

Computational method and application using Newton Algorithm

Cornelia Victoria Anghel

Computer Science Department, “EFTIMIE MURGU” University, Resita, 320085, Romania

Summary

The article presents some aspects about Newton method and algorithm and a numerical example. The C++ program illustrated the important steps and advantages to apply the Newton method to solve the nonlinear equations.

KEYWORDS: Newton (tangent) method, Newton algorithm, C++ program.

1. INTRODUCTION NEWTON METHOD (TANGENT METHOD)

The Newton Method (or Tangent Method) is used to solve the un-linear equations, and to reduce substantially the number of iterations.

If we considered x^* - a separate solution of equation $f(x) = 0$ on $[a, b]$ interval and $f(x)$ is continue and monotone on this interval, the values of function in a and b points $f(a)$ and $f(b)$ have opposed signs (such as in Figure 1).

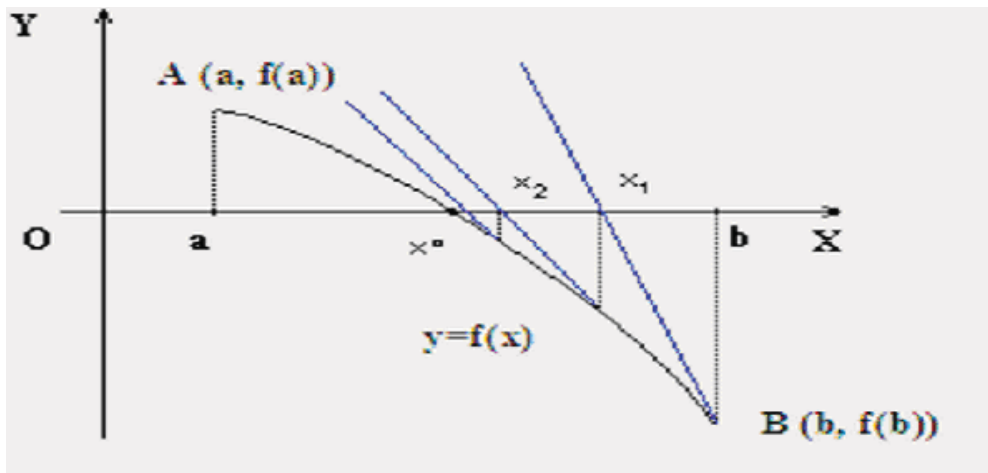


Figure 1.

We write the tangent equation in $A(a, f(a))$, point
$$y - f(a) = f'(a) \cdot (x - a)$$

intersect the Ox axis.

We obtain
$$x = a - \frac{f(a)}{f'(a)} \text{ or } x_1 = a - \frac{f(a)}{f'(a)}.$$

From geometrical point for view (figure 1) signifies the fact that the arch/spring curve is replaced by the tangent, and the place of the exact value solution x_1 (the abscissa/x-coordinate of the intersection point of the curve and the axis Ox) it is taken as an approximate value x_1 (the abscissa of the intersection point of the tangent at the curve with the axis Ox).

By repeatedly applying Newton’s method we can correct the first approximation, finding closer values to the exact one.

The approximate values result from the series:

$$x_n = x_{n-1} - \frac{f(x_{n-1})}{f'(x_{n-1})}$$

2. THE ALGORITHM OF THE TANGENT METHOD (NEWTON)

- We draw the tangent at the curve in the point **B(b, f(b))** and we find the intersection point of the tangent and the axis OX – $(x_1, 0)$. The abscissa of this point **x1** is taken as I the solution approximation.

- Computing the function value in **x1** we could deduce the tangent at the curve in the point with the coordinates **(x1, f(x1))**. The tangent will intersect the axis OX in the point with the coordinates **(x2, 0)**. The abscissa of this point **x2** taken as I solution approximation.

- Continuing this process several times, we can observe that we obtain a value series **x1, x2, x3, ...**, which tend towards the equation solution **x°**.

3. NUMERICAL APPLICATION

We propose to solve the equation $x^3 - 2x - 5 = 0$.

Solution: We notice that if we note $f(x) = x^3 - 2x - 5$, then $f(1) = -6$; $f(2) = -1$; $f(3) = 16$.

From the conditions $f(2) < 0$ and $f(3) > 0$ we deduce that a solution of the equation appears in the interval (2, 3).

We consider the first approximation $x_1 = 2$.

We determine $x_2 = 2 - \frac{f(2)}{f'(2)}$.

For $f(x) = x^3 - 2x - 5$, $f'(x) = 3x^2 - 2$ and $f(2) = -1$; $f'(2) = 10$

$$x_2 = 2 + \frac{1}{10} = 2 + 0.1 = 2.1.$$

We repeat the sentence and we get: $x_3 = 2.1 - \frac{f(2.1)}{f'(2.1)}$

where $f(2.1) = (2.1)^3 - 2 \cdot (2.1) - 5 = 0.061$.

$$f'(2.1) = 3 \cdot (2.1)^2 - 2 = 3 \cdot 4.41 - 2 = 13.23 - 2 = 11.23.$$

$$\text{It results } x_3 = 2.1 - \frac{0.061}{11.23} = 2.1 - 0.0054 = 2.0946$$

Then we determine $x_4 = x_3 - \frac{f(x_3)}{f'(x_3)}$

$$\text{By substitution we get: } x_4 = 2.0946 - \frac{f(2.0946)}{f'(2.0946)} = 2.09455.$$

We approximate $x_4 = 2,095$.

The value of the function is:

$$f(2,095) = (2,095)^3 - 2 \cdot (2,095) - 5 = 9,195 - 4,190 - 5 = 9,195 - 9,190 = 0,005$$

hence $f(2,095) > 0$.

From the conditions $f(2) = -1 < 0$ and $f(2,095) > 0$ we determine that the value $x = 2,095$ can be considered the solution of the given equation.

As an observation, we can affirm that if the graphic of the function $f(x)$ is almost parallel to the ax Ox, i.e. the size of the derivative $f'(x)$ is closed of zero, then the Newton method is not applicable, but another method is recommended, for example the string/cord method.

4. PROGRAM C++

The program written in C++ which determines the solution of the function given in the above mentioned example, using the algorithm of the tangent method (Newton) is:

```
#include <stdio.h>
#include <conio.h>
#include <math.h>
```

```

float Func(float x)
{
    return x*x*x-2*x-5;
}
int Newton(float Func(float, float *x), float *x)
{
    const float eps=1e-6;
    const int itmax=100;
    float df, dx, f;
    int it;

    for(it=1; it<=itmax; it++){
        f=Func(*x, &df);
        dx=(fabs(df) > eps) ? -f/df : -f;
        *x += dx;
        if (fabs(dx) <= eps*fabs(*x)) return 0;
    }
    printf("maximum no. of iterations exceeded within the Newton method! \n");
    return 1;
}

```

The following notations were used:

- Func** – for the user function
- a, b** - the limits for the search interval
- *x** - the found zero (output)
- it** - the number of iterations
- itmax** – the maximum number of iterations

The error number is returned:

- 0** – for a normal execution
- 1** – if the maximum number of iterations is exceeded
- 2** – when the interval does not contain a root.

After each partition of the interval, not only the ends of the interval are upgraded, but also the corresponding values of the function $f(a_i)$ and $f(b_i)$.

5. CONCLUSIONS

This method helps us to efficiently obtain the solution of the problem. The small number of iterations necessary for the determination of the equation solution from the presented example indicates that the choice of the tangent method (Newton) in

the solving of this equation was the right one. These observations can be picked out from the analysis of the results obtained after the development of the program implemented in the above presented programming language C++.

If the graphic of the function $f(x)$ is almost parallel to the Ox axis, i.e. the size of the derivative $f'(x)$ is closet o zero, then the Newton method is not applicable, but another method is recommended, for example the string/cord method.

References

1. Anghel C.V. – *Metode numerice. Algoritmi și programe de calcul*. Ed. Orizonturi Universitare, Timișoara 2005 (in Romanian);
2. Anghel, I., Anghel, C.V.- *Algebra liniară. Programare liniară*, Curs vol.1, Ed. Eftimie Murgu, Reșița, 2003 (in Romanian);
3. Precup, R. ș.a – *Matematici asistate de calculator. Aplicații*. Ed. Politehnică, Timișoara, 2002 (in Romanian);
4. Kilyeni, Șt. – *Metode numerice*, vol.1, Ed. Orizonturi Universitare, Timișoara, 1997 (in Romanian).

Partial substitution of Cement in Concrete by Finely Ground Brick Body

Libuše Beckerová, Gergely Bölckei and Jiří Brožovský

^{1,2,3} Faculty of Civil Engineering, Brno University of Technology, Brno, 602 00, Czech Republic

Summary

Brick chippings are the waste which can partially substitute the cement. Therefore this waste is utilized, in light of the environment, into the useful new product - the concrete. The finely ground brick body is characterized by certain pozzuolana activity which enables the partially substitution of the energetically demanding binder which is the cement. The paper indicates the observations concerning the tests of concrete in which the cement was substituted by 10% and 20% of finely ground brick bodies from the brick plants Kryry and Šlapanice.

KEYWORDS: brick body, concrete, additive to concrete, pozzuolana activity.

1. INTRODUCTION

The brick plants produce on the average 1 till 5 % of waste, which is recycled only in low range and utilized as opening material. The rest is stored in deposits. The price of this waste material rarely overreaches 5 till 10% of the cement price. It is true that for the utilization as substitute for cement it is necessary to prepare it (by grinding, separation etc.). However also after this preparation its price does not overreach 20% of cement production costs. The finely ground brick body shows pozzuolana activity so that we can hold it for the active pozzuolana admixture and we can substitute the part of binder in cement composite by this material.

By the addition of finely ground brick body we can achieve, with comparable concrete parameters, the decrease of production costs.

The reaction extent of the burned brick body with the hydrating cement is given on the one hand by the composition of raw materials and on the other hand by the burning conditions.

The brick products are on the present as a rule burned at the temperature 1000 – 1100°C. The brick body is formed by raw glass surrounded by other crystals and it can show variable pozzuolana activity in dependence on the used earth and on the burning temperature. The greatest portion in the resulting product forms as the rule the glassy phase with high content of silicon and of alkalis and it contents further

also aluminium, different iron oxides, calcium and magnesium surrounded by crystals of mullite, silicon and sometimes also cristoballite. The brick products with high lime content can also contain considerably amounts of feldspars which support the increase of activity.

The reaction activity is highest mostly in the temperature range between 600 – 900°C. Higher temperature causes nucleation and crystallization of new phases in the body and the reaction activity rather decreases. The glassy phase excels during cooling and it is in dependence on the composition more or less active [4].

The following active admixtures were applied in practice:

- Finely ground brick body from the brick plant KRYRY
- Finely ground brick body from the brick plant ŠLAPANICE

The effect of the cement substitution in concrete by finely ground brick body, on its physico-mechanical characteristic, was tested in experimental work.

2. METHODS OF EXPERIMENTAL WORK AND THE COMPOSITION OF CONCRETE

The experimental work is based on the properties comparison of concrete made with different batch of finely ground brick body (substitution 10 % and 20 % of the cement weight) with the properties of reference concrete which was made without the use of brick body.

2.1. Input materials:

The following components were used for the production of concrete:

- cement CEM 42,5R from cement plant Mokrý
- sand fraction 0-4 mm from the locality Žabčice
- crushed aggregate fraction 4-8 mm from the locality Želešice
- crushed aggregate fraction 8-16 mm from the locality Želešice
- admixture: finely ground brick body from the brick plant KRYRY and ŠLAPANICE
- The volume weight of these brick bodies are 2750 kg/m³
- Additive: poly-carboxyl-ether ACE 40, from the firm BASF which shows liquefying effects, increases the initial and the final strength of concrete
- batch water – it fulfils the demands of the EN 1008.

The basic parameters of the aggregate are in table 1.

Table 1: Basic parameters of the aggregate

Parameter	Unit	Žabčice 0/4 mm	Želešice 4/8 mm	Želešice 8/16 mm
Volume weight	[kg/m ³]	2630	2650	2730
Bulk weight in shed state	[kg/m ³]	1770	1670	1710
Porosity	[%]	32,7	37,0	37,4

2.2. Composition of concrete

The composition of concrete is in table 2.

Table 2. Composition of concrete in 1 m³

Component	Reference concrete	Concrete with 10% of brick body	Concrete with 20% of brick body
CEM I 42,5 R Hranice cement	400 kg	360 kg	320 kg
Finely ground brick body	0 kg	40 kg	80 kg
Sand 0 to 4 mm from the Žabčice Gravel Pit	745 kg	740 kg	739 kg
Aggregates 4 to 8 mm from the Želešice Gravel Pit	235 kg	230 kg	229 kg
Aggregates 8 to 16 mm from the Želešice Gravel Pit	980 kg	972 kg	971 kg
Plasticizer BASF ACE 40	4 kg	4 kg	4 kg
Mixing Water	151 kg	147 kg	141 kg
Water/Cement Ratio	0,38	0,37	0,35

2.3. Observed parameters

The following parameters were observed with tested concrete:

- fresh concrete - flow table test F (EN 12350-5 Standard)
- density of fresh concrete D (EN 12350-6 Standard)
- density of hardened concrete D (EN 12390-7 Standard)
- compression strength $f_{c,cu}$ (EN 12390-3 Standard) in the age of concrete 1, 3, 7, and 28 days
- bending strength f_{cf} (EN 12390-6 Standard) in the concrete age 28 days
- depth of penetration of water under pressure h_n (EN 12390-8 Standard)
- dynamic modulus of elasticity E_{bu} (CSN 731371 Standard) in the age of concrete 1, 3, 7, 14 a 28 days.

Marking of individual tested concrete:

- REF** - reference concrete (strength class C 55/67)
S10 - concrete with 10% substitution of cement by finely ground brick body from brick plant Šlapanice
S20 - concrete with 20% substitution of cement by finely ground brick body from brick plant Šlapanice
K10 - concrete with 10% substitution of cement by finely ground brick body from brick plant Kryry
K20 - concrete with 10% substitution of cement by finely ground brick body from brick plant Kryry

3. TEST RESULTS

The test results are in table 3 and for selected parameters they are represented graphically in figures:

- Fig.1: Effect of the finely ground brick body addition on the compression strength of concrete with different age

Fig.2: Effect of the finely ground brick body addition on the bending strength of concrete and on the ingress of pressure water - age of concrete 28 days

- Fig.3: Effect of the finely ground brick body addition on the dynamical elasticity modulus – for different ages of concrete.

Table 3: Results of concrete tests

Properte	Age [days]	Unit	REF	S10	S20	K10	K20
FRESH CONCRETE							
<i>F</i>	--	[mm]	370	435	450	420	435
<i>D</i>	--	[kg/m ³]	2500	2480	2460	2470	2460
HARDENED CONCRETE							
<i>D</i>	28	[kg/m ³]	2520	2490	2480	2490	2480
<i>f_{c,cu}</i>	1	[MPa]	39,8	30,2	20,8	28,6	20,4
	3		49,8	40,4	34,9	36,5	33,6
	7		59,6	54,6	43,1	52,6	44,1
	28		74,0	68,6	56,6	69	52,1
<i>f_{cf}</i>	28		7,8	6,5	5,5	6,6	5,5
<i>h_v</i>	28	[mm]	11	8	6	10	7
<i>E_{bu}</i>	1	[GPa]	47,5	42,8	40,3	40,8	40,7
	3		52,2	46,5	44,5	44,6	44,5
	7		56,7	52,8	50,3	51,1	49,8
	14		57,1	53,0	51,7	52,2	51,5
	28		57,4	54,6	52,0	52,5	52,5

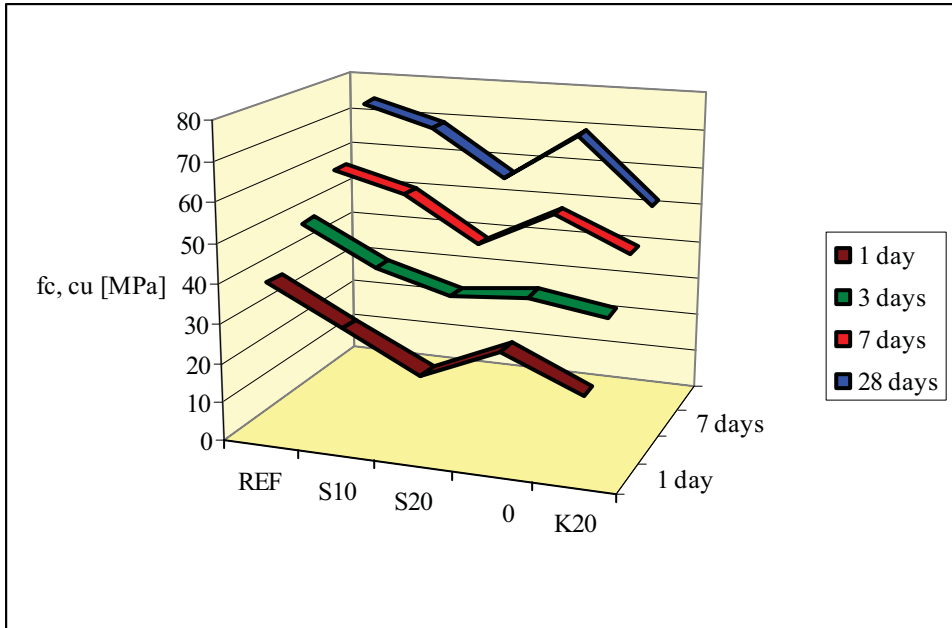


Figure 1. Compression strength in dependence on the quantity of added brick body and on the hardening time of concrete

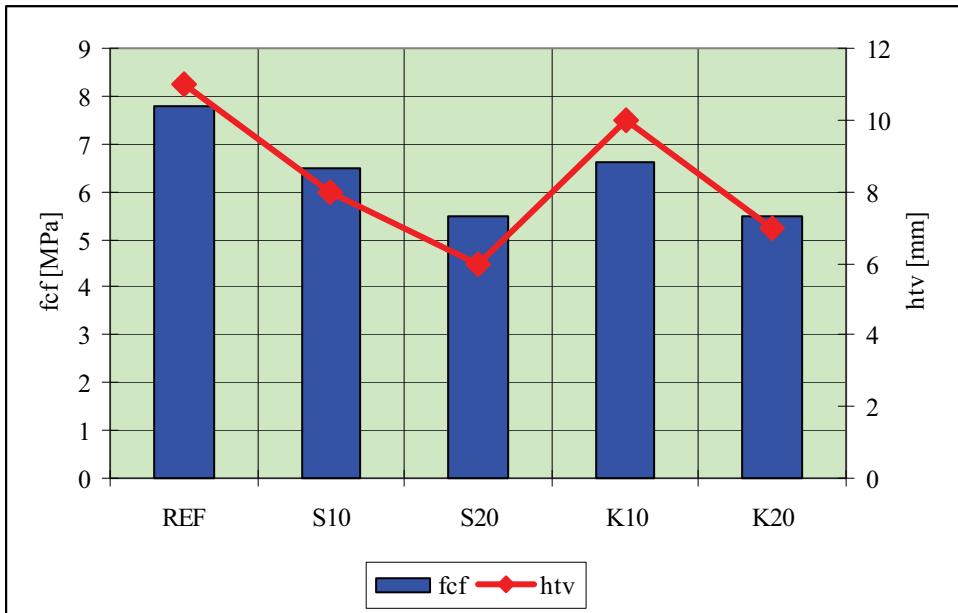


Figure 2. Effect of the quantity of added brick body on the bending strength and on the depth of the pressure water ingress

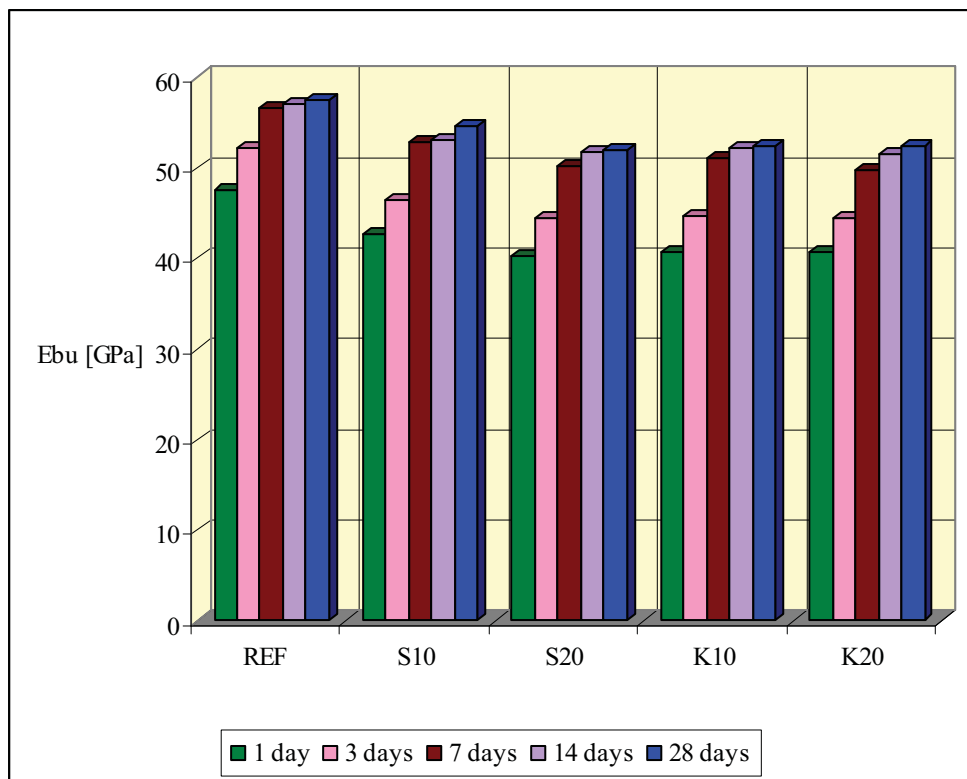


Figure 3. The dynamical elasticity modulus in dependence on the quantity of added brick body and on the hardening time of concrete.

4. CONCLUSION

Experimental works proved the usability of finely ground brick body as active admixture into concrete. The test results showed that the utilization of this active admixture is also adequate for the improvement of some special concrete properties.

a) Compression strength:

The concrete with the substitution of 10 % cement by finely ground brick body achieved after 28 days 92 - 93% of the reference concrete compression strength values.

The concrete with the substitution of 20 % of cement by finely ground brick body achieved after 28 days 71 – 73% of the reference concrete compression strength values.

b) Bending strength:

The bending strength decreases with the increasing content of the brick body. The highest strength had the reference concrete.

c) Depth of the pressure water ingress:

The depth values of pressure water ingress into the reference concrete were comparable with the water ingress into concrete with the addition of brick body and they are very favourable.

d) Dynamical modulus of elasticity:

The dynamical modulus of elasticity decreases with the increasing content of the brick body. The reference concrete had the highest value.

The results of experimental works show that better values of compression strength are achieved in the case of 10 % cement substitution by brick body – the concrete class corresponds with the concrete class of the reference concrete. Concrete with 20 % cement substitution by brick body achieves values which are by a class lower.

We can conclude that the utilization of finely ground brick body in concrete is useful from the ecological and also from the economical point of view.

ACKNOWLEDGEMENTS

The work was supported by the MSM 0021630511 Plan: Progressive Building Materials with Utilization of Secondary Raw Materials and Impact their on Structures Durability.

References

1. Drochytka, R. et al. Progressive Building Materials with Utilization of Secondary Raw Materials and their Impact on Structures Durability. Brno University of Technology, *Final report of the project VVZ CEZ MSM: 0021630511*, Brno 2006. Brožovský, J.: Subtask 3 (in Czech).

2. Brožovský, J. and Martinec, P. Durability of Concrete with Fly Ash. *In Proceedings of the 2^d International Conference on Concrete and Reinforced Concrete: Concrete and Reinforced Concrete – Development Trends*. NIIZHB, Moscow, Russia, Vol. 4, 2005. (in Russian).
3. Brožovský, J., Zach, J., Brožovský, J., Jr.: Durability Of Concrete Made From Recycled Aggregates. *In Proceedings Of The International Rilem Jci Seminar Concrete Durability And Service Life Planning: Curing, Crack Control, Performance In Harsh Environments*, Ein-Bokek, Dead Sea, Israel, 2006
4. Wild, S., Gaillius, A., Hansen, H., Pederson, L., Szabowski, J.: Pozzolanic properties of a variety of european clay bricks. *Building research and information* vol. 25, number 3, 1997
5. EN 12350-5 Testing fresh concrete - Part 5: Flow table test
6. EN 12350-6 Testing fresh concrete - Part 6: Density
7. EN 12350-3 Testing hardened concrete - Part 3: Compressive strength of test specimens
8. EN 12350-5 Testing hardened concrete - Part 5: Flexural strength of test specimens
9. EN 12350-7 Testing hardened concrete - Part 7: Density of Hardened Concrete
10. EN 12350-8 Testing hardened concrete - Part 8: Depth of penetration of water under pressure
11. CSN 73 1371 Method of Ultrasonic Pulse Testing of Concrete
12. EN 1008 Mixing Water for Concrete. Specification for Sampling, Testing and Assessing the Suitability of Water, Including Water Recovered from Processes in the Concrete Industry, as Mixing Water for Concrete

Minimum weight buildings design using inequalities method

Constantin Amariei¹, Iulian Gabriel Mihai²

¹Structural Mechanics Department, TU “Gh. Asachi” Iași, 700050, România

²S.C. EdilConst S.A Câmpina, Prahova, 105600, România,

Summary

Based on inequalities method and on possibilities of solving by automatic computation mathematical computation model of minimum weight steel structures is presented.

KEY WORDS: optimum design, minimum weight, inequalities method, linear algorithm.

1. GENERAL PROBLEMS

Optimization computation due to weight criterion can be done in many ways, according to structure equilibrium equations which are designed function of weight reduction condition formulation. Most important ways are presented below:

1. Establishment, function of a certain cross-section previously chosen, of all possible solutions, determination for each of it of the allowable load and choosing from all “sure” (for which the capable load is bigger than real load) of the one with the smallest one. The procedure is very elaborated and represents an empirical way for obtaining of some economic solutions.

2. The computation is based on choosing the most efficient solution from a variety of solutions, using one of the post-elastic computation methods. Such a possibility is given by the bending moments distribution in plastic domain, in its usual form or in a generalized operation form with mechanical work measures. [1] Using of this method supposes a certain experience in choosing the adjusting way of nodes, bars and kinematic chains equilibration, respectively in choosing of some combinations and constructive constraints which have to be taken in view.

3. Static methods, based on plastic yielding conditions (safety) corresponding to critical cross-sections of the structure, as presented below:

$$-S_{p(i)} \leq S_i \leq S_{p(i)} \quad (1)$$

where: $S_{p(i)}$ is the capable effort (plastic) of the critical cross-section “i”;

S_i is the effective effort in the critical cross-section “i”.

In the case of bar structures subjected mostly in bending, relation (1) becomes:

$$-M_{p(i)} \leq M_i \leq M_{p(i)} \quad (2)$$

Choosing a statically determined system and writing the bending moments M_i as:

$$-M_i = M_{0i} + \lambda \cdot M'_{0i} + \sum_{h=1}^n x_h \cdot m_{0i}^h \quad (3)$$

where: M_{0i} - bending moments on the base system, produced by permanent loads;

λ - loading coefficient;

M'_{0i} - bending moments in the base system by $\lambda = 1$;

x_h - statically undetermined values;

m_{0i}^h - bending moments produced in the base system by each $x_h = 1$.

The limit state computation is reduced to a linear algorithm problem consisting in increasing at maximum the loading factor λ in obtained relations by replacing the equations (3) and (2). By utilizing bending moment diagrams in equilibrium with external loads, disposed on base systems, judiciously choused, and which can differ from a load case to another, the plastic yielding conditions become [7]:

$$-M_p \leq M_p^0 + \sum x_i \cdot m_i \leq M_p \quad (4)$$

where (for a critical cross-section "i"):

M_p - plastic moment of the cross-section;

M_p^0 - bending moment produced by several loads on a certain base system;

x_i - proportionality coefficients (statically undetermined values);

m_i - bending moments from auto equilibrium diagrams.

Using unknown factors decomposing or axes translations, are obtained resolvable formulations by simple procedure, due to which is determined the minimum of weight function.

4. The method based on using the elementary mechanisms combination and on the minimum weight solution theory elaborated by J.Foulkes and B.G.Neal.

5. The method proposed by J.Heyman and W.Prager, based on the general conditions of the limit state computation and on the minimum weight design theories and following the static way, in a two cycles of solving, each cycle consisting of two stages.

Generally, additionally to general hypothesis of the post elastic computation domain, at minimum weight structures design are also taken into consideration some supplementary hypothesis:

- a) There exist an infinite variety of cross-sections (rolled steel shapes or composed cross-sections);
- b) It is known the variation law on the weight per unit length of elements (q), due to plastic strength modulus (W_p). If there are graphically represented the pairs of values of (q, W_p) for the usual :I” rolled steel shape, is obtained the curve presented in figure 1 (approximated as being a continuous curve), which can be expressed by an exponential relation as :

$$q = k \cdot W_p^\alpha \tag{5}$$

or:

$$q = k \left(\frac{M_p}{\sigma_c} \right)^\alpha = k' \cdot M_p^\alpha \tag{6}$$

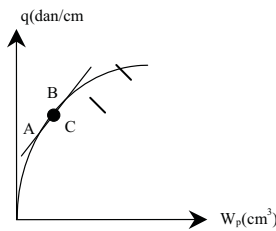


Fig. 1

The coefficients k and α vary function of the cross-section type.

Since for a certain structure the used cross-sections don't vary generally between very high limits, the curve (q, W_p) can be approximated with a polygonal diagram. For example, if the values of plastic module corresponding to points A and B from the figure 1 have a 1:2 ratio, the error coming from the approximation of the curve on the specified portion with a straight line, is only of 1%. Due to this assumption, the weight per unit length of the element can be written as a linear function:

$$q = a + b \cdot M_p \tag{7}$$

The total weight of the structure is:

$$Q = \sum_{i=1}^n q_i \cdot l_i = \sum_{i=1}^n (a + b \cdot M_{p(i)}) \cdot l_i = a \cdot \sum_{i=1}^n l_i + b \cdot \sum_{i=1}^n M_{p(i)} \cdot l_i \tag{8}$$

where l_i represents the lengths of the bars, $M_{p(i)}$ are the plastic bending moments of the bars cross-sections, and the number „n” is the number of bars having different values of plastic bending moments.

Because $a \cdot \sum_{i=1}^n l_i$ and b are constant, results that the determination of the minimum weight is reduced to determination of the minimum solution of the equation:

$$X = \sum_{i=1}^n M_{p(i)} \cdot l_i \quad (9)$$

called weight function.

Regarding the loads considered for minimum weight structures computation, according to American norms, they will be considerate as follows:

- for the combination consisting of permanent and live loads, they will be multiplied with a unic coefficient 1,7;
- for the combination consisting of permanent loads, live loads and wind action or earthquake action, they will be multiplied with a unic coefficient 1,3.

2. COMPUTATION MODEL BASED ON INEQUALITIES METHOD

Adaptation of the inequalities method for optimization computation

Inequalities method, usually used as determination way of loading limit factor can be adapted for a structure weight optimization computation, representing some important advantages, as simple and direct way of writing the constraining relations (especially of plastic yielding conditions), and the fact that it can be taken into consideration in the optimization computation of axial force influence, fact that can influence a lot the conceiving and behavior of certain structures categories.

Adaptation of inequalities method for weight optimization computation requires two important elements:

- a) Taken in consideration as unknowns – in the relations that express plastic yielding conditions – of the plastic moments and introducing in these relations of the loading factor with imposed values by real loads acting on the structure.
- b) Joining to these relations the weight function (linear or nonlinear) which has to be optimized.

The relations which compose the mathematic model for optimum design in this way are the following:

1. Static equilibrium equations:

a) for loaded bars (figure 2.a):

$$M_s^{(k)} \cdot b_k + M_c^{(k)} \cdot l_k + M_d^{(k)} \cdot a_k = \lambda_k \cdot a_k \cdot b_k \tag{10}$$

where: $k=1,2,\dots,b$ (b being the number of loaded bars over the length).

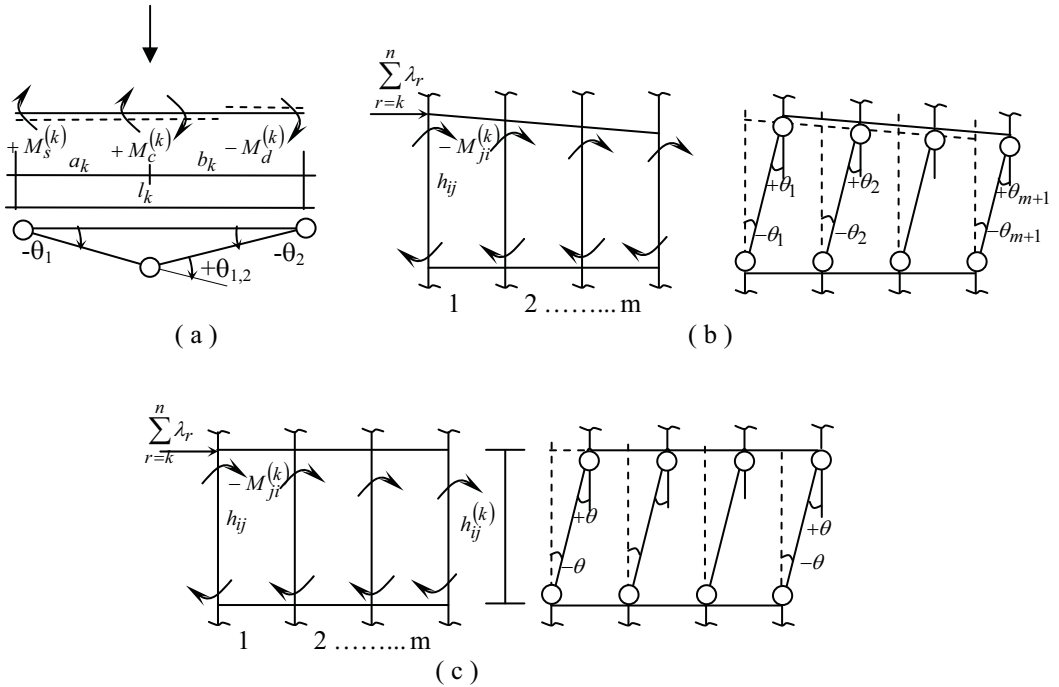


Fig. 2

b) for kinematic chains:

-unequal columns over the level (figure 2.b):

$$\sum_{i=1}^s \left(\frac{M_j^{(i)} + M_s^{(i)}}{h_i} \right) = H_k \tag{11}$$

where: $i=1,2,\dots,s$ (s being the number of the columns from a level);

$k=1,2,\dots,m$ (m being the number of levels of the structure);

h_i =column height;

H_k =sliding load for a level.

- unequal columns over the level (figure 2.c):

$$\sum_{i=1}^s (M_j^{(i)} + M_s^{(i)}) = h_k \cdot H_k \quad (12)$$

h_k level height.

c) for nodes:

$$\sum [\pm M_{ij}^{(k)}] = 0 \quad (13)$$

$k=1,2,\dots,n$ (n being the number of nodes).

2. Relations which express plastic yielding conditions:

$$-M_{p(i)} \leq M_i \leq M_{p(i)} \quad (14)$$

where: $M_{p(i)}$ is the plastic moment of the critical cross-section "i" (the unknowns of the problem);

M_i is the effective bending moment in the critical cross-section "i", $i=1,2,\dots,c$ (c being the number of critical cross-sections).

Totally are written a number of (e) statically equilibrium relations ($e=b+m+n$) and a number of (2c) inequalities – plastic yielding conditions.

3. Weight function, which has the usual form:

$$X = \sum_{i=1}^p l_i \cdot M_{p(i)}^\alpha \quad (15)$$

$i=1,2,\dots,n$ (n being the established number of different plastic bending moments of the structure).

In a matrix form, the relations can be written as:

- statically equilibrium relations:

$$[B] \cdot \{M\} = \{\bar{\lambda}\} \quad (16)$$

- plastic yielding conditions:

$$-\{M_p\} \leq \{M\} \leq \{M_p\} \quad (17)$$

- weight function:

$$X = \{C\}^T \cdot \{M_p\} \quad (18)$$

where:

$[B]$ is the matrix of coefficients from the statically equilibrium relations;

$\{M\}$ vector of bending moments in the critical cross-sections;

$\{\bar{\lambda}\}$ is the vector of constants from statically equilibrium;

$\{M_p\}$ is the vector of plastic moments in critical cross-sections;

$\{C\}$ is the vector of plastic moments coefficients from the weight equation.

Removing from the plastic yielding conditions a number of (e) bending moments by their replacing with the values obtained in the (e) statically equilibrium equations, function of the other (c-e) bending moments, will result (2c) inequalities with [p+(c-e)] variables, [p necessary plastic bending moments and (c-e) bending moments in the critical cross-sections, as:

$$[A] \cdot \{M\} \geq \{\lambda\} \tag{19}$$

Some inequalities will be eliminated, obtaining a reduced number of constraining conditions which, together with the weight function, compose the relations of programming problem for minimum weight determination.

From the constraints number reducing problem, the most important are the following:

a) Imposing – constructively taking – of some ratios between necessary plastic moments, meaning:

$$M_{p(i)} > M_{p(k)} \tag{20}$$

which will have as effect the decreasing of the unknowns number of the optimization problem and also will eliminate some constraining relations referring to plastic joints appearance possibility on each bar in nodes.

b) “Selection” of inequalities meaning eliminating the least restrictive relations (which are satisfied including the remained inequalities).

c) Partially or totally knowing the shape of failure bending moments distribution (based on static and loading schemes), which makes possible to write – for critical cross-sections where is certainly known the sign of bending moment – only some simple inequalities, instead of double ones which usually appear in plastic yielding conditions:

$$-M_{p(i)} \leq M_i \tag{21}$$

or:

$$M_i \leq M_{p(i)} \tag{22}$$

In case of a linear weight function, **simplex method** can be used for solving, when is necessary the transformation of constraints inequations in equalities relations, by introducing of some compensation variables \overline{M} , so the matrix relation [19] becomes (eventually after elimination of some constraints conditions):

$$[A] \cdot \{M\} - [E] \cdot \{\overline{M}\} = \{\lambda\} \quad (23)$$

where: $\{\overline{M}\}$ is the vector of compensation variables;
 $[E]$ is the unit matrix.

Or, can be used the extended form of the problem, by introducing of some auxiliary variables M' :

$$[A] \cdot \{M\} - [E] \cdot \{\overline{M}\} + [E] \cdot \{M'\} = \{\lambda\} \quad (24)$$

or:

$$[A] \cdot \{M\} + [E] \cdot \{M^*\} = \{\lambda\} \quad (25)$$

where:

$$\{M^*\} = \{M'\} - \{\overline{M}\} \quad (26)$$

in this case, is necessary to respect the negativity conditions for all three variables categories:

$$M, \overline{M}, M' \geq 0 \quad (27)$$

and the extended weight function (the lower bound of the weight function X) is:

$$X^* = \{C\}^T \cdot \{M_p\} + \{0\}^T \cdot \{M_i\} + \{\mu\}^T \cdot \{M^*\} \quad (28)$$

where: $\{M_p\}$ is the vector of necessary plastic bending moments, which makes the minimum weight structure;

$\{M_i\}$ is the vector of remain bending moments;

$\{M^*\}$ is the vector of auxiliary compensation variables.

The simplex solution contains also the values of “p” necessary plastic bending moments, and the values of remain bending moments in (c-e) critical cross-sections; the other (e) values of bending moments are determined with statically equilibrium equations, so it is possible a complete statically analyze for checking the plastic yielding conditions fulfill, and also the failure mechanism establishment.

In case of some big dimensions, the problem will be solved with a linear or nonlinear computer program.

3. COMPUTATION EXAMPLE

Determination of minimum weight solution for the frame in the figure 3.a.

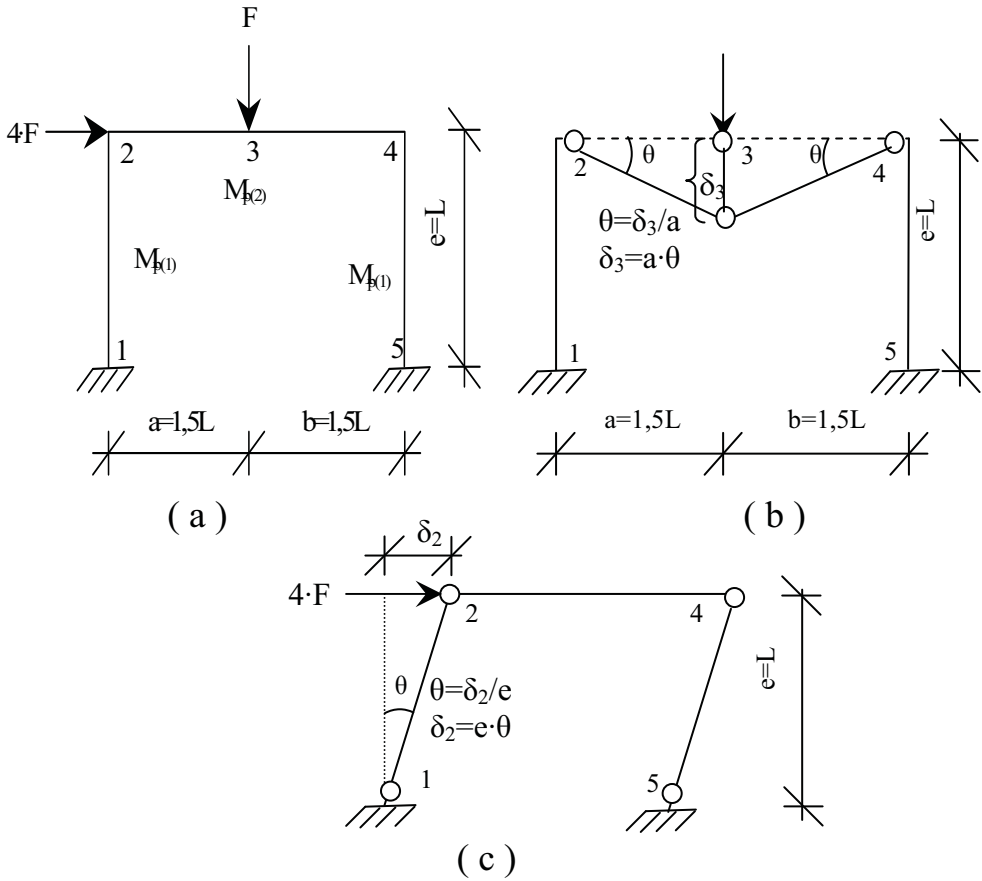


Fig. 3

It is considered: $F=1$; $L=1$.

It will be noted: $M_{p(1)}=Y_1$ și $M_{p(2)}=Y_2$ which are the necessary plastic bending moments for the columns and beams.

Will be noted the bending moments in the five critical cross-sections **(1,2,3,4,5)** of the frame, as: $M_3=Y_3$; $M_4=Y_4$; $M_5=Y_5$; $M_1=Y_6$; $M_2=Y_7$

The relations which compose the mathematical model of the minimum weight frame design problem by **inequalities method** are the following:

1) Statically equilibrium relations:

a) bar equilibrium (figure 3.b):

$$M_2 \cdot \theta + M_3 \cdot \theta + M_3 \cdot \theta + M_4 \cdot \theta = F \cdot \delta_1$$

$$\text{or: } M_2 + M_3 + M_3 + M_4 = F \cdot a$$

having the established notations:

$$Y_7 + Y_3 + Y_3 + Y_4 = F \cdot 1,5 \cdot L$$

$$\text{or } Y_7 + 2 \cdot Y_3 + Y_4 = 1,5$$

b) displacement equilibrium (figure 3.c):

$$M_1 \cdot \theta + M_2 \cdot \theta + M_4 \cdot \theta + M_5 \cdot \theta = 4 \cdot F \cdot \delta_2$$

$$\text{or: } M_1 + M_2 + M_4 + M_5 = 4 \cdot F \cdot e$$

having the established notations:

$$Y_6 + Y_7 + Y_4 + Y_5 = 4 \cdot F \cdot L$$

$$Y_6 + Y_7 + Y_4 + Y_5 = 4$$

2) Plastic yielding conditions:

$$-Y_1 \leq Y_6 \leq Y_1; -Y_1 \leq Y_7 \leq Y_1; \quad -Y_2 \leq Y_7 \leq Y_2; -Y_2 \leq Y_3 \leq Y_2; -Y_2 \leq Y_4 \leq Y_2; -Y_1 \leq Y_4 \leq Y_1; \quad -Y_1 \leq Y_5 \leq Y_1$$

These relations can also be written:

$$Y_1 + Y_6 \geq 0; Y_1 + Y_7 \geq 0; Y_2 + Y_7 \geq 0; Y_2 + Y_3 \geq 0; Y_2 + Y_4 \geq 0; Y_1 + Y_4 \geq 0; Y_1 + Y_5 \geq 0$$

respectively:

$$Y_1 - Y_6 \geq 0; Y_1 - Y_7 \geq 0; Y_2 - Y_7 \geq 0; Y_2 - Y_3 \geq 0; Y_2 - Y_4 \geq 0; Y_1 - Y_4 \geq 0; Y_1 - Y_5 \geq 0$$

3) Weight function:

$$X = \sum_1^n l_i \cdot M_{p(i)}$$

so: $X=2 \cdot M_{p(1)}+3 \cdot M_{p(2)}+0 \cdot M_3+0 \cdot M_4+0 \cdot M_5+0 \cdot M_1+0 \cdot M_2$

or: $X=2 \cdot Y_1+3 \cdot Y_2+0 \cdot Y_3+0 \cdot Y_4+0 \cdot Y_5+0 \cdot Y_6+0 \cdot Y_7$

Using a usual computation program for solving linear problems, will be obtained the following results:

-plastic bending moments values:

$Y_1=M_{p(1)}=1.625; Y_2=M_{p(2)}=0.375$

-valorile momentelor din secțiunile critice:

$Y_3=M_3=0.375; Y_4=M_4=0.375; Y_5=M_5=1.625; Y_6=M_1=1.625; Y_7=M_2=0.375$

-value of the weight function:

$X=4.375$

Knowing the values of plastic bending moments on the columns and beams will be established the cross-section of bars:

a) the column:

$$M_{p(1)} = \sigma_c \cdot W_{column} \quad so : W_{column} = \frac{M_{p(1)}}{\sigma_c}$$

or: $W_{stalp} = \frac{b_{column} \cdot h_{column}^2}{4}$

Will be imposed: $h_{column} = 1,5 \cdot b_{column}$

and results : $\frac{b_{column} \cdot (1,5 \cdot b_{column})^2}{4} = \frac{M_{p(1)}}{\sigma_c}$

where $b_{column} = \sqrt[3]{\frac{4 \cdot M_{p(1)}}{2,25 \cdot \sigma_c}}$

$h_{stalp} = 1,5 \cdot \sqrt[3]{\frac{4 \cdot M_{p(1)}}{2,25 \cdot \sigma_c}}$

b) the beam:

$M_{p(2)} = \sigma_c \cdot W_{beam} \quad deci : W_{beam} = \frac{M_{p(2)}}{\sigma_c}$

$$\text{or: } W_{beam} = \frac{b_{beam} \cdot h_{beam}^2}{4}$$

It will be imposed: $h_{beam} = 1,5 \cdot b_{beam}$

$$\text{and results: } \frac{b_{beam} \cdot (1,5 \cdot b_{beam})^2}{4} = \frac{M_{p(2)}}{\sigma_c}$$

$$\text{where: } b_{beam} = \sqrt[3]{\frac{4 \cdot M_{p(2)}}{2,25 \cdot \sigma_c}}$$

$$h_{beam} = 1,5 \cdot \sqrt[3]{\frac{4 \cdot M_{p(2)}}{2,25 \cdot \sigma_c}}$$

References

1. Amariei C. – Calculul structurilor în domeniul plastic, I.P.Iași, 1974 (in Romanian)
2. Bălan Șt, Petcu V. – Calculul structurilor în domeniul plastic – Optimizări, Editura Academiei R.S.R., București, 1979 (in Romanian)
3. Dancea I. – Metode de optimizare, Editura Dacia, Cluj Napoca, 1976 (in Romanian)
4. Gheorghiu Al. – Concepții moderne în calculul structurilor, Editura Tehnică, București, 1975 (in Romanian)
5. Mihăilă N. – Introducere în programarea liniară, Editura Didactică și Pedagogică, București, 1980 (in Romanian)
6. Nădejde I. – Probleme de cercetare operațională. Programare matematică, Editura Academiei R.S.R., București, 1971 (in Romanian)
7. Răutu S., Chiroiu V. – În legătură cu calculul construcțiilor cu greutate minimă (in Romanian)
8. Vuc I. – Modele matematice în proiectarea construcțiilor, Editura Facla, Timișoara, 1981 (in Romanian)

Scientific Perspectives for Future Research Work in Fundamental Properties of Short-Lived Radionuclides from Decay and from in-Beam Studies

Brindusa Ciobanu¹, Ion Silisteanu² and Irina Radinschi³

¹ Department of Physics, “Gh. Asachi” Technical University, Iasi, 700050, Romania

² “Horia Hulubei” Natl. Inst. of Physics & Nuclear Engrg., 077125, Bucharest-Magurele, Romania

³ Department of Physics, “Gh. Asachi” Technical University, Iasi, 700050, Romania

Summary

The aim of this paper is to point out some scientific perspectives for future research work in fundamental properties of short-lived radionuclides from decay and from in-beam studies, arisen in the frame of our research project. The project approaches one of the most important themes of nuclear physics. In recent years the investigation of unstable short-lived nuclei has gained world-wide interest as well on the experimental as on the theoretical side. These nuclei are characterized by unique structure properties: the weak binding of the outermost nucleons and the effects of the coupling between bound states and the particle continuum. Particularly, the modification of the effective nuclear potential leads to the formation of the nuclei with very diffuse nucleon densities, to the occurrence of the nucleon skin and halo structures. Our first goal is to formulate a reaction theory for cluster decay in which the clustering and reaction amplitudes will be represented by means of resonance formulas. A brief outlook of the experimental results and theoretical ideas which define the field is presented together with quantitative estimations for the resonance decay widths and relative intensities. The resonance solution of systems of coupled equations is obtained by a direct numerical integration using step-by-step methods on computer. Thus, we obtain most complete information on the development of typical structures from stable to exotic loosely-bound nuclei by: improving the structure models in order to describe essential features and to obtain spectroscopic information on a number of nuclei that can then be tested against data extracted from decay and in-beam studies; extending the range of applicability of reaction models by using accurate reaction channels methods (e.g. via additional channels including deformation, exchange effects, antisymmetrisation, etc); including microscopic structure information in coupled channel reaction models and treating more carefully of "intermediate" systems that are more or less bound or have mixed composition.

KEYWORDS: short-lived radionuclides, cluster decay, numerical integration of coupled channel equations, computational methods.

1. INTRODUCTION

In recent years the investigation of unstable short-lived nuclei has gained worldwide interest as well on the experimental as on the theoretical side. These nuclei are characterized by unique structure properties: the weak binding of the outermost nucleons and the effects of the coupling between bound states and the particle continuum. Particularly, the modification of the effective nuclear potential leads to the formation of the nuclei with very diffuse nucleon densities, to the occurrence of the nucleon skin and halo structures. These phenomena will also affect collective vibrations and rotations of unstable nuclei, particularly the electric dipole and quadrupole excitations, and new modes of excitations and decay might arise in nuclei near the drip line.

Apart from general structure aspects in the physics of nuclei far from stability, there is also strong relations to the question of clustering in nuclei and to few-body physics. Furthermore, there will be a strong coupling to the continuum both in static and dynamic descriptions. Nuclear clustering and fine structure are two of the most important typical structures in nuclear physics which are strongly connected to the stability and deformation.

Superheavy elements (SHE) probe the extremes of nuclear structure with respect to the number of nucleons that can form a bound system. Their existence and decay properties are one of the most fundamental problems in nuclear physics [1-4]. There are data that confirm the existence of $Z=111$ and 112 and their connection to lighter decay chains [1]. The first data for $Z=113, 114, 115$ and 116 also exist [3, 4], with suggested $A=288-292$, respectively, but the A values are not certain since the connection to lighter nuclei is not known. A new element with atomic number 118 was synthesized for the first time in the $^{249}\text{Cf} + ^{48}\text{Ca}$ reaction.

Atomic and mass numbers of the isotope of element 118 were determined from the measured excitation functions and decay characteristics of the daughter nuclei produced in cross-bombardments [5]. Theoretical models for SHE have evaluated from microscopic-macroscopic models [6] to fully microscopic deformed Hartree-Fock (HF) models [7]. In addition to their importance for many-body nuclear structure, theoretical models for the prediction of the decay properties of the SHE are important when designing experiments since the technique used will depend on half-life and decay mode.

In order to obtain the most complete information on these new nuclei, effects and phenomena a use of radioactive beams in a wide range of isospin and energy is necessary. High energy beams produced by in-flight fragmentation and post-accelerated beams proved to be complementary with the respect to their intensity, purity, and optical quality. When one analyses a proper reaction model, the measurements of core or halo momentum distributions after breakup, can provide important information on the structure of a such nucleus. The detection of gamma-

rays from outgoing fragments allows to access experimentally whether core excited components are present in a halo state.

The experimental signatures of clustering and "fine structure" (FS) far from stability are supported by data from selective excitation in nucleon and α -transfer reactions, α -decay, heavy cluster decay, and by rotationally spaced energy levels, enhanced transition strengths and intensities, and appreciable emission width for the resonant states above the decay threshold. Recent decay and in-beam studies of unstable nuclei are revealing an unexpected diversity and richness of shapes, and new decay modes and typical structures which are related to very low binding energy and the strong influence of the continuum.

To treat the decay rates for these nuclei we describe the nuclear clustering and penetration of the particle through the potential barrier taking into account the correspondence between different decay channels and different final states of the daughter nucleus.

The decay process being governed by nuclear clustering and quantum tunneling over the Coulomb barrier is strongly influenced by couplings of the relative motion of the fragments to several nuclear intrinsic motions. We address to effects of coupling between the intrinsic degrees of freedom and relative motion by solving numerically the coupled channel equations, including all the relevant reaction channels.

Our first goal is to formulate a reaction theory for cluster decay in which the clustering and reaction amplitudes will be represented by means of resonance formulas. A brief outlook of the experimental results and theoretical ideas which define the field is presented together with quantities estimations for the resonance decay widths and relative intensities. The resonance solution of systems of coupled equations is obtained by a direct numerical integration using step-by-step methods on computer.

Thus, we obtain most complete information on the development of typical structures from stable to exotic loosely-bound nuclei by: improving the structure models in order to describe essential features and obtain spectroscopic information on a number of nuclei that can be tested against data extracted from decay and in-beam studies; extending the range of applicability of reaction models by using accurate reaction channels methods (e.g. via additional channels including deformation, exchange effects, anti-symmetrization, etc); including microscopic structure information in coupled channel reaction models and treating more carefully of "intermediate" systems that are more or less bound or have mixed composition.

The modern facilities (EUROBALL, GAMMASPHERE, RIA, etc.) or recent research projects (SPIRAL-2, etc.) of the important international centers in Oak

Ridge (USA), Darmstadt (Germany), Dubna (Russia), etc., are mainly devoted to the laboratory investigation of exotic nuclear structures [6].

The very large number of publications and conferences in this field underlines its importance and define it as an excellence research area. The research team has a long-term experience in the research fields approached by the project, as:

- short lived nuclear production with secondary beams;
- spectroscopy of exotic nuclei by transfer and breakup reactions. One notes experimental methods like resonant particle spectroscopy (RPS) method [8], recoil decay tagging (RDT) method [9], cross-sections measurements in breakup reactions and theoretical methods (highly unstable states spectroscopy, semiclassical models for the evaluation of one-nucleon breakup reactions at intermediate energies, calculation and design for detection methods, RPS and RDT);
- theoretical modelling of spontaneous decay, transfer and break-up reactions (clustering and “fine structure” at limits of stability, coupled channel approximation for cluster decay including rotational degrees of freedom, quantum tunneling induced by rotational coupling, multichannel resonant decay).

In the following we will shortly present the current status and directions within the topics related to our project.

2. RESULTS AND PERSPECTIVES

2.1. Short lived nuclei production with secondary beams

One tries to estimate the most favourable projectile - target combination to maximize the fusion cross section at energies near the Coulomb barrier, taking into account the deformation degrees of freedom and mass asymmetry.

These thematics investigate the orientation effect by considering the role of quadrupolar and hexadecapolar deformations for the projectile and the role of rotational degrees of freedom for the target. In this propose one developes coupled channel approximation for the Schrödinger equation, treating the cold fusion as a scattering problem with appropriate boundary conditions.

Both Numerov and Runge-Kutta numerical methods will be use for the computing of the radial wave functions. One establishes the succesfull application to the description of fusion of ^{48}Ca on actinide nuclei ^{238}U and ^{248}Cm , recently performed at the Flerov Laboratory Dubna. It was estimated that this projectile-target combination is one of the most promising one to reach the superheavy island of stability [1,2,10].

2.2. Spectroscopy of decay, transfer and breakup reactions

One attempts to measure one nucleon breakup cross sections for proton and neutron rich nuclei. One estimates breakup cross sections for weakly bound exotic nuclei. One performs the design and simulation of complex experimental setup for reactions with secondary beams.

Exotic nuclei (far from stability valley) play an important role in the structure studies, as well in the modern astrophysical studies (nucleosynthesis, structure an evolution of neutron stars, black holes, etc.)

One of the most sophisticated and succesful experimental methods has been proposed by Romania (C. Borcea et al.) in which a measurement of total reaction cross section and the inclusive breakup one nucleon cross section for ^8B and ^{11}Be have been proposed for the definite establishment of the existence of halo states [11]. In these experiments, a secondary beam of (e.g.) ^{11}Be has been produced by fragmentation of a primary beam of ^{18}O at 70 MeV/nucleon on a thick target of ^9Be . Fragmentation products have been separated with the doubly achromatic LISE separator in GANIL (France). An approximately 1000 ^{11}Be counts/sec has been obtained in impinged on a stack of 17 Silicon detectors which served as a degrader, target and analysing media for reaction products. In front of the telescope a position sensitive detector x-y (position sensitive parallel plate avalanche detector-PPAD) has been placed to define the beam spot on the detector. The telescope segmentation allowed identification of the reaction products as well as the identification of reaction mechanisms such as stripping or nuclear dissociation. The first mechanism has been identified by an increased rate of reaction events in adjacent segments of the telescope, following an reaction event in a given segment. Later on in a subsequent experiment at Michigan the nuclear dissociation mechanism has been identified by a supplementary energy loss deposition by the proton in the breakup reaction of ^8B on a silicon target. The method is based on the assumption that to a good approximation after breakup the heavy fragment will have 10/11 or 7/8 from the incident energy. This is based on the common understanding of halo states (i.e. low separation energy and low angular momentum characterising the state). This small change in the energy translates into a different range in the detector which can be measured. Backwards to the telescope an array or 32 neutron detectors has been placed in an attempt to better identify reaction mechanism such as nuclear dissociation.

A similar experiment has been performed recently in a Oberlin -Michigan - Bucharest collaboration. A cocktail of proton rich nuclei has been impinged on a silicon telescope. The experiment allowed identification of new candidates for proton halos, weakly bound nuclei, close to the proton drip line, which shows a very low separation energy and a wave function dominated by low angular momenta (p-waves). This work is in progress. These exeperments have a very nice future. New plannigs are projected at GANIL for studies of neutron rich nuclei in

the f-shell with the improvements that core states will be identified by an array of efficient gamma detectors [12-16].

2.3. Spontaneous decay, transfer and breakup theoretical modelling

The experimental results and theoretical ideas which define the clustering and "fine structure" is presented together with quantitative estimations for the resonance emission widths. We present both formal considerations, derived from a microscopic (shell model) formulation of the reaction theory, and practical computational programs based on coupled channel methods, with many-body effects included in formation and reaction amplitudes, energy shifts and total decay widths.

The main conceptual issues in reaction theory are identified and their relative importance is assessed: these include, couplings between the relative motion of the fragments and several nuclear collective motions, the existence and convergence of the resonance scattering solution, account the effects of non-linear couplings to all orders, self-consistence of the scattering potential, and the rotational excitation of nuclei by the cluster transfer.

The cluster decay properties of heavy drip-line nuclei are considered and some spectroscopic information on the continuum states populated in the unbound intermediate systems in the decay channel is obtained. The limitations and advantages of current computational approaches are addressed, with particular regard to quantitative experimental comparisons for superheavy nuclei [1- 4], [17, 18].

2.4. Numerical computer codes for nuclear reactions with exotic nuclei

The aim is to obtain with good accuracy the eigenstates (bound and resonant) of deformed nuclei for realistic studies of phenomena like fission, alpha decay and proton emission.

The motion of a particle in a deformed potential is governed by the tri-dimensional Schrödinger equation. When the potential is axially symmetric, the wavefunction can be expanded in partial waves with angular and radial components. The radial wavefunctions are the solutions of a set of coupled differential equations of second order. In order to obtain the eigenstates (either bound, resonant or antiresonant) one has to solve (numerically) the eigenvalue problem for this system subject to some physically consistent boundary conditions. For this purpose several tasks should be accomplished: the calculation of the solution at the boundaries of the numerical domain (near the origin and at large distances), the propagation of the solution on the integration interval, the determination of the eigenvalues and the construction of the normalized wave functions. Many investigations have been devoted to this

subject. See for example [19-24], including our own experience [4,17,18,25]. In the present project one intends to improve the existing procedures, increasing the accuracy and reducing the amount of computer time and memory requirements. Thus realistic cases with important deformations and large number of equations could be handled, allowing the study of nuclear processes in complex systems (like exotic and heavy nuclei).

2.5. Role of charge density in cold fusion reactions

Cold fusion barriers are studied with respect to the change of the charge density within the overlapping region. Charge evolution from separated target and projectile up to the compound nucleus is taken into account by meaning of a deduced transition formula which depends on geometric parameter variation defining the shape. Macroscopic shell correction and total deformation energy for fusion like configurations are calculated for different charge density paths.

The way geometric parameters influence on the total deformation energy is also studied and compared with already published work [26, 27]. Influence of changes on isotopic composition of the reaction is emphasized in final shell corrections, and an analogy is made with isospin equilibration observed and calculated in [28]. Total barriers are computed as a function of charge density taken as free parameter, a procedure also accounted in [29]. Minimization along this coordinate produces variations of about 4 MeV for light nuclei and up to 8 MeV for superheavy synthesis, for the deformation energy in the last part of the process.

4. CONCLUSIONS

The aim of this paper is to point out some scientific perspectives for future research work in fundamental properties of short-lived radionuclides from decay and from in-beam studies, arisen in the frame of our research project. Our first goal is to formulate a reaction theory for cluster decay in which the clustering and reaction amplitudes will be represented by means of resonance formulas. A brief outlook of the experimental results and theoretical ideas which define the field is presented together with quantitative estimations for the resonance decay widths and relative intensities. The resonance solution of systems of coupled equations is obtained by a direct numerical integration using step-by-step methods on computer.

The degree of novelty is given by the field of the proposal itself: exotic nuclear systems are intensively investigated by different experimental and theoretical groups in all important international centers during the last decade. Important experimental and computing facilities were assigned to this field in this period and many conferences and workshops were organized in order to analyse the obtained

results. The complexity is given by sophisticated experimental techniques and theoretical methods.

The participants are well recognized scientists in several related to this field areas. This project is a good opportunity to enlarge the international cooperation with our foreign partners and to prepare the participation within the framework of various international projects.

Acknowledgements

Research of authors was supported by MedC- CERES in the framework of the grant CEX05-D10-08/03.10.2005.

References

1. Yu. Ts. Oganessian, et al., *Phys. Rev. Lett*, 83, 1999, pp. 3154.
2. Yu. Ts. Oganessian, et al., *Phys. Rev.*, C70, 2004, pp. 242.
3. S. Hofmann and G. Münzenberg, *Rev. Mod. Phys.*, 72, 2000, pp.733.
4. I. Silişteanu, W. Scheid, A. Sandulescu, *Nucl. Phys. A*, 679, 2001, pp. 317.
5. Yu. Ts. Oganessian, et al., Synthesis of the isotopes of elements 118 and 116 in the ^{249}Cf and $^{245}\text{Cm} + ^{48}\text{Ca}$ fusion reactions, *C* 74, 2006, 044602.
6. G. Münzenberg, Perspectives for nuclear structure research at GSI- from halo nuclei to superheavy elements, Proceedings of the 174. WE- Heraeus- Seminar, *Il Nuovo Cimento*, Vol. 110 A, N. 9- 10, 1997, pp. 1103.
7. S. G. Nilsson, I. Ragnarsson, *Shapes and Shells in Nuclear Structure*, Cambridge University Press, ISBN-13 978-0-521-01966-8, ISBN-10 0-521-01966-4, 2005, pp. 50, 72, 157.
8. D. Robson, *Nucl. Phys.*, A 204, 1973, pp. 204.
9. R. S. Simon et al., *Z. Phys.*, A 325, 1986, pp. 197.
10. Y. S. Tsyganov, Detection of ultra rare α decays of super heavy nuclei, *Nuclear Instruments and Methods in Physics Research*, A 573, 2007, pp. 161-164.
11. N. K. Skobelev, R. Anne, C. Borcea, D. Guillemaud - Mueller, S. Grevy, Z. Dlouhy, F. Carstoiu, M. Lewitowicz, S. M. Lukyanov, A. C. Mueller, F. Negoita, Yu. E. Penionzhkevich, M. G. Saint - Laurent, O. Sorlin, Reactions of breakup of ^{11}Be Nuclei interacting with ^{28}Si Nuclei, *Bull. Rus. Acad. Sci. Phys.*, 63, 1999, pp. 771.
12. A. De Vismes, P. Roussel-Chomaz, F. Carstoiu, Global analysis of proton nucleus cross sections, *Phys. Rev.*, C 62, 2000, 064612.
13. E. Sauvan, F. Carstoiu, N. A. Orr, J. C. Angelique, W. N. Catford, N. M. Clarke, M. Mac Cormick, N. Curtis, M. Freer, S. Grevy, C. Le Brun, M. Lewitowicz, E.Liegard, F. M. Marques, M. Mac Cormick, P. Roussel-Chomaz, M. G. Saint Laurent, One-neutron removal reactions on neutron-rich psd-shell nuclei, *Phys. Rev.*, C 69, 2004, 044603.
14. E. Sauvan et al., *Phys. Rev.*, C 69, 2004.
15. L. Trache et al., *Phys. Rev. Lett.*, 271102, 2001, pp. 87.
16. L. Trache et al, *Phys. Rev.*, C 69, 2004, 032802(R).
17. I. Silisteanu, A. O. Silisteanu, W. Scheid, B. I. Ciobanu, Alpha Half-Time Estimates for the Superheavy Elements, Proceedings of the Carpathian Summer School of Physics 2005, *Exotic Nuclei and Nuclear/ Particle Astrophysics*, World Scientific, 2006, pp. 423.
18. I. Silisteanu, A. Sandru, A. O. Silisteanu, B. Popovici, A. Neacsu, B. I. Ciobanu, Alpha Half-Time Estimates for the Superheavy Elements, Proceedings of the Predeal International Summer School in Nuclear Physics, *Collective Motion and Phase Transition in Nuclear Systems*, World Scientific,

- 2006, pp. 569.
19. S. Cwiok, J. Dudek, W. Nazarewicz, J. Skalski, T. Werner, Single particle energies, wave functions, quadrupole moments and g-factors in axially deformed Woods - Saxon potential with applications in the two - centre - type nuclear problems, *Comp.Phys.Commun.*, vol. 46, 1987, pp.379.
 20. E. Maglione, L. S. Ferreira, R. J. Liotta, Nucleon decay from deformed nuclei, *Phys.Rev.Letters*, vol. 81, 1998, pp. 538.
 21. K. Rykaczewski, J. C. Batchelder, C. R. Bingham, T. Davinson, T. N. Ginter, C. J. Gross, R. Grzymack, M. Karny, B. D. MacDonald, J. Mas, J. W. McConnel, A. Piechaczek, R.C. Slinger, K.S. Toth, W. W. Walters, P. J. Woods, E. F. Zganjar, B. Barmore, L.Gr. Ixaru, A.T. Kruppa, W. Nazarewicz, M. Rizea, T. Vertse, Proton Emitters: Probing the Structure of Unbound Nilsson Orbitals, *Phys.Rev.,C*, vol. 60, 1999, 011301.
 22. T. Vertse, A. T. Kruppa, B. Barmore, W. Nazarewicz, L. Gr. Ixaru, M. Rizea, Proton emission from Gamow resonance, *AIP Conference Proceedings 518*, Proton-Emitting Nuclei, First International Symposium, Oak Ridge, Tennessee U.S.A., 2000, pp. 184.
 23. H. Esbensen, C. Davids, Coupled-channel treatment of deformed proton emitters, *Phys.Rev.,C*, vol. 63, 2000, 014315.
 24. M. Rizea, PERSYS - A program for the solution near the origin of coupled channel Schrödinger equation with singular potential, *Comput. Phys. Commun.*, vol.143, 2002, pp. 83.
 25. I. Silişteanu, W. Scheid, A. O. Silisteanu, *Rom. Rep. Phys.*,57, 2005, pp. 4.
 26. C. Y. Wong, *Phys. Rev. Lett.*, 31, 1973, pp. 766.
 27. L. C. Vaz, J. M. Alexander, *Phys. Rev.*, C 18, 1978, pp. 2152.
 28. B-A. Li, S. J. Yennelo, *Phys. Rev.*, C52, 1995, R1746.
 29. K. Satou, H. Ikezoe, S. Mitsuoka, K. Nishio, S. C. Jeong, *Phys. Rev.*, C 65, 2002,054602.

Experimental and numerical analysis of compressed concrete elements confined with FRP composites

Gabriel Oprisan, Nicolae Taranu and Vlad Munteanu

Civil Engineering Department, "Gh. Asachi" Technical University, Iasi, 700054, Romania

Summary

Confinement of concrete by suitable selection of transverse internal reinforcement or by externally bonded reinforcement results in significant increase in both the compressive strength and the ductility of concrete subjected to compressive loading. Traditional confinement solutions have been developed using steel hoops or steel jackets and only recently fibre reinforced polymer composites (FRP) have been perceived as reliable confinement solutions for concrete elements. Extensive research projects have been performed since 1990s and theoretical and experimental results confirm the validity of confinement with FRP composites jackets. An experimental program has been initiated at the Faculty of Civil Engineering, the Technical University of Iasi, to evaluate the confining effect with glass fibre/epoxy and carbon fibre/epoxy composites. The influence of the material type and the thickness of FRP confining jacket were the variables involved.

The results obtained have proven the effectiveness of confinement solutions based on FRP composites. Both compressive strength and ductility of the confined specimens have shown dramatic increase compared to unconfined concrete specimens. The experimental set-up, the testing procedure and the main results are presented, emphasizing the influence of the composite nature and the thickness of the confining jacket.

KEYWORDS: confining, FRP jackets, compressive strength, ductility

1. INTRODUCTION

To establish the mechanical characteristics of unconfined concrete, cylindrical specimen and standard cubes adequate to compression test were cast. Also in order to determine the concrete class and the compressive strength, 9 concrete cylinders, 100 mm in diameter and 250 mm high, and 9 cubes, 100 mm in side, have been tested in uniaxial compression under standard condition. To avoid a rapid failure of the unconfined concrete cylinder and determine the complete stress-strain curve including the post peak strength domain of the material it was necessary to use a special installation for the post elastic testing of brittle materials. The arrangement

of all transducers is illustrated in figure 1, for both unconfined and confined samples.

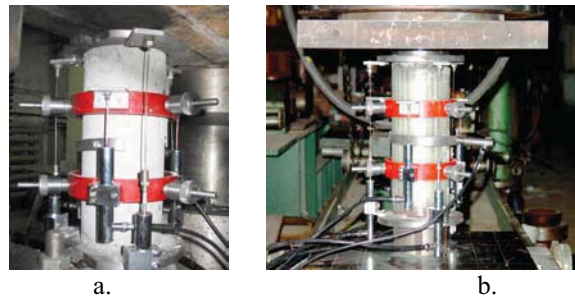


Figure 1. Instrumentation of test samples with LVDTs a. unconfined concrete cylinder specimen; b. confined concrete cylinder specimen

The compressive strength determined on plain concrete samples, after 28 days is 31.64 N/mm² on the concrete cylinders and 32.16 N/mm² on the concrete cubes, and a complete stress-strain curve for unconfined concrete is illustrated in Figure 2.

2. EXPERIMENTAL PROGRAM

To avoid a rapid failure of the unconfined concrete cylinder and determine the complete stress-strain curve including the post-yielding domain of the material it was necessary to use a genuine installation for the post elastic testing of brittle materials. Before the experimental testing of the specimen, the testing machine had been calibrated and the equipment had been prepared for data acquisition, fig. 2. Data processing was done with a developed soft based on “Test Point” program.

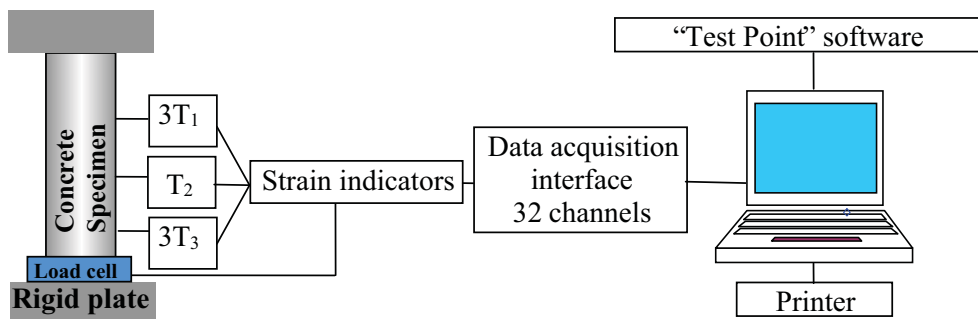


Figure 2. Acquisition and processing experimental data

Stress-strain curve obtained on unconfined concrete cylinders (fig.3) has two branches, a rising one associated with elastic, viscous and plastic strains, and a

falling one corresponding to pseudo plastic strain and characterized by an accelerated decrease in load and increase in strain over time. The maximum value on the curve corresponds to the ultimate compressive strength of concrete. The compressive strength determined on plain concrete samples, after 28 days was 31.64 N/mm^2 on the concrete cylinders and 32.16 N/mm^2 on the concrete cubes.

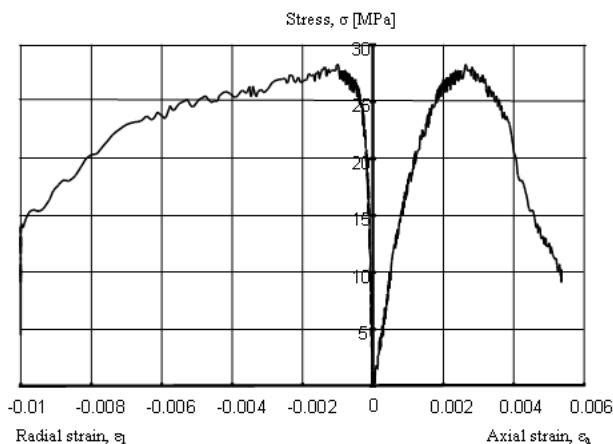


Figure 3. The complete stress-strain curves for unconfined concrete specimens

Nine specimens with 2, 3 and 4 unidirectional CFRP and GFRP layers (three of each type) with main fibers orientated in the hoop direction have been prepared using a wet hand lay-up technique. Prior to the application of the FRP layers the surface of the samples has been properly prepared to provide a hard, dry and clean surface. The main characteristics of GFRP for epoxy resins are presented in table 1 whilst the properties for glass and carbon fibers are given in table 2 and table 3.

Table 1 - Properties of epoxy resin

Appearance	Component A: light/yellow to amber Component B: pale yellow to clear liquid
Mixing ratio	A:B = 100:34,5
Density	$1,16 \text{ g/cm}^3$
Tensile strength (ASTM D 638)	7 days at $+21 \text{ }^\circ\text{C}$: 55 N/mm^2
Tensile modulus (ASTM D 638)	7 days at $+21 \text{ }^\circ\text{C}$: 2000 N/mm^2
Fracture elongation (ASTM D 638)	7 days at $+21 \text{ }^\circ\text{C}$: 3,2%

Confined concrete specimens with GFRP and CFRP have been tested with the same installation used for the unconfined concrete samples. The confined specimens have been kept under laboratory conditions kept for 7 days to enable the complete cure of the polymeric resin after confinement.

Table 2 - Properties of glass fiber reinforcement

Fiber type	E-Glass fibers
Fiber orientation	0 ⁰ C (unidirectional)
Construction	93% warp, 7% weft
Areal weight	920 g/m ²
Fabric thickness	0,36 mm
Density of glass fibers	2,58 g/cm ³
Tensile strength of fibers	2250 N/mm ²
Tensile E-modulus	72400 N/mm ²
Ultimate fiber strain	3,7 %

Table 3 - Properties of carbon fiber reinforcement

Fiber type	Carbon fibers - high modulus
Fiber orientation	0 ⁰ C (unidirectional)
Construction	97% warp, 3% weft
Areal weight, [g/m ²]	610
Fabric thickness, [mm]	0,34
Tensile strength of fibers, [N/mm ²]	3900 (nominal) 3700 (minimal)
Tensile E-modulus, [N/mm ²]	231000
Ultimate fiber strain, [%]	1,5

Three stages have been observed on the stress-strain curve of confined concrete specimens:

- the first stage is linear and it corresponds to the stiffness of the unconfined concrete specimens, fig.4;
- in the second stage the concrete specimen exhibits larger lateral strains and the GFRP jacket creates a confining pressure on the concrete core. When the concrete specimen is cracked, a dramatic change in curve configuration occurs. At this stage much higher stresses and strains are attained than in the case of unconfined concrete;
- in the third stage, the concrete specimen is thoroughly cracked and the GFRP maintain the concrete confined specimen intact till the explosive failure of the jacket occurs. The stress-strain curve increases by a constant angle up to the rupture, fig.4.

A comparative set of curves for unconfined and CFRP confined samples is illustrated in fig.5; the confined samples have been wrapped with 2, 3 and 4 layers of CFRP composites.

The stress-strain curves of the CFRP composites have a bilinear shape with sharp softening in the transition area around the strength of the unconfined concrete. In the first stage the slope of the stress-strain curve is similar to that of the unconfined concrete. In the second stage the concrete is cracked and the confinement is activated. The stress of the confined concrete linearly increases with increasing the

CFRP strain. All experimental results confirm the similar work published in the field of structural rehabilitation with composites [1].

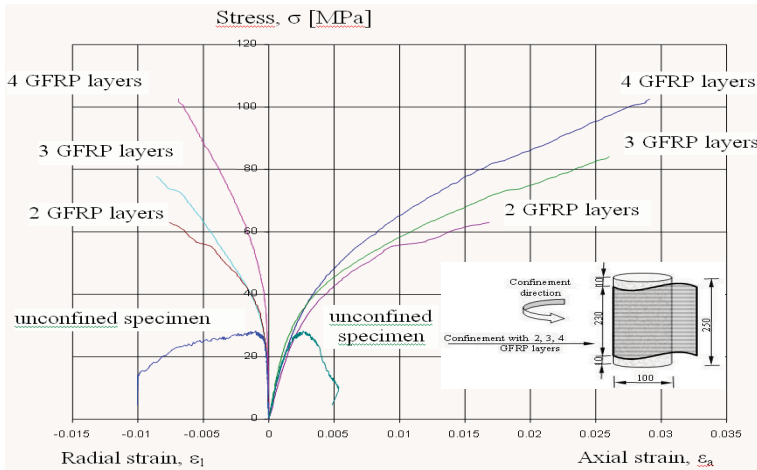


Figure 4 - Stress-strain curves of compressed unconfined and confined concrete specimens with GFRP

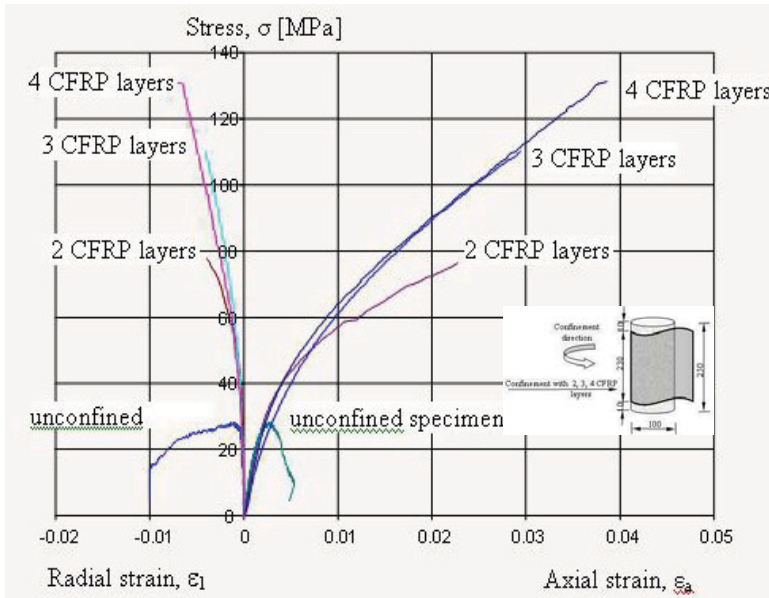


Figure 5 - Stress-strain curves of compressed unconfined and confined concrete specimens with CFRP

When the test is properly carried out the maximum stress is reached at the CFRP rupture. Some samples failed prematurely due to separation of the composite layers

at the lap joints. A step forward of the experimental program has been the cyclic loading of the confined samples as a first stage to seismic retrofit with polymeric composites. Some preliminary results are shown in fig.6 [2].

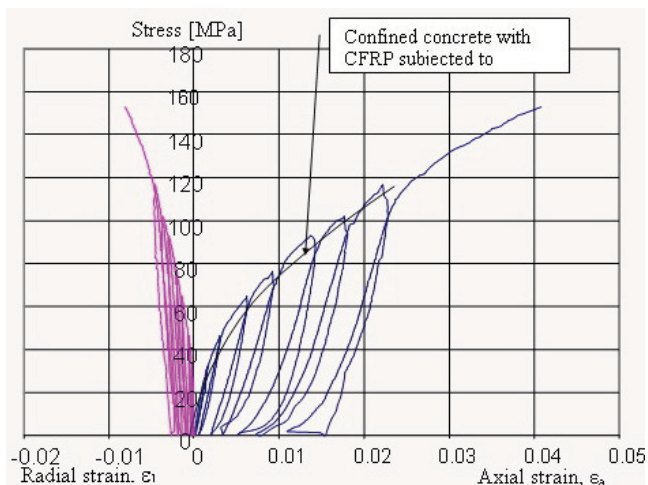


Figure 6 - Stress-strain curves of confined specimens subjected to cyclic load

3. NUMERICAL ANALYSIS

In order to verify the suitability of a FEM based software (LUSAS) for modelling concrete confinement problems, a numerical analysis was performed.

A statical non-linear analysis was conducted on a model that was built under the same dimensional conditions with the experimental program.

The concrete cylinder was modelled as a 3D solid element. In order to obtain a radial regular meshing it was first modelled a quarter of the final concrete element. The CFRP jacket was modelled as a sum of thick shell elements, “glued” onto the concrete surface using the SLIDELINE option, proper for contact problems, as in this case. The attributed thickness of the jacket was equivalent to a 3 layers disposal of CFRP sheets.

3D solid elements were used for the concrete cylinder meshing, as long as for the jacket, 3D surface elements were used. Although the software allows the use of higher order finite elements, only linear interpolation between nodes option was used in order to reduce the total number of elements and nodes for having a reasonable solving time.

The cylinder was considered as simply supported at the top end and totally restrained at the bottom end. The load was applied as a uniformly distributed force at the top end of the concrete element. In order to ensure a good convergence of the load increments, an initial value of 1 N/mm^2 was used and variable load increments (3 and 10) were used afterwards in the Solution Software Manager.

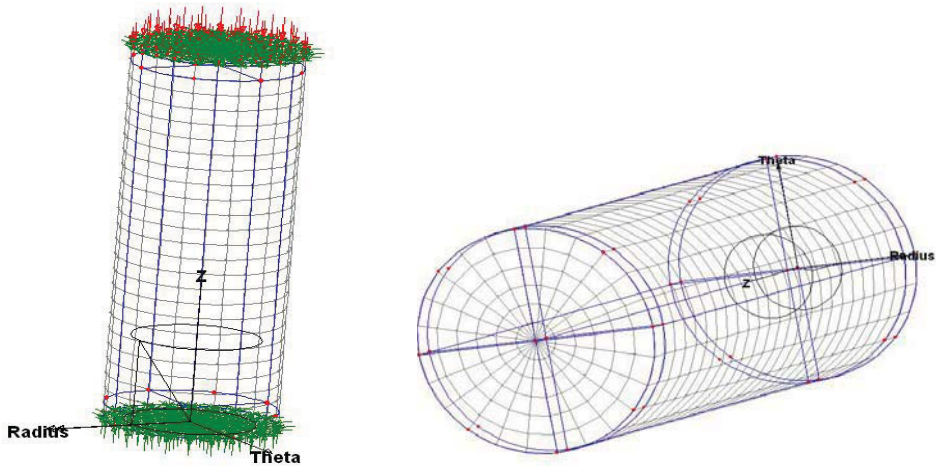


Figure 7 Support and load conditions of the concrete cylinder; radial meshing of the concrete volume

A Ducker-Prager material model based was used for defining the material properties for concrete as long as for the composite CFRP jacket an orthotropic material model available in the software's material options was used.

The mechanical properties for both concrete and composite jacket were defined in accordance with the materials that were used in the laboratory tests, and then attributed to the geometric elements.

From the large range of numerical and graphical results available after performing the run of the program, representative data charts and maps were selected and presented below. They are related to stresses, strains, displacements data needed in order to realise a good picture of the confined concrete cylinder behaviour under axial loading.

LOAD CASE = 14
Increment 14 Load Factor = 30.0000
RESULTS FILE = 1
STRESS
RESULTS CARTESIAN= 1
CONTOURS OF S_{zz}
-36.87
-36.29
-35.71
-35.14
-34.56
-33.99
-33.41
-32.83
-32.25
-31.67
-31.1
-30.52
-29.95
-29.37
-28.79
-28.22
-27.64
-27.06
-26.48
Max: 23.58 at Node 2511
Min: 36.90 at Node 2287

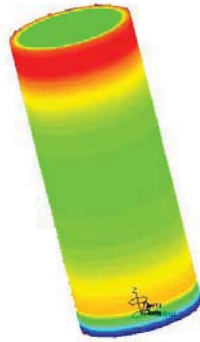


Figure 8. Normal stresses (unconfined concrete cylinder)

LOAD CASE = 12
Increment 12 Load Factor = 130.0000
RESULTS FILE = 1
STRESS
RESULTS CARTESIAN= 1
CONTOURS OF S_{zz}
-137.292
-136.360
-135.462
-134.595
-133.897
-133.9
-131.903
-131.005
-130.100
-129.211
-128.314
-127.448
-126.510
-125.622
-124.724
-123.827
Max: 123.6 at Node 13470
Min: -136.0 at Node 0



Figure 9. Normal stresses (CFRP confined concrete cylinder)

LOAD CASE = 14
Increment 14 Load Factor = 30.0000
RESULTS FILE = 1
DISPLACEMENT
RESULTS CARTESIAN= 1
CONTOURS OF D_{zz}
-0.2091
-0.2554
-0.2497
-0.228
-0.2142
-0.2096
-0.1868
-0.1731
-0.1594
-0.1460
-0.1319
-0.1192
-0.1046
-0.09070
-0.07704
-0.06352
-0.04969
-0.03588
-0.02219
Max: 0.0000E+00 at Node 1
Min: -0.2091 at Node 2195



Figure 10. Longitudinal displacements (unconfined concrete cylinder)

LOAD CASE = 12
Increment 12 Load Factor = 130.0000
RESULTS FILE = 1
DISPLACEMENT
RESULTS CARTESIAN= 1
CONTOURS OF D_{zz}
-1.29187
-1.29562
-1.16117
-1.09892
-1.02047
-0.956116
-0.900765
-0.828416
-0.756005
-0.682716
-0.628585
-0.563016
-0.487665
-0.422316
-0.369805
-0.301616
-0.236205
-0.170016
-0.105665
Max: 0.0000E+00 at Node 1
Min: -1.292 at Node 2165



Figure 11. Longitudinal displacements (CFRP confined concrete cylinder)

LOAD CASE = 14
Increment 14 Load Factor = 30.0000
RESULTS FILE = 1
DISPLACEMENT
RESULTS CARTESIAN= 1
CONTOURS OF D_{rr}
0
0.5624E-3
1.125E-3
1.687E-3
2.25E-3
2.812E-3
3.374E-3
3.937E-3
4.499E-3
5.062E-3
5.624E-3
6.186E-3
6.748E-3
7.311E-3
7.874E-3
8.436E-3
8.999E-3
9.561E-3
0.01912
Max: 0.1103E-01 at Node 17159
Min: -0.2283E-17 at Node -803



Figure 12. Transversal displacements (unconfined concrete cylinder)

LOAD CASE = 12
Increment 12 Load Factor = 130.0000
RESULTS FILE = 1
DISPLACEMENT
RESULTS CARTESIAN= 1
CONTOURS OF D_{rr}
-0.567643E-3
-0.110182E-3
0.287277E-3
0.844738E-3
1.3222E-3
1.79966E-3
2.27712E-3
2.75467E-3
3.23203E-3
3.70949E-3
4.18925E-3
4.66941E-3
5.14187E-3
5.61933E-3
6.09979E-3
6.57425E-3
7.05171E-3
7.52917E-3
8.00653E-3
Max: 0.8747E-02 at Node 2516
Min: -0.8181E-03 at Node 12502

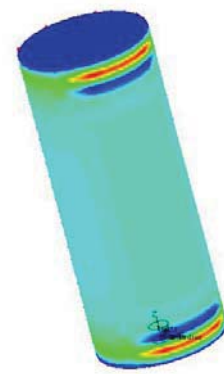


Figure 13. Transversal displacements (CFRP confined concrete cylinder)

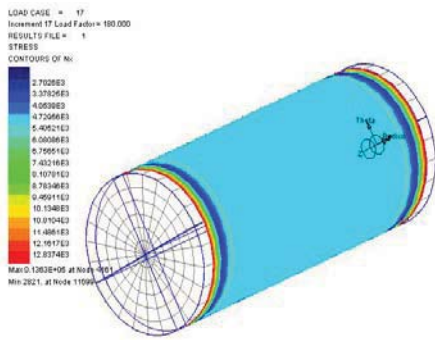


Figure 14. Longitudinal stress resultants in the CFRP jacket

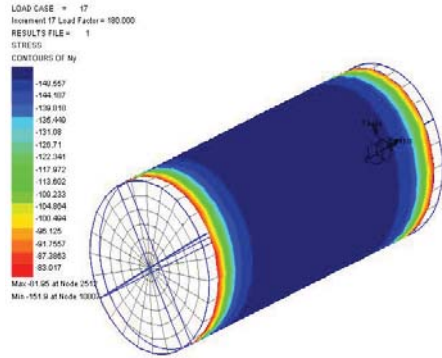


Figure 15. Transversal stress resultants in the CFRP jacket

Characteristic stress-strain curves for both confined and unconfined concrete were obtained; they are very similar to those obtained from the experimental analysis.

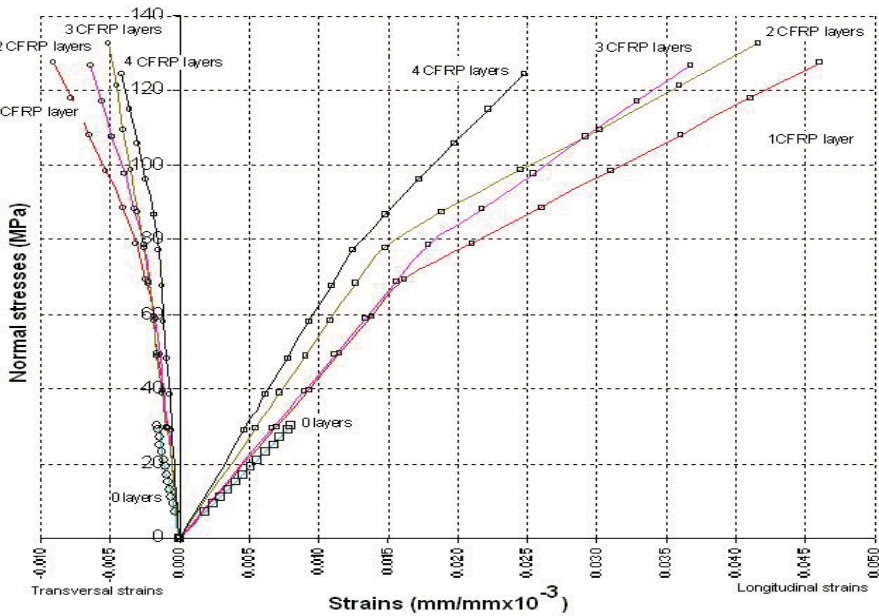


Figure 16. Stress-strain characteristic curves (CFRP confined / unconfined cylinder)

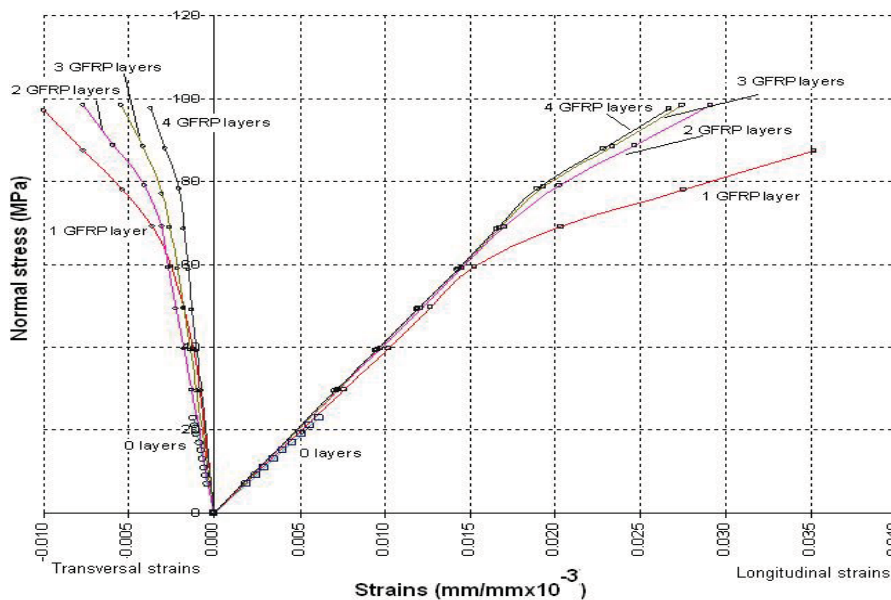


Figure 17. Stress-strain characteristic curves (GFRP confined / unconfined cylinder)

4. CONCLUSIONS

The use of FRP confinement significantly improves compressive strength and ductility of concrete. It should be noted that epoxy resins adhere well to the concrete surface, being also an excellent adhesive. Strengthening solutions with FRP used for reinforced concrete columns prove to be very good for several reasons. On the one hand, the strength and ductility values obtained are favourable and on the other hand, the weight of the consolidated system and the cost related to execution time and work are considerably reduced. Experience has shown that the failure modes of FRP are different and they depend on a series of factors which can influence the results obtained, such as: the characteristics of the concrete to be confined, casting moulds and vibration methods, fibre volume fraction, confinement techniques and accurate application by qualified workers.

References

1. Teng, J.G., Chen, J.F., Smith, S.T., Lam, L., *FRP strengthened RC structures*, John Wiley, Chicester, 2002.
2. Oprisan, G. *Soluții moderne de consolidare a structurilor pentru construcții industriale*, Teză de doctorat - U.T. Iasi, (2002). (in Romanian)

Rayleigh models coefficients

Florin Țepeș Onea

Universitatea “Ovidius” Constanța

Summary

The propose of this work is to study the effect of the superior vibration modes on the energy dissipation in the backlash between two plots of a idealized concrete dam.

The intern energy dissipation inside the structural material is generating material internal variations or hysterical damping. For viscous damping this energy is frequency balanced. The Rayleigh damping could be considered as a linear combination between structural masses matrix and stiffness matrix. The damping matrix is obtained from the Cauchy sequence:

$$C = M \sum_{k=0}^{p-1} a_k (M^{-1}K)^k \quad (1)$$

Where the coefficients a_k , $k=1,2..p$ are obtained from p simultaneous equations:

$$\xi_i = \frac{1}{2} \left(\frac{a_0}{\omega_i} + a_1 \omega_i + a_2 \omega_i^2 + \dots + a_{p-1} \omega_i^{2p-3} \right) \quad (2)$$

For $p=2$:

$$C = \alpha M + \beta K \quad (3)$$

Where α and β are constants that can be obtained from two dumping ratios of two different frequencies.

This study is made for an idealized symmetric concrete dam

It was used two calculus models for the dam-foundation ensemble; a plain one and spatial model, with simultaneous calculation.

KEYWORDS: Rayleigh, spatial mesh, excitation, dumping

1. STRUCTURAL ANALYSYS

The plane finite element mesh is made by 80 quadrilateral elements for the foundation and 56 elements for the dam. The elasticity modulus for the dam was pick $E_b = 300000 daN / cm^2$ and for the foundation $E_f = 150000 daN / cm^2$, with the dam's high of 30m and the slope $\lambda_1 = \lambda = 0,5$.

The dam is made by two plots 15m width each other separate for a backlash of 1mm. The two plots adjacent nodes, corresponding with the space, have the same quota on x and z axis. This nodes can be connected with the help of springs in order to model the friction.

We can notice that in the case of plane mesh the fundamental vibration mode is flexural on upstream-downstream, the second mode is flexural too but on the high of the dam, the others modes are of torsion.

For the spatial mesh the first vibration mode implies a symmetrical displacement and flexural on upstream- downstream direction of the two plots, and for the second mode a antisymmetrical displacement. To start with the 6's vibration mode it appear also a rotation of the two plots, imples a relative moving of the plots surfaces in the spae between them. The propose of this work is to study the effect of the superior vibration modes on the energy dissipation in the backlash between the two plots.

Because both masses and stiffness matrix are orthogonal, damping matrix is orthogonal too. From orthogonal condition we obtain:

$$\phi_i^T (\alpha M + \beta K) \phi_j = 2\omega \quad (4)$$

Where ϕ_i, ϕ_j are eigenvectors, ω_i is circular frequency, ξ_i fraction of critical dumping. The equation become:

$$\alpha + \beta\omega_i^2 = 2\omega_i\xi_i$$

For determine the α and β coefficients influence, it was made a parametric study for plane and spatial dam- foundation discrete mesh. Critical damp fraction was taken as constant $\xi = 0,05$ for whole vibration modes because of the fact that massive structure as a concrete dam is, it is possible to obtain, after the structure excitation (with a value lower that the seismic value), only the fraction of critical dumping corresponding to the first vibration mode.

The calculus was made in both cases of finite elements, for the first 10 vibration modes.

If we coupled $\omega_1 + \omega_i$ and solving the equation systems obtained result α and β coefficients. So for plane discrete mesh $\alpha = 1,44, \beta = 1,51E - 3$ for ω_1 and ω_3 and $\alpha = 1,97, \beta = 5,66E - 4$ for ω_1 and ω_{10} . We can observe that the effect of the mass matrix increase and the effect of stiffness matrix decrease in the same direction with the increase of the second frequency taken into account.

In spatial mesh case, the fundamental vibration mode is reduce $\omega_1 = 13,48rad/s$ and for the plane mesh $\omega_1 = 21.3rad/s$. This difference appears because in spatial mesh we take account of the torsion vibration modes also.

For the spatial mesh and for the frequency ω_1 and ω_3 $\alpha=0,893$ and $\beta = 2,5E - 3$ while if use the frequency ω_1 and ω_9 $\alpha = 1,063$ and $\beta = 1,56E - 3$.

In the case of spatial discrete mesh we can notice a mass matrix influence grow and a stiffness matrix influence diminution in the same time as the pulsation value grow. The variation of the α and β factors is much reduce when is use the spatial mash. For the spatial mash case we obtain a mean value $\alpha_{Ed} = 0,99$ and for the plane mesh $\alpha_{med} = 1.72$. All the results are presented in tables 3.1 and 3.2

Table 1 Plane mesh

Num.	Ω_i (rad/s)
1	21.3
2	38.59
3	44.43
4	79.44
5	87.59
6	96.43
7	109.0
8	118.8
9	121.3
10	155.1

$\omega_1 + \omega_i$	α	β
1+3	1,44	1,519E-3
1+5	1,71	9,17E-4
1+7	1,78	7,67E-4
1+10	1,97	5,66E-4

Table 2 Spatial mesh

Num.	ω_i
1	1
2	17,44
3	26,49
4	34,28
5	37,21
6	42,17
7	45,64
8	49,8
9	50,25

$\omega_1 + \omega_i$	α	β
1+3	0,893	2,5E-3
1+5	0,989	1,97E-3
1+7	1,041	1,689E-3
1+9	1,063	1,567E-3

The calculus was resumed for a critical dump fraction 8% in witch case we obtain for spatial mash and the pears ω_1 and ω_9 the following results $\alpha=1.69$ and $\beta=2.51E-3$, results with no big difference compare with the case of critical dump fraction of 5%.

It is obvious that only for a spatial discrete mash the obtained results are close to reality. The influence of superior modes use in the case of spatial mash have no significant effect on the α and β coefficients as it presented in table 2.

It is noticed that in the same time with the increase of the frequency the mass matrix effect increase to and also the stiffness matrix effect decrease.

So, we can say that the stiffness matrix effect connected with frequency is major.

After coefficients calculus, it was analyzed the dam response at the same excitation with and without damping matrix effect. It was followed the effect of using vibration modes 1-3, 1-5,1-7,1-10 in mass end stiffness matrix coefficients on the stress and displacement response. In the table 3,4,5,6 are presented stress and displacement values for different coefficient pairs α and β , for plane and spatial mesh.

1.1 Plane mesh-displacements compare

(nods was select on a vertical for the coping of the weir to the foundation of the dam)

Table 3

Node	Without damping	$\omega_1 + \omega_3$	$\omega_1 + \omega_5$	$\omega_1 + \omega_7$	$\omega_1 + \omega_{10}$
161	0.728E-2	0.4200E-2	0.4184E-2	0.4178E-2	0.4104E-2
152	0.6079E-2	0.3508E-2	0.3495E-2	0.3490E-2	0.3429E-2
143	0.4149E-2	0.2407E-2	0.2399E-2	0.2396E-2	0.2876E-2
124	0.3706E-2	0.2154E-2	0.2147E-2	0.2144E-2	0.2107E-2
94	0.2404E-2	0.1406E-2	0.1401E-2	0.1399E-2	0.1375E-2

1.2 Plane mesh-stress compare (stress are presented in upstream-downstream points)

Table 4

	Without damping	$\omega_1 + \omega_3$	$\omega_1 + \omega_5$	$\omega_1 + \omega_7$	$\omega_1 + \omega_{10}$
$\sigma(-)$ daN/cm ²	-18.2	-10.93	-10.92	-10.91	-10.75
$\sigma(+)$ daN/cm ²	14.9	7.57	7.54	7.53	7.37

1.3 Spatial mesh-displacements compare (nods was select on a vertical for the coping o the weir to the foundation of the dam)

Table 5

	Without damping	$\omega_1 + \omega_3$	$\omega_1 + \omega_5$	$\omega_1 + \omega_7$	$\omega_1 + \omega_{10}$
161	0.433E-2	0.3319E-2	0.3326E-2	0.3325E-2	0.3326E-2
152	0.3646E-2	0.2778E-2	0.2783E-2	0.2786E-2	0.278E-2
143	0.3096E-2	0.2352E-2	0.2357E-2	0.236E-2	0.236E-2
124	0.2328E-2	0.1764E-2	0.1769E-2	0.1771E-2	0.1773E-2
94	0.1593E-2	0.1205E-2	0.1209E-2	0.1212E-2	0.1213E-2

1.4 Spatial mesh – stress compare (stress are presented in upstream – downstream points)

Table 6

	Without damping	$\omega_1 + \omega_3$	$\omega_1 + \omega_5$	$\omega_1 + \omega_7$	$\omega_1 + \omega_{10}$
$\sigma(-)$ daN/cm ²	-12.03	-9.2	-9.2	-9.2	-9.2
$\sigma(+)$ daN/cm ²	7.16	5.2	5.2	5.2	5.2

It is presented in the table 7 displacement comparative values for the spatial mesh for two critical dumping ratios of 5% and 8%.

Table 7

	5% Rayleigh	8% Rayleigh	Diference %
323	-0.3878E-3 -0.8799E-2 -0.2340E-2	-0.3623E-3 -0.7545E-2 -0.2272E-2	-6.57 -14.25 -2.9
314	-0.2895E-3 -0.7398E-2 -0.2276E-2	-0.2678E-3 -0.6348E-2 -0.2210E-2	-7.49 -14.19 -2.89
299	-0.1890E-3 -0.5644E-2 -0.2144E-2	-0.1738E-3 -0.4849E-2 -0.2082E-2	-8.04 -14.08 -2.89
278	0.1383E-3 -0.4047E-2 -0.1965E-2	0.1354E-3 -0.3480E-2 -0.191E-2	-2.09 -14.01 -2.79
256	0.1032E-3 -0.2943E-2 -0.1779E-2	0.1024E-3 -0.2529E-2 -0.1731E-2	-0.77 -14.06 -2.69

The displacement comparative graphics are presented in figures 1 and 2 and the stress calculus points in figure 3.

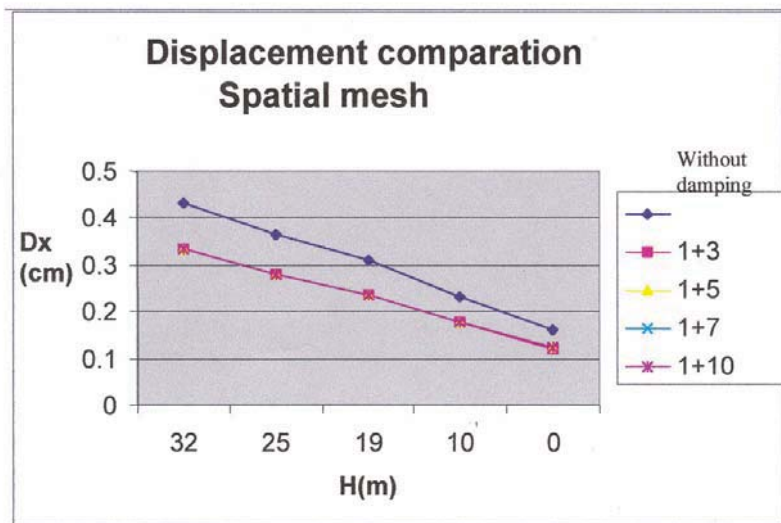


Figure 1 Displacement comparison for spatial mesh

It is also notice that as well as for plane and spatial discrete mash, if damping matrix is used, the stress and efforts values are almost similar for all the coefficient pairs α and β used. It was also noticed that for Rayleigh models use, only the first 3 vibration modes are required.

Major response differences of 14% are obtained only between 2 critical dams of 2% and 8%.

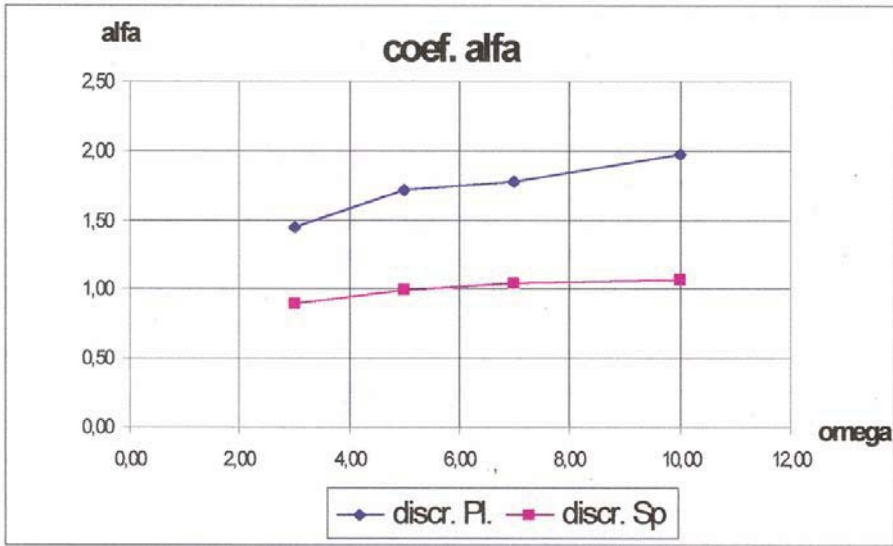


Figure 2 $\alpha(\omega)$ for plane mesh and spatial mesh

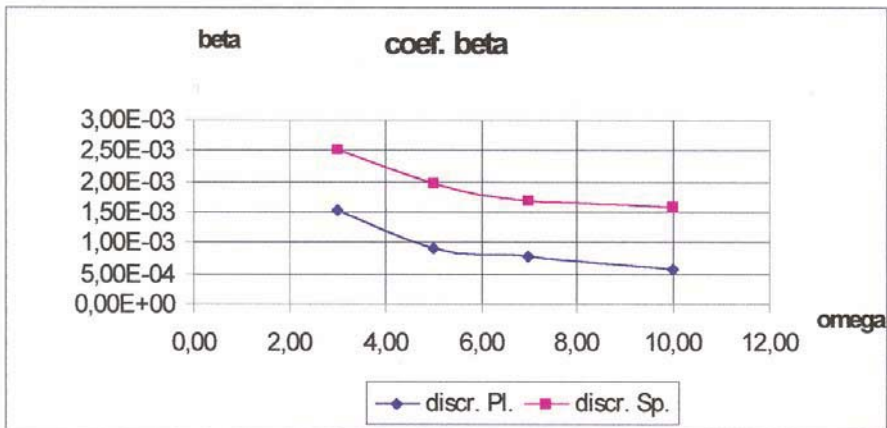


Figure 3 $\beta(\omega)$ for plane mesh and spatial mesh

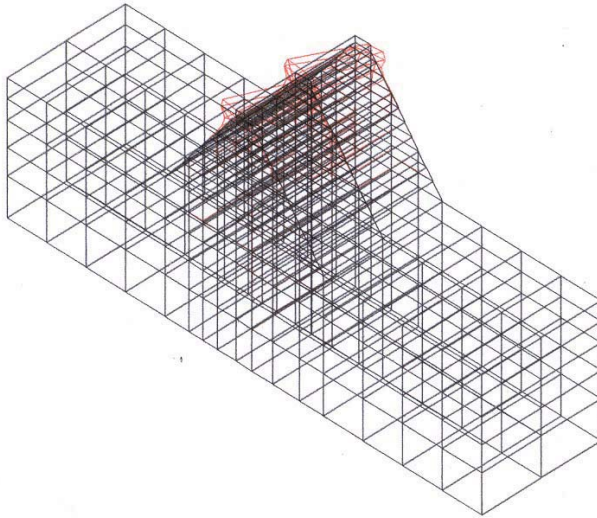


Figure 4 Modal analyze. Spatial mesh for a concrete dam. The six vibration mode
Freq=42.17rad/s; T=0.149s

References

1. Clough. R.W., Penzien J., Dynamics of Structures, New York: McGraw-Hill Book Co.1975
2. Bathe. K.J. and Wilson, E.L. Numerical Methods in Finite Element Analysis. Englewood Cliffs, N.J.: Prentice-Hall,Inc.,1976
3. D.Stematiu, Calculul structurilor hidrotehnice prin metoda elementelor finite, Editura Tehnică București, 1988. (in Romanian)

NDT Devices as Long-Term Vision in Assessing of Old Masonry Buildings by Probabilistic Approach

Magda Broșteanu¹ and Teodor Broșteanu²

¹CCI Department, Faculty of Civil Engineering, Technical University of Iasi, Romania

²CFDP Department, Faculty of Civil Engineering, Technical University of Iasi, Romania

Summary

Assessment and retrofitting of existing buildings made by masonry structure represent a huge engineering challenge as a distinct problem versus the design of a new building. Structural Strengthening and Thermal Renovation have to be applied at the same time.

This article refers to Two Non-Destructive Testing Devices in Diagnostic and Assessing under realistic conditions of Old Masonry Buildings evaluated to the real performance. It focuses on flat-jacks technique to determine the state of stress in masonry, and on monitoring of buildings health using IR thermal-graphic method. Minimum Equipment for Compressive Strength Qualifying Test on Masonry Large Specimen, and Minimum Equipment for Infrared Thermal-Graphic Test in Quality Control of Thermal Insulation are presented.

The results deal with the Masonry Strengths of walls and columns for the computation of Nominal Assurance Degree of Seismic Action of the existing masonry dwellings and monumental buildings according to the Strengthening Structural Design for Compressing Loading and Lateral Loading of damaged buildings.

Other results deal with the Surface Temperature Distribution and Moisture Content in Visible and Infrared Images for Quality Control of Thermal Insulation according to the Thermal Renovation Design for Heat Losses and Yearly Thermal Balance of damaged buildings.

The measured values are random variables. The characteristic values of random variables as fractiles for a given probability will be computed using the Probabilistic Approach.

KEYWORDS: monitoring, non-destructive testing (NDT), flat-jacks technique, infrared thermal-graphics, masonry characteristic compressive strength, surface temperature, random variables, input data in strengthening design.

1. INTRODUCTION

Many masonry structures were built over long periods of time using different technologies and materials. There are hidden damages out of a professional control. There are dwellings and monumental buildings made by masonry structure, placed on seismic hazard zone that need to be retrofitted at new performance levels.

The Romanian law L10:1995 concerning the quality in constructions defines one main component from 11 ones of quality system such as serviceability behavior and remedies during the life span of buildings.

Investor and/or owner or users have to be able to define correctly the users' requirements on custom mode offer and contract form of technical project for assessment or retrofitting.

Structural Safety (strength and stability) and Thermal Protection (thermal insulation and moisture protection for heat energy saving) are two essential performance requirements of buildings. Assessment and retrofitting of existing buildings made by masonry structure represent a huge engineering challenge as a distinct problem versus a new building design. Framing of damages into potential risk degrees has a cultural, social and economic impact.

Structural Strengthening and Thermal Renovation have to be applied at the same time.

The existing buildings are big consumers of energy. The volume of existing buildings is so big and it contains many masonry buildings that need an upgrading of the insulating by thermal retrofitting that means no interstitial condensation risk and no surface dew point temperature. There are almost 8.0 million of dwellings as 2.8-rooms conventional apartments with an amount of fuel required for one season's heating of 10.4-21.5 mil tones conventional fuel per year. By summing-up almost 20% for other buildings, the Romanian annual energy consumption for the heating of buildings is between 12.5-25.8 mil tones conventional fuel per year.

There are damaged old buildings placed on seismic hazard zones. Local remedies were been applied from economic reasons. Few local inventories were been performed with modest results. The existing buildings with classified damages need an upgrading of cross walls structure in order to reduce the seismic risk for users' safe.

No general rules are expected. Case-studies will be performed. Few official inventory and preliminary decisions of alternative spaces of living or working about were been performed. This is a worried factor.

There will be a sustainable activity to restore old buildings and monuments, not matter where. The trends in building costs in Germany (7) for new buildings and existing buildings are presented in the Fig.1.

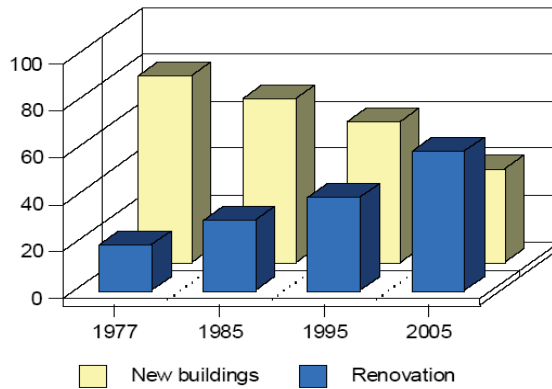


Fig.1. Trends in building costs in Germany

This article refers to the non-destructive testing device in assessing of old masonry buildings which were originally built over a long time ago, and it focuses on flat-jacks technique to determine the state of stress in masonry, and on health monitoring using IR thermal-graphic method, as input data for strengthening structural design of masonry members in compression, and thermal renovation design.

2. DIAGNOSTIC SURVEYS

Diagnostic strategy is presented in the Fig.2. Keywords of diagnostic strategy using the probabilistic approach are the followings: sources of risk, damages, weak points, indicators, probability of failure, limit states, monitoring, early damages survey, random variables, input re-design data, costs etc.

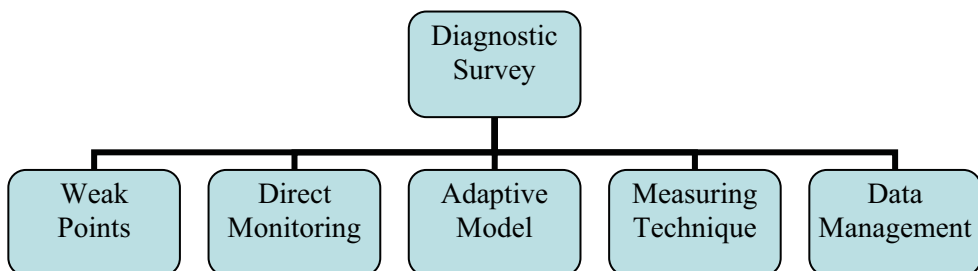


Fig.2. Diagnostic Strategy

Preliminary surveys focus on:

- (i) geometric survey using topographic method and photogram-metric technique to identify the geometry of building;
- (ii) crack-detection using piezoelectric arrays to identify static pattern and probable causes of instability.

Final aim of preliminary surveys of the overall pattern of cracks is the framing of existing buildings with classified damages into 4 potential classes of seismic risk **RS** /5/. **RS1** means a high risk of collapse. **RS2** means a low probability of collapse but there are major damages of bearing elements. **RS3** means that the damages of bearing elements do not disturb the structural safety but there are major damages of nonbearing elements. **RS4** means that the expected seismic answer of the existing building and the designed seismic answer for a new building are the same.

Note that should be kept in mind the influence factors of quantifying: the design seismic zone, the structural pattern on height, the aseismic conformity of structure, the nominal assurance degree to seismic action, the probable nature of collapse of bearing elements (either a ductile nature, a semi-ductile one or a breakable one), the reinforcement details, the building importance factor, the building life span, and the building inventory.

Diagnostic surveys focus on:

- (iii) coring survey using coring and sampling technique to provide specimens for material testing;
- (iv) X-ray survey inside the boreholes using a rotating micro-camera to provide 3-D image of wall;
- (v) non-destructive testing using flat-jacks technique (6) to determine the state of stress in masonry realistic specimen, and the strengths of masonry: the f_k compressive strength, the f_{vk} shear strength, and the f_{xk} tensile strength in bending, and the f_{vk} shear strength of mortar layer;
- (vi) sonic testing using an ultrasonic pulse excitation through, to perform a detailed survey of sound velocity distribution over;
- (vii) radar-screen survey using high frequency electro-magnetic waves to investigate the interfaces between material layers having different dielectric constants;
- (viii) health monitoring using fiber optical sensors and IR thermal-graphics for data capture to control any change in behavior, such as temperature distribution, moisture distribution, strains in all directions, relative movements, inclination etc;
- (ix) material-destructive testing on coring samples using axial compression and other tests to assess the masonry strengths, and the degree of physical-chemical damages.

The calibration is a very important step.

3. FLAT-JACKS TECHNIQUE

Characteristic values of the compressive strength for the computational design purpose of new masonry structures are only regulated by design codes. Hence, the behavior of old masonry structures in compression has to be investigated to provide strength values.

Flat-jacks technique is a non-destructive testing method for quantification of phenomenon with regard to the state of stress in masonry.

Minimum Equipment for Compressive Strength Qualifying Test on Masonry Large Specimen consists of:

Loading Devices: Electric Drill, Core Drill, Hydraulic Pump, Hydraulic Flat-Jacks, Hydraulic Presses, Service Gauges, and Flexible Hose;

Recorder and Dataloggers: Data Acquisition Board, Inductance Strain Gauges Transducers, Wheastone Bridge Circuit, Graphic Recorder (Printer), Deformeters (Comparing Devices), Micrometers, Dilatometers, Sonic Detector, and Software.

Testing Method consists of: Stress-Strain Analysis of Large Specimen in Compression, Modulus of Elasticity, Shear and Dilatometer Tests on Masonry Sample Area, Diagnostic Surveys, Sonic Surveys, Structural Monitoring, and Structural Strengthening.



Fig.3. Flat-Jacks Compressive Starter Kit

Flat-Jacks Compressive Starter Kit is shown in the Fig.3. It contains: 5 flat-jacks, 10,000 psi capacity hydraulic hand pump, 1,000 psi test quality pressure gauge, 2,...,6 feet hydraulic hoses with quick connect fitting, removable extensometer of 0.0001 inch resolution, inch reference bar, marking gauge, 100 extensometer gauge points, rugged field case, where $1 \text{ psi}=10^{-3} \text{ ksi}=10^{-3} \text{ kip.sqin}^{-1}=0.006895 \text{ MPa}=0.006895 \text{ N.mm}^{-2}$, $1 \text{ in}=25.4 \text{ mm}$, $1 \text{ ft}=12 \text{ in}=0.3048 \text{ m}$.



Fig.4. Flat-Jacks Shear Starter Kit

Flat-Jacks Shear Starter Kit is shown in the Fig.4. It contains: 10,000 psi capacity hydraulic hand pump, 10,000 psi test quality pressure gauge, 5,000 psi test quality pressure gauge, 10 feet hydraulic hose, 10 tones capacity hydraulic ram with tilt saddle, 2-3.5 inch x 2.0 inch x 0.5 inch hardened steel bearing plates, 2 inch Φ x 1.4 inch cylindrical aluminium spacer, 2 inch Φ x 4.0 inch cylindrical aluminium spacer, rugged field case.



Fig.5. Survey to perform flat-jacks test

The survey using flat-jacks technique carried out without scaffolding is presented in the Fig.5.

Masonry sample will be marked by two horizontal cuts into which two flat jacks will be inserted and it will be subjected to an axial compression. The pressure of flat-jacks will be increased up to the re-establishment of the initial degree of deformation. It is possible to find the masonry compressive strength f_k in

MPa=N.mm⁻² by increasing of compression load until the first vertical crack will arise in the brick (1), (2), (3) because the lateral strain of mortar will only meet the effect of adhesion and friction between bricks and mortar.

Masonry sample will be marked by two vertical cuts, a brick will be removed out, and two small horizontal-acting hydraulic flat jacks will be inserted. It is possible to find either the shear strength of mortar layer f_{vk} or the friction angle between bricks and mortar by modifying the vertical and horizontal stresses.

Masonry strengths are random variables. By the probabilistic approach (9), the characteristic value of a material strength is the probability $p=0.05$ of lower values than this. The fractiles x_p will be computed as follows:

$$x_p = m_x \pm k\sigma_x \quad (1)$$

where,

m_x is the mean of random variables;

k is the factor or standard deviation number depending on the p probability and the type of distribution;

σ_x is standard deviation.

From the field data arranged into an increasing row, data selection, graphic probability distribution such as histogram and frequency polygon, on recommends Henry's line for checking of the theory-testing concordance, and the elimination of the absurd results. If the mean line that rectifies the plotted line is very close by the middle field points, it will be a concordance between the measured values distribution and the theoretical distribution. A few values will be rejected, and a few values will be kept.

The intersection of Henry's line with the abscissa is m_x point. The intersection of Henry's line with the 16% line is the a angle between Henry's line and the ordinate, where σ_x is tangent of a . The intersection between Henry's line with the 5% line means the x_p fractile.

Mean value with relative frequency named first moment or math hope and the variance named central second moment are computed using locating and spreading of statistical evaluation from Table 1 and Table 2, using Eq.2 and Eq.3.

Fractile is computed using Eq.1 for 0.05 probability of lower value than x_p .

Table 1. Data selection

Intervals	Central Value	Absolute Frequency	Relative frequency	Sum	Diagram of events on interval	
R	N.mm ⁻²	N _i	f _i =n _i /n	Σn _i	Σf _i %	N _i
1.46-1.50	1.48	6	0.1111	6	11	x x x x x x
1.51-1.55	1.53	8	0.1482	14	26	x x x x x x x x
1.56-1.60	1.58	9	0.1666	23	43	x x x x x x x x x
1.61-1.65	1.63	12	0.2222	35	65	x x x x x x x x x x x x
1.66-1.70	1.68	8	0.1482	43	80	x x x x x x x x
1.71-1.75	1.73	6	0.1111	49	91	x x x x x x
1.76-1.80	1.78	5	0.0926	54	100	x x x x x
7	1.63	54	1.0000	54	100	5 10

Table 2. Mean and standard deviation computation

Central value	Relative frequency	Multiplication	Central deviation	Variance
X _i	F _i =n _i /n	f _i X _i	A _i = X _i - m _x	σ ² = f _i (X _i - m _x) ²
1.48	0.1111	0.1644	-0.1424	0.0022
1.53	0.1482	0.2267	-0.0924	0.0012
1.58	0.1666	0.2632	-0.0424	0.0002
1.63	0.2222	0.3621	0.0076	0.0001
1.68	0.1482	0.2489	0.0576	0.0005
1.73	0.1111	0.1922	0.1076	0.0013
1.78	0.0926	0.1648	0.1576	0.0023
1.63	1.0000	1.6224		0.0078

$$m_x = \sum_1^8 f_i X_i = 1.6224 \tag{2}$$

$$\sigma_x = \sqrt{\sum f_i (X_i - m_x)^2} = 0.0883 \tag{3}$$

The characteristic compressive strength of masonry large specimen **f_k** computed as fractile of 1.4771 MPa:

$$x_p = 1.6224 - (1.645)(0.0883)=1.4771 \tag{4}$$

4. IR THERMAL-GRAPHICS

The key feature to reduce the amount of heat losses through the building envelope to a very low value is a very high standard of thermal insulation. Hence, the thermal behavior of masonry envelopes has to be investigated to provide thermal resistance **R**-values and thermal transmittance **U**-values (4).

Lock in thermal-graphics is a picture-based method for visualization and quantification of phenomenon with regard to the heat transfer.

The thermal energy caught by the IR camera from an object is focused by the radiation detector and the electronic system converts the electrical signal produced by detector into a video signal on monitor screen.

The total energy emitted by a body's surface is defined by Eq.5:

$$E_T = \int_{\lambda=0}^{\infty} \epsilon_{\lambda} E_{\lambda} d\lambda = \epsilon_T \sigma T^4 \quad (5)$$

where,

E_T is the total radiation energy emitted with the wavelength λ at T temperature;

ϵ_{λ} is the body's emissive power for the radiation with the wavelength λ ;

E_{λ} is the radiation energy emitted with the wavelength λ ;

ϵ_T is the body's emissive power for the radiation with the whole wavelength spectrum;

$\sigma = 5.672 \cdot 10^{-8} \text{ W} \cdot \text{m}^{-2} \cdot \text{K}^{-4}$ is Stefan Boltzmann's constant.

Minimum Equipment for Infrared Thermal-Graphic Test in Thermal Insulation Quality Control consists of: Thermocouples Meters and Probes, Equipment for Recording, Stocking, and Processing, Thermal CAM P-Series (professional infrared camera), and Thermal CAM Connect Software.

Testing Method consists of: Data Acquisition of Temperature, Temperature Control, and Thermal Imaging System.

IR equipment can catch the body's thermal image in real time using a receiving and recording system (IR camera), and a processing system of the thermal images (computer and software). IR camera consists of a scanning system, an infrared radiation detector, an electronic system, and a microprocessor.

Working parameters are as follows: temperature range from -20°C till 500°C with the sensibility increment of 0.1°C , working autonomy of 3 hours, and operation temperature from -15°C till 45°C . The calibration between the surface emissive power and the surface temperature is given.

A few results are presented (11). In the Fig.6, the visible image and IR image with cold bridges zones are presented. In the Fig. 7, the earth moisture infiltration at the building ground floor level (12) is presented. In the Fig.8, temperature values on a window with the layering effect are presented as screened results.

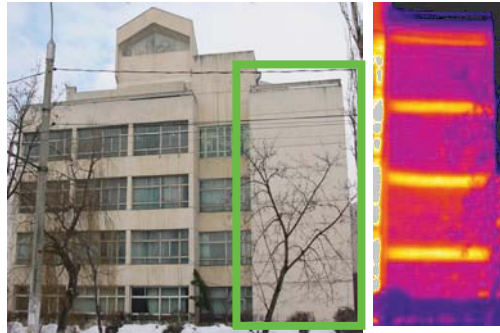


Fig.6. Visible and infrared images with defects due to the cold bridges

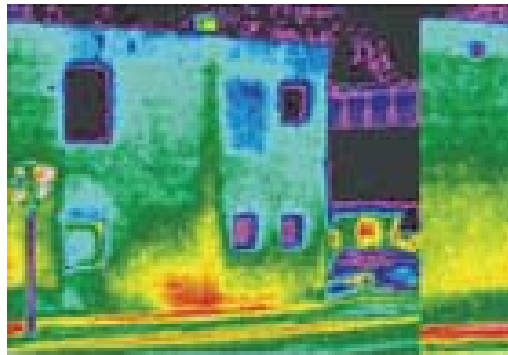


Fig.7. Infrared image of the earth infiltration tracing

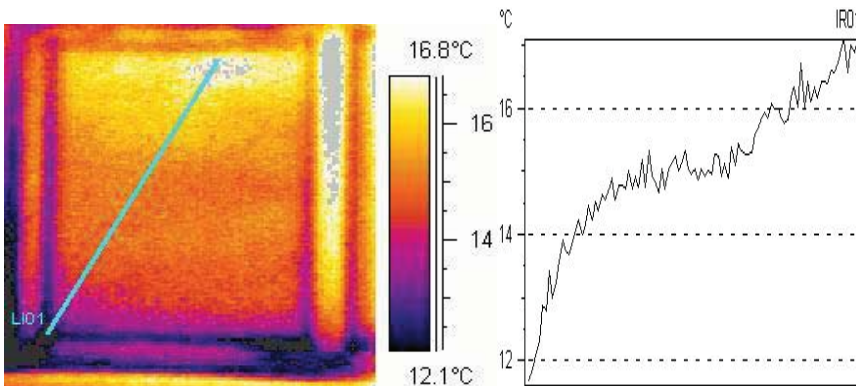


Fig.8. Screened results of temperature distribution

5. CONCLUSIONS

There will be a sustainable activity to restore old buildings and monuments, not matter where it will be. In Germany, trends in building costs for new and existing buildings confirm this.

Assessment and retrofitting of existing buildings made by masonry structure represent a huge engineering challenge as a distinct problem versus a new building design.

Inspection techniques via monitoring and parallel testing i.e. the diagnostic surveys under realistic conditions are presented.

Flat-jacks technique as a non-destructive testing method is suggested for input data capture of masonry strengths in strengthening design of damaged old buildings. Note that for high buildings, few experts have to be rock-climbers.

Lock in thermal-graphics as a picture-based method for visualization and quantification of phenomenon with regard to the heat transfer, but not only is suggested for input data capture of masonry thermal resistance in thermal renovation design of damaged old buildings. It is attractive. IR thermal-graphics is an important instrument to stimulate the interest concerning the quality of works. The right decision is taking the best insulation available. Note that for high buildings, few experts have to be rock-climbers, too.

Lock in acoustics and thermal-graphics is suggested for research.

On recommends the equivalent rigid frame pattern for simplified structural design (10), and for the best approximation to the specimen experimental behavior (8), and for actual brick shear walls structure, as well.

The equivalent rigid frame consists of columns with the same features as posts, and slabs with the same features as lintels. The frame columns will substitute the posts spanning between posts centre lines. The slabs will substitute the lintels on the entire span of columns centre lines.

References

- 1 xxx The EC 6-1-3:1996 *“Design of Masonry Structure-General Rules for Buildings-Rules for Reinforced Masonry”*.
- 2 xxx CR 6:2006 *Codul de proiectare pentru structuri din zidarie*.
- 3 xxx The EN 1052-3:1996 *“Methods of tests for masonry”*.
- 4 xxx SR EN ISO 13790:2005:2004 *Evaluarea performantei termice a cladirilor*.
- 5 xxx P 100:2006:2004 *Codul de proiectare seismica cap. 1”Prevederi de proiectare pentru cladiri”, cap.3 “Prevederi pentru evaluarea si proiectarea consolidarii constructiilor vulnerabile seismic, cap.8 “Prevederi pentru proiectarea consolidarii monumentelor istorice si a constructiilor cu valoare arhitecturala”*.

- 6 xxx The former ISMES spa “*Building and Monument Restoration-Surveys and Control*”, Bergamo, Italy, 1996.
- 7 xxx Collaborative Research Center SFB 477, founded by the German Science Foundation (DFG), “*Life Cycle Assessment of Structures via Innovative Monitoring*”, University Carola-Wilhelmina-Braunschweig, Germany, <http://www.sfb477.tu-bs.de>
- 8 Hendry, A.W., Sinha, B.P., Davies, S.R. -*Design of Masonry Structures*, Third edition of Load Bearing Brickwork Design, E& FN Spon Publishing House, An Imprint of Chapman & Hall, London, Weinheim, New York, Tokyo, Melbourne, Madras, 1997, ISBN0 419-21560-3.
- 9 Brosteanu, M. -*Constructions. Philosophy of Design*, The first edition. Cerni Publishing House, Iasi, 1998, ISBN973-9378-13-7.
- 10 Brosteanu, M., Brosteanu, T. -*Selection of theoretical method for lateral load analysis of brick shear walls structures*, In the Proceedings of International Symposium “Computational Civil Engineering”, “Matei-Teiu Botez” Academic Society Publishing House, Iasi, May 26, 2006, ISBN(10)973-7962-89-3, ISBN(13)978-973-7962-89-8.
- 11 Avram, C. -*Investigatii IR pentru controlul calitatii protectiei termice*, Satisfacerea exigentelor de izolare termica si conservare a energiei in constructii, “Matei-Teiu Botez” Academic Society Publishing House, Iasi, 2003, ISBN973-85882-7-8.
- 12 xxx The former <http://www.agma.com>; <http://www.flir.com>.

IT Approach in Heat Transmission Visualizing through Opaque Walls

Magda Brosteanu¹ and Teodor Brosteanu²

¹CCI Department, Faculty of Civil Engineering, Technical University of Iasi, Romania

²CFDP Department, Faculty of Civil Engineering, Technical University of Iasi, Romania

Summary

This article refers to the 2-D thermal field computation in the steady-state conditions for thermal design of the building envelope. A procedure to analyze the heat transfer through the opaque wall is provided. The results are as follows: Heat Flow Image and Density, Surface Temperature Distribution, and Isothermal Lines. Computing programs are very useful instruments in the designing of adjustment to R-value and in the solving of problems.

KEYWORDS: building, envelope, opaque wall, heat transfer, steady-state conditions, computational analysis, surface temperature visualizing.

1. INTRODUCTION

The Romanian standard SR EN 10211-2:2001 /1/ is identical to the European Standard EN ISO 10211-2:2001-Thermal bridges in construction-Calculation of heat flows and surface temperatures-Part2: Linear thermal bridges.

Solving problems by 2-D analysis has required using the dedicated software and computer aided design systems.

2. THERMAL FIELD

The thermal field represents all temperatures $\theta(x, y, z, \tau)$ -values, where x, y, z are the spatial co-ordinates of the point and τ is the time.

The thermal field is computed from the Laplace's Eq., as follows:

$$\lambda \Delta \theta = c \rho \frac{\partial \theta}{\partial \tau} + I \quad (1)$$

where,

- λ is the thermal conductivity of the material, in $\text{W.m}^{-1}.\text{K}^{-1}$;
- \mathbf{c} is the heat capacity of the material, in $\text{J. kg}^{-1}.\text{K}^{-1}$;
- ρ is the density of the material, in kg.m^{-3} ;
- \mathbf{I} is the source of heat, in W.m^{-3} .

There are many heat transfer problems from which **2-D** problem in steady-state conditions is the most useful formula for $\theta(\mathbf{x}, \mathbf{y})$ -values computation by the Numerical and Computational Techniques:

- in steady-state conditions $\tau=0$, and in transient ones $\tau \neq 0$;
- in linear conditions with $\lambda, \mathbf{c}, \rho = \text{constants}$, and non-linear ones with $\lambda(\theta), \mathbf{c}(\theta), \rho(\theta)$;
- 1-D** problem of $\theta(\mathbf{x})$, **2-D** problem of $\theta(\mathbf{x}, \mathbf{y})$, and **3-D** problem of $\theta(\mathbf{x}, \mathbf{y}, \mathbf{z})$.

3. MATHEMATICAL MODEL

By the Finite Difference Method or Finite Element Method, the Differential Equations with second partial derivative of θ with respect to dx^2 squared at constants (m, n) have to be changed into a system of Algebraical Linear Equations using difference operators or finite operators:

$$\lambda \frac{\partial^2 \theta}{\partial x^2} + \lambda \frac{\partial^2 \theta}{\partial y^2} = 0 \tag{2}$$

The digitization after \mathbf{x} and \mathbf{y} in elementary layers supposes the nodes disposal at the borders, at intermediary surfaces between different materials, and in the same material. The differential operators could be approximated with the help of two levels schemes resulted from $\theta(\mathbf{x}, \mathbf{y})$ development in the Taylor’s series around the node with (m, n) co-ordinates.

Finally, the formulae have resulted by the imposed, uniqueness conditions, initial and at the limits ones:

the 1st case condition (Dirichlet’s one) in steady-state conditions has indicated that the inside air temperature θ_i and the outside air temperature θ_e are fixed;

the 2nd case condition (Newman’s one) has indicated the occurrence of a continuous density of heat flow \mathbf{q}_s at the boundaries, i.e. we have to consider many nodes up to the breadth of the influence zone \mathbf{l}_p of the cold bridge limited by the normal heat flow on both surfaces of the element:

$$\mathbf{q}_s = \frac{\Delta\theta}{R} \quad (3)$$

the 3rd case condition (Fourier's one) has indicated the heat transfer on the internal surface and external surface of the element:

$$\alpha_i(\theta_i - \theta_{si}) = \lambda \frac{\theta_{si} - \theta_2}{\Delta y} \quad \text{and} \quad \lambda \frac{\theta_3 - \theta_{se}}{\Delta y} = \alpha_e(\theta_{se} - \theta_e) \quad (4)$$

the 4th case condition has indicated the heat transfer between different materials deduced from the conservation Eq.:

$$\sum \mathbf{q} = 0 \quad (5)$$

4. HANDLING THE PROGRAM

There are thermal bridges as parts or portions of a built element, given by the technological or structural reasons, in which the insulating material is completely absent, i.e. **the insulation is bridged**.

The heat flow increases across the thermal bridges and the inside surface becomes cooler, giving the reason of **“the cold bridge term”**. There is also an increased risk of condensation.

Sometimes, it is necessary to calculate the thickness of **the additional insulating material** in order to produce the same specified R_0 -value as in the current section. The best position of thermal insulating material is at the outside surface of building element.

Thermal resistance of the envelope R_0 in $m^2 \cdot K \cdot W^{-1}$ can be found from the Eq. as:

$$R_0 = R_i + R + R_e \quad (6)$$

All details selected can be developed for the claimed input data.

The results of computational approach are as follows:

- the image of heat flow;
- the density of heat flow \mathbf{q}_s , in $W \cdot m^{-2}$;
- the distribution of the outer surface temperature, $\theta_{es}(\mathbf{x}, \mathbf{y})$ in $^{\circ}C$;
- the distribution of the inside surface temperature $\theta_{is}(\mathbf{x}, \mathbf{y})$, in $^{\circ}C$;
- the isothermal lines $\theta(\mathbf{x}, \mathbf{y}) = \text{constant}$;
- the zones of almost constant temperatures;
- the lines of almost constant densities of heat flow;
- the zones of almost constant densities of heat flow.

Considering a case-study /2/ of a building outer wall joint subjected to 2-D heat flow through, in the winter time conditions, for a masonry wall with a cold bridge due to a concrete column with and without adjustment at the outside surface using an EPS layer, the results are shown in the Fig. below. Wall structure thermal properties and indoor-outdoor surface resistances are taken, and the temperatures remain steady.

Wall Joint Digitization is presented in the Fig. 1.

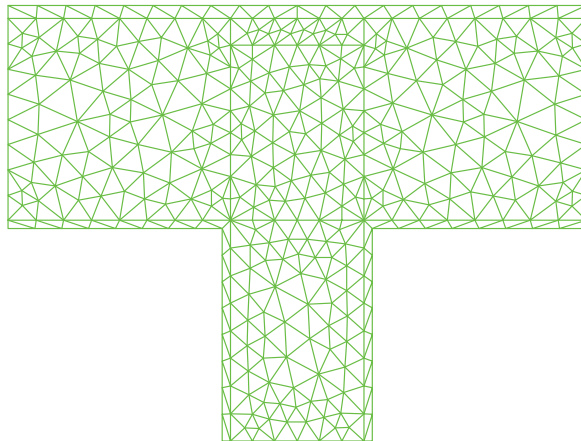


Fig.1. Wall Joint Digitization

The image of lines of conductive heat flow through the outer wall after the thermal adjustment is presented in the Fig.2. There is a non-uniform heat flow through because of the effect of lateral heat flow is significant.

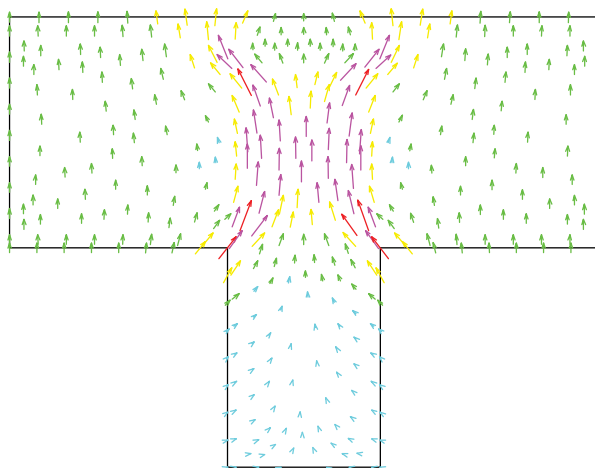


Fig.2. Image of Heat Flow through

The distribution of heat flow density and surface temperature on a wall joint with and without adjustment of R_0 -value is compared in the Fig. 3, 4, 5, 6, 7, and 8.

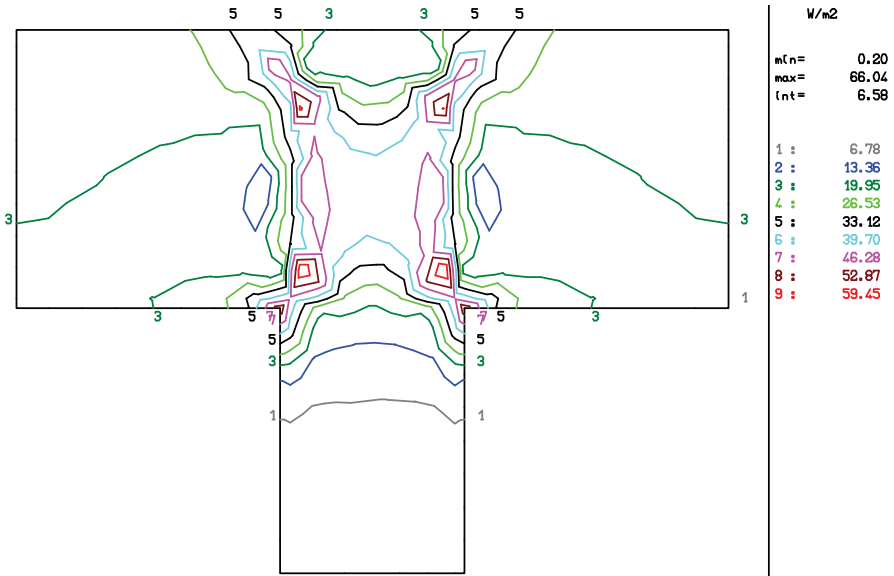


Fig.3. Variation of the Density of Heat Flow after the Adjustment

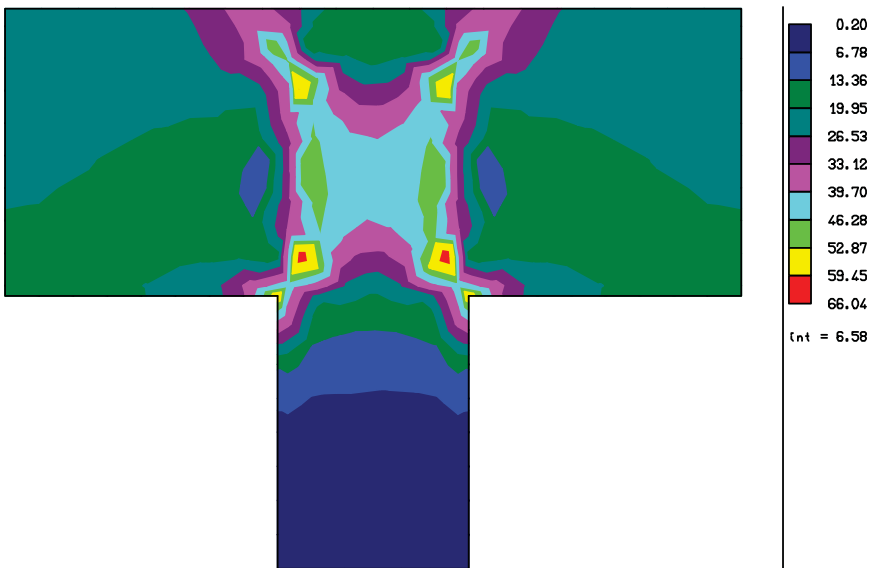


Fig.4. Zones of almost Constant Densities of Heat Flow after the Adjustment

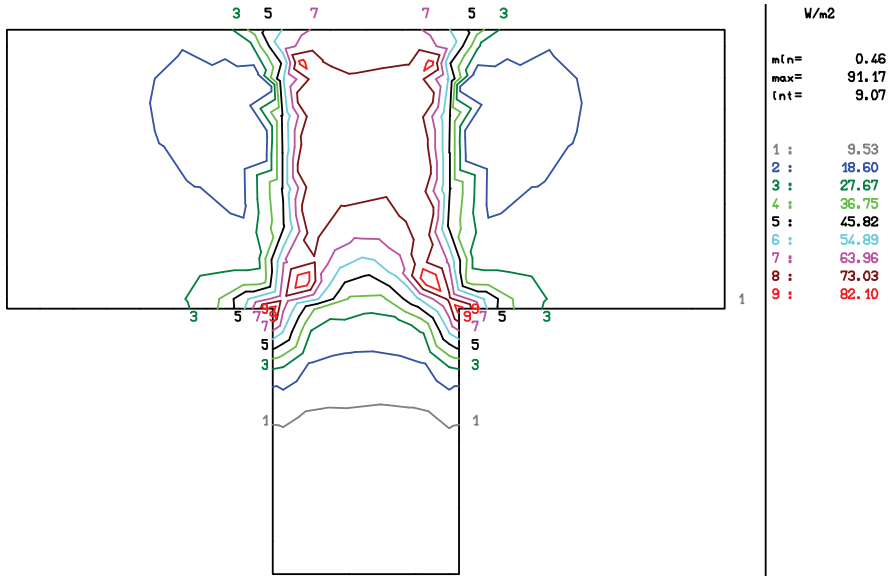


Fig.5. Variation of the Density of Heat Flow before the Adjustment

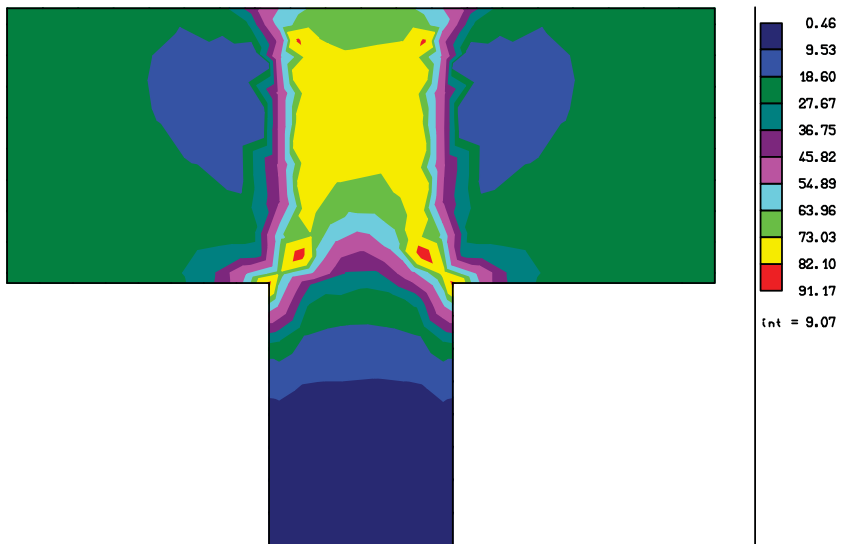


Fig.6. Zones of almost Constant Densities of Heat Flow before of the Adjustment

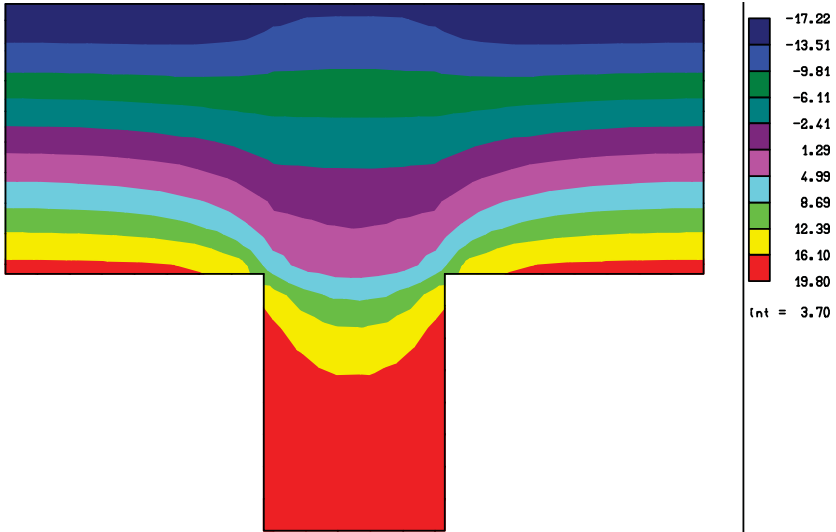


Fig.7. Zones of almost Constant Temperatures after the Adjustment

After the adjustment, the isothermal lines are almost parallel to the wall external surface and the effect of lateral heat flow is not significant.

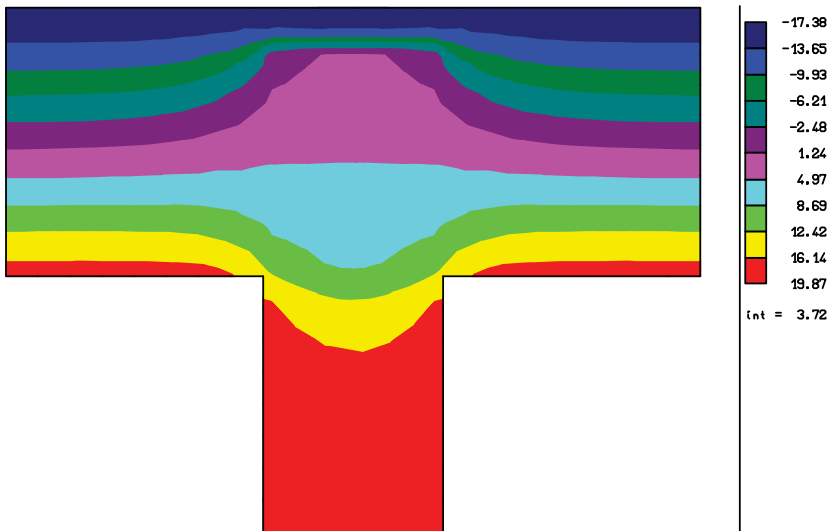


Fig.8. Zones of almost Constant Temperature before of the Adjustment

5. CONCLUSIONS

Thermal comfort and protection requirements mean a positive state of mind due to a friendly inside environment, and a lower cost of heating for energy conservation resulting from the best thermal isolation available concerning the improvement of relative humidity, condensation risk, comfort temperature, thermal resistance, thermal transmittance, and heat losses.

2-D FEM wall pattern in the steady-state conditions is suggested for the design of the adjustment of R_0 -value. After the adjustment, the effect of lateral heat flow is not significant. Note that the best position of thermal insulating material is at the outside surface of building element.

IT Approach is an important instrument to stimulate the taking of right decision by heat transmission visualizing. It is attractive.

On recommends the dynamic heat transmission through the building envelope with solar gain and material thermal storage, for research and effective design, as well.

References

- 1 xxx The Romanian code SR EN ISO 10211-2:2001 “*Thermal bridges in construction- Calculation of heat flows and surface temperature. Part2: Linear thermal bridges*”.
- 2 Moss, J. Keith –*Heat and Mass Transfer in Building Services Design*, “E&FN Spon” Publishing House, an imprint of Routledge, London, 1998, ISBN 0 419 22650 8.

Comparative Study on the Results of Analytical and Experimental Analysis of a Steel Taintor (Radial) Gate

Adrian Prodescu and Daniel Bîtcă

Steel Structures Department, University of Civil Engineering, Bucharest, Romania

Summary

The main load of a hydraulic gate is the water pressure, especially for the submerged gates. A good accuracy of the computation methods leads to a more secure structure.

The paper presents a comparison between different computation methods of this type of structures. A radial gate was analyzed. The size of the submerged outlet is 4,0 x 4,0 m and the water depth is 20,0 m

The following methods were used in the analysis:

- *The finite elements method, using a mesh of the structure of the gate.*
- *Model studies. An 1:4 scale model was built in order to perform this study. The model was subjected to water pressure. In several points of this model, strain measuring devices were installed and the strains were measured at several water pressure magnitudes.*

The results of the first two computation methods are compared in some points of the structure. With the aid of the second method, the strains were computed in order to compare them with the strains measured on the model.

These comparative studies try to establish the accuracy of each of the methods presented above.

KEYWORDS: *radial gate, water pressure; experimental study*

1. STUDY'S OBJECT

In this paper it is analyzed a depth radial gate, which have the dimensions 4,00x4,00m, located on 20,00m depth. The structure of radial gate is presented in figure 1.

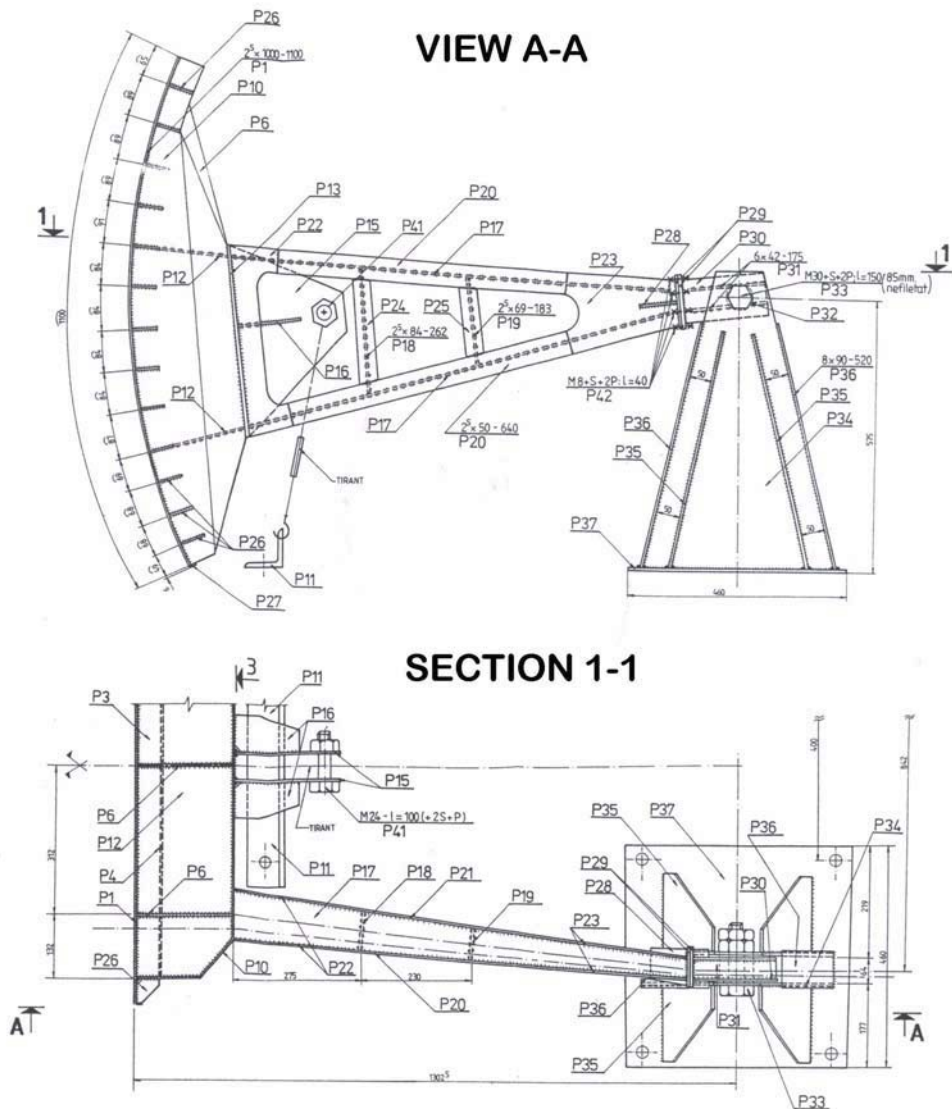


Figure 1. The structure of analyzed radial gate

The main dimensions of the 1:4 scale model are:

- the outlet dimensions $L \times h = 1050 \times 1000$ mm;
- the plate radius is 1300 mm;
- the plate thickness is 2,5 mm, in order to be 1:4 by the thickness of the gate's plate (10 mm);

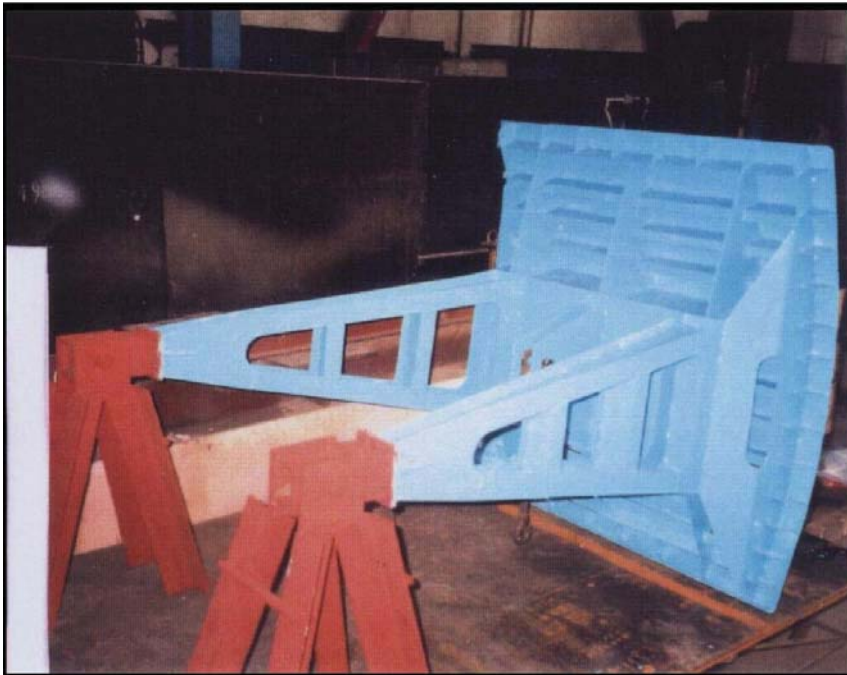


Fig 2 Assembling the scale model

2. THE HYDRAULIC PRESSURE TEST OF THE SCALE MODEL

In order to apply water pressure on the model, a steel tank was built such as the model would fit on one of the tank's lateral faces. The tank was made out of 6 mm thickness sheet, which was stiffened with angle steel shapes.

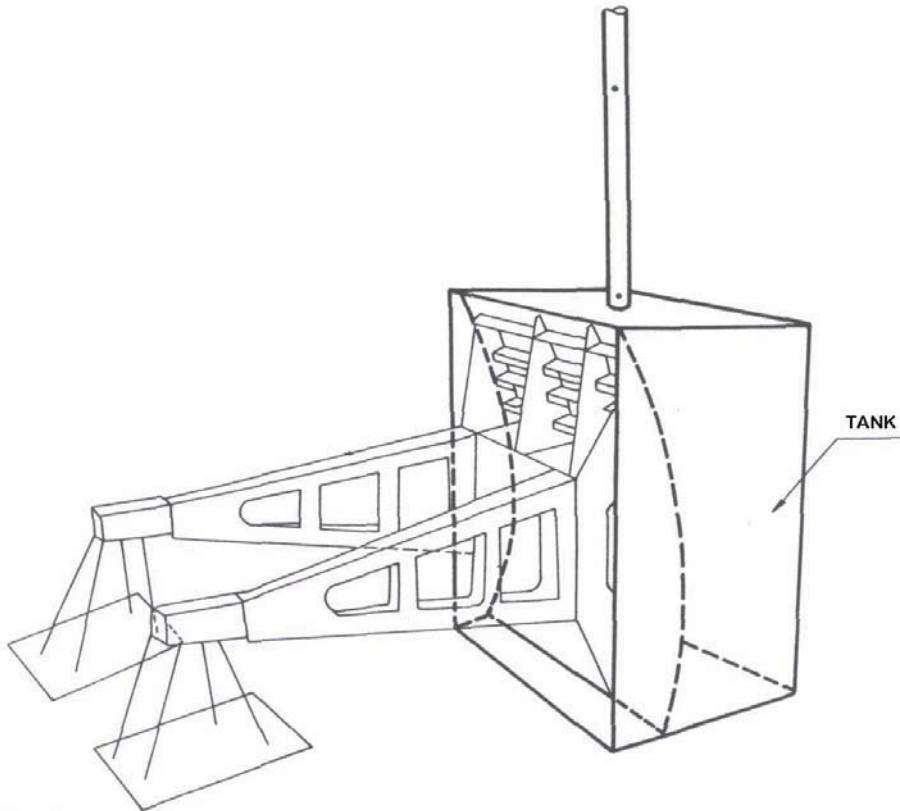


Fig. 3. The scheme of the hydraulic pressure test

The sealing between the model and the tank was made using siliconic sealant with good elastic properties, in order to allow the displacements between the tank and the model.

The boundary conditions were made similar to the real ones, when the gate is closed.

A vertical pipe was attached to the top face of the tank. This pipe allows the increase of water pressure in 1 m steps, the maximum pressure being 6 m above the tank.

The deflections of the model were measured in 6 load steps; the water pressure was increased with 1 m in each step.

The deflections of the model in the upstream - downstream direction were measured with the aid of some measuring devices with 1/100 mm precision. The points in which these measuring devices were placed are shown in fig. 4 and 5. In pts 1 and 2 (where the displacements should be 0) two measuring devices were installed in order to correct the other measured deflections.

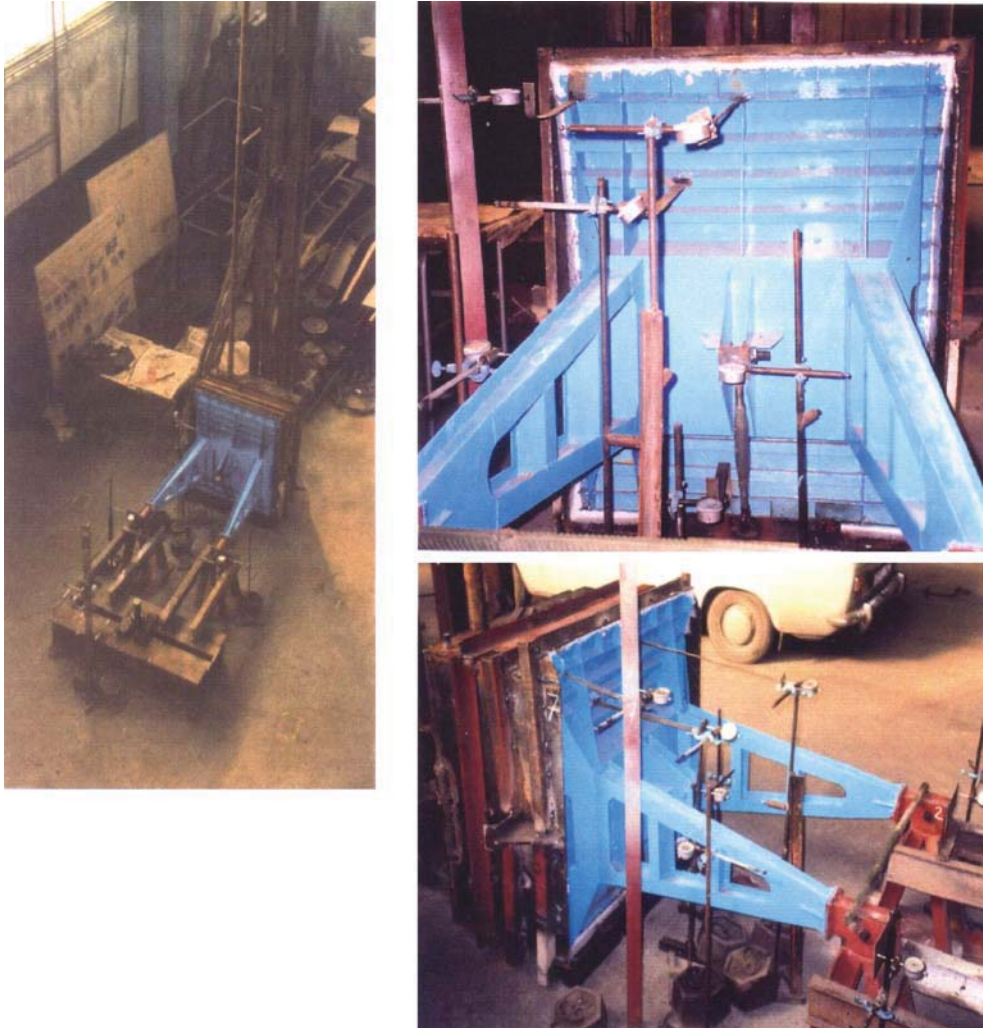


Fig. 4. Aspects during the test

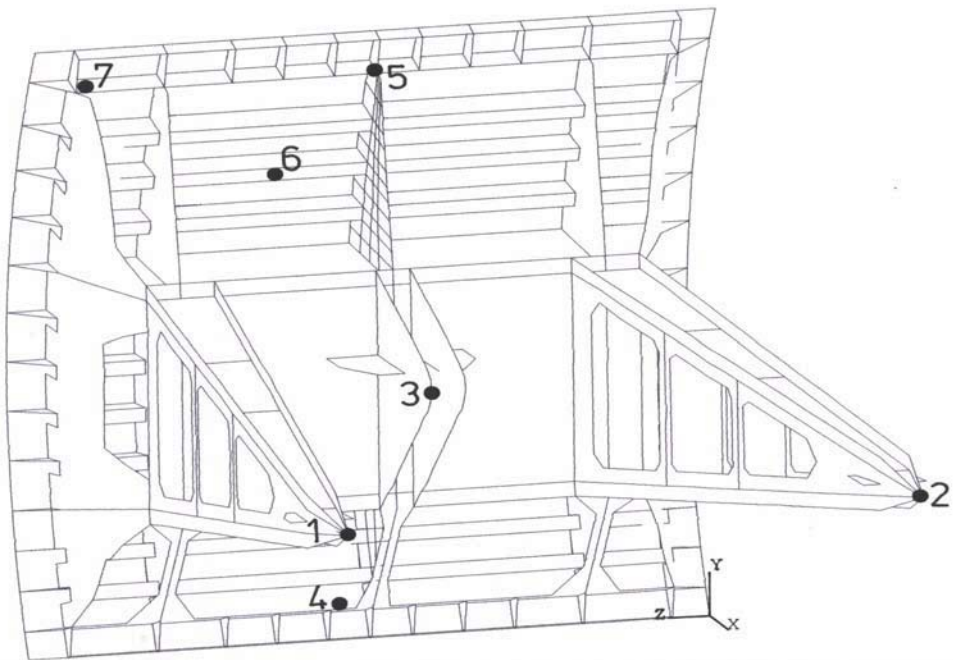


Fig. 5. The points where the measuring devices were installed

The corrected deflections in points 3 to 7 are shown in fig. 6. The corrections were made using the deflections measured in points 1 and 2 (which are the bearings where, theoretically, the displacement is null)

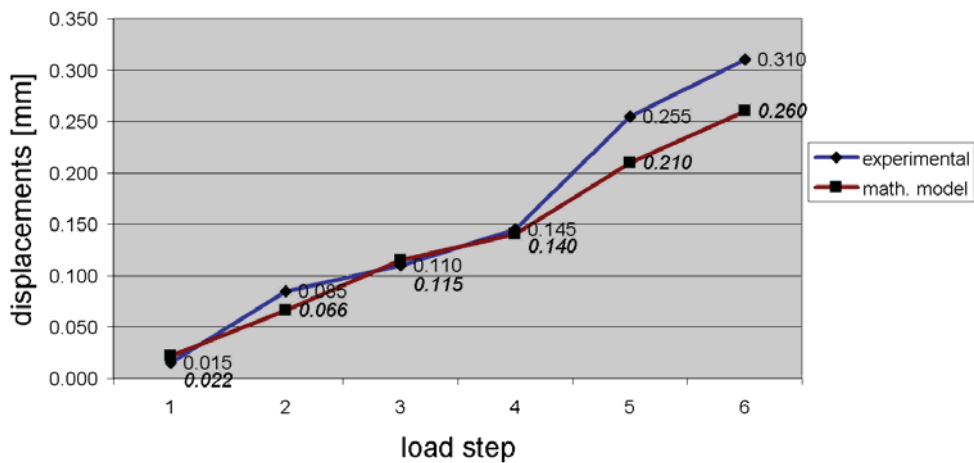


Figure 6. The corrected deflections in points 3 to 7.

3. COMPARRISON BETWEEN THE RESULTS OF THE TEST AND THOSE OBTAINED BY COMPUTATIONS

A finite elements model was build, having the same characteristics as the scale model. The load steps were similar to the ones from the test.

The graphs in fig. 7, 8 and 9 shows comparisons between the displacements obtained in the test and in the computations.

One can notice a good match between the results obtained using the two methods, especially in the first four loading steps.

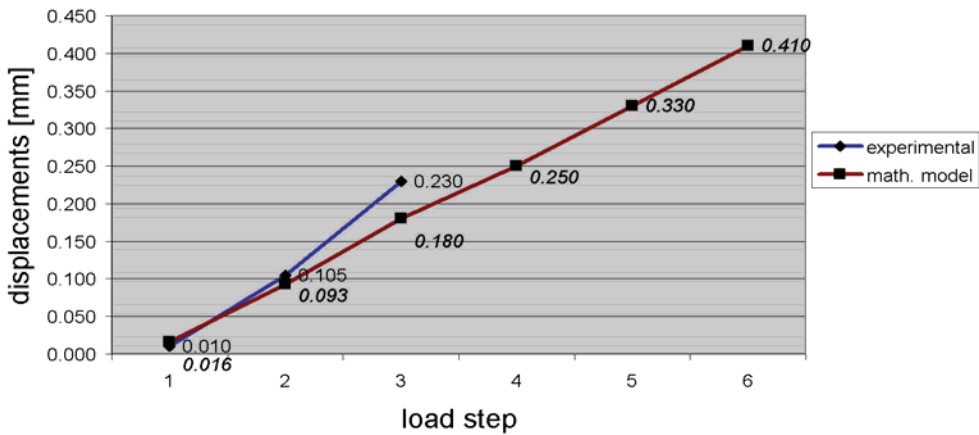


Fig 7. Displacements in point 3

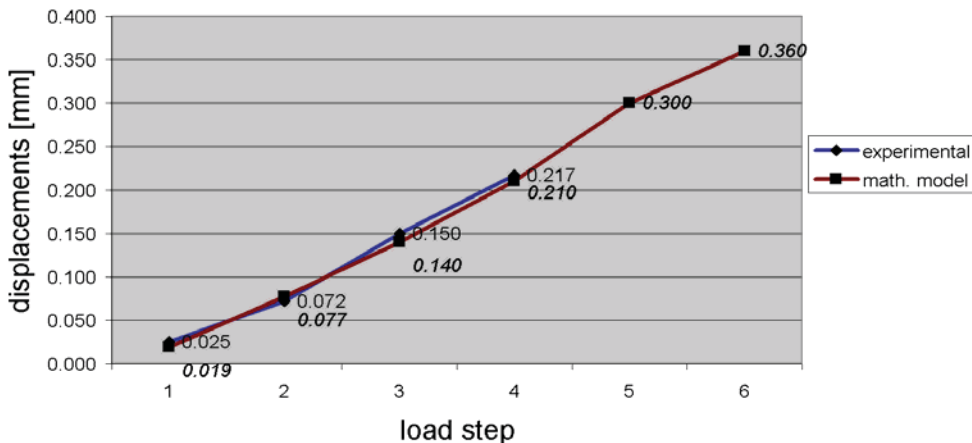


Fig 8. Displacements in point 6

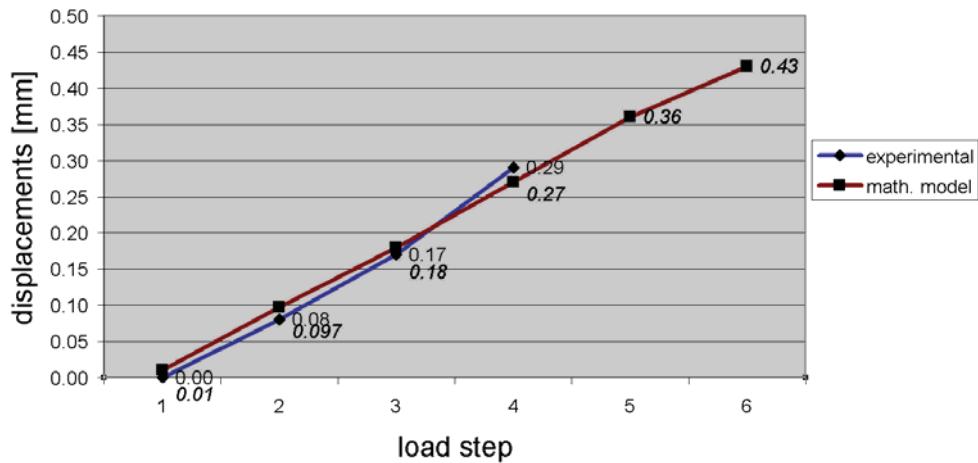


Fig 9. Displacements in point 7

In points 3 and 6, situated in areas of the structure having rather big stiffness, one can see the results are very close, the maximum differences being of about 19 % for point 3 and about 26% in point 6.

As a conclusion, the closeness between the results confirms the reliability of the finite element method, if the mesh is appropriate and sufficiently detailed.

References

- 1 Prodescu, A. *Acuratețea modelelor de calcul folosite la analiza stăvilor segment*, Teză de doctorat, Universitatea Tehnică de Construcții, București, 1998
- 2 Beleş, I; Răduică, N. *Construcții metalice și elemente de construcții; Stăvile metalice* Institutul de Construcții București 1979

Contribution to non-linear constitutive modelling of masonry structures in 2D

Jiří Brožovský¹, Alois Materna² and Ivan Kološ¹

¹Dept. of structural mechanics, VSB – Technical University of Ostrava, CZ708 33, Czech Republic

²Dept. of building structures, VSB – Technical University of Ostrava, CZ708 33, Czech Republic

Summary

This paper discusses a non-linear constitutive model for modelling of masonry in 2D. The model consists from two independent parts: the model for mortar and the model for bricks or stones.

The reason of using two different constitutive models is our need to be able to modell individual bricks (or stones in the case of a stone masonry) and the mortar between the bricks.

We have decided to use a smeared crack approach for the modelling fo a mortar. It is an approach that is widely and successfully used for a constitutive modelling of concrete and we assume that it can be also applied to a mortar that is very similar to a concrete.

The model of mortar is based on an equivalent one-dimensional stress-strain relation that depends also on 2D state of stress (through the Kupfer's failure criteria that is used to obtain the limit stresses for the one-dimensional stress-strain relation) and on some special material properties such is fracture energy of mortar.

Bricks are modelled in a different way, As a generally brittle, they often can't be effectively modelly by the smeared crack approach. The damage of the brick (a crack) usually goes through the whole brick and it can be assumed that its occurrence depends on a stress intenzity on an area and not on the stress size in an individual material point. Thus we have decided to use a simple approach that can be describes as a very basic non-local material model.

After the ckack on the brick is detected the material properties are changed in a moment. Unlike the model for a mortar, it is assumed that there is no unloading curve for this model,

KEYWORDS: finite element method, constitutive modelling, masonry, mortar, bricks, crack band model, smeared cracks.

1. INTRODUCTION

The static analysis of masonry can be done in several ways. The most common is approach is a linear elastic constitutive modelling. It allows to provide a relatively simple computational analysis and many structures can be analysed with very simple computational models (beams and frames) and often even without need of a computer. Also the finite element analysis can be relatively easy and non-complicated. It is often said that linear elastic modelling is enough for a design of masonry structures because they are not allowed to work in situations when their behaviour can be non linear (under tension loads, for example).

But there are situations when the assumption of the linear elastic behaviour is not sufficient. For example there are often needs of analysis of already existing buildings or of historic structures and monuments that can work in a non-optimal mode for masonry. For these cases a lot of different non-linear constitutive models have been developed by many authors (for example [1]). Many of these approaches are very complex and they can offer a high level of accuracy of results if they are properly used. But it isn't often easy (or even possible) to get all the necessary input data that are needed for such models. In these cases the results can be even less precise than the traditional computing approaches. There are also a lot of not so advanced models that cannot offer so high precision of results but they usually require lower number of input data and may they may be easier to use.

In this paper we present a constitutive model for masonry that we are developing. This model was designed as a compromise between needs and possibilities of computing and access to input data (however, the proposed model still can be too complicated in some cases).

2. CONSTITUTIVE MODEL DESCRIPTION

2.1. Overview

The constitutive model includes two independent parts: the model for mortar and the model for bricks. These parts are based on different assumptions and they are implemented in different ways. The mortar is implemented using the smeared crack approach and the crack-band model. Bricks are modelled with a simple variation of a non-local model approach. This division of the model into two parts allows us to create a models that can include individual bricks (or stones in a case of stone masonry that is common in historic buildings) and also locate the mortar in positions that correspond with the real structure.

The proposed constitutive model is developed for 2D cases (for the plane stress case).

2.2. Model for mortar

The constitutive law for mortar is controlled by an equivalent uniaxial stress-strain relation. The simplification of the problem from 2D to 1D is not ideal but it is relatively easy to develop and understand. To make the uniaxial relation to be more corresponding with the real behaviour the limits of the relation (strengths in tension and in compression) are computed from a 2D failure criteria (the Kupfer's criteria is used here) and depends on the actual 2D stresses.

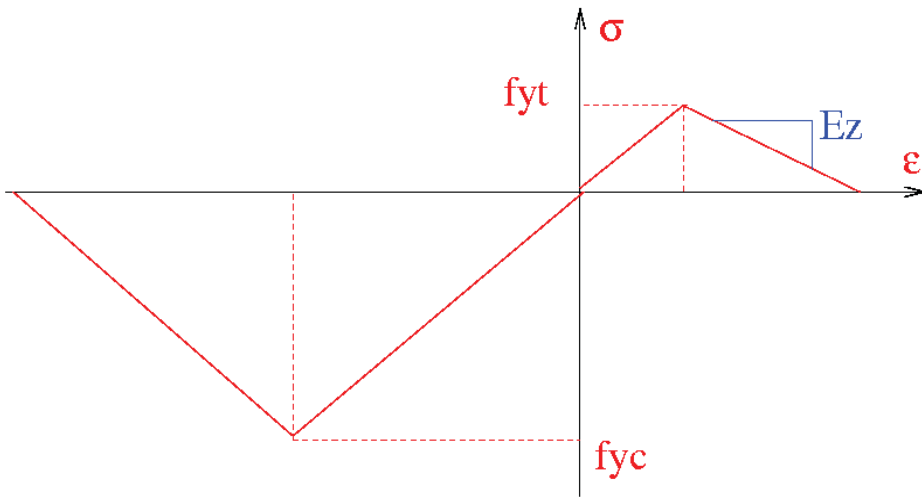


Figure 1. Uniaxial stress-strain relation for mortar

The used approach has several disadvantages. The one of the most important is that results depend on properties of a finite element mesh. It is obvious, because when a “damage” is detected the properties of the material become reduced and they are reduced on the whole area of the element (or – in our case – on a whole area that corresponds with an integration point of a finite element).

This issue can be minimized by usage of the Bazant's crack-band model when the properties of the stress-strain diagram (the “Ez” value in Figure 1) depends on the size of the cracked area (value L on Figure 2) and the material properties (the fracture energy G_F). The fracture energy can be obtained from special experiments or it can be (with limited precision) computed (Karihaloo []).

The behaviour of the material in the compression is modelled in a similar way.

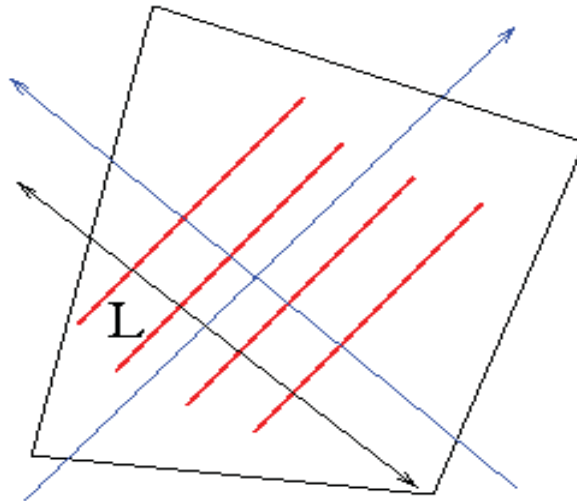


Figure 2. Length L of the cracked area

2.3. Model for bricks

The real bricks (or stones in stone masonry) have a different behaviour. They usually are much more brittle than the mortar. The material model for mortar can be also used for a modelling of bricks but it usually isn't ideal for this purpose.

We have prepared a different constitutive model. We assume that behaviour of bricks is linear elastic until the damage (crack) is detected. Usually, the crack goes through the full height (or width) of brick so it is obvious that the failure condition must respect this.

We have proposed a use an approach that is similar to non-local material models: the stresses in the brick are controlled on an area A with dimensions that are comparable with height of the brick. It should guarantee that crack is detected if the stresses in the brick are big enough to be able to create a crack. Thus a brittle damage of the brick should occur.

After the brick is damage the material properties should be changed. Now we have adopted the elasto-plastic behaviour of a material. After the crack is detected then the normal stiffness of the material (represented by Young's modulus) is reduced to zero. It is not an ideal approach because it means that the cracked material still carry the previous stresses but we selected it for the relatively ease of the implementation. After we will test the other parts of the algorithm (namely the computation of the failure condition) we will improve the behaviour of the cracked material to be more realistic.

3. ILLUSTRATIVE EXAMPLE

Model description

To show the behaviour of the model we have prepared a simple (not very realistic) numerical example. The geometry is shown on the Figure 3. The sizes of bricks are 270x160 mm and the width of mortar is 10 mm in all cases.

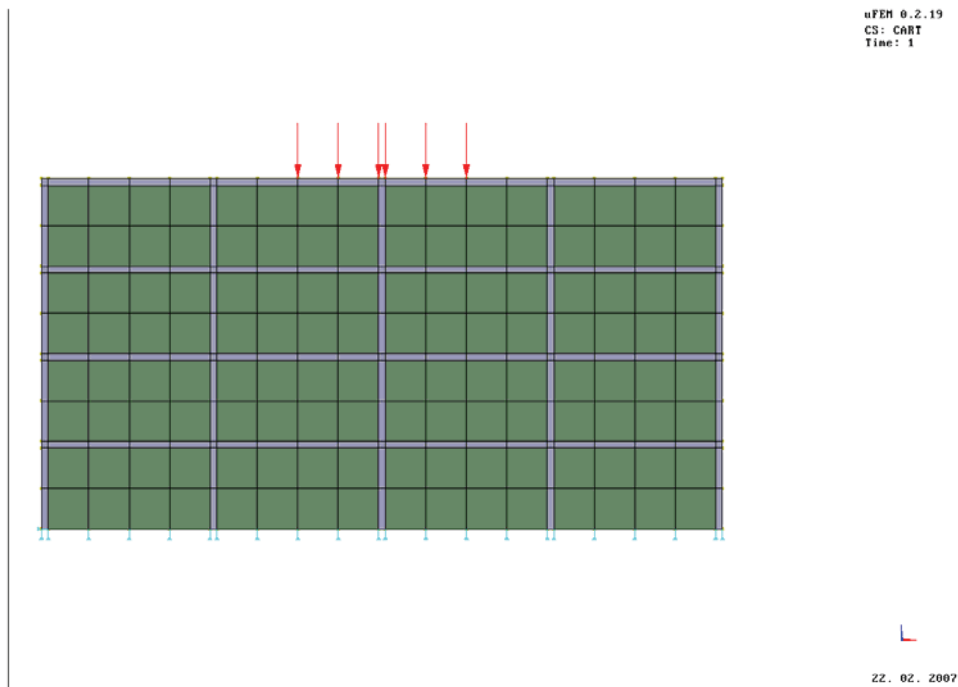


Figure 3. Illustrative example – finite element model

The Figure 4 shows the load-displacement relation that was obtained from the analysis of the model.

The relatively sharp change of the stress-strain curve is the result of a selected constitutive model of mortar – the bricks under the loading cracked in a moment and then the strength of the structure became reduced. From the Figure 4 it is obvious that the mortar has a relatively small influence of the results in this case.

The relatively high strength of a damaged material in this case was a result of a relatively large residual stiffness of a bricks (we used a elastoplastic model with hardening for the bricks here to help the convergence of solution).

The results show that the model features a behaviour that we have expected to obtain.

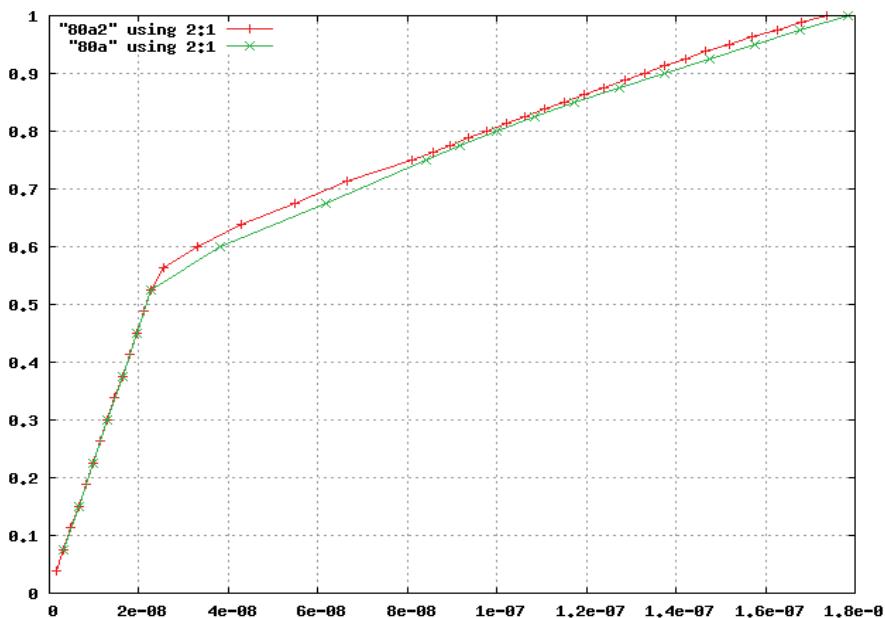


Figure 4. Computed stress-strain relation

4. CONCLUSIONS

The article shows a basic material model for masonry. It can be improved in several ways, namely in the area of the modelling of bricks.

Acknowledgements

The works are supported from the Czech state budget through the Czech Science Foundation. The project registration number is GA CR 103/03/P389.

References

1. Bazant Z. P., Planas, J., *Fracture and size effect in concrete and other quassibrittler materials*, CRC Press, Boca Raton, 1998.
2. Cervenka V., *Constitutive models for cracked reinforced concrete*, ACI Journal, vol. 82, 1985.
3. Cervenka V., *Inelastic finite element analysis of of reinforced concrete panels under in-plane load*, University of Colorado, Colorado, 1970

Behavior of newly developed FRP reinforcement in structures under various load schemes

David Horak¹, Martin Zlamal¹, Petr Danek²

¹Department of Concrete and Masonry Structures, Brno University of Technology, Czech Republic

²Department of Building Testing, Brno University of Technology, Brno, Czech Republic

Summary

An own reinforcement based on glass or carbon fiber reinforced polymers in frame a Czech ministry of industry and trade research task was developed. A set of experiments was made for reinforcing of concrete structures with this FRP internal reinforcement.

The developed reinforcement was used for reinforcing of several concrete elements. These elements were exposed to different types of loading. Their behavior was monitored to verify the functionality of new reinforcement. Based on this results it is possible to determine required properties of reinforcement used for every sort of reinforcing (longitudinal or shear reinforcement).

This reinforcement was also used to additionally strengthen the masonry vaults loaded with static and dynamic loads. Obtained results are compared with theoretic results of nonlinear numerical analysis of constructions.

KEYWORDS: Longitudinal and shear GFRP reinforcement, reinforced concrete structures, strengthened masonry vaults.

1. INTRODUCTION

At present non-metallic reinforcement is used very frequently (because of their resistibility) in constructions that are exposed to aggressive environment's influence. It makes possible to reduce costs needed for special arrangements for protection the common reinforcement and eventually consecutive repairs.

However the price of the non-metallic reinforcements is quite high (see Fig. 1). And because this reinforcement form the significant part of the final costs of the cross-section price, it is very advisable to (next to economical optimizing of the cross-section [1]) use local non-imported (i.e. probably cheaper) materials.

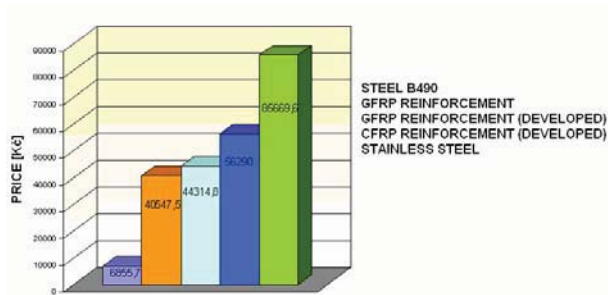


Figure 1. Comparison of the average prices in the Czech Republic (common materials and developed reinforcement)

The economic aspect mentioned above isn't in the Czech Republic so strong, because there isn't any native producer of this kind of reinforcement. While using it is necessary to import the reinforcement from abroad, which makes construction sometimes more expensive.

In terms of research in frame of the Czech Ministry of Industry and Trade, development of “home” reinforcement based on glass and carbon fibers has begun. It is of course necessary to check out functionality of this system – i.e. functionality of interaction of reinforcing bar and surrounding concrete.

But not only new concrete structures are in the centre of interest. Masonry continues to be popular because of its relative simplicity of application in the technical practice. Indeed, for a new use of structural masonry reasonable constructional rules are required, because conventional approach based on the experience is unacceptable nowadays. In addition, most methods of carrying capacity assessment and of strengthening for the existing masonry construction are increasingly based on analyses of mathematical simulation and appropriate (linear and nonlinear) computational models. One method of load-bearing elements strengthening is application of additional external non-prestressed reinforcement into chases in masonry on intrados of vaults, which will provide stiffening and increasing of load carrying capacity of the individual load-bearing elements.

The existing and especially historical masonry structures are nowadays considerably monitored. Many of them are in need of some retrofitting or strengthening. In such cases the non-metallic with minimal requirements for reinforcement cover even in aggressive environment could be the best solution. Therefore some tests were undertaken to learn about behavior of masonry vaults additionally strengthened with GFRP bars. These test logically followed previous research of the additionally strengthened masonry structures.

To achieve good usable results it is necessary to provide also statistical evaluation and theoretical backgrounds for further designs of such structures. Therefore all data obtained from the tests are used to create and verify the numerical model of

FRP reinforcement material used in calculations. This model should allow to predict as accurate as possible the behavior of concrete and masonry structures reinforced with FRP bars.

Mathematical model is created in physically non-linear FE software based on fracture mechanics of quasi-brittle materials. Results obtained from real tests are used as input data for all materials. It means all material characteristics for both concrete (strengths, modulus of elasticity, fracture energy, etc.) and non-metallic bars (tensile strength, load-deflection diagram, modulus of elasticity). The cohesion between reinforcement and concrete (grouting) is modeled via cohesion parameters for each type of the surfacing.

Comparison of the real and numerical results shows very good correspondence (some results are shown in the text below and in [2] and [3]).

1.1. Concrete reinforcement

Tests are performed in several partial fields:

- obtaining physical-mechanical characteristics of reinforcement,
- obtaining cohesion between reinforcement and concrete,
- monitoring behavior of specimens reinforced with non-metallic reinforcement (i.e. real function of reinforcement in loaded construction).

The first two research points were completed and all the results were analysed [2]. Choice of the most suitable type of reinforcement was achieved based on obtained results. The best cohesion with the concrete, material properties and demand factor of the production of the reinforcement and the surface preparation were confronted. All these parameters influence the price and the efficiency of the developed reinforcement.

After the decision about the surfacing of the reinforcement it was necessary to confirm the functionality of the reinforcement. Therefore several tests were performed on the concrete specimens. GFRP bars were used as both longitudinal and shear type of reinforcement.

1.2. Strengthening of the masonry structures

The method of additionally inserted non-prestressed reinforcement allows additional strengthening of masonry structures without a necessity of large intervention into vaults especially in case of external application. This system is capable redistributing newly originated stresses from load that act on a strengthened construction. The aim of reinforcement is to restrict the development of existing cracks and eliminate possibly an origin of the new ones, and to improve load-bearing capacity of vaulted masonry constructions.

From the static viewpoint, unreinforced masonry structure is unable to transfer tensile forces that can originate on existing structure from following action:

- action of the higher imposed load against the designed one,
- action of either identical or the lower load against the designed one.

Another consequence of the retrofit reinforcement application into masonry structures is the rigidity improvement. The effect is evident especially at the structures cracked by the previous traffic utilisation. Nevertheless, from the practical viewpoint this consequence could be smaller for railway bridges.

For reinforcing the masonry structures it were used two types of reinforcing materials (shape of this reinforcement bars can be seen in Figure 2):

- commonly used steel reinforcement (Helifix),
- non-metallic reinforcement (GFRP bars).



Figure 2. Shape of Helibar and wrapped surface GFRP

As a binding (transferring) medium between reinforcement and origin masonry was used special mortar (grouting substance). It is important to mention that it is essential the reinforcing bars compose with grouting substance and with origin masonry the reliable and durable system.

2. CONCRETE MEMBERS WITH LONGITUDINAL GFRP REINFORCEMENT

These tests are related to concrete beams (dimensions 350 x 100 x 2200 mm) reinforced only with longitudinal GFRP reinforcement (diameter 14 mm, one-side-wrapped bars).

This test was classical four-point bending test (Figure 3). The span of the beam was 2.2 m and the loading forces were applied at 1/3 of the length of the beam. Beams were designed to obtain failure caused by a bending moment. During the experiment following input data were monitored – force load, deflection on several points and strain of the reinforcing bars (monitoring units build into the reinforcement [2]).

Three specimens with the longitudinal reinforcement were exposed to load forces. Also three specimens without the reinforcement were loaded to provide reference data and to make possible the comparison of effects of the reinforcement. Results

of specimens without reinforcement allowed also validating the input data (i.e. material model of the concrete) used in FEM numerical model.



Figure 3. Deflection of the loaded beam before the collapse

All three reinforced beams collapsed because of exceeding the tensile strength of the GFRP bars. Two of them collapsed under the load force, one beam collapsed in the middle. Maximal average load carrying capacity of this beam improved from total 6.11 kN (calculation presumption 6.09 kN) to 17.19 kN (calculation presumption 16.38 kN - according to ACI 440.1R-03 without any safety factors). The tests results demonstrated the functionality of the developed non-metallic reinforcement.

The development of the load-deflection curve is in Figure 4. Also comparison of the behavior between reinforced beams (specimen 1-3), non-reinforced beams (reference specimens 1-3) and numerical model of the reinforced beam (Atena 3D results) can be found there.

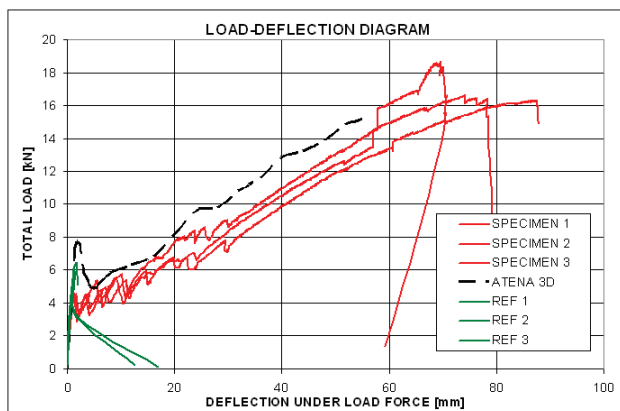


Figure 4. Deflection of the beam with longitudinal GFRP reinforcement

2. CONCRETE MEMBERS WITH LONGITUDINAL AND SHEAR GFRP REINFORCEMENT

The non-metallic reinforcement was tested also as shear reinforcement. The longitudinal reinforcement in these beams were the GFRP bars (diameter 14 mm, one-side-wrapped bars – same as mentioned before). The shear reinforcement was created from one GFRP bar (diameter 8 mm, one-side-wrapped bars) shaped into spiral looped around all longitudinal reinforcement bars – see Figure 5.

This reinforcement had to be shaped before hardening. Thus the curing method was changed and the curing of the already shaped and fixed reinforcement proceeded at the room temperature. The hardening of the bar took more time, but the material characteristics were not reduced.



Figure 5. Shear reinforcement shaped into spiral

All beams (dimensions 115 x 240 x 2100 mm) were loaded by the same way as the beams with longitudinal reinforcement only. It means the load scheme was classical four-point bending test with load points at 1/3 of the span. Supposed failure mode was exceeding the shear capacity in the area near supports.

Again the test set was made from three test specimens with shear reinforcement and from three “reference” specimens without shear reinforcement. The reinforcement influenced positively the shear capacity of the tested beam and confirmed its functionality. The shear capacity improved from 54.7 kN (reference specimens without shear reinforcement) to 82.2 kN (reinforced specimens).



Figure 6. Cracked beam with GFRP shear reinforcement

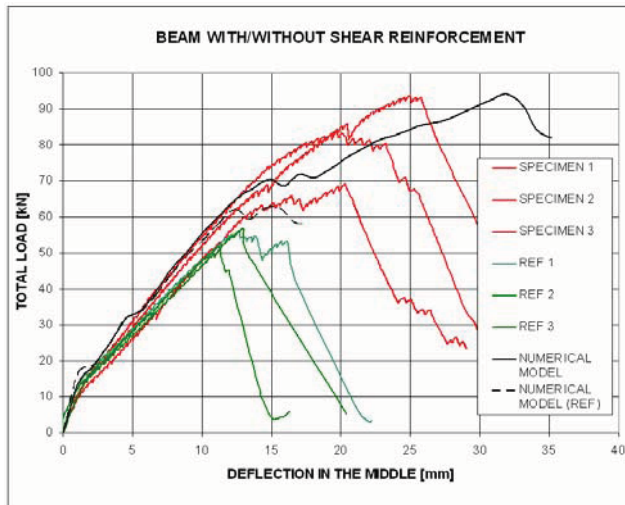


Figure 7. Deflection of the Beam with GFRP Shear Reinforcement (REF Specimens are Reference Specimens Without Shear Reinforcement)

The tests results demonstrated the functionality of the developed non-metallic reinforcement.

3. MASONRY STRUCTURES STRENGTHENED WITH GFRP BARS

Within experimental parts of the project three sets of masonry vaults with for various loading types were manufactured. For the distinction of individual vaults are used notation jKi , where „j” corresponds to series number (1-3) and „i” to the strengthening method (1-3). The vaults were symmetrically loaded in $\frac{1}{2}$ of the span

- 1.series ($j=1$), asymmetrically in $\frac{1}{4}$ of the span - 2.series and symmetrically in both quarters of the span - 3.series ($j=3$).

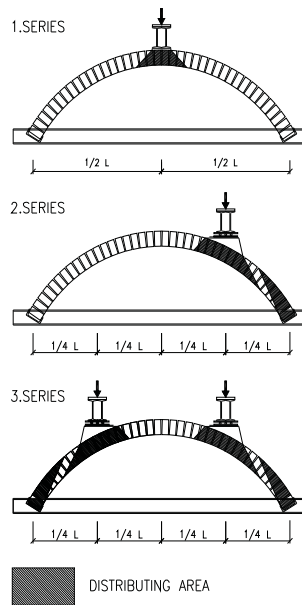


Figure 8. Loading scheme of the vaults and distribution zones of the load in the vaults

Each series consists of three vaults: non-strengthened – comparative ($i=1$), a vault reinforced in two chases ($i=2$) and a vault reinforced in three chases ($i=3$). The vaults were bricked up from full burnt bricks on lime-cement mortar of the width 890 mm, span 2600 mm, deflection 750 mm and radius 1500 mm.

Into every reinforcing chases were embedded 2 bars. First experiments were performed with reinforcement HeliBar of special helical shape of diameter 8 mm and the second set of test specimens were reinforced with GFRP bars of diameter 6 mm (one-side wrapped). Only unsymmetrical loading in $\frac{1}{4}$ of the span was used for testing vaults with non-metallic reinforcement (it is the case of the biggest influence of the additional strengthening [4]).

3.1. Behavior under static load

From the comparison of the load-bearing capacity of the individual vaults in the series results that essential growth of the load-bearing capacity was achieved especially in the case of 1st series and 2nd series of the vaults, namely more than eight multiple growth. This growing of carrying-capacity can be watch for both cases of reinforcement – helical metallic and non-metallic. It was related to the

vaults stressed by either concentrated or one-sided load, at which the vaults were loaded by the interaction of normal forces and bending moments.

In the case of 3rd series the experiments did not prove the effects of strengthening by additionally inserted reinforcement on the vaults load-bearing capacity; no effects of reinforcement demonstrated themselves because the vaults were mainly compressed.

In the case of non-strengthened vaults of 1st and 2nd series the failure was acute, main crack was opened and the vault ruptured. In the case of the strengthened vaults of 1st and 2nd series came to the gradual opening of separate cracks until the failure, which was accompanied by the rupture of the metallic reinforcement from the chases. All glass reinforcing bars were in the ultimate limit state ruptured.

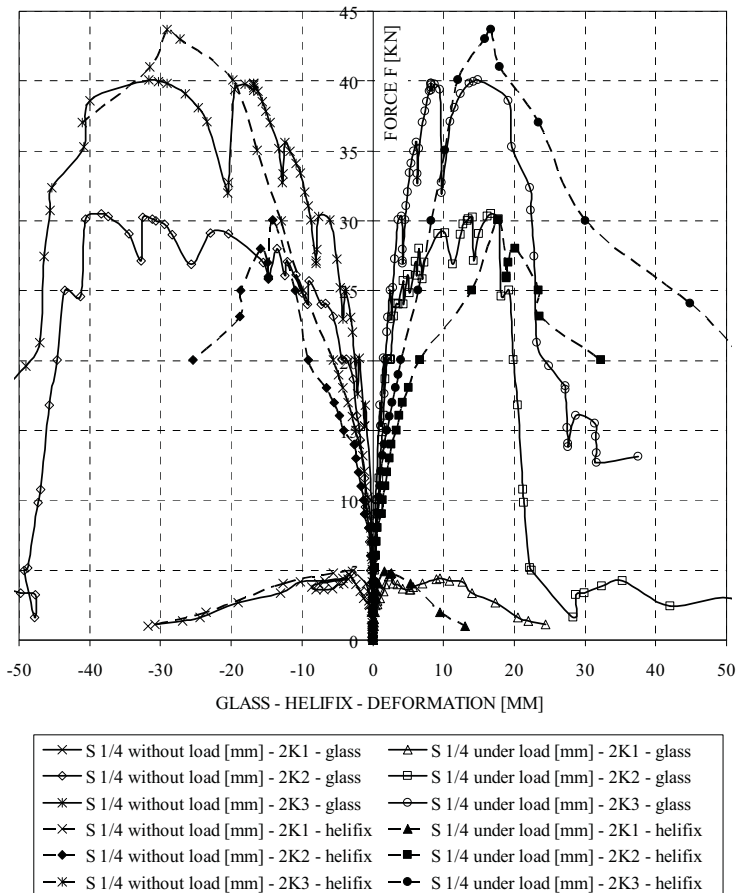


Figure 9. Comparison of deformations on vaults loaded in $\frac{1}{4}$ of the span strengthened with GFRP and metallic helical reinforcement

On the basis of thus obtained results from numerical studies and on the base of the designed algorithm, it will be possible to obtain (substantiate) simple constitutive relations for the evaluation and design of strengthening by simplified designed methods used in the practice and to set up simple algorithms for design and checking calculation of the masonry vaulted construction with additional reinforcement for the practice.

3.2. Behavior under dynamic load

Dynamical tests were performed on vaults loaded asymmetrically in 1/4 of the span and reinforced with glass reinforcement (GFRP) only. From results of first dynamical tests it is visible increasing of load-bearing capacity of the reinforced vaults (2K2, 2K3) compared to the non-reinforced vault (2K1) (Figure 10).

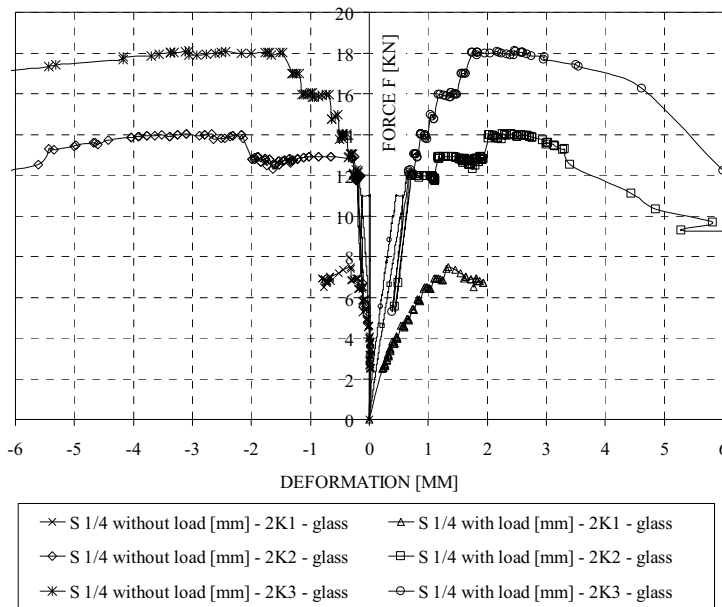


Figure 10. Comparison of deformations on vaults loaded in 1/4 of the span strengthened with GFRP reinforcement – dynamical test

Unfortunately the low set of tested specimen prohibited comparison with the test data from statical experiments. The results are also influenced by the big non-homogeneity of masonry structure. Also the fracture mode (i.e. failure of the vault by opening of tension cracks in the bed joint) is not uniform and the position of cracks can influence the final load bearing capacity.

Strengthened vaults can be partially compared by relation of their load-bearing capacity. Ratio of the load-bearing capacity of the vaults with three reinforcing chases and with two chases (2K3/2K2) at static loading is 1,33 and at dynamical loading is 1,29.

3. CONCLUSION

The tests showed that the developed system is functional. The reinforcement bars can work as concrete reinforcement and they are capable to transfer the load forces generated in the construction during the loading.

There is also very positive benefit for the strengthening of the masonry vaults. This system can be used to repair the historical structures with minimal impact to the structure itself (thanks to low requirements for cover – there is no need to provide additional layers of cover materials).

So far only short term tests were performed. To fully confirm the functionality and safety of the newly developed reinforcing system it will be necessary to verify the long term characteristics of the reinforcement. The main subjects of research will be the behavior of the reinforced structures under the long term loads. Also the resistibility of the reinforced structures in the aggressive environment has to be verified.

Acknowledgements

This research has been proceeded with support of Czech ministry of industry and trade (MPO) in frame research task 1H-PK2/57 – “Durable concrete structures” and also has been prepared with the financial support of Ministry of Education, Youth and Sports, project No. MSM0021630519 “Progressive reliable and durable load bearing structures”.

References

1. Plsek, J., Stepanek, P., Optimisation of design of cross-section in concrete structures, *Proceeding of the 4th International Conference Concrete and Concrete Structures*, 2005.
2. Stepanek, P., Fojtl, J., Horak, D., Pull-out test of non-metallic FRP reinforcement for concrete structures, *Proceedings of the 4th International Specialty Conference on Fibre Reinforced Materials*, 2006, Hong Kong.
3. Horak, D., Krupa, P., Stepanek P., Prokes, J., Development of the new methods of measurement of the strain in GFRP concrete reinforcement, *Workshop NDT 2006 – Non-destructive testing in engineering practice*, 2006, Brno, Czech Republic.
4. Stepanek, P., Zlamal, M.: Additional strengthening of masonry vaults with non-prestressed additional reinforcement, *Proceeding “STRUCTURAL FAULTS + REPAIR-2006”*, 2006, Edinburgh, Scotland.

New Shear Connectors for Composite Girders – Experiences with ABAQUS Push-Out Test Simulations

Josef Fink¹, Lubomir Ondris²

Institute of Steel Structures, TU Vienna, Karlsplatz 13/212, A-1040 Vienna, Austria

Summary

Composite structural members consisting of steel and concrete parts utilize the advantages and suppress the disadvantages of individual material components. The shear loading between steel and concrete parts is transferred by shear connectors. They have to be designed to maximize the shear load capacity and ductility and to minimize the overall manufacturing costs.

At the Technical University of Vienna, Institute of Steel Constructions, new shapes of shear connectors for composite steel and concrete beam structures are being developed. The composite structure consists of steel I-beam with connector welded lengthwise in the middle of the flange and surrounded by a concrete reinforced slab. The first sheet-type crown shaped connector has already been accepted for patent procedure. To verify its efficiency both numerical analyses and physical experiments with push-out tests were carried out. For numerical analyses of composite structures the well-established FE-program ABAQUS is used. Results depend on many material and control parameters therefore first an extensive parametric study was necessary /1/. Here missing information is given, originally suppressed in /1/ because of patent protection procedure. Further numerical experiences with different loading velocities, with ABAQUS option NLGEOM and experiences relating to results evaluation are described. Different results of ABAQUS versions 653 and 662 are mentioned. Necessity of a very careful preparation of numerical simulation and of using realistic material data for concrete is emphasized.

A comparison in /2/ shows a very good matching between physical tests and numerical simulation.

KEYWORDS: Composite steel and concrete beam structure, welded shear connector, push-out test, finite element modeling, ABAQUS, material model for concrete, loading velocity, geometric nonlinearity, kinetic energy, total strain energy, new shape of shear connector.

1. INTRODUCTION

Developing of new sheet-type connectors at the Technical University of Vienna, Institute of Steel Structures consists of physical tests with push-out specimens and of their numerical simulation as well. A recent extensive parametric study /1/ of options given in the known FE-program ABAQUS /3-5/ was concerned with a new sheet-type crown shaped connector. After accepting it by European Patent Office in Vienna for patent procedure under proposed name "VieCro", the information originally suppressed in /1/ can here be given for completeness.

The welded steel parts of the specimen can be seen in Fig. 1. In Fig. 2 the complete specimen with reinforced concrete slabs is ready for testing in a horizontal loading machine. In Fig. 3 the basic parts of the FE-model utilizing twofold symmetry are shown. Because of their very high stiffness, the head plate and the I-beam could be removed from the FE-model and replaced by corresponding boundary conditions. The loading was simulated by prescribing boundary condition on the lower surface of the steel connector (welded to the I-beam) in longitudinal direction. ABAQUS static and dynamic nonlinear procedures have been invoked, using quadratic FE-elements C3D20R and linear FE-elements C3D8R, respectively.

In /1/ results of 123 FE-calculations are given in form of P-d diagrams, d being the actual value of the prescribed connector displacement, P being the corresponding total reaction force in supported right side surface in Fig. 4. In diagrams the influence of ABAQUS material parameters, of friction coefficient in frontal and lateral contact surfaces and of clamped or contact support while using static and dynamic solution procedures can be observed.

2. DIFFICULTIES WITH NUMERICAL SIMULATIONS

The difficulties are caused by highly nonlinear character of the problem and by missing specific material parameters for concrete. If there is no P-d diagram from physical test and/or if the material data are not reliable then it is not easy to decide whether the calculated peak load, post-peak response and failure load are "true" i.e. whether they correspond to the parameters chosen only or whether they are influenced also by potential "internal" numerical instabilities.

In a recent EU-Project FE-packages ABAQUS, ANSYS, DIANA, GEFDYN and LUSAS used for solution of concrete dams have been compared /6/. It has been confirmed that the result of a complex highly nonlinear problem often depends on nonlinear control parameters used. According to /6/, correct estimating of the failure load using a non-convergence stopping criterion is problematic because with a "wrong" criterion the non-convergence on relatively small loads can occur. The quotation marks signalize some uncertainty always present while solving complicated nonlinear problems: The result depends on the solution path, this

again depends on a set of parameters used. Every change in parameters used means a different solution path, sometimes with surprising effects.

Because of problems described a very careful preparation of solution strategy and mesh data and a very thorough results evaluation is necessary. Even then it is always useful to carry out more calculations with slightly changed parameters to check the result sensitivity.

Throughout the study /1/ emphasis has been placed on the highest possible accuracy and reliability of the system answer rather than on efficiency of calculations. As far as possible, for the most control and material parameters ABAQUS default values were used uniformly throughout all calculations.

With static calculations maximum number of iterations as a general stopping criterion was set sufficiently high (and never reached), for starting and minimum increments very small values were set. With dynamic calculations the ABAQUS default automatic incrementation with global stable increment estimator was used.

3. SOLUTION PROCEDURES

From ABAQUS nonlinear procedures tested in /1/ (*STATIC,RIKS, *STATIC,STABILIZE, *DYNAMIC,EXPLICIT) the last one seems to be the most suitable for simulation of physical push-out tests. The reasons why just an explicit integration package like ABAQUS/Explicit should be used for solving highly nonlinear problems are convincingly given in /7/. Practical comparison of results obtained by particular procedures is given in /1/.

4. FE-MODEL FOR DYNAMIC ANALYSES

With the *DYNAMIC,EXPLICIT procedure of ABAQUS/Explicit package only linear elements can be used. However, the FE-model has to take into account material and contact nonlinearities and the geometry of the connection.

The authors prefer a rather conservative solution with some "FE-overkill". The mesh for dynamic analyses (Fig. 4) consists of following parts: steel connector: 6474 linear 8-node hexahedrons C3D8R (3 elements crosswise on the half-thickness of 10 mm), concrete slab: 30495 elements C3D8R, reinforcement: 525 elements T3D2, each anchor rod: 1 element T3D2. This mesh is able to register high stress gradients occurring in interactions between sheet connector and concrete parts near connector.

5. MATERIAL MODELS

ABAQUS material models used are completely described in /1/, thus the description will not be repeated here. It is to emphasize that for concrete parts a characteristic material curve with loss of strength after reaching the tensile strength has been used instead of artificial material features.

For steel parts an elastic-ideal plastic model without hardening was used.

6. FRICTION IN CONTACT SURFACES

In /1/ each calculation has been carried out three times with friction coefficients 0.3, 0.5, 0.7. For simplicity, between frontal surfaces (Fig. 5) the same friction coefficient was used as between lateral surfaces (Fig. 6). Generally, P-d curve from physical experiment, especially in post-peak area, can better be approximated in numerical simulation using small friction coefficient. Calculations in /8/ confirm this conclusion and analyse the contribution of frontal and lateral friction.

7. RESULTS EVALUATION – ENERGIES AND VISUAL INSPECTION

In dynamic calculations used for simulation of quasi-static processes an important role plays the ratio of kinetic energy to internal energy $ALLKE/ALLIE$ with a peak value accompanying distortion. ABAQUS-recommendation that $ALLKE/ALLIE$ should not be over 0,05-0,1 has to be used with some caution. The ultimate value can be different if the distortion is localized in a small area and the energy output in history output request is required for the whole FE-model. This is the way how the ratio $ALLKE/ALLIE$ is judged usually, at least in first calculations. In all calculations described in /1/ and here energies were output for the whole model.

It turns out that in the curve $ALLKE/ALLIE$ -d sometimes the existence of the peak regardless of its magnitude determines the distortion process. Usually, the peaks are very narrow and disappear soon. Often they can not be observed because of such a trivial reason as too big distance between output points. Also in such cases a careful visual inspection of deformed mesh using deformation scale factor > 1 can detect beginning of distortions or numerical difficulties since the accompanied oversized unnatural displacements do not disappear.

8. LOADING VELOCITY

Dynamic explicit calculations in /1/ have been carried out conservatively with a very small constant velocity of $v=0.5$ mm/s (prescribed connector displacement linear increasing with time). Using higher velocities can shorten the computer times substantially, on the other side inertial forces can arise and influence the result. Therefore it would be useful to find the upper bound of admissible velocities for quasi-static calculations of structures in question.

First, push-out test simulations based on an anvil connector shape (red in Fig. 7) and utilizing two planes of symmetry have been carried out. ABAQUS concrete material model CDP with dilation angle $\psi=30^\circ$, friction coefficient $f=0.5$ between interaction surfaces, clamped support surface and loading in the same way as in /1/ but using five constant loading velocities v were used. The corresponding P_{\max} - v diagram (Fig. 8) was however unacceptable, contradicting expectations. By detailed inspection of particular solutions it has been found out that, in contrary to /1/, the pre-peak response in P - d diagrams is characterized by several irregularities (Fig. 9). For example, upon velocity $v=1$ mm/s, the first peak value at $d=0.5$ mm (blue in Fig. 9) is followed by a downcome caused by local numerical problems which can clearly be seen in Fig. 7 (excessive local displacements; deformation scale factor: 10) and on ALLKE/ALLIE- d curve in Fig. 10. Just the curve for $v=2$ mm/s could be accepted for estimating P_{\max} as a measure for inertial effects. Differences in P_{\max} and irregularities are not caused by inertial forces directly but by the extreme numerical instability of the solution: Already a negligible parameter change (in this case the loading velocity v) effects on the solution path. Thus, simulations based on an anvil connector shape could not be used to identify the range of admissible velocities.

After this experience the influence of the loading velocity has been examined using the simplest possible example. The test beam $100 \times 100 \times 200$ mm consisting of concrete only (without any contact interactions and steel parts) was clamped on one end and loaded by prescribed displacement of -25 mm on the opposite surface. Again, linear increasing displacement was prescribed. Following constant velocities were used: $v=0$ (static solution), 0.5, 5, 25, 100, 500, 1000 mm/s.

ABAQUS CDP material model and C3D8R elements were used. Because of twofold symmetry only $1/4$ of the beam has been meshed. In Fig. 11 the final deformed shape with Mises stress upon $v=5$ mm/s can be seen. The corresponding P_{\max} - v diagram in Fig. 12 conforms to expectations. In Fig. 13 the pre-peak response up to $v=5$ mm/s is free of irregularities (diagram parts with $d > 2$ mm do not contain any substantial information and are omitted). Clear visible is the force delay upon $v=100, 500$ and 1000 mm/s due to the distance between the surface on the left with applied displacement d and the clamped surface on the right with the reaction force P . Thus, upon higher velocities the solution is ever more dominated

by inertial effects unacceptable in a quasi-static structural response. ALLKE/ALLIE values in Fig. 14 confirm the conclusion that in this type of problems the constant loading velocity should not exceed, let's say, just to be sure, 10 mm/s.

However, also the difference between ABAQUS procedures is to be noticed. With the procedure *STATIC ($v=0$) the peak load of $P_{max}=115.2$ kN is slightly higher than with the procedure *DYNAMIC,EXPLICIT ($v=5$ mm/s: $P_{max}=109.9$ kN), both being used with NLGEOM=YES..

At last, push-out test simulations based on a crown shaped connector (in /1/ loaded by $v=0.5$ mm/s) have been recalculated using additional loading velocities $v=5, 25, 100, 1000$ mm/s. As in /1/, support with contact interaction, concrete material CDP M2, dilation angle $\psi=36.31$, friction coefficient $f=0.3$ and NLGEOM=YES were used.

Corresponding P-d curves can be seen in Fig. 15 (diagram parts with $d>10$ mm do not contain any substantial information and are omitted). The P-d curve for $v=0.5$ mm/s was already given in Fig. 27 of /1/.

Generally, P-d curves for support with contact interaction are characterized by oscillations, the same curves for clamped support are smooth (Fig. 28 in /1/). In Fig. 15 only the curves $v=0.5$ and $v=5$ mm/s are acceptable. The bifurcation of P-values after reaching peak area could not be explained yet. The reason is probably again an extreme numerical instability of the solution process.

With $v=25$ mm/s and more, oscillations become dominant and influenced by inertial effects. Also the force delay is clear visible. The ALLKE/ALLIE values in Fig. 16 are acceptable for $v=0.5$ and $v=5$ mm/s only.

In Fig. 17 Mises stress is shown to demonstrate the influence of inertial effects. Upon the velocity $v=1000$ mm/s the lower red part of the steel connector moving to the right is already upon $d=0.76$ mm (ideally) plastic, whereas the support reaction force on the specimen right side still equals zero. The yielding area in this case is not originating around contact points with concrete as usually but due to prescribed fast growing displacement on lower connector surface.

A general recommendation concerning the highest admissible loading velocity for numerical simulation of push-out tests can not be given. It is not easy to distinguish whether the difference in peak values and/or calculation break were really caused by inertial effects or by taking a different solution path. The critical velocity value depends on many parameters, e.g. connector shape, mesh quality, boundary conditions used, way how the loading is applied, and so on. Therefore, not only P-d curves should be compared but also ALLKE/ALLIE values have to be checked and the deformed mesh should be carefully visually inspected throughout the solution. At least two calculations with different loading velocities are to be carried out. If the results differ substantially, the reasons have to be investigated in more detail.

9. USING NLGEOM AND DOUBLE PRECISION

This option on the data card *STEP controls the inclusion of nonlinear effects of large displacements. With static procedures in ABAQUS/Standard default setting is NLGEOM=NO, with the procedure *DYNAMIC,EXPLICIT in ABAQUS/Explicit default setting is NLGEOM=YES.

In /1/ all calculations have been carried out taking into account the nonlinear effect of large displacements. In dynamic calculations in post-peak response this has led to very long calculations offering at last nonrealistic distorted FE-mesh by far not corresponding to the brittle behavior of concrete especially in situations with no or little reinforcement. E.g. the curve $v=0,5$ mm/s in Fig. 15 ends at $d=23,6$ mm, but between $d=11,8$ mm (expressive ALLKE/ALLIE-peak) and $d=23,6$ mm (calculation collapse) the structure in Fig. 18 (suppressed Fig. 30 in /1/) is nonrealistic distorted and the calculation does not give any real information. Therefore, using NLGEOM=NO can be a reasonable alternative generally, not only if BRITTLE material model is used.

Generally, always DOUBLE PRECISION solution should be used. Upon SINGLE PRECISION the solution process aborts prematurely and using NLGEOM=YES does not change the situation substantially.

10. ABAQUS VERSIONS 653 AND 662

For calculations in /1/ ABAQUS version 653 was used. At TU Vienna shortly a new computer system came into service using ABAQUS version 662. Calculations on both systems with the same input file showed in P-d diagram considerable differences in post-peak area. The reason could not be explained yet.

11. CONCLUSIONS

The basic question is which goals are to be fulfilled by numerical simulation of physical push-out tests. A pure matching of the P-d curve from an existing physical test can be achieved also by using a coarse FE-mesh, inadequate material model "sometimes without regard to the reasonableness of the material input variables" /9/ and controversial calculation parameters. Such a simulation, of course, keeps the simulation costs minimal. However, it proves rather the versatility of the FE-program and the user's inventiveness than an accurate representation of the physical behavior itself.

A consequent numerical simulation should not only match the data record from a foregoing physical test. It also should be able to reduce the number of physical tests in the course of selecting more effective connector shapes. This goal can be achieved only by a detailed visual inspection of analysis results get by a reliable FE-calculation. This has to be based on a sufficiently fine mesh (one linear finite element crosswise the modeled steel connector half-thickness is not sufficient to follow stress gradients), on a realistic material model (no "ideal plastic concrete" in tension), on a tolerable loading velocity (for safe excluding of additional inertial forces), etc. In case of doubts the influence of an unknown (e.g. material) parameter has to be checked by changing its value and repeating the calculation.

In near future the authors will continue developing of new connector shapes accompanied by exploring the influence of reinforcement location on properties of specific connector shape in composite steel and concrete beam structures.

Acknowledgment

The corresponding author thanks to Wojciech Lorenc for valuable and inspiring discussions /10/. Other research colleagues are encouraged to join and exchange experiences, too.

References

1. Fink J., Petraschek Th., Ondris L.: Push-Out Test Parametric Simulation Study of a New Sheet-Type Shear Connector, in: Projekte an den zentralen Applikationsservern, Berichte 2006, Zentraler Informatikdienst (ZID) der Technischen Universität Wien, Wien 2007, pp. 131-153, also: <http://www.zid.tuwien.ac.at/projekte>
2. Fink J., Petraschek Th., Ondris L.: Neuartige Schubverbinderleisten – experimentelle Untersuchungen und numerische Vergleichsbetrachtungen, ÖIAZ, accepted for publishing 2007
3. Hibbitt, Karlsson & Sorensen, Inc.: ABAQUS/CAE, ABAQUS/STANDARD, ABAQUS/EXPLICIT, Dokumentation Ver. 6.5.3, <http://www.abaqus.com>
4. ABAQUS Verification Manual, 2.2.24
5. ABAQUS Example Problems Manual, 2.1.15
6. Jefferson A.D., Bennett T. and Hee S.C.: Fracture Mechanics Based Problems for the Analysis of Dam Concrete, NW-IALAD-Final Technical Report-Task Group 2.4, Cardiff University (UWC), 15. March 2005
7. Zimmermann S.: Finite Elemente und ihre Anwendung auf physikalisch und geometrisch nicht-lineare Probleme, Report TUE-BCO 01.05, Technische Universität Eindhoven, Niederlande, März 2001
8. Iwancsics M.: Numerische Untersuchungen zu neuartigen Schubverbindern, Diplomarbeit, Institute of Steel Structures, TU Vienna 2007
9. Evaluation of LS-DYNA Soil Material Model 147, Report No. FHWA-HRT-04-094, November 2004, Federal Highway Administration, 6300 Georgetown Pike, McLean, VA 22101-2296
10. Lorenc W., Institute of Building Engineering, Wroclaw University of Technology: Private Communication 2006-2007



Fig. 1 Push-out specimen's welded steel parts

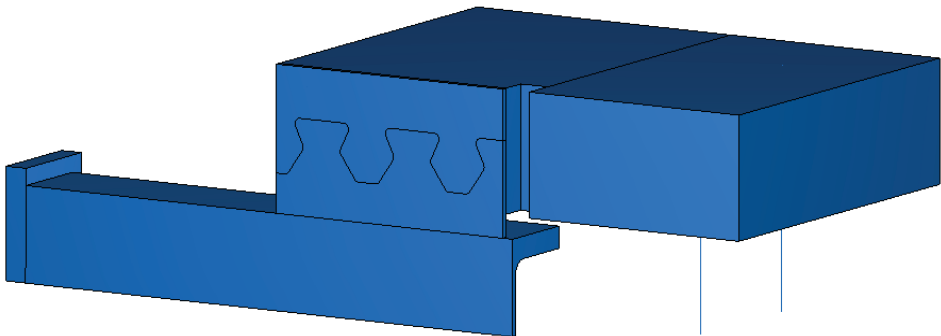


Fig. 3 Basic parts of the FE-model with twofold symmetry



Fig. 2 Complete push-out-specimen ready for testing

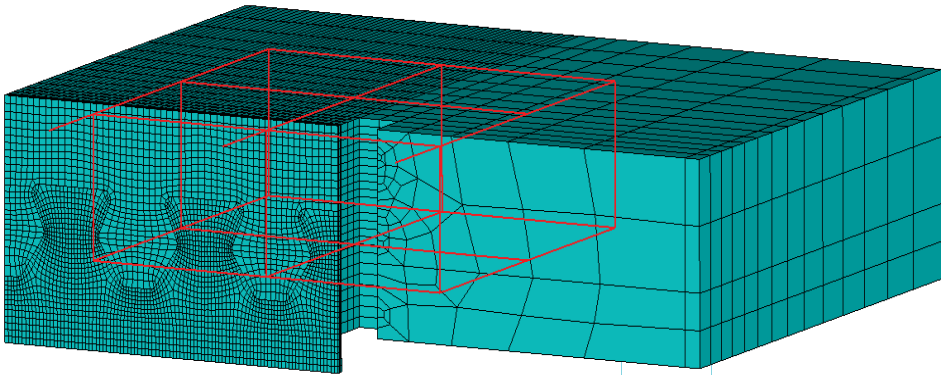


Fig. 4 FE-mesh for dynamic analyses incl. reinforcement, contact support on the right

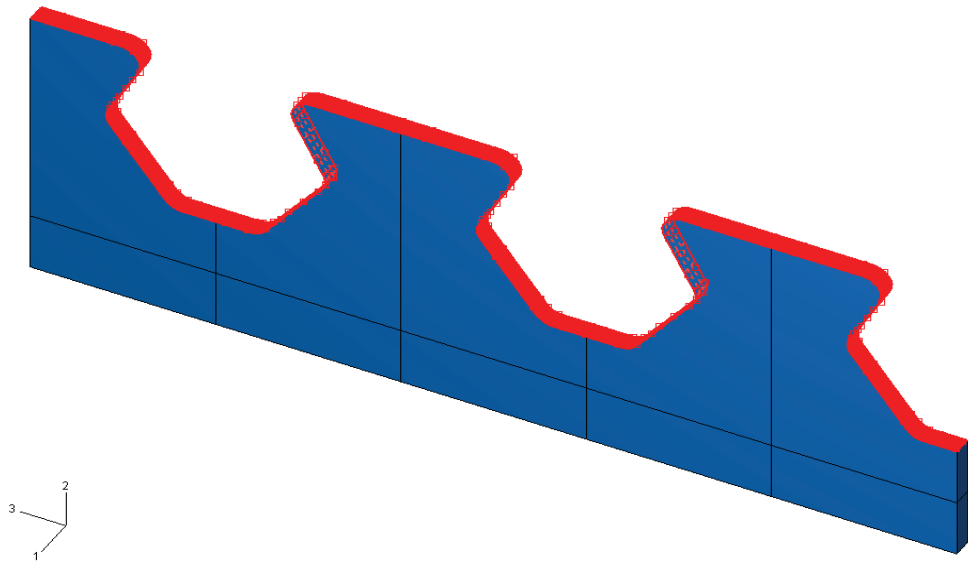


Fig. 5 Frontal master contact surface of the steel connector

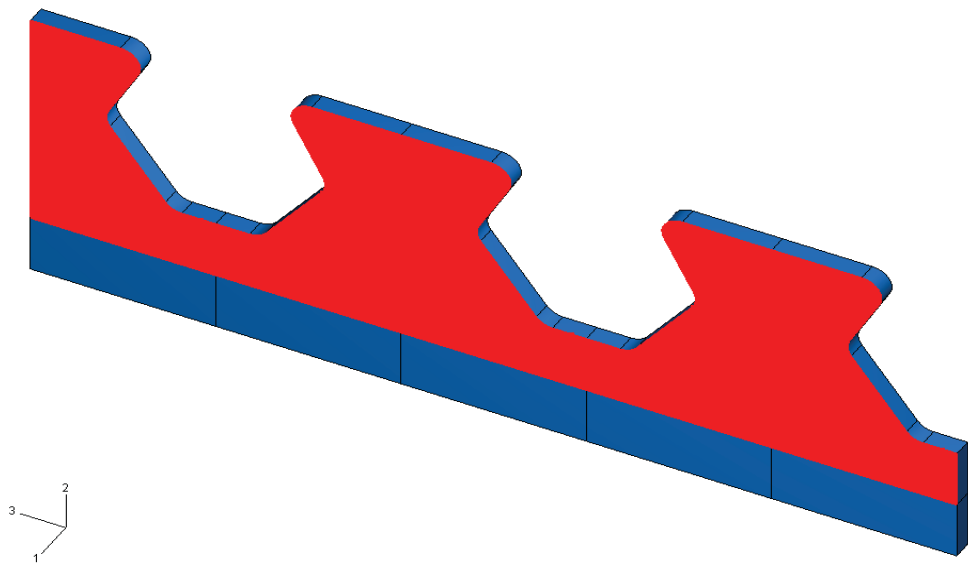


Fig. 6 Lateral master contact surface of the steel connector

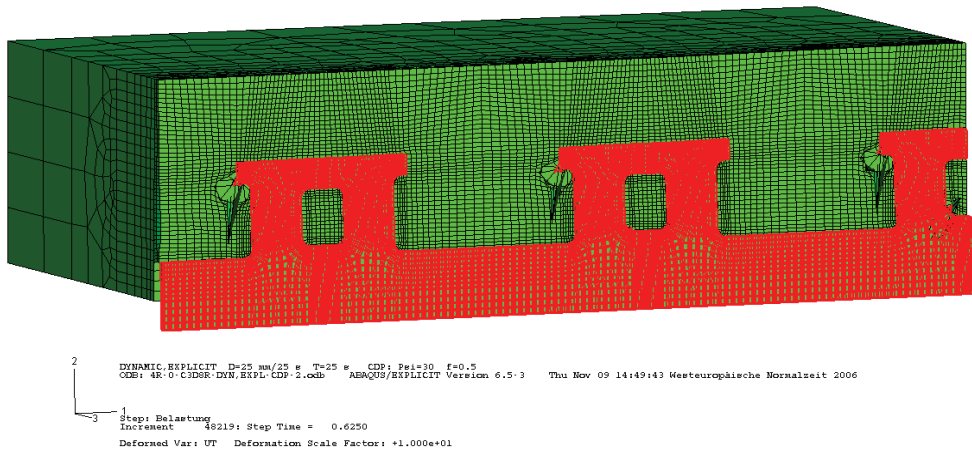


Fig. 7 FE-simulation with anvil shape connector, $v=1$ mm/s, $d=0.625$ mm

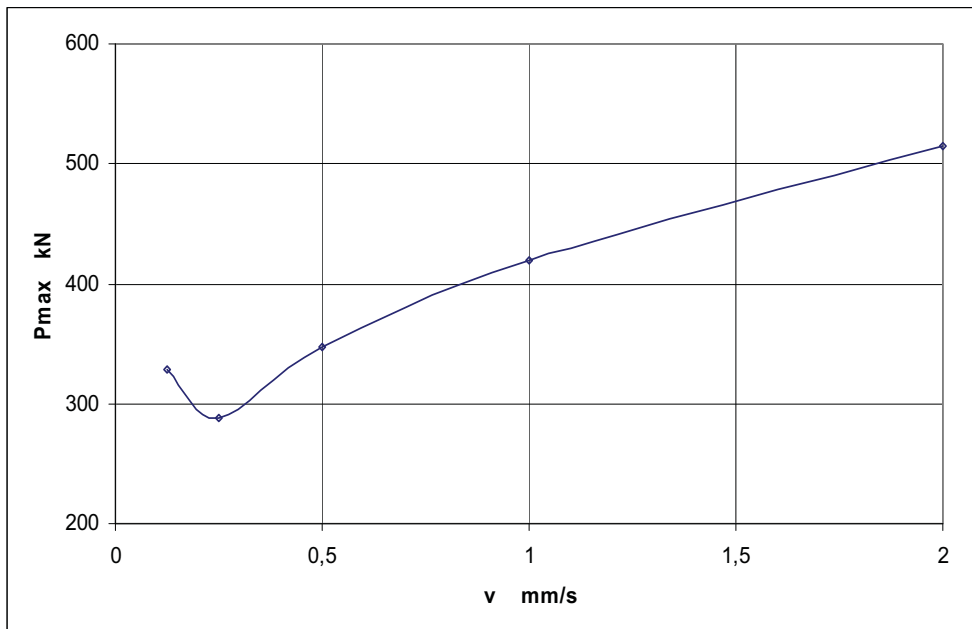


Fig. 8 Pmax – v curve, anvil shape connector

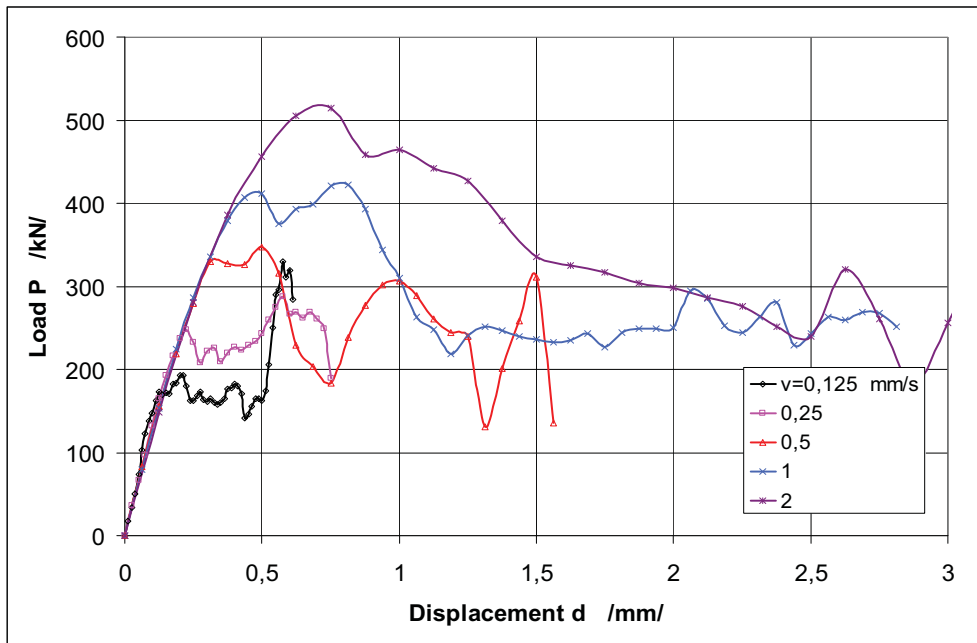


Fig. 9 P-d curves, anvil shape connector

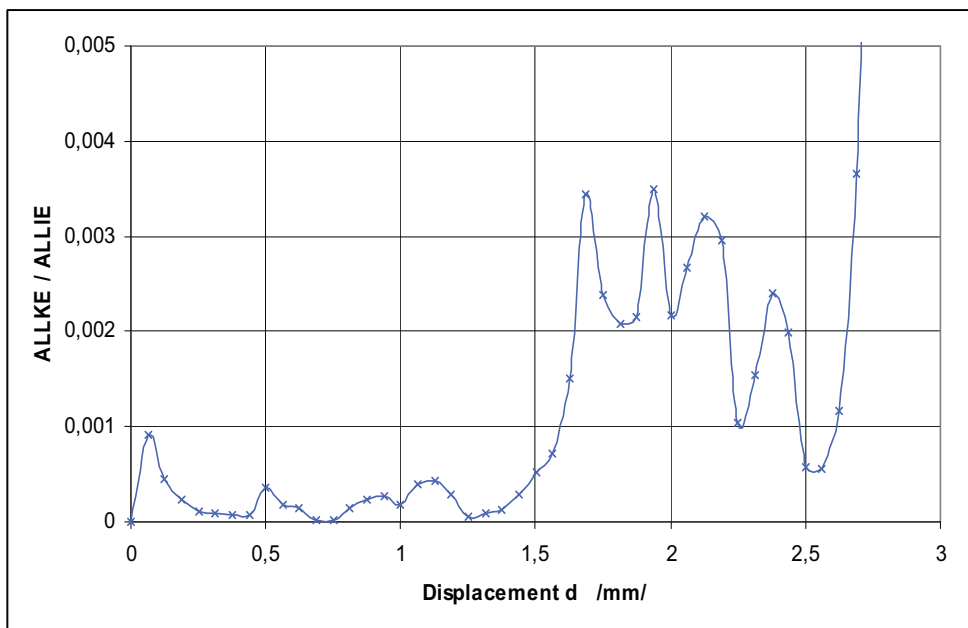


Fig. 10 ALLKE/ALLIE-d curve, anvil shape connector, $v=1$ mm/s

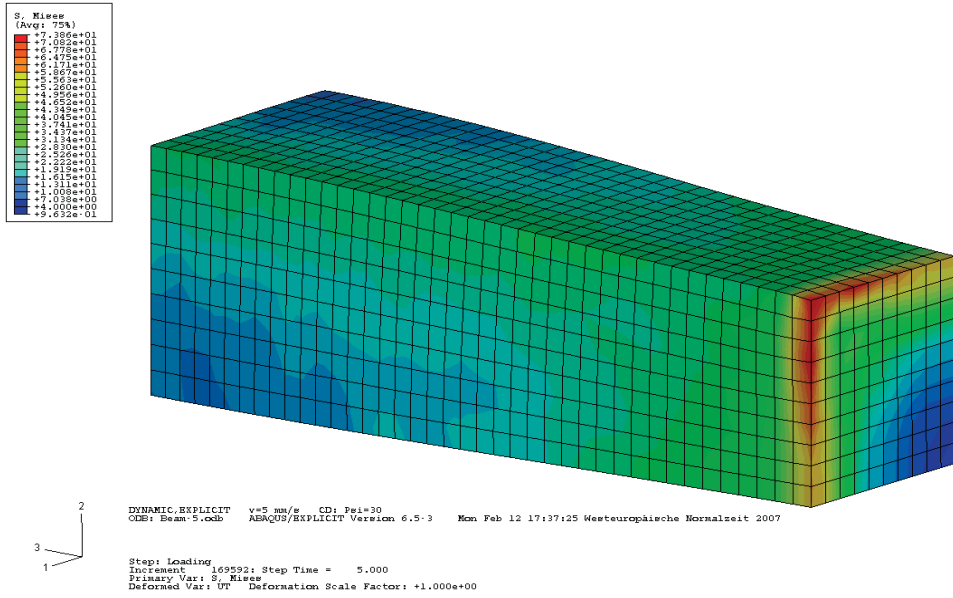


Fig. 11 Simple concrete beam with displacement controlled loading

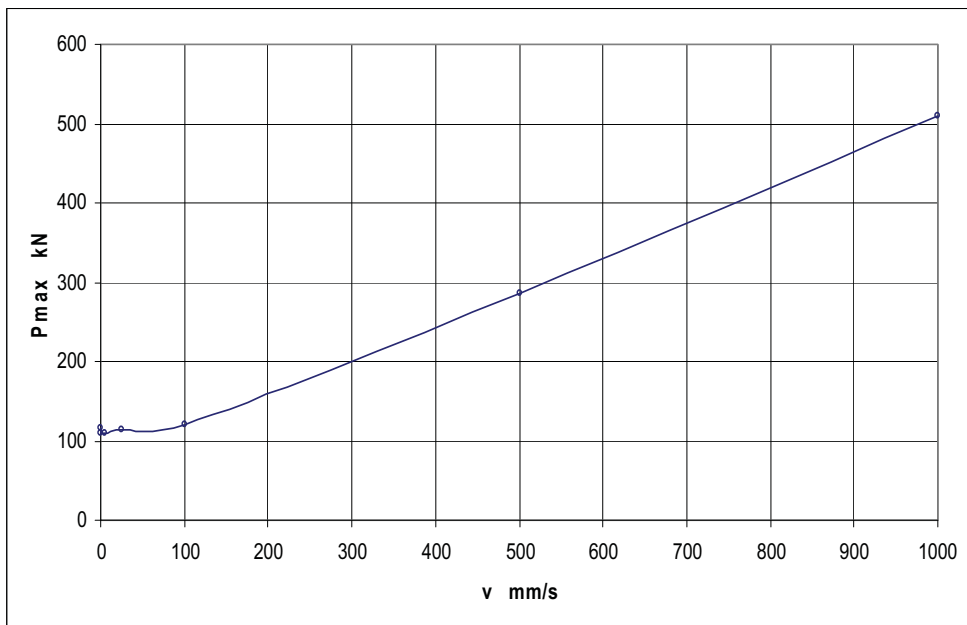


Fig. 12 Pmax – v curve, simple concrete beam

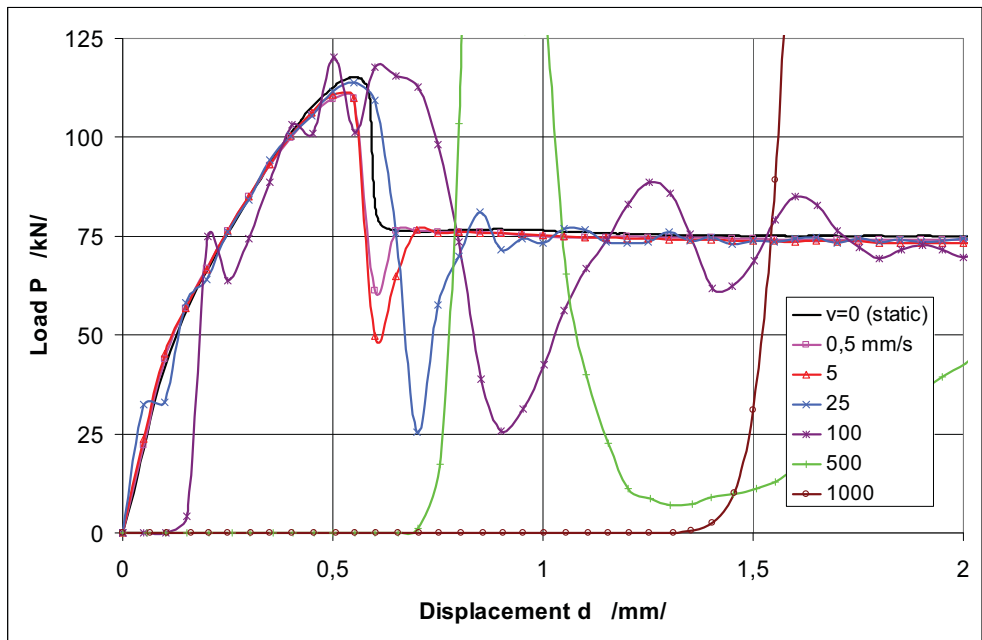


Fig. 13 P-d curves, simple concrete beam

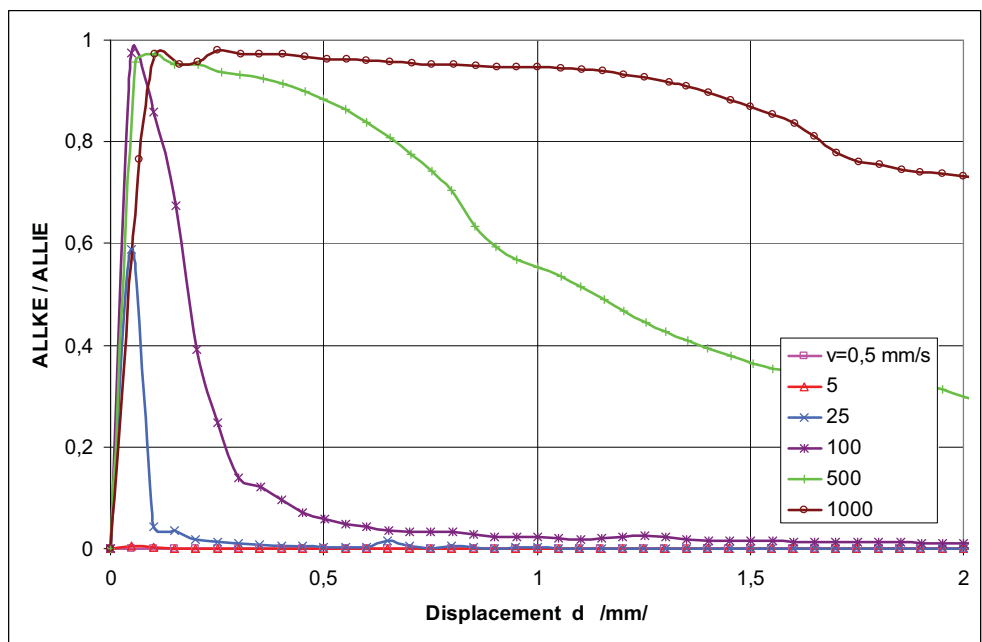


Fig. 14 ALLKE/ALLIE-d curves, simple concrete beam

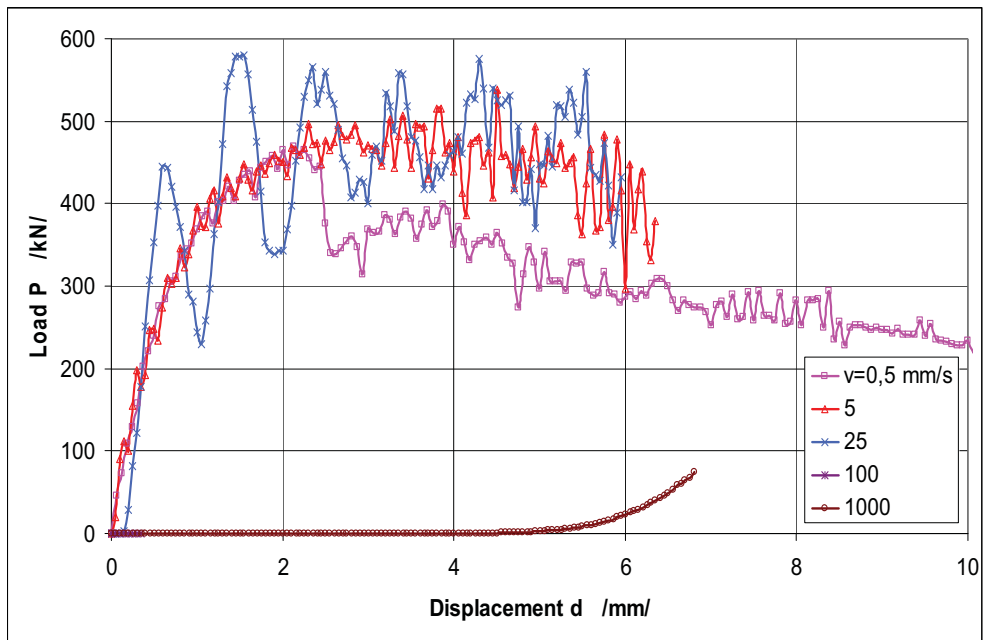


Fig. 15 P-d curves, crown shaped connector /1/, NLGEOM=YES

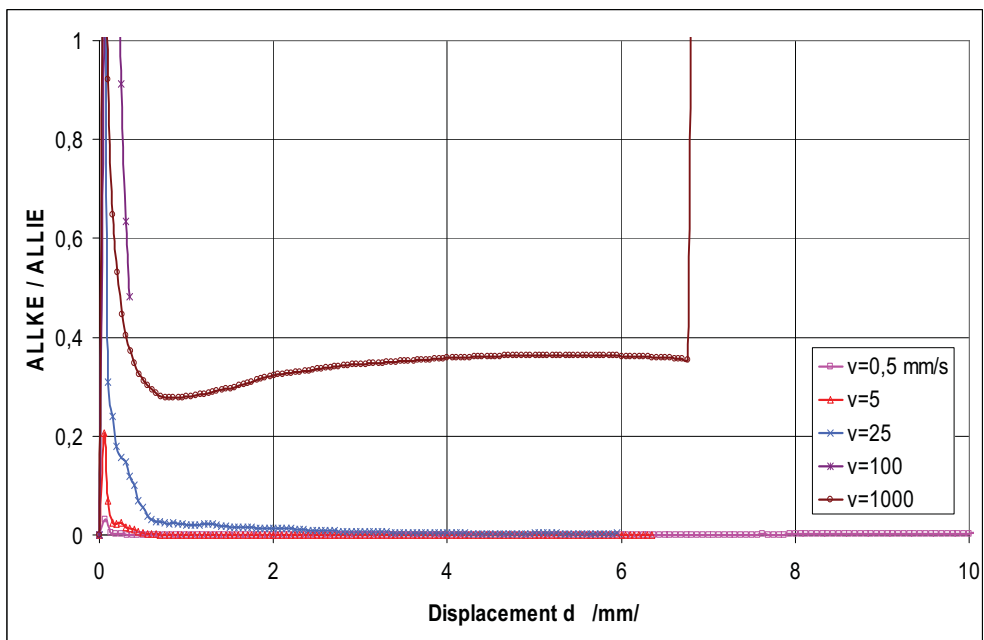


Fig. 16 ALLKE/ALLIE-d curves, crown shaped connector /1/, NLGEOM=YES

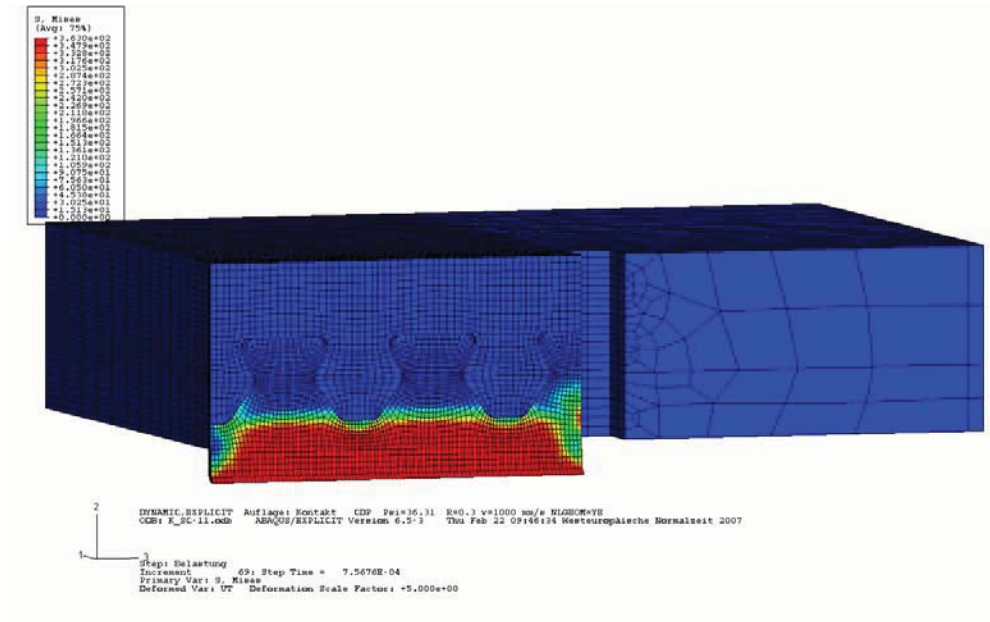


Fig. 17 Crown shaped connector /1/, NLGEOM=YES, v=1000 mm/s, d=0.76 mm

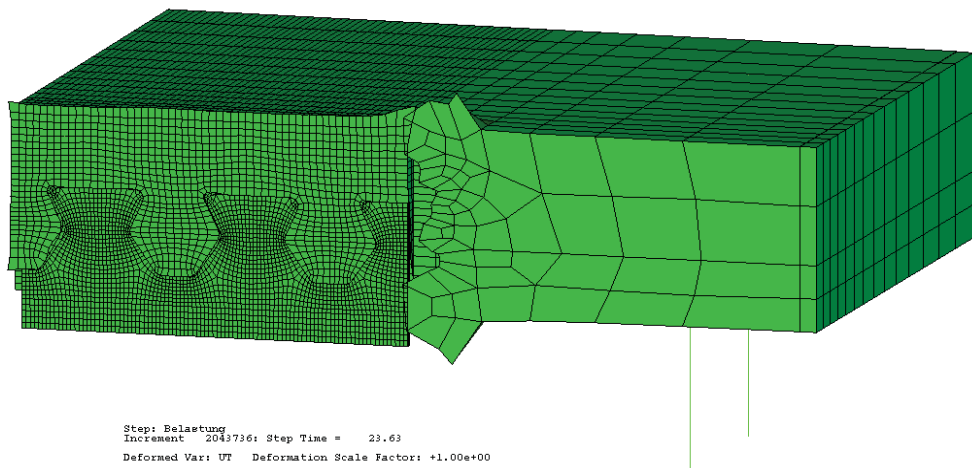


Fig. 18 Crown shaped connector /1/, NLGEOM=YES, v=0,5 mm/s, d=11,8 mm

The Structural Expertise of Steel Cables

Ludovic G. Kopenetz, Ferdinand-Zsongor Gobesz

*Department of Structural Mechanics, Faculty of Civil Engineering and Building Services, Technical
University of Cluj-Napoca, Cluj-Napoca, 400020, Romania*

Summary

Considering the fact, that steel cables are structural elements forming statically determinated systems, their rupture can lead to catastrophe. In this context, the structural assessment of steel cables represents a primary necessity, generated by the requirement to assure security and safety in use.

Generally the main causes which induce degradation/deterioration of cables are: fatigue and corrosion.

The effects of corrosion and fatigue are displayed usually through fiber laceration sequent to a certain service time, after which the number of ruptures and lacerations increases exponentially.

This paper covers some problems of structural expertise along with numerical simulation aspects of corrosion and fatigue, as well as a methodology for the deduction of the presumed service life of steel cables.

KEYWORDS: steel cable, structural expertise, corrosion, fatigue.

1. INTRODUCTION

The irrefutable qualities of bearing cable structures justify, from one part the extension of their application area, from another part the remarkable effort for world-over research concerning a better insight and knowledge about their behavior under corrosion and fatigue, envisioning a safer and more judicious design.

The aim of the authors through the submission of this paper is to present some aspects of their research done by the Faculty of Civil Engineering and Building equipments from the Technical University of Cluj-Napoca.

Since the middle of 70' the pursuit of this kind of research was focused in the following directions:

- Tests carried out in situ (generally considering only statical behaviour, just infrequently considering dynamical too), including the exact quantification of cable structure geometry based on survey techniques. Due to the fact that those kinds of structures are located usually at considerable heights, the applicable survey techniques have a dynamic character, recording also the swing and vibration of the structure and the movements induced by dynamic loads (wind, functioning equipment, traffic).
- Laboratory tests, in order to identify the structural materials through physico-mechanical and chemical analysis.
- Statical and dynamical analysis and calculus, including the evaluation of the service time for every structural component considering possible future loads and actions over the operative period.

It has to be pointed out the complex and time consuming character of any credible structural expertise in this field, considering the vastity of involved factors which are combined with the unstationary character of the loads (wind, temperature, vibrations from equipment and traffic etc.) [9], [10], [11].



Figure 1. The Agigea Bridge from Romania

2. CABLES AND TIE-BACKS IN MEMBRANOUS CABLE STRUCTURES

Common materials used in cable fabrication during history were: papyrus, camel hair, flax and hemp, until in 1834 when the first cables and ropes from steel wires were made. This new building material soon became indispensable in many fields, due to its special properties – high breaking strain compared to its self weight, great flexibility and durability [17]. In the field of construction, cables were used initially as bearing parts for suspended bridges, and much more lately for covering large areas without intermediate holders [18].

In the last period, in highly corrosive environments, cables made from polypropylene (specific cable weight / specific water weight = 0.91), polyester and nylon (specific cable weight / specific water weight = 1.14) are used.

2.1. Steel qualities and brands for cables and tie-backs [19], [20]

Cables and tie-backs are made from high- and very high-grade steel, with an average carbon content of 0.5% and a breaking strain around 60 daN/mm². Considerable growth of mechanical strength can be obtained through repeated deformations applied on steel rods during the fabrication process of wires. Thus, a cylindrical steel bar is transformed on the drawbench in wire, while its breaking strain rises up to 120 – 200 daN/mm². After that, the wire is subdued to a thermal treatment and hereby the material regains its plastic properties. The wire yarns are entwisted on a central wire, in one or more layers, composing strands. At their turn, the strands are coiled around a central core, forming the cable.

Nowadays in Romania two types of steel are used in the fabrication of wires which can be embodied in cables:

- carbon steel with 0.6 – 0.9% C and 0.3 – 0.7% Mn,
- thin alloyed steel, usually with manganese and silicon.

From carbon steel are wires with smooth (SBP) or marked (SBPA) surface made, each type in two qualities (I and II). From thin alloyed steel, high strength rods (PC90) are produced, with geometrical, chemical, mechanical and technological properties prescribed by the STAS438/1-74 standard.

The semi-product which is used in the fabrication of strands and cables is the proprietary carbon steel wire (through initial thermal treatment the steel is heated up to 880 – 930 °C, followed by a quick cooling to 450 – 500 °C in a lead bath after which the cooling continues slowly in the air) and drawn SBP type wire (the laminated wires are forced on a drawbench through a smaller hole than the actual diameter of the wire) without final annealing treatment.

The cables can be classified upon several criteria:

- Classification based on shape: The cables can be flat or round shaped. At their turn, round shaped cables can be simple (made from a single strand), double (composed from several strands) or coupled (formed by wrapping double cables around a central core).
- Classification according to the number of strands: Cables can be made from 1, 6, 8, 18 or 36 strands.
- Classification upon the core material: The cable core can be manufactured from vegetal, mineral, metallic or synthetic wires.
- Classification after the quality of fibers: Steel cables can be produced from uncoated (mat) or zinc coated wires.
- Classification upon the laying of strands: The wire yarns can be coiled in a strand towards right (Z) or left (S). At their turn, the strands can be wrapped within a cable towards right (Z) or left (S).

2.2. Bearing structures with cables

From the point of view of structural analysis, bearing structures with cables can be divided in the following two categories:

- isolated cables,
- cable nets and suspended structures.

Considering these structures, cables can be:

- isolated parallel or twisted wires,
- fascicles of stranded wires,
- ropes,
- thin steel rods,
- ribbons,
- chains,

arranged in one direction or in different directions (Fig. 2).

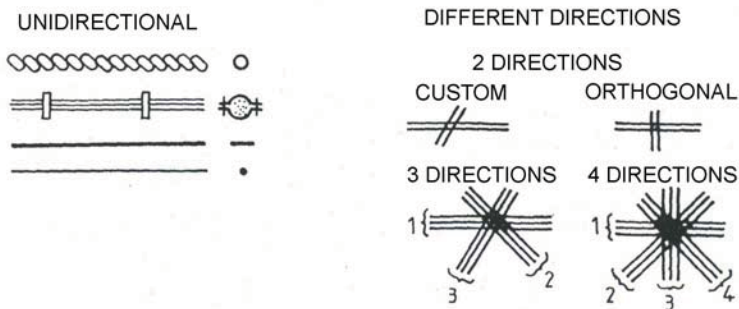


Figure 2. Different cable types

A synthetically exhibition of bearing structures with cables is presented in fig. 3.

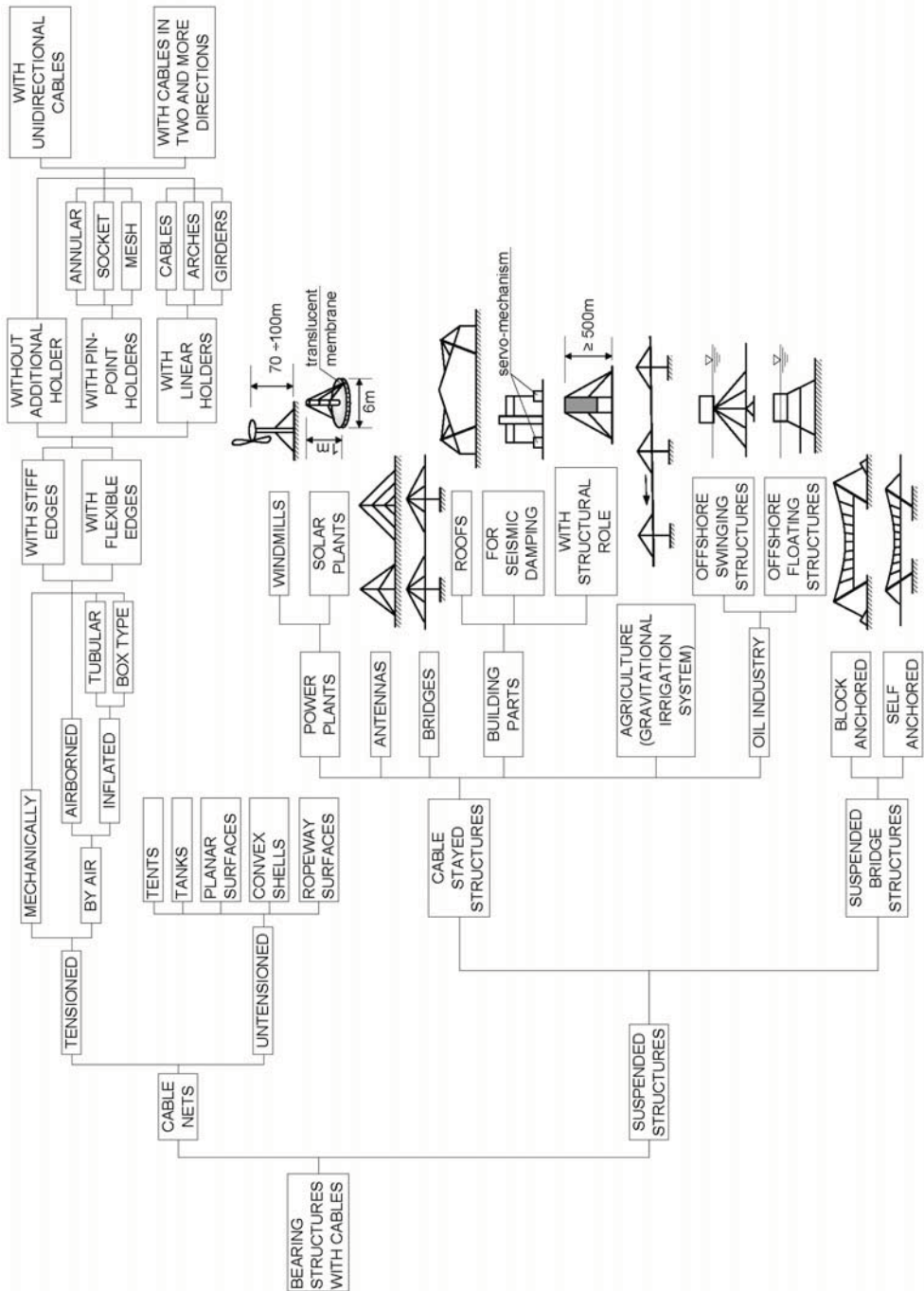


Figure 3. A classification of bearing structures with cables.

3. EXAMINATION FACETS FOR STRUCTURAL CABLES

In case of structural cables the problems which are generating noticeable modifications of the structural safety can be grouped in the following classes:

- Problems concerning the quality of the constitutive material (cold flow, brittle or breaking in different manners etc.).
- Fatigue problems due to repeated stress.
- The problem of considerable displacements caused by static and dynamic loads.
- Corrosion and erosion problems.

Bearing structures with cables are characterized by loads which are strongly depending from the basic geometry of the structure, namely by the initial balanced state (including also the geometrical and physical imperfections) induced by the steady and working loads and by eventual prestressing.

The expertise and checking of these structures must be done by studying the nonlinear geometrical (eventually physical) behaviour and all the factors upon which relies the structural safety. As a decisive element rises in this context the occurrence of corrosion and endurance to oligocyclic fatigue. The resistance to oligocyclic fatigue will be studied from secondary stresses (from vibrations or from daily thermal expansion – contraction) considering the intensity of the stress range.

3.1. Loads on structures with cables

The main loads applied on bearing structures with cables are arising from self weight, wind pressure, temperature, working loads with connected dynamic effects and support displacements.

3.1.1. *The influence of weight*

The following effects will be considered from dead load, combined also with other loads and forces from different causes:

- active loads, containing self weight and snow build-up, ice (frost);
- inactive loads, containing the self weight of the structural element and other permanent loads.

3.1.2. *The influence of wind*

This action will be considered in the context of KÁRMÁN vortices, combined from case to case with the phenomena of galloping and fluttering.

3.1.3. *The influence of temperature*

The low environmental temperature must be considered in any cases. Structural elements with lower working temperature than 0 °C will be additionally loaded with ice (frost) through the condensation of the moisture from the atmosphere.

In case of cable sustaining tubular structures with closed ends, through the cooling of the built-in gas or steam the inner pressure can drop enough to create vacuum inside the tube. In such case these tubular structural parts must bear up to the external pressure at low temperature.

3.1.4. *The influence of dynamic effects*

Buildings with structural cables are checked against the detrimental effects of vibrations that can arise from several sources, such as:

- impact forces;
- resonance developing from the operation of equipments (including air conditioning and ventilation appliances, loud musical gears, traffic etc.);
- seismic actions and wind.

3.1.5. *The influence of thermal effects (expansion, contraction)*

Thermal effects should be considered in combination with loads and forces from other causes:

- thermal actions through constraints and restraints;
- effects due to different coefficients of thermal expansion in case of structures with mixed materials (like steel and aluminium).

3.2. Case of laboratory-tests

The minimal bench tests which are carried out in a laboratory in order to identify the compounding materials of bearing structures with cables are:

- axial extension test, at different velocities;
- repeated bending test;
- torsion test;
- chemical test of the base material;
- simulation of corrosion and fatigue.

3.3. Site investigations [21]

Examining the behavior in time (ageing property) of steel cables is a special assay, imposed primary by the necessity to insure operational safety. In situ tests will pursue:

- Diminution of cable section, namely *loss of metallic cross sectional area* (LMA) due to corrosion, plastic deformation (afterflow) etc. [22].
- Modification of the shape (geometry).
- Broken wires, laceration and other *local faults* (LF) due to fatigue [22].

In principle the following methods are used for site investigations:

- visual inspection,
- electrochemical (potential, electrochemical sounds, magnetic etc.) methods,
- other nondestructive testing (microscopical examination, gravimetry, infrared thermography, gammagraphy, radiography and radar processing) [23], [24], [25].

For structural cables only a few of these methods give adequate results.

For visual inspection carried out in site, the authors are advising a new method: MOV_CAM (currently under patenting), using sliding digital cameras in order to view and process the image of the cable (fig. 4).

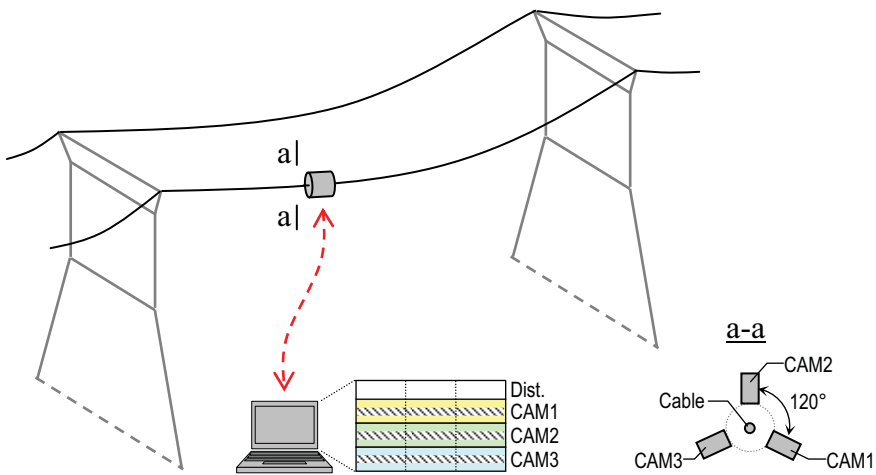


Figure 4. Visual investigation with digital cameras (currently under patenting).

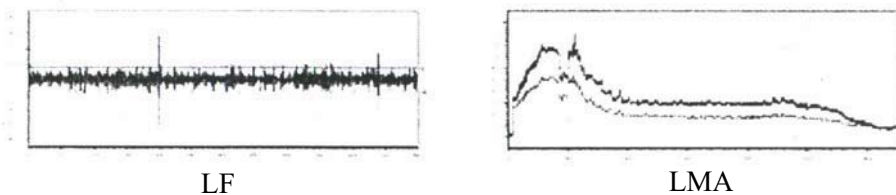


Figure 5. Sample results from LF and LMA testing.

For LMA and LF type investigations electromagnetic processes are successfully used lately, based on a magnetic head equipped with strong permanent magnets and sensors with distance meter. The software enables to inspect and to display the local faults (LF) and the sectional area diminishments (LMA) in a synthetically manner (fig. 5).

The investigation of the occurrence of corrosion in situ has a peculiar meaning, on one side due to the increasing intensity of the polluting agents in the environment, on the other side due to the requirement regarding the prolongation of the operational service time of cables.

Cables are highly sensitive to corrosion because their self constructional embodiment enables the penetration and stagnation of moisture.

One of the most delicate problems of structural engineering is to track and to keep under control the evolution of degradations caused by corrosion, because this aspect entail in time changes in the physico-mechanical properties and therefore in the strength of materials, leading also to stress redistribution in the structural elements. That is the reason why in the following part a method for monitoring the corrosion of steel cables and the principle of numerical simulation for this process will be described.










The acquisition of primary data about corrosion, in the case of cables, can be done with the method of electric resistance, which is easily applicable in situ. The method of electric resistance is based on the principle that cable corrosion is accompanied by cross sectional reduction. In this way, if there is no intercrystalline corrosion, the raising of electric resistance is produced by the diminution of the cross section.

In case of intercrystalline corrosion, the area of the cross section is not modified significantly, but the specific resistance increases. Thereby, measuring the electric resistance on different portions of a steel cable, considering 500 – 1000 mm long segments, the commencement of corrosion can be promptly recorded. Monitoring the corrosion of steel cables by the means of the electric resistance method enables the undelayed signaling of the occurrence of corrosion, including intercrystalline corrosion. This method is simple, safe and relatively cheap, implying low costs.

4. NUMERICAL SIMULATION OF CABLE CORROSION

The numerical simulation of corrosion can be done in order to study the phenomena in time, using probabilistic degradation functions or data acquired through monitoring. Some of the most frequently encountered fault types are presented in table 1.

Table 1. Typical patterns of wire rope degradation and failure [25]

Illustration	Short explanation
	<p>A “bird cage” caused by sudden release of tension and resultant rebound of rope from overloaded condition. These strands and wires will not return to their original positions.</p>
	<p>A close-up of a rope subjected to drum crushing. The distortion of the individual wires and displacement from their normal position is noticeable. This is usually caused by the rope scrubbing on itself.</p>
	<p>A wire rope jumped from a sheave. The rope itself is deformed into a “curl” as if bent around a round shaft. Close examination of the wires show two types of breaks – normal tensile “cup and cone” breaks and shear breaks which give the appearance of having been cut on an angle with a cold chisel.</p>
	<p>Localized wear over an equalizing sheave. The danger of this type wear is that it is not visible during operation of the rope. This emphasizes the need of regular inspection of this portion of an operating rope.</p>
	<p>A wire which has broken under tensile load in excess of its strength. It is typically recognized by the “cup and cone” appearance at the point of the fracture. The necking down of the wire at the point of failure to form the cup and cone indicates that failure occurred while the wire retained its ductility.</p>
	<p>An illustration of a wire which shows a fatigue break. It is recognized by the squared off ends perpendicular to the wire. This break was produced by a torsion machine which is used to measure the ductility. This break is similar to wire failures in the field caused by excessive bending.</p>
	<p>A wire rope which has been subjected to repeated bending over sheaves, under normal loads. This results in “fatigue” breaks in individual wires, these breaks being square and usually in the crown of the strands.</p>
	<p>An example of “fatigue” failure of a wire rope which has been subjected to heavy loads over small sheaves. The usual crown breaks are accompanied by breaks in the valleys of the strands, caused by “strand nicking” resulting from the heavy loads.</p>
	<p>A single strand removed from a wire rope subjected to “strand nicking”. This condition is the result of adjacent strands rubbing against one another and is usually caused by core failure due to continued operation of a rope under high tensile load. The ultimate result will be individual wire breaks in the valleys of the strands.</p>

The SACOC (*Structural Analysis of Corrosion for Cables*) software package is based on the finite element method and it proved to be very useful in the study of the corrosion of structural cables. A schematic block diagram of this program is presented in figure 6 [21].

The user can take advantage of several available degradation functions simulating cable corrosion in time, or he can use quantifications from site investigations gathered in a data base.

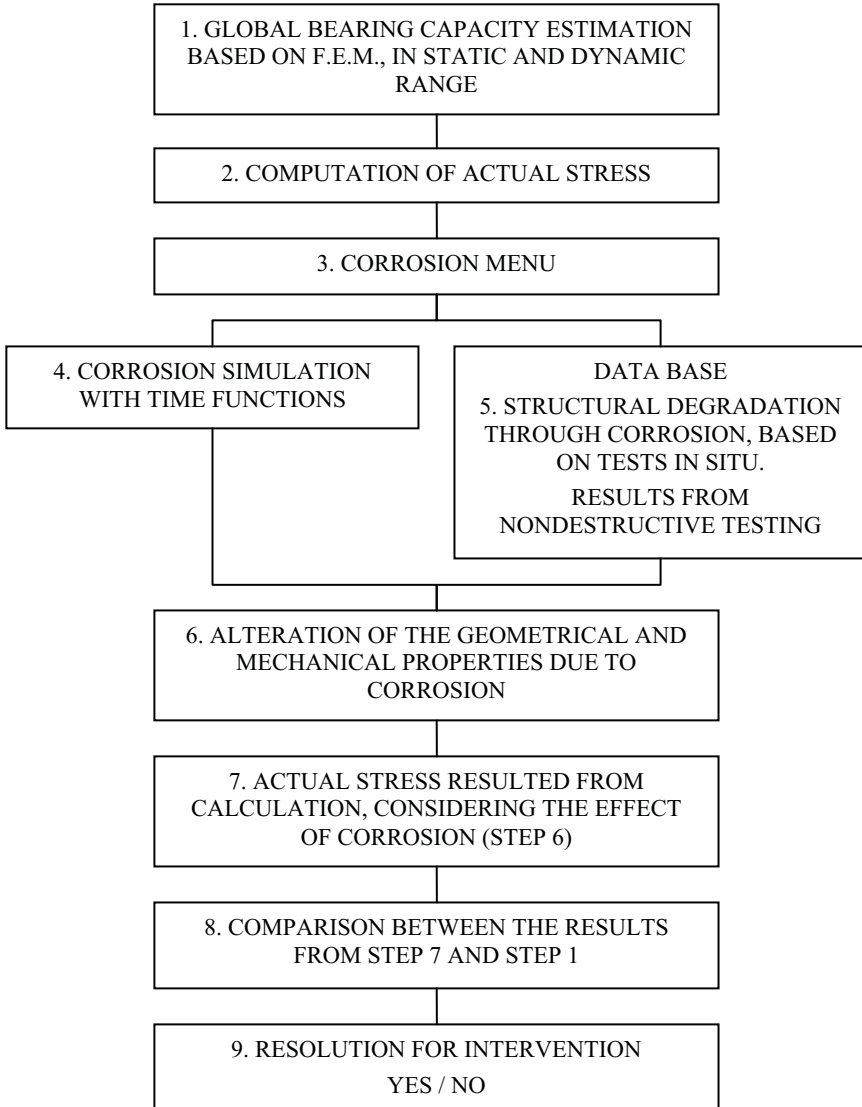


Figure 6. The schematic block diagram of the SACOC software.

5. CABLE QUALITY CERTIFICATION

The quality of cables is guaranteed by the manufacturer through quality assurance certificates, released for each product range. Deviations in dimensions, properties and shape shall not exceed the prescribed limits from the relevant Romanian technical regulations, nor those stated by the manufacturer. The list of standards for wires and steel cables is presented in table 2.

Table 2. The list of Romanian standards (STAS) in use

Pos.	Title	STAS code
1	Materials	880-66
2	Cold-drawn steel wires for drag ropes	1298-80
3	Steel cables. Concept and classification.	1710-79
4	Steel cables. Simple structure cables. Shapes and dimensions.	1513-80
5	Steel cables. Technical requirements.	1352-78
6	Steel cables. Double cables. Combined structure. Shapes and dimensions	1689-80
7	Steel cables. Combined cables. Double cables. Ordinary structure. Shapes and dimensions	1535-71
8	Steel cables. Combined cables. Triple structure. Shapes and dimensions	2693-80
9	Steel cables. Combined flexible double cables. Shapes and dimensions	1353-80
10	Steel cables. Flat cables. Shapes and dimensions	1559-80
11	Alternate bending test for steel wires	1177-74
12	Testing of metals. Torsion test for wires	1750-80
13	Testing of metals. Coiling test for wires	6622-70
14	Testing of metals. Tensile test for wires	6951-76
15	Testing of metals. Tensile test for steel cables	2172-74
16	Combined double concentric cables	2590-80
17	Steel wire for prestressed concrete	6484-77

6. CONCLUSIONS

Bearing structures with cables are liable to generate unappointed phenomena in comparison with conventional structures. Thus, beside the great displacements originated from their custom designed structural shapes, displacements arise due to the $\sigma_{breaking} / E$ ratio. While this ratio in case of conventional structures, considering OL37 steel is $3700 / 2100000 = 1 / 568$, in case of using cables becomes $15000 / 1650000 = 1 / 110$, namely five times bigger.

Zinc coated cables are able to withstand to corrosion approx. 10 – 15 years. For this reason, in case of highly corrosive environment should be remembered that high quality ropes and cables made from synthetic materials with outstanding endurance are available too.

The required anchoring of cables must be done by wrapping their end with cast zinc inside threaded pipes instead of using clamps, because the cable may slip out from the clamp at high dynamical stress.

Cables should be prestressed in a jointly manner with their anchors (thus the anchoring is tested) before installation, with a force equal to approx. 1.10 times the computed actual stress, in order to consume the significant remnant elongations and to avoid subsequent loosening and relaxation.

References

1. Falk, S., *Lehrbuch der Technischen Mechanik*, Springer Verlag, Berlin-Heidelberg, 1967.
2. Leonhardt, F., Zellner, W., Vergleiche zwischen Hängebrücken und Schrägkabelbrücken für Spannweiten über 600 m, *International Association for Bridge and Structural Engineering*, vol. 32, 1972.
3. ***, Bibliography and Data Cable-Stayed Bridges, *Journal of the Structural Division*, ST10, 1977.
4. Knut, G., Merkblatt-496, Ebene Seiltragwerke, *Beratungstelle für Stahlverwendung*, Düsseldorf, 1980.
5. Kopenetz, L. G., Ionescu, A., Lightweight Roof for Dwellings, *International Journal for Housing and its Application*, vol. 9, No. 3, Miami, Florida, USA, 1985.
6. Haug, E., Engineering Contributions to the Design of Lightweight Structures via Numerical Experiments, *2nd International Symposium Weitgespannte Flachentragwerke*, University of Stuttgart, 1979.
7. Jensen, J. J., *Das Dynamische Verhalten Eines Vorgespannten Kabelnetz*, University of Trondheim, Norway, 1972.
8. Goschy, B., Dynamics of Cable-Stayed Pipe Bridges, *Acier-Stahl-Steel*, No. 6, 1961.
9. Szabó, J., Kollár, L., *Függőtetők számítáása*, Műszaki Könyvkiadó, Budapest, 1974.
10. Otto, F., *Das Hängende Dach*, Bauwelt Verlag, Berlin, 1959.
11. Oden, J. T., *Finite Elements of Nonlinear Continua*, McGraw-Hill, 1972.
12. Krishna Prem, *Cable-Suspended Roofs*, McGraw-Hill, London & New York, 1979.
13. Fuller, B. W., *Weathering of neoprene-coated Nylon fabric*, E. I. Dupont de Nemours & Co., Report BL-327, 1956.
14. Otto, F., Trostel, R., *Zugbeanspruchte Konstruktionen II*, Ullstein Verlag, Frankfurt-Berlin, 1966.
15. O'Brien, T., General Solution of Suspended Cable Problems, *Journal of the Structural Division*, ST1, Febr. 1967.
16. Sofronie, Ramiro, Vertical Deflection of Suspension Bridges, *Revue Roumaine Scientifique Technique-Mécanique Appliqué*, Tome 24, No. 3, București, 1979.
17. Mollmann, H., *A Study in the Theory of Suspension Structures*, Copenhagen, 1965.
18. ***, *Recommendation for Guyed Masts*, The Working Group on Guyed Masts of I.A.S.S., 1981.
19. Kopenetz, L. G., Cătărig, A., *Cabluri structurale*, Simpozionul Tehnologie și Siguranță, U.T. Pres, Cluj-Napoca, 2004. (in Romanian)
20. Kopenetz, L. G., Cătărig, A., *Teoria structurilor ușoare cu cabluri și membrane*, U.T. Pres, Cluj-Napoca, 2006. (in Romanian)
21. Kopenetz, L. G., Cătărig, A., *Probleme ale coroziunii cablurilor din oțel*, Lucrările celei de a VII-a Conferințe de Construcții Metalice, vol. 2, Timișoara, 1994. (in Romanian)

22. ***, GTU Documentation, USA (Nondestructive Testing Technical Diagnostics).
23. Knut, G., On the Fatigue Strength of Wires in Spiral Ropes, *Journal of Energy Resources Technology*, vol. 107, 1985.
24. ***, Internal Report, Bethlehem Wire Rope, USA.
25. ***, Technical Report No. 107, Wire Rope Corporation, St. Joseph, MO, USA.
26. Bârsan, G. M., Kopenetz, L. G., Alexa, P., Theil, S., Gedanken zum Entwurf Leichter Zusammengesetzter Tragwerke, Proceedings of the 4th Conference on Steel Structures, Timisoara, Romania, 1985.

Computer aided building diary

Mária Kozlovská¹ and Michal Danko²

¹Technical University of Kosice, Faculty of Civil Engineering, Slovakia

²Inzinierske stavby, a.s. Kosice, Slovakia

Summary

One of the main and also generally obligatory tools for building site works management is the site diary. The building code orders to building manager the building diary leading. In the sense of the code, the building site diary is the document, which is the part of documentation available on building site and in the document are noticed all relevant events, which have happened on the site.

The article describes possibilities of better building diary leading, as the main document for managing and monitoring of works on building site by computer support. Also describes design, structure and architecture of electronic tool as well as collaboration of database environments. The article presents real examples of computer aided building site diary paper forms.

KEYWORDS: building, site diary, electronic tool

1. INTRODUCTION

The code also determines that the building diary has to be written from the first day of preparation works till construction works finish and also who is competent to write into the diary. According to law, by which are executed some dispositions of the building code, into the building diary are written all important conditions concerning a structure building up:

- notes about divergences from project documentation verified by surveyors office in building process or from conditions dedicated in building permission or in other resolution or proceeding,
- facts influencing building works and building process, especially time flow of works, temperature in relation to building works, especially with wet production process, weather,
- date of building site visit, found facts and steps of the person competent to do state building surveyor and the person doing state inspection,

- records of project engineer and of partial projects designer or of architectonic product author, geodesist and cartographer of the structure,
- records of investor or his empowered person or the structure owner, if he is not investor,
- records of the person making building inspection or capable person, which manages building process, building contractor,
- data about elimination of building faults and back-logs according to structure inspection decree conditions.

But the reality on many building site is such, that the records are not written daily, often are made after longer time period, sometimes only before the building disposition. Then they are only short information about weather, worker and equipments amount, in better case are written performed building processes but only in outline version.

2. THE BUILDING DIARY VALUE

The building site diary leading has its purpose, as well as irreplaceable value for all building participants. That is why are in following text presented some principles and good advices how write the diary in the manner, that the diary should be an effective management tool. The building diary presents also the most effective form of communication among building participants, which flows from law practice principles, demanding reliable presentation of all facts connected with building. The building diary in the sense of effective management tool must imply complex data, which are necessary not only for real state monitoring, but also for the building process management. The records written into building diary by particular building participants are the basis for follow change management what is inseparable part of every building activity. That is why the building site diary is the main tool of operative works management on building site.

The areas, which management is for the building diary essential:

- the building processes performance (data about workers, machines, products, materials, practices,)
- time schedule of works, building works quality
- occupational health and safety
- environment protection
- conditions of building site (production, social, operative, climatic...)
- financial controlling (performed works billing, internal accounting, ...)
- contract parameters accomplishment (eventually change actions)

In small or technically simple buildings can be the diary retrieved by simple record about the structure, which investor writes and also person who special inspections do, signs the record. In the record must be written also building works amount, which perform on building site other corporate and natural persons besides the investor.

RECOMMENDED STRUCTURE (MAP) OF THE SITE DIARY

INTRODUCTION PAPERS

Cover front page	<ul style="list-style-type: none"> ▫ Contractor ▫ Diary number ▫ Registration numbers of records sheets ▫ The building
General part	<ul style="list-style-type: none"> ▫ Main sheet – the building name, place and date of the beginning, building number, contractor, project engineer, building manager, technical supervyvor of investor, investor, subcontractors ▫ List of main evidences about building: contracts of building participants, protocol of building site transmission, additions and changes of contracts, ... ▫ List of building documentation – evidence of documentation available on building site ▫ Survey of performed exams and measurements – evidence of protocols from exams and measurements of building constructions, technological equipments, nets, ... ▫ List of other documents originated in time of building production – records from control negotiations, protocols, ...

DAILY RECORDS

Site diary establishment	<ul style="list-style-type: none"> ▫ Record of contractor about works beginning ▫ Record of investor about empowered workers competent for records into the diary writing (building supervisor) and for the project engineer (author supervisor) ▫ Record of contractor about empowered workers to do notes into the diary ▫ Name of contractor employer responsible for OHS and FP on building site ▫ Verification of investor about acceptance of the diary front page
---------------------------------	---

Beginning of works	<ul style="list-style-type: none"> ▫ Works beginning date ▫ Found facts, which influence negatively the working process ▫ Requirements on the faults elimination (limitation)
Products, machines and equipments taking	<ul style="list-style-type: none"> ▫ Appeal to investor into preparation of materials, machines and equipments, if they are not the part of contractor supplies ▫ Appeal to transport and supplying of supplies on building site in limitation ▫ Found inadequacies of investor supplies
Occupational health and safety and fire prevention insuring	<ul style="list-style-type: none"> ▫ Skull session on building site including workers roster ▫ Record about control of workers certificates validity, special works performance competences ▫ Difference from safety arrangements in works race condition, with investor operations or with other contractors works ▫ Records about work accidents ▫ Records about building site control performed by occupational safety inspectorate
Works on building site performance	<ul style="list-style-type: none"> ▫ Climatic conditions influencing works process and quality ▫ Type, amount and time schedule of performed works ▫ Works assurance by workers, machines and products, ... ▫ Building site readiness for subcontractor taking up ▫ Building parts finishing ▫ Requirements on investor in connection with restrictions in works performance
Works breaks and technological breaks	<ul style="list-style-type: none"> ▫ Writing of all facts, which menace or preclude works continuance ▫ Writing of all and also short-time break
Continuation of works	<ul style="list-style-type: none"> ▫ Date and time of interrupted works beginning and break reason record ▫ Requirements on correction and revisions performance
Works covering	<ul style="list-style-type: none"> ▫ Appeal to control of quality and covered works integrity ▫ Record about control results
Auxiliary works specification	<ul style="list-style-type: none"> ▫ Investor writes the works amount approved by him and by contractor ▫ Contractor specify amount and process of performed auxiliary works, capacity and terms point
Changes specification	<ul style="list-style-type: none"> ▫ Record of all found divergences from executed and approved plans ▫ Record of performed divergences from previous plans, including their approbation, documentation and evidence
Coordination of (sub)	<ul style="list-style-type: none"> ▫ In field of transport - requirements on transport with object and term introducing

contractors on building site	<ul style="list-style-type: none"> ▫ In building works field – requirements on amount and terms, verification about their performance ▫ Works performance requirements – building site equipments demands ▫ Other works – lending of machines and equipments, method of using of building site objects, building site patrol, ...
Facts necessary for billing	<ul style="list-style-type: none"> ▫ working out hours amount (works charger by hour tariff) ▫ undone machines-hours, time of machines and equipments using ▫ increase of costs from reasons of impossibility of expected calculation incompliance because of changed organizational and technological conditions ▫ usage of energies (electrics, water, gas, ...) taking method, operation time, used equipments
Exams and measurements performance	<ul style="list-style-type: none"> ▫ time, process and results of exams and measurements ▫ investor statement into their result (in detail in control and exam plan of building)
Extraordinary events	<ul style="list-style-type: none"> ▫ raised damages on possession – reason writing (natural forces, swag, ...), damage amount, names and address of witnesses, performed arrangements ▫ illegitimate using of machines and equipments
The building acceptance and handover	<ul style="list-style-type: none"> ▫ date of written appeal to transfer action beginning ▫ place, date and time of transfer action beginning ▫ transfer action process ▫ place, date and time of transfer action finish (writing of protocol about transfer and acceptance between contractor and investor, including list of faults and inadequacies)
Competent institutions standpoints	<ul style="list-style-type: none"> ▫ record of competent workers and institutes about their determinations ▫ competent institutes statements
Complex examination	<ul style="list-style-type: none"> ▫ appeal on participation on equipments examination ▫ exams process, including achieved results ▫ complex examination beginning and finish date ▫ list of complex examination participants

Nowadays the form of the building diary can be various. From standard “blind” form, which can be bought in shops with paper forms (standardized notebooks) to structured forms, which form and structure is selected by firm itself in dependence on data management system. Basically the investor must accept the form of the building diary.

In contract relations writing, concerning often used formulation of commercial code “if contractor parties do not agree otherwise...” right and careful leading of the building diary has got big importance. The records in building diary are often only obligatory verification presenting real building process and accomplishment of duties among building participants. Timely and good made record in the building diary is also often an only entry basis for conventional sanctions, damages reparation, changes or additions of contract applying.

3. E-BUILDING DIARY – APPLICATION ENVIRONMENT

The building diary can be considered as some collection of information and records. In order to make work with these information and records easier and more effective, it is necessary to use computers with suitable software. This software must be dedicated specially for work with information. Also it has to be able to observe all functions and conditions for the building diary leading. A useful alternative presents the product of company Microsoft – Access, which is part of today often used office packs Microsoft Office. By this program is possible to create database applications, which are the most suitable for work with information. Particular database applications are made from database objects namely from charts, into which are inserted information, questions, paper forms, combinations, data pages, macros and modules.

The main characteristic of the program Microsoft Office is simple and especially wide possibility of work with information. Besides that it has got many other advantages, which in the case of the site diary leading as fully functional program, can do leading of the diary and work with it do more effectively. At the present is communication by net and internet connection a common stuff. Similar possibilities provides also Access 2003, from which is possible to export data into different external database systems. Also is possible to install all database software Microsoft Access into computer net server or publish application data at the internet. The advantage is also the form of outgoing records by program Word or joining of tabs from program Excel. It is possible to join own databases of companies with the site diary database, by what is user work easier. User will not must write some data (about machines or employers), but only choose from database.

Next advantage of Access is database application insurance. There are many possibilities how to non-authorised entries. Database applications created in Access 2003 version is possible to sign by electronic signature. The user by his signature confirms that information contained in this file is valid and from sign immediate was not changed. If the file will not be changed, is possible to add signatures of other users. Added digital signature informs that, signature author insure the

project safety. This possibility is in case of the building diary very important, because records in the diary have to be signed.

4. E-BUILDING DIARY – APPLICATION OF STRUCTURE AND VISUAL ASPECT

Application of building diary e-form structure comes from higher presented map (tab. 1) of building diary. This application consists of 28 paper forms (fig. 1) which are each other connected. They are divided into two groups, into forms for data import into database and forms for browsing the data yet saved in database

The main structural element of electronic building diary is the forms. Each form consists of three parts: head-line, body and heel. In head-line is presented the name of database “Site diary” and “date” which is daily actualized. In place of heel of forms generality is inserted command button “Back” which can switch over the user into past form. Body of forms is different depending on contents and function. The forms dedicated for data insert are similar, only fields describes are different. In order to visual site of program will be agreeable for user, all forms are orange with black texts. Pictures 2 – 11 present selected forms (screens).

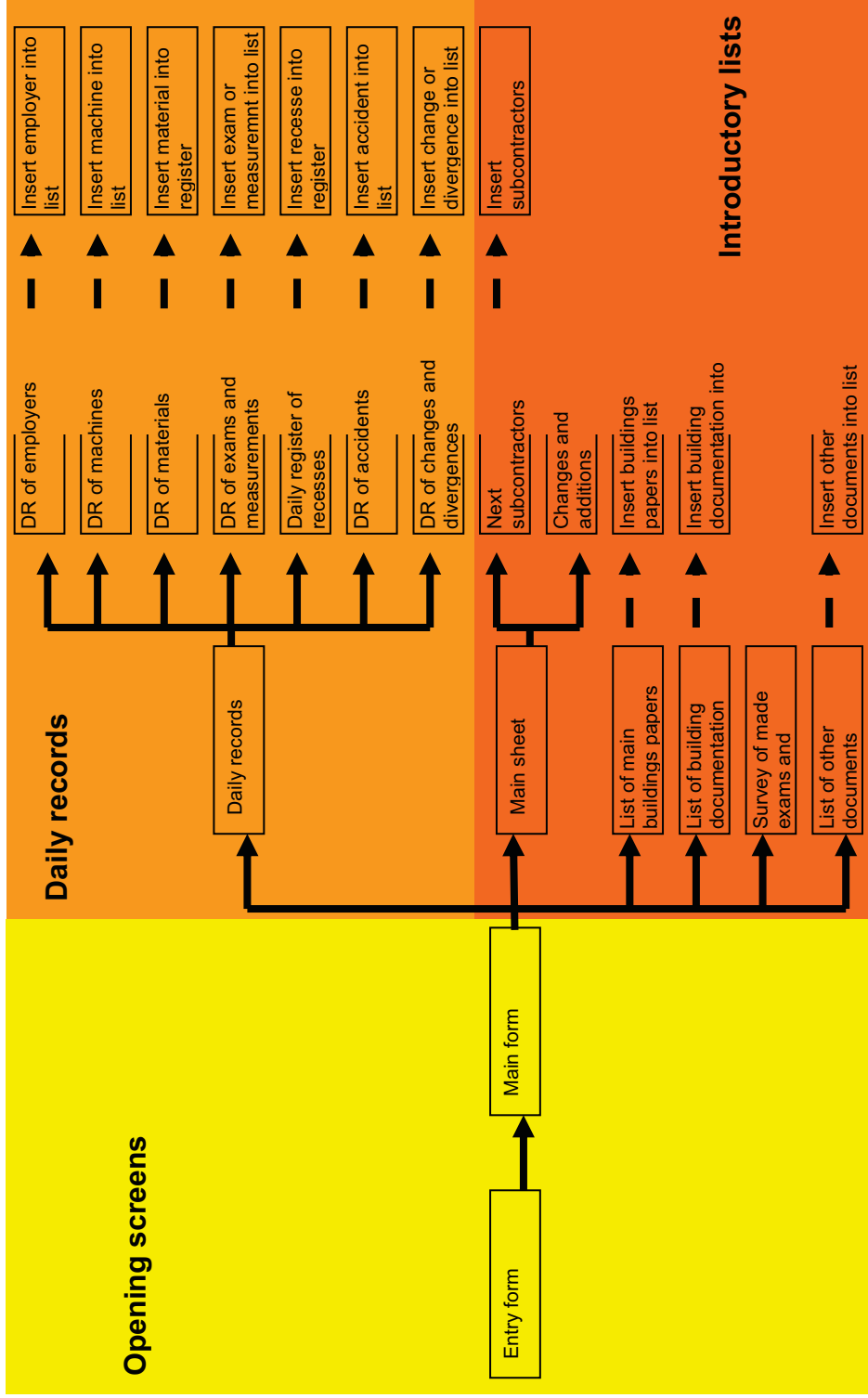


Fig.1 Structure of building diary

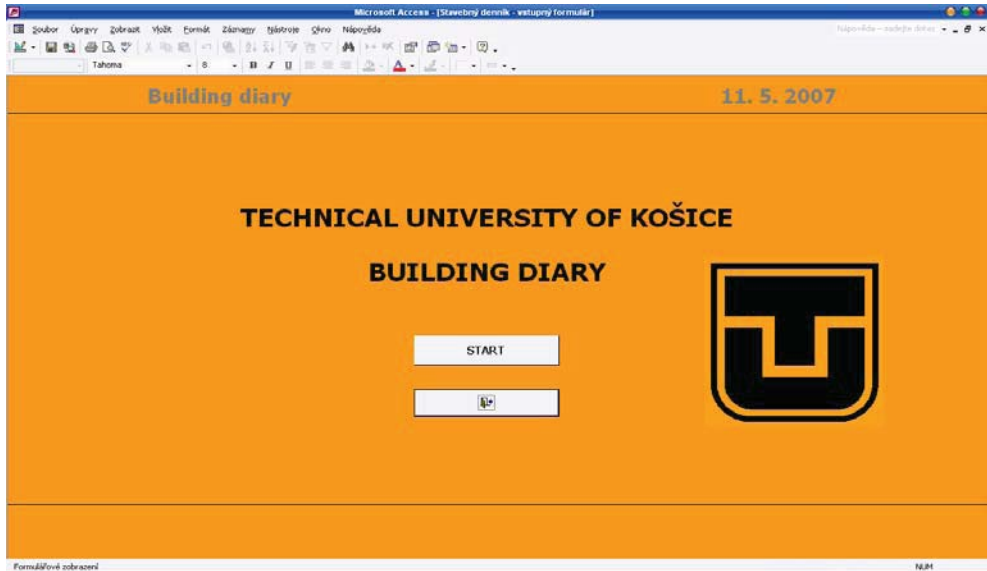


Fig.2 Opening screen

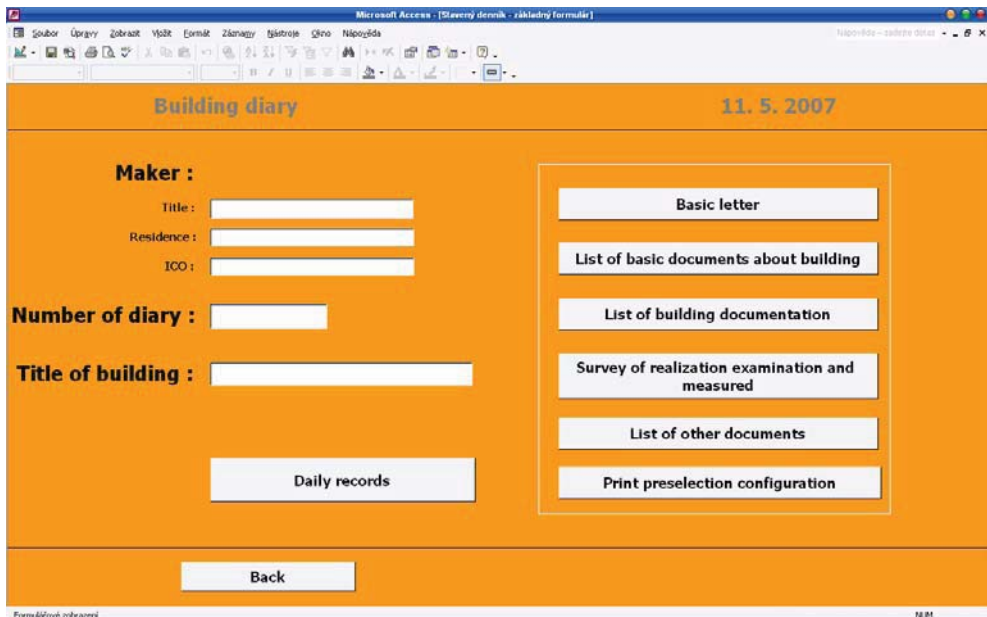


Fig.2 Main formular

Building diary 11. 5. 2007

Basic letter

Title of building :

Number of building :

Date beginning of building :

Place beginning of building :

Other subcontractors

Changes and complements

Print basic letter

Parties concerned (poop resp. representative)

	Name and surname	Address	Phone number
Straight investor :	<input type="text"/>	<input type="text"/>	<input type="text"/>
Top investor :	<input type="text"/>	<input type="text"/>	<input type="text"/>
Central investor :	<input type="text"/>	<input type="text"/>	<input type="text"/>
Main investor :	<input type="text"/>	<input type="text"/>	<input type="text"/>

Back

Engineering supervision of investor :

Constant :	<input type="text"/>	<input type="text"/>	<input type="text"/>
Occasional :	<input type="text"/>	<input type="text"/>	<input type="text"/>

General contractor :	<input type="text"/>	<input type="text"/>	<input type="text"/>
Construction manager :	<input type="text"/>	<input type="text"/>	<input type="text"/>
Section engineer :	<input type="text"/>	<input type="text"/>	<input type="text"/>

Overall projector :	<input type="text"/>	<input type="text"/>	<input type="text"/>
Responsible projector :	<input type="text"/>	<input type="text"/>	<input type="text"/>
Author supervision :	<input type="text"/>	<input type="text"/>	<input type="text"/>

Back

Formulářové zobrazení 10.01

Fig.3 Basic information

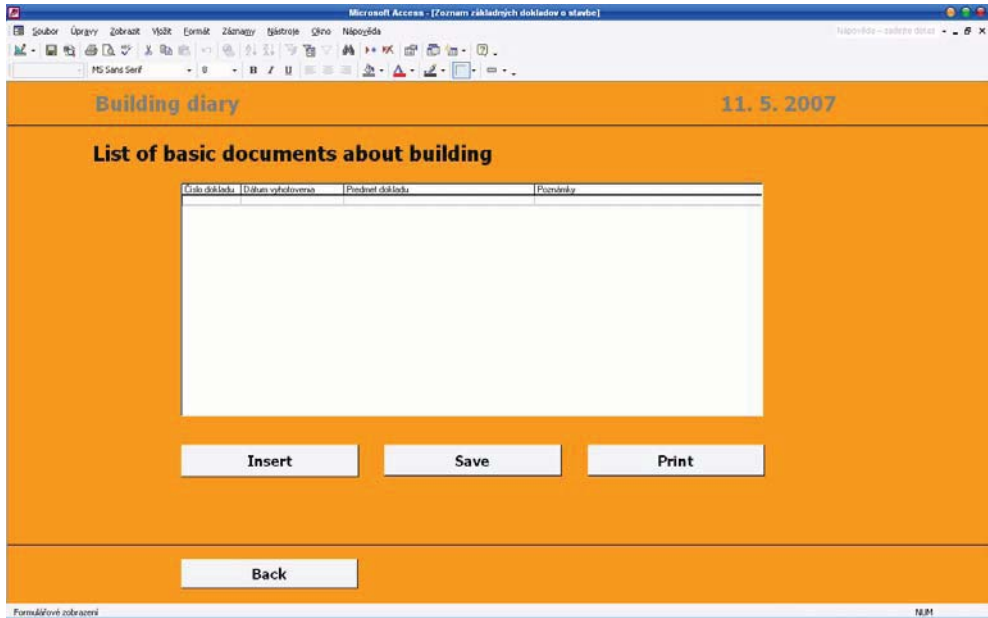


Fig. 4 List of basic documents about building

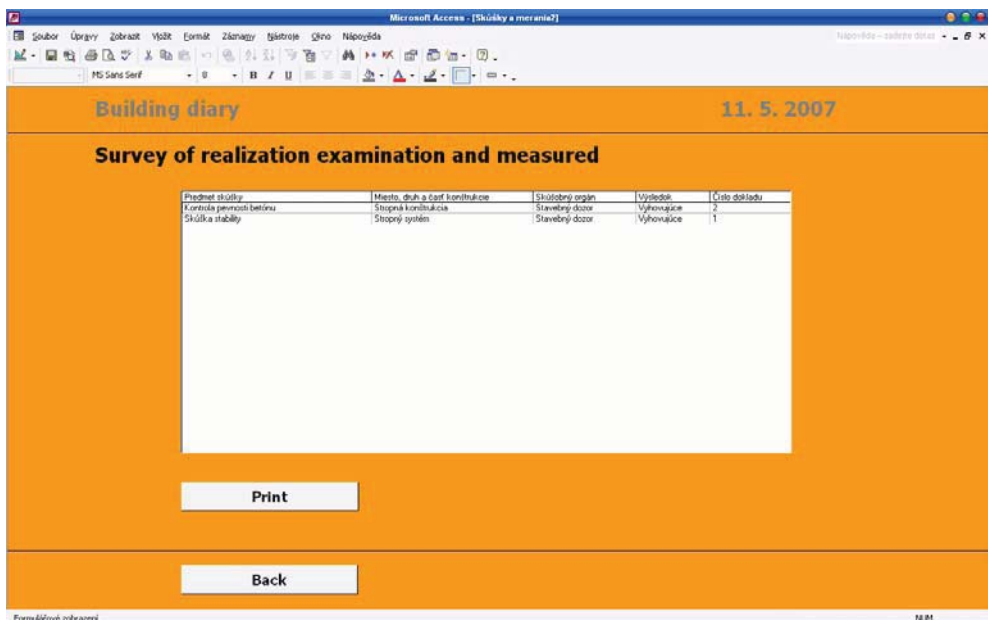


Fig.5 Survey of made exam and measure

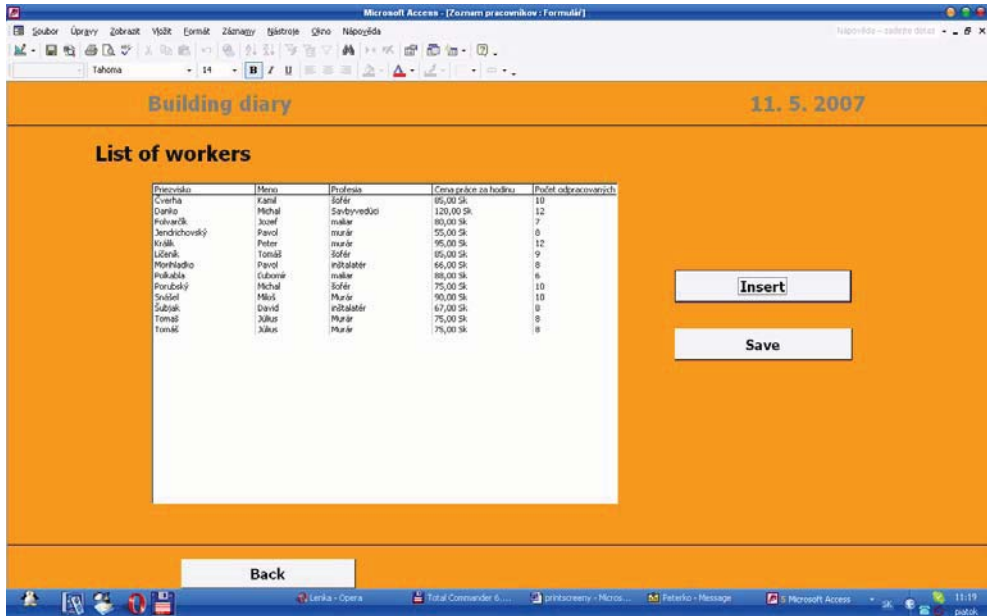


Fig. 6 List of workers

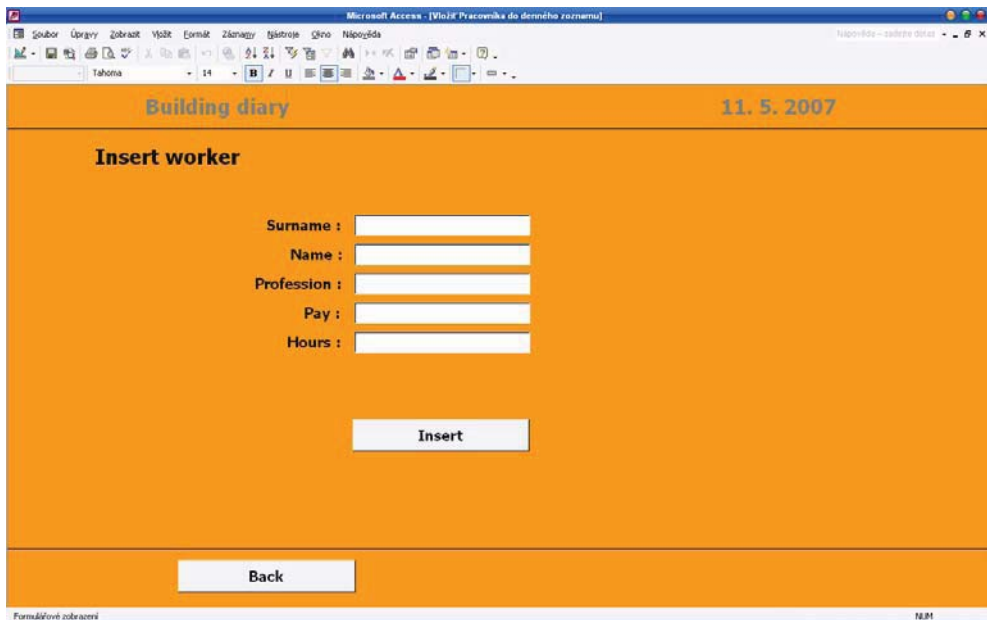


Fig.7 Formulary for workers inserts

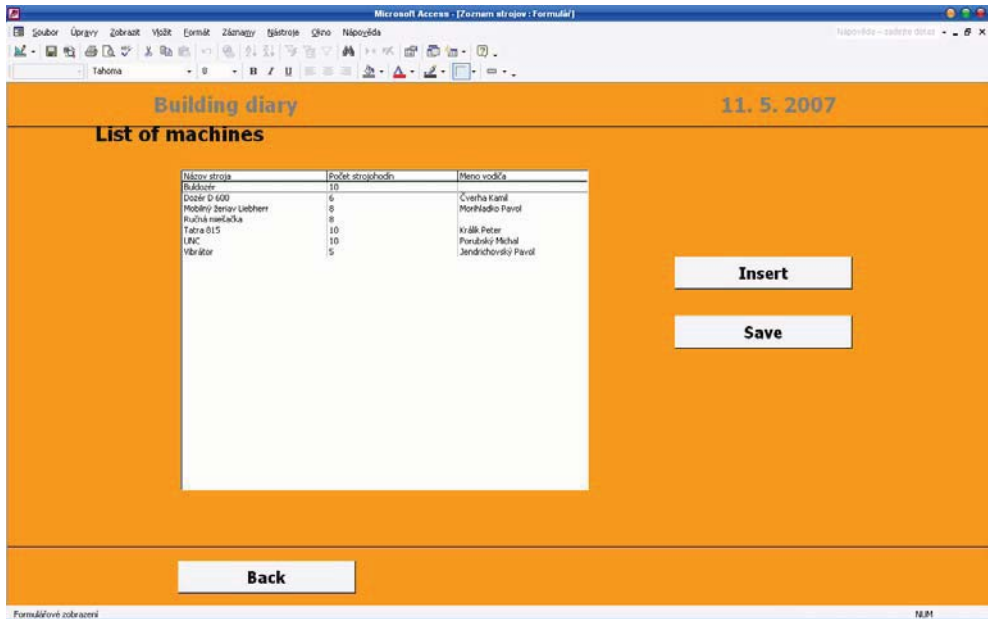


Fig.8 List of machines

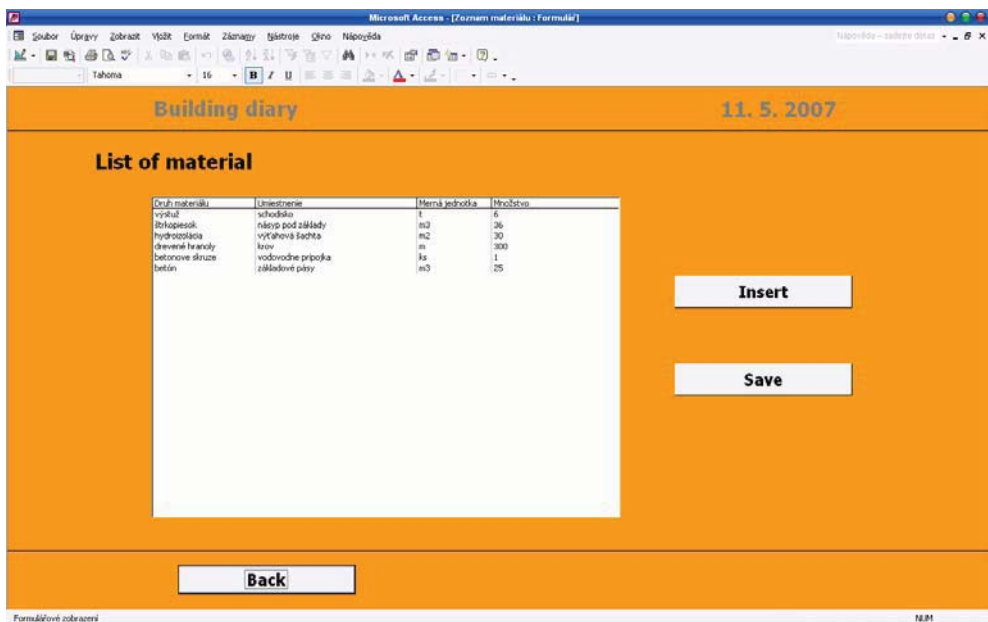


Fig.9 List of materials

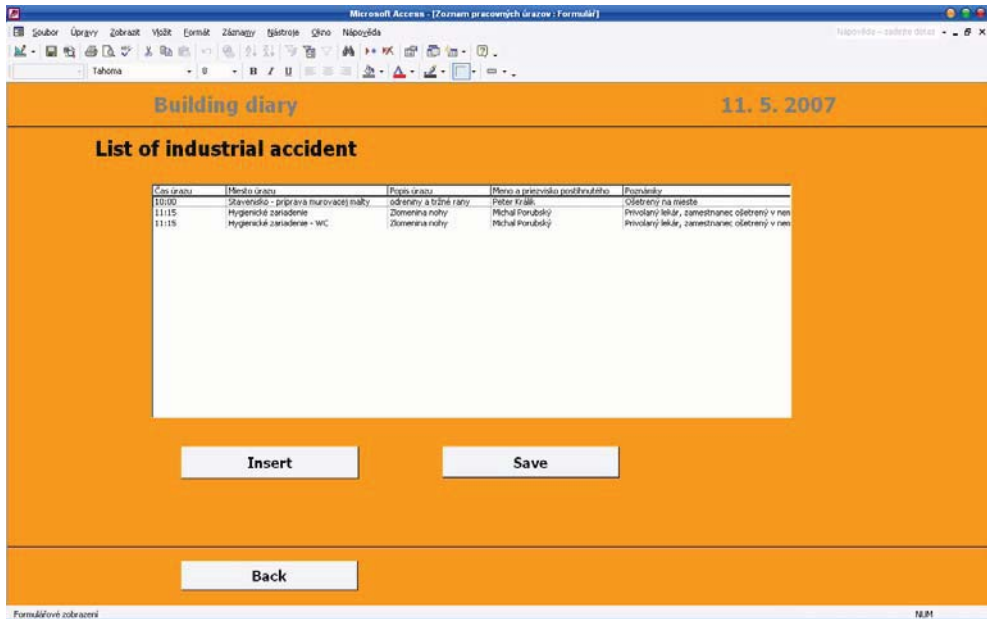


Fig.10 List of accidents

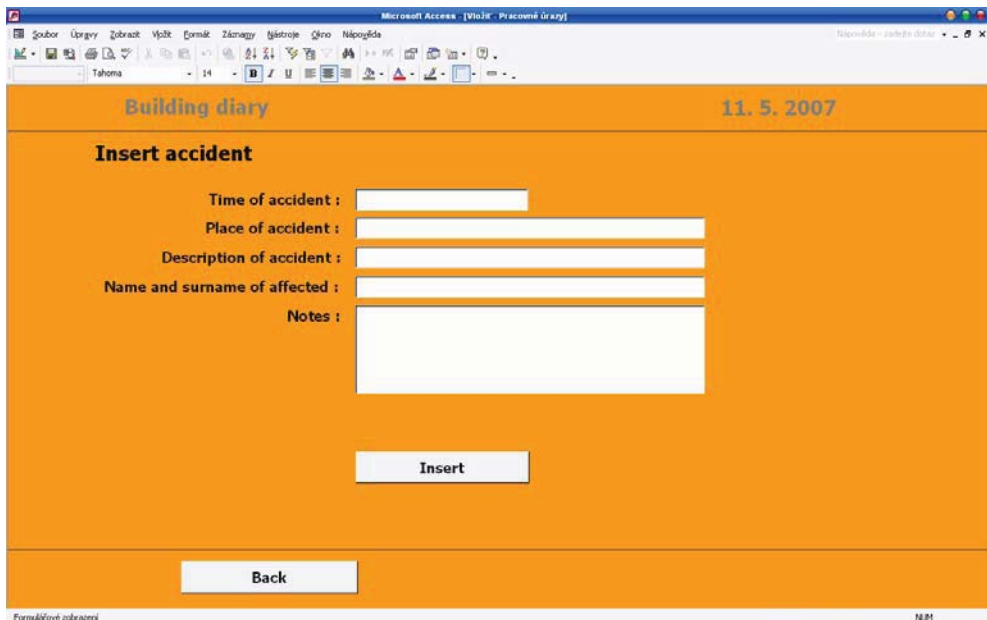


Fig.11 Formulary for accident inserts

5. CONCLUSION

The high rate of construction, necessity of fast transport of information, including their fidelity, create force on new tools development, which can effectively insure activities connected with building realization. Development and design of application supporting electronic leading of the site diary is a contribution, supporting these necessities. Nowadays information and communication technologies including personal computers are more often the natural “co-operator” of building managers. Developed application presents the tool, which can essentially do work of managers more effective.

The article is the part of the project KEGA 3/4004/06 MM program for building educate support.

References

- [1] Kozlovská, M., Hyben, I.: *Works foreman – manager of the building process*. 1. edition. Bratislava: Eurostav, 2005.
- [2] *Building law No.76/1976* in later regulations version.
- [3] Korínek, M.: *Access 2000*. České Budějovice : Kopp, 2000.

Determination of the heat flows, of the solar and luminous characteristics of the glazing and of the devices for the solar protection. Automaton calculus program “SOLAR”

Ioan Moga and Ligia Moga

Physics of Constructions, Faculty of Civil Constructions and Installations, University of Cluj-Napoca, Cluj-Napoca, 400027, Romania

Summary

The automaton calculus program “SOLAR” has resulted from the activity for establishing the annex A94 from “THE METHODOLOGY FOR CALCULUS THE ENERGETICS PERFORMANCE FOR BUILDINGS - PART I”, for the applying of the requirements of the law 372/2005.

The calculus program has at its basis the stipulations of the normative EN 13363-2:2005.

With the help of the automaton calculus program, it can be determined for any type of glazing with or without solar protection devices, the solar energy total transmission factor, luminous transmission factor and the normalized thermal emission flow.

KEYWORDS: heat engineering for constructions, solar protection devices, energy savings, rehabilitation of buildings.

1. CALCULUS ALGORITHM

1.1. Calculus program description

The calculus program is realized using the programming language Delphi under Windows system.

The calculus program was made out taking into consideration the stipulations from the normative SR EN ISO 10211/1-98 concerning the geometrical model, the layout of the sectioning plans through the glazing system with the solar protection that forms the calculus network. Regarding the convergence conditions of the obtained solutions a more important requirement than the one in the normative SR EN ISO 10211/1-98 was imposed. The requirement considers obtaining the convergence of the numeric calculus results by assuring the energy balance condition, in every

node of the calculus network, according to relation (17), with a accuracy of 0,0001W.

1.2. Glazing system and the solar protection devices

The glazing unit and the solar protection devices are made from a sequence of layers of material separated by spaces filled in with gas. The layers of the material are considered homogeneous and with thermal conductivities, that are not varying with temperature.

The heat and solar radiation flow are considered to transfer unidimensional. For the ventilated spaces, the expressions for the two-dimensional convection are converted into unidimensional formulas.

The layers for material and spaces are numbered with the subscript j from 1 to n , space n representing the interior environment and space 0 the exterior environment. The physical model does not limitate the number of layers.

The basis formulas indicated for the solar radiation and for the heat transfer express the energy balance for each layer.

For resolving the non-linear dynamic system of equations obtained, it is recommended the use of a iterative calculus process.

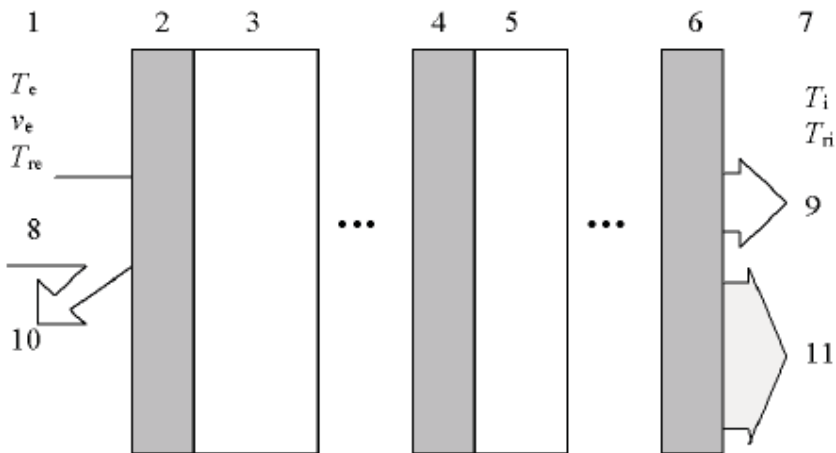


Figure 1 . System made of layers of material and spaces

Legend

- | | | |
|---|------------|---|
| T_e Exterior air temperature | 1 Exterior | 8 Solar radiation |
| T_{re} Exterior radiating temperature | 2 Layer 1 | 9 Direct solar and luminous transmission factor |

v_e	Exterior wind speed	3	Space 1	
T_i	Interior air temperature	4	Layer j	10 Direct solar and luminous reflection factor
T_{ri}	Interior radiating temperature	5	Space j	
		6	Layer n	11 Radiative and convective (direct and indirect) thermal transfer
		7	Interior	

NOTE: The interior and exterior environs are characterised by the interior air temperature and the radiating temperature; the exterior environment is also characterised by the speed wind.

1.3. Solar and optical characteristics of the glazing

For each wave length λ and for each layer of the glazing j, next equilibrium equations can be written (Figure 2) for the normalized spectral radiative flow I_j si I'_j :

$$\begin{aligned}
 I_j(\lambda) &= \tau_j(\lambda) \cdot I_{j-i}(\lambda) + \rho'_j(\lambda) \cdot I'_j(\lambda) \\
 I'_j(\lambda) &= \rho_j(\lambda) \cdot I_{j-i}(\lambda) + \tau'_j(\lambda) \cdot I'_j(\lambda)
 \end{aligned}
 \tag{1}$$

where:

- $\tau_j(\lambda)$ spectral transmission factor of the face exterior oriented ;
- $\tau'_j(\lambda)$ spectral transmission factor of the face interior oriented ;
- $\rho_j(\lambda)$ spectral reflection factor of the face exterior oriented ;
- $\rho'_j(\lambda)$ spectral reflection factor of the face interior oriented ;
- $I_j(\lambda)$ normalized spectral radiative flow interior oriented ;
- $I'_j(\lambda)$ normalized spectral radiative flow exterior oriented ;

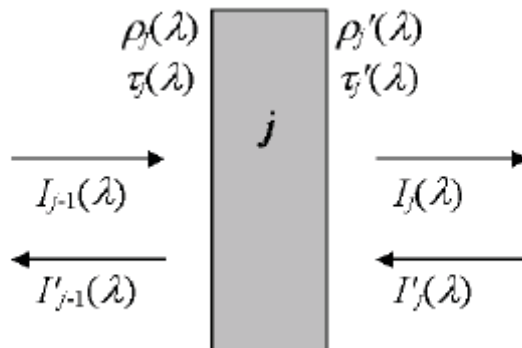


Figure 2. The scheme with the characteristic data of the layer j and related spectral flows

By writing the equation (1) for each layer j of the glazing, a system with n equations will result, having as unknowns the values for $I_j(\lambda)$ și $I'_j(\lambda)$.

The limit conditions for resolving the system of equations will be:

$$I_0(\lambda) = 1 \text{ and } I_n(\lambda) = 0 \quad (2)$$

After resolving the system of equations and obtaining for each layer j the values for the spectral radiative flow $I_j(\lambda)$ și $I'_j(\lambda)$, the next factor will be obtained:

$$\text{spectral transmission factor : } \tau_j(\lambda) = I_n(\lambda) \quad (3)$$

$$\text{spectral reflection factor : } \rho_j(\lambda) = I'_0(\lambda) \quad (4)$$

spectral absorption factor:

$$\alpha_j(\lambda) = (1 - \rho_j(\lambda) - \tau_j(\lambda)) \cdot I_{j-1}(\lambda) + (1 - \rho'_j(\lambda) - \tau'_j(\lambda)) \cdot I'_j(\lambda) \quad (5)$$

The direct solar transmission factor τ_e , the direct solar reflection factor ρ_e , and the spectral absorption factor α_{ej} for each layer will be calculated taking into account the spectral data, determined according to the methodology from SR EN 410:1998;

In the same way the direct luminous transmission factor τ_v and direct luminous reflection factor ρ_v will be calculated.

1.4. Heat transfer

1.4.1 Thermal radiation

The heat flow through radiation depends upon the temperature of the system double with other heat flows that appear in the system.

For the thermal radiation the scheme from figure 3 is used, where the next characteristics are presented for each face of the layers that compose the system, glazing or solar protection layer.

- T_j absolute temperature ;
- $\tau_{th,j}$ direct solar transmission factor ;
- ε_j effective emissivity of the face exterior oriented ;
- ε'_j effective emissivity of the face interior oriented ;
- $q_{th,j}$ radiative flow density towards interior ;
- $q'_{th,j}$ radiative flow density towards exterior.

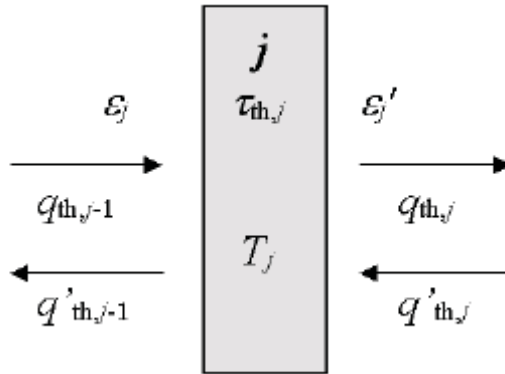


Figure 3. Characteristic data of the layer j and related radiative flow densities

The effective emissivity ε is derived from the normal emissivity ε_n , determined with the help of a infrared spectrophotometer, with the related correction from the procedure described in SR EN 673 annex A.2.

For each layer j of the system of the glazing equations of radiative energy balance will be written resulting a complex equations system, where the temperature are at the fourth value :

$$\begin{aligned}
 q_{th,j} &= \tau_{th,j} \cdot q_{th,j-1} + (1 - \varepsilon'_j - \tau_{th,j}) \cdot q'_{th,j-1} + \varepsilon'_j \cdot \sigma \cdot T_{j-1}^4 \\
 q'_{th,j-1} &= (1 - \varepsilon_j - \tau_{th,j}) \cdot q_{th,j-1} + \tau_{th,j} \cdot q'_{th,j} + \varepsilon_j \cdot \sigma \cdot T_j^4
 \end{aligned}
 \tag{6}$$

Limit conditions are given by the interior and exterior radiative conditions, $T_{r,e}$ și $T_{r,i}$:

$$q_{th,0} = \sigma \cdot T_{re}^4 ; \quad q_{th,n} = \sigma \cdot T_{ri}^4
 \tag{7}$$

After resolving the system of equations and determining the temperatures T_j , the next will be calculated :

the net radiative flow toward exterior

$$q_e = q'_{th,0} - q_{th,0}
 \tag{8}$$

the net radiative flow toward interior

$$q_i = q'_{th,n} - q_{th,n}
 \tag{9}$$

retained net heat, from thermal radiation, in layer j

$$q_{th,a,j} = \varepsilon_j \cdot q_{th,j-1} - \varepsilon'_j \cdot q'_{th,j} + (\varepsilon_j + \varepsilon'_j) \cdot \sigma \cdot T_j^4
 \tag{10}$$

1.4.2 Heat transfer through thermal conduction and thermoconvection in enclosed spaces with glazing surfaces

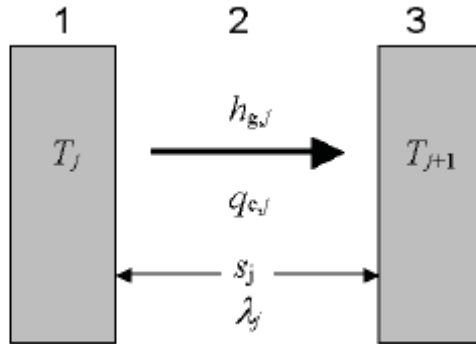


Figure 4. Scheme presenting the characteristic data for an enclosed space and the heat flow density through thermal conduction and thermoconvection

Legend

- 1 Layer j
- 2 Space of gas j
- 3 Layer $j+1$

λ_j Thermal conductivity of gas in a space j at temperature $T_m = \frac{(T_j + T_{j+1})}{2}$

s_j The thickness of the gas layer from the layer j

$h_{g,j}$ Thermal conductance of the gas in layer j

$q_{c,j}$ Heat flow density through thermal conduction and thermoconvection starting from layer j to $j+1$

Thermal conductivity of gas in a limited space j , at medium temperature

$$T_{m,j} = \frac{(T_j + T_{j+1})}{2}$$

, enclosed between glazing surfaces (Figure 4), is given by the relation:

$$h_{g,j} = \frac{Nu_j \cdot \lambda_j}{s_j} \quad (11)$$

where:

- λ_j thermal conductivity of the gas from the enclosed space j ;
- s_j the thickness of the gas layer ;
- λ thermal conductivity of the gas at the temperature T_m ;

Nu Nusselt dimensionless number, determined according to the stipulations from the standard SR EN ISO 673:2000;

Limit conditions for exterior are:

for the air temperature : $T_0 = T_e$;

for the thermal transfer through thermoconvection:

$$h_{g,0} = h_{c,e} ; \quad (12)$$

Limit conditions for interior are:

for the air temperature : $T_{n+1} = T_i$;

for the thermal transfer through thermoconvection:

$$h_{g,n} = h_{c,i} ; \quad (13)$$

After resolving the system of equations and after determining the temperatures T_j , in each node of the calculus network, the next will be calculated :

resulted net heat in layer j (through thermal conduction and thermoconvection), is given by :

$$q_{c,aj} = h_{g,j-1} \cdot (T_{j-1} - T_j) + h_{g,j} \cdot (T_{j+1} - T_j) \quad (14)$$

heat flow density through thermoconvection toward exterior environs is given by :

$$q_{c,e} = q_{c,a,0} = h_{g,0} \cdot (T_1 - T_e) \quad (15)$$

heat flow density through thermoconvection toward interior environs is given by :

$$q_{c,i} = q_{c,a,n} = h_{g,n} \cdot (T_i - T_n) \quad (16)$$

A non-linear algebraic system of equations will result, after writting the equation for the energy balance, in each node of the calculus network. Because of the dynamic and non-linear nature of interaction between temperature and the radiative and convective heat transfer, for resolving the resulted system of equations, it is recommended the use of an iterative process. The dynamic nature is assess a rewritting for the system of equations, because of the modification of coefficients belonging to the system of equations, for each step of the iterative calculus.

2. VALIDATION OF THE “SOLAR” AUTOMATON CALCULUS PROGRAM

The validation of the automaton calculus program was made using the examples from annex C of the norm EN 13363-2:2005.

Next entry data were used:

1. exterior blind: blind- 50 mm air space- 4 mm glazing- 13 mm air space- 4 mm glazing
2. interior blind: 4 mm glazing- 13 mm air space- 4 mm glazing- 50 mm air space- blind.
3. inbuilt blind: 4 mm glazing - 13 mm air space- blind- 13 mm air space- 4 mm glazing.

Properties of the materials:

Glass:

- 4 mm clear normal glass;
- solar energy transmission factor $\tau_e = 0,82$, reflection factor $\rho_e = 0,07$;
- thermal emissivity $\varepsilon = 0,84$.

Blind:

- solar energy transmission factor $\tau_e = 0,2$, reflection factor $\rho_e = 0,4$;
- thermal emissivity $\varepsilon = 0,9$;
- without thermal radiation transmission.

The obtained results depend on several factors:

- number of decimals with which the thermotechnic parameters are taken (2,3,4,...);
- number of decimals for working (algorithm calculus accuracy);
- number of calculus steps at which the thermotechnic parameters of air are changing numeral;
- interpolation manner of those parameters, when this operations are made etc .

After performing the calculus in double precision, is inferred that the values displayed in norm EN 13363-2:2005 in the annex C, are obtained as intermediate calculus values before the energetic balancing of the glazing system layers with solar protection.

After carrying out the calculus up to the energetic balance, until assurance with 3 decimals the energetic balance, the obtained results differ meaningful from the displayed values in annex C of the norm EN 13363-2:2005. The obtained results with the automaton calculus program “Solar” are the proper one by the thermotechnic point of view, taking into consideration the energy balance in each layer of the glazing assembly with solar protection.

The listing with the obtained results is given for the analyzed examples.

In the listing the results are obtained for: direct solar transmission factor τ , radiation factor G_n , convection factor G_c , ventilation factor G_v , secondary thermal transfer interior oriented G_{hcv} , total energy transmission factor G_{hcv+T}

On the right side of the tables in the listing is presented the energy balance for each surface of the glazing assembly- solar protection. It can be observed that the results

displayed in tables in annex C of the norm EN 13363-2:2005, are the intermediate calculus values before the energy balancing of the surfaces of the system.

3. CONCLUSIONS

The automaton calculus program “SOLAR” has a prompt practicability in the designing phase and also in the phase for energetic rehabilitation for new and existing buildings.

This program covers the required necessity of the experts in the field. Its applicability is general and can be taken into consideration for any type of glazing, filled with various gases, with the surfaces of the clear or treated glass, with or without solar protection in three variants of emplacement: in exterior, in interior and between leaves of glass.

References

1. SR EN 410:2003, *Glass for constructions. Determination of the solar and luminous characteristics of glazing.*
2. SR EN 673:2000, *Glass for constructions. Determination of the thermal transmittance U. Calculus method.*
3. SR EN 673:2000/A1:2002, *Glass for constructions. Determination of the thermal transmittance U. Calculus method.*
4. SR EN 673:2000/A1:2002/A2:2004, *Glass for constructions. Determination of the thermal transmittance U. Calculus method.*
5. SR EN ISO 10077-2:2004, *Thermal performance of windows, doors and shutters. Calculus for the thermal transmittance- Second part: General method*
6. SR EN ISO 10211-1:1998, *Thermal bridges in constructions. Thermal flows and superficial temperatures. First part: General calculus method.*
7. SR EN ISO 10211-1:1998/AC :2003, *Thermal bridges in constructions. Thermal flows and superficial temperatures. First part: General calculus method.*
8. SR EN 13363-2:2006, *Solar protection devices applied for glazings. The calculus of the solar and luminous transmission factor. Second part: The detailed calculus method.*

Stor exterior si Doua geamuri Vara (neventilat)

I t	Ir = 500.0				Rezultate				Echil. energetic Ir=0.0					
	Radiatie	Convecti	Ventilat	Total	Ga	Gc	Gv	Gchv+T	Supr1	Supr2	Supr3	Supr1	Supr2	Supr3
0	0.000	0.000	0.000	29.664	-13.500	0.000	0.027	0.086	0.228	0.000	0.000	168.310	158.146	-65.156
1	0.000	0.000	0.000	38.213	-13.500	0.000	0.027	0.103	0.245	0.000	0.000	-234.837	70.656	4.321
2	0.000	0.000	0.000	35.707	-13.500	0.000	0.027	0.098	0.240	0.000	0.000	-4.669	-0.944	-11.977
3	0.000	0.000	0.000	35.586	-13.500	0.000	0.027	0.098	0.240	0.000	0.000	-0.293	-0.463	-12.815

Calculul Exact

I t	Ir = 500.0				Rezultate				Echil. energetic Ir=0.0					
	Radiatie	Convecti	Ventilat	Total	Ga	Gc	Gv	Gchv+T	Supr1	Supr2	Supr3	Supr1	Supr2	Supr3
0	0.000	0.000	0.000	45.827	-17.440	0.000	0.035	0.127	0.268	0.000	0.000	-46.260	2.477	-18.885
1	0.000	0.000	0.000	32.944	-12.204	0.000	0.024	0.090	0.232	0.000	0.000	-0.849	-0.114	-0.558
2	0.000	0.000	0.000	32.562	-12.047	0.000	0.024	0.089	0.231	0.000	0.000	-0.028	-0.004	-0.018
3	0.000	0.000	0.000	32.550	-12.042	0.000	0.024	0.089	0.231	0.000	0.000	-0.001	-0.000	-0.001
4	0.000	0.000	0.000	32.550	-12.042	0.000	0.024	0.089	0.231	0.000	0.000	-0.000	-0.000	-0.000

Doua geamuri Si Stor interior Vara (neventilat)

I t	Ir = 500.0				Rezultate				Echil. energetic Ir=0.0					
	Radiatie	Convecti	Ventilat	Total	Ga	Gc	Gv	Gchv+T	Supr1	Supr2	Supr3	Supr1	Supr2	Supr3
0	0.000	0.000	0.000	98.395	-45.000	0.000	0.090	0.287	0.429	0.000	0.000	62.806	46.753	-190.389
1	0.000	0.000	0.000	97.226	-45.000	0.000	0.090	0.284	0.426	0.000	0.000	64.361	36.899	-197.830
2	0.000	0.000	0.000	97.298	-45.000	0.000	0.090	0.285	0.426	0.000	0.000	62.327	37.244	-197.331
3	0.000	0.000	0.000	97.346	-45.000	0.000	0.090	0.285	0.426	0.000	0.000	61.265	37.306	-196.981

Calculul Exact

I t	Ir = 500.0				Rezultate				Echil. energetic Ir=0.0					
	Radiatie	Convecti	Ventilat	Total	Ga	Gc	Gv	Gchv+T	Supr1	Supr2	Supr3	Supr1	Supr2	Supr3
0	0.000	0.000	0.000	73.304	-31.781	0.000	0.064	0.210	0.352	0.000	0.000	-29.390	-38.773	-35.905
1	0.000	0.000	0.000	59.367	-26.005	0.000	0.052	0.171	0.313	0.000	0.000	-6.512	-13.835	-1.985
2	0.000	0.000	0.000	57.176	-25.228	0.000	0.050	0.165	0.307	0.000	0.000	-2.328	-3.165	-0.109
3	0.000	0.000	0.000	56.716	-25.079	0.000	0.050	0.164	0.305	0.000	0.000	-0.820	-1.064	-0.029
4	0.000	0.000	0.000	56.564	-25.030	0.000	0.050	0.163	0.305	0.000	0.000	-0.302	-0.390	-0.010
5	0.000	0.000	0.000	56.509	-25.012	0.000	0.050	0.163	0.305	0.000	0.000	-0.114	-0.147	-0.004
6	0.000	0.000	0.000	56.489	-25.005	0.000	0.050	0.163	0.305	0.000	0.000	-0.043	-0.056	-0.001
7	0.000	0.000	0.000	56.481	-25.003	0.000	0.050	0.163	0.305	0.000	0.000	-0.017	-0.021	-0.001
8	0.000	0.000	0.000	56.478	-25.002	0.000	0.050	0.163	0.305	0.000	0.000	-0.006	-0.008	-0.000
9	0.000	0.000	0.000	56.477	-25.001	0.000	0.050	0.163	0.305	0.000	0.000	-0.002	-0.003	-0.000
10	0.000	0.000	0.000	56.476	-25.001	0.000	0.050	0.163	0.305	0.000	0.000	-0.001	-0.001	-0.000
11	0.000	0.000	0.000	56.476	-25.001	0.000	0.050	0.163	0.305	0.000	0.000	-0.000	-0.000	-0.000

Effect of moulding humidity on the properties of dry pressed ceramic tiles

Radomir Sokolar

*Department of Technology of Building Materials and Components, Faculty of Civil Engineering,
Brno University of Technology, City, Veveri 331/95, 602 00 Brno, Czech Republic*

Summary

The aim of the work was to describe moulding humidity influence on the properties of dry pressed ceramic tiles from fly ash – clay mixture (70 % fly ash and 30 % stoneware clay). It was determined properties of green body (bulk density) and fired body (water absorption, bending strength, bulk density and apparent porosity according to EN ISO 10545 standards) by the mathematical functionalities.

KEYWORDS: Dry pressed ceramic tiles, pressing water content, bulk density, water absorption, green ceramic body, fired ceramic body.

1. INTRODUCTION

The enormous amount of fly ashes generated during mineral coal burning is still far from being used in its totality as a product or by-product, making technological alternatives needed in order to reduce its possible environmental impact. The paper present one of the possibilities how to use fly ashes – as a basic raw material for the production of ceramic tiles. It is evident, that moulding moisture influenced properties of dry pressed green or fired ceramic body very much. It was determined optimal water content to get maximal compact green body and the best properties of the firing fly ash - clay bodies according to EN ISO 10545 standards (e.g. water absorption, bending strength) and properties of the fly ash body microstructure. The properties of firing fly ash – clay body (water absorption, bending strength) were compared in accordance with requirements of EN 14411 for dry pressed for ceramic tiles (Table 1).

Table 1 - The choose properties of ceramic tiles - group B

Characteristics		B Ia	B Ib	B IIa	B IIb	B III
Water absorption [%]	average individually	$\leq 0,5$ Max. 0,6	0,5 - 3 Max. 3,3	3 - 6 Max. 6,5	6 - 10 Max. 11	$> 10^2$ Min. 9
Bending strength [MPa]	average individually	≥ 35 Min. 32	≥ 30 Min. 27	≥ 22 Min. 20	≥ 18 Min. 16	$\geq 15^1$
Breaking strength ($t \geq 7,5$ mm)		1300 N	1100 N	1000 N	800 N	600 N

2. RAW MATERIAL PROPERTIES

The fly ash utilized in this work was originated in the burning process of mineral brown coal in a pulverized coal-fired plant of Thermoelectrical Power Station, which is located in Melnik (Czech Republic). This thermoelectrical process has good efficiency in the combustion of the mineral coal and the residual carbon is very low - 1,2 wt%. Stoneware clay (from region Postorna CZ) was used as a binder for non plastic fly ash grains. The chemical composition of raw materials is showed in Table 2.

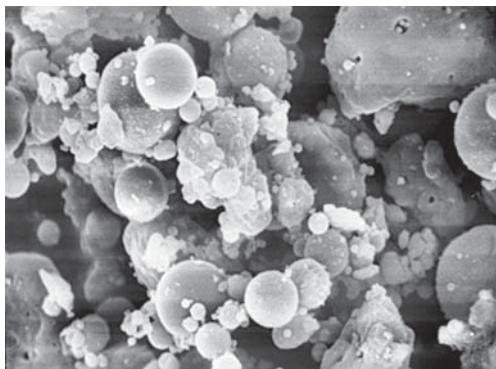


Figure 1. Microstructure of used fly ash (2000x).

Table 2. Average chemical composition of used raw materials

[mass-%]	SiO ₂	Al ₂ O ₃	Fe ₂ O ₃	TiO ₂	CaO	MgO	K ₂ O	Na ₂ O	S	IL
Fly ash	55,9	29,3	4,7	1,7	2,2	1,4	1,6	0,1	0,1	1,2
Clay	62,2	18,8	4,2	1,5	1,4	1,4	2,3			9,3

Particle size distribution of fly ash was studied by using of the floating method through the 0,063 mm sieve. The fly ash was grinded in the dry laboratory ball mill with clay together to get minimal residue on the 0,063 mm sieve.

Table 3. Particle size distribution of fly ash

	Original	After Ball grinding with clay
Sieve residue 0,063 mm [%]	43,2	5,9

3. SPECIMEN SHAPING AND FIRING

The mixture of raw materials (70 % mass fly ash + 30 % mass clay) was milled in dry ball mill together. Test specimens measuring 100 mm x 50 mm x 10 mm were

shaped in a laboratory press from granulate = moistened mixture with a different water content were pressed through a 1 mm sieve. The pressing pressure corresponds to used values for dry pressed ceramic tiles industrial production from spray-dried granulates (40 MPa).

The firing of test specimens proceed in the industrial tunnel kiln – maximal firing temperature 1020 °C with 5 hours soaking time in this temperature. After firing, It was determined properties of firing body: E – vacuum water absorption, B – bulk density (B_g – bulk density of green (not fired, only after drying) body, B_f – bulk density of fried body), P – apparent porosity, T – apparent relative density according to EN ISO 10545 – 3 and capillarity in dependence on moulding humidity. Frost resistance of firing body was determined by using indirect method - T – value (saturation value according to DIN 52253 – 3) describes the amount of open pores capable of filing with water under atmospheric pressure, in relation to the pores which fill with water at a vacuum of 30 mbar. Frost resisted bodies embody low T – values (under 0,75).

5. RESULTS

According to figures 2, 3 and tables 4, 5 it is evident, that all determined properties of green or fired bodies are depended on the pressing moisture of pressing granulate – it is concerned linear dependence. With increasing of pressing moisture the body is more compact and decreased the capillarity of fired fly ash – clay dry pressed body.

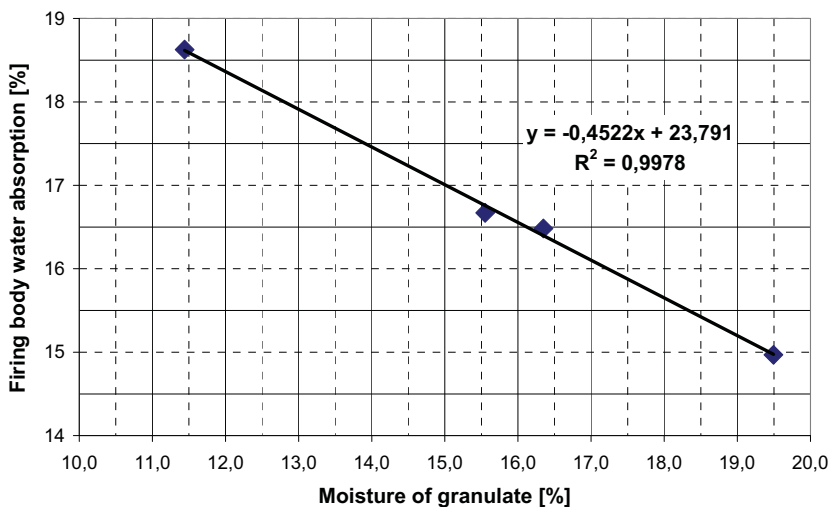


Figure 2. Fired body water absorption in dependence on pressing moisture of granulate

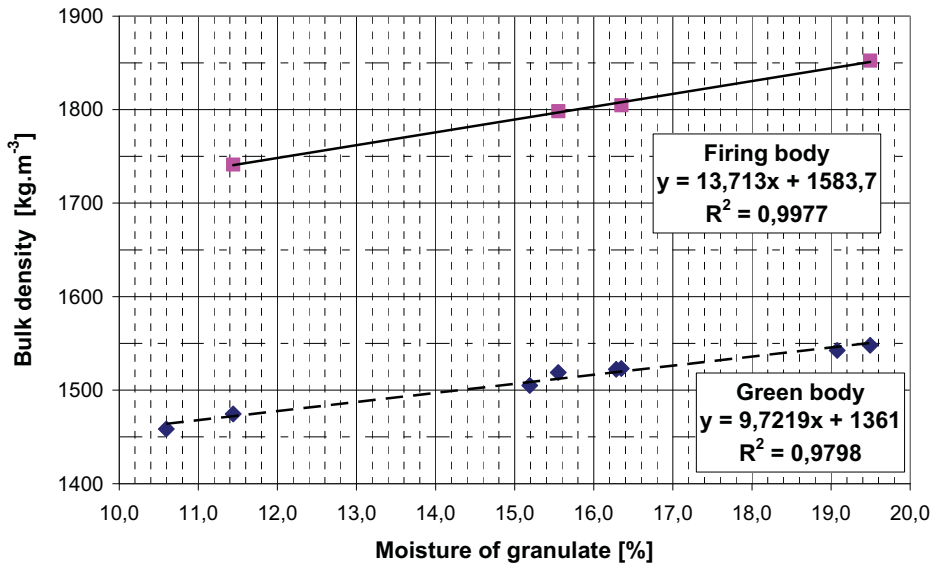


Figure 3. Bulk density of green and fired body in dependence on pressing moisture of granulate

Table 4. Properties of green and fired body

Moisture [%]	B _g [kg.m ⁻³]	B _f [kg.m ⁻³]	P [%]	E [%]	T [kg.m ⁻³]	T-value [-]
10,6	1458					
11,4	1475	1741	32,4	18,6	2577	0,988
15,2	1505					
15,6	1519	1798	30,0	16,7	2568	0,981
16,3	1523	1804	29,7	16,5	2569	0,976
19,1	1542					
19,5	1548	1852	27,7	15	2563	0,963

Table 5. Capillarity of fired bodied in dependence on pressing moisture of pressing granulate

Moisture [%]	Capillarity [mm] – after 5-10-20-30-40-50-60-70 min							
	5	10	20	30	40	50	60	70
11,4	47	64	76	85	all			
15,6	40	54	65	74	83	95	all	
16,3	36	50	60	69	77	83	all	
19,5	34	45	54	62	69	75	86	all

6. CONCLUSION

Possibility of dry pressed ceramic tiles production explicitly on base of Czech fly ashes is quite real. To get optimal properties of final fired body it must be determined optimal water content of pressing granulate.

Acknowledgements

This Research project was financed with MSM 0021630511 „Progressive Building Materials with Utilization of Secondary Raw Materials and their Impact on Structures Durability“

References

1. MAAGE M. Frost resistance and pore size distribution of bricks 1-2, Ziegelindustrie International, 1990, no. 9, p. 472-481, no. 10, p. 582-588.
2. BENTRUP H., FRANKE L.: Evaluation of the frost resistance of bricks in regard to long service life, Ziegelindustrie International, 1993, no. 7-8, p. 483-492, no. 9, p. 528-536.
3. FRIESE P.: Predictions of the Frost Resistance of Bricks, Ziegelindustrie International, 1995, no. 12, p. 952-963.
4. SOKOLAR, R. Dry Pressed Ceramic Tiles on the Basis of Fly Ash. Interceram 2007. DVS-Verlag GmbH, Vol. 56, no.1, p. 30-35, ISBN.

Application of damage model for analysis of masonry structures

Jerzy Szołomicki

Department of Civil Engineering, Wrocław University of Technology, Wrocław, 50-370, Poland

Summary

The predictive modelling of the masonry structures behaviour, in the non-linear range represents a challenge due to their semi-discrete and composite nature. An adequate computational model should include the fundamental mechanisms that characterize the masonry behaviour at failure. This paper presents the application of a damage model, based on the finite elements method, to simulate the ultimate response and the mode of failure of different masonry structures. To take into account the mechanical properties degradation, a damage variable is introduced in the constitutive law of the material.

KEYWORDS: Masonry structures, damage model, computational simulations

1. INTRODUCTION

The masonry structures are widely used in civil engineering. These structures are characterised by a softening response. Indeed, the non-linear behaviour of masonry is due to the damage and plastic micromechanical processes. From a microscopic point of view the damage is linked to the growth and coalescence of micro-cracks, leading to the formation of macro-cracks which can induce the collapse of the structure. The plasticity is due to intergranular displacements and accounts for inelastic deformations occurring during the loading process. Various nonlinear models have been proposed in the literature to describe the softening response of masonry structural elements. The available models adopted for structural computations are mainly based on macro-mechanical approaches using damage mechanics and plasticity theory.

As known, any macro-model of masonry structures always includes some approximations, since the different failure mechanisms of masonry (cracking of the mortar joints, sliding along bed and/or head mortar joints, cracking of the bricks under direct tension, masonry crushing) are not exactly reproduced, but are smeared out in the continuum.

This paper presents the application of a damage model, based on the finite elements method, to simulate the ultimate response and the mode of failure of different masonry structures.

2. THE CONCEPTION OF DAMAGE MODEL

The nonlinear behaviour of masonry can be modelled using concepts of damage theory. In this case an adequate damage function is defined for taking into account different response of masonry under tension and compression states. Cracking can, therefore, be interpreted as a local damage effect, defined by the evolution of known material parameters and by one or several functions which control the onset and evolution of damage. The model takes into account all the important aspects which should be considered in the nonlinear analysis of masonry structures such as the effect of stiffness degradation due to mechanical effects and the problem of objectivity of the results with respect to the finite element mesh.

A useful concept for understanding the effect of damage is that of effective stress. The damaged σ_d and effective undamaged σ stress tensors are correlated, according to continuum damage mechanics, by the relation:

$$\sigma_d = (1 - d)\mathbf{D}\boldsymbol{\varepsilon} = (1 - d)\boldsymbol{\sigma} \quad (1)$$

where d is a scalar value, ranging from 0 to 1 and representing the local damage parameter, \mathbf{D} is the elastic stiffness matrix and $\boldsymbol{\varepsilon}$ is the strain tensor.

The damage function $g(\bar{\tau}, r)$ defines the limit of the region of undamaged response and is written at time t as:

$$(g(\bar{\tau}, r))^t = (\bar{\tau})^t - (r)^t \leq 0 \quad (2)$$

where the undamaged complementary energy norm is defined as:

$$(\bar{\tau})^t = \gamma \sqrt{2\Lambda^0(\boldsymbol{\sigma})^t} \quad (3)$$

where $\Lambda^0(\boldsymbol{\sigma})$ is the elastic complementary energy.

For Simo’s damage model $\gamma = 1$.

$(r)^t$ in the damage function of Equation (2) is the current damage strength measured with an energy norm and can be given as:

$$(r)^t = \max\left\{(r)^0, (\bar{\tau})^t\right\} \quad (4)$$

where $(r)^0$ denotes the initial damage threshold of the material.

The initial damage threshold $(r)^0$, can be considered to carry out a similar function to the initial yield stress in an analysis involving an elasto-plastic material. However, in a damage analysis, the value of the damage threshold influences the degradation of the elastic modulus matrix. A value for $(r)^0$ may be obtained from:

$$(\mathbf{r})^0 = \frac{\sigma_d^t}{(E_0)^{1/2}} \tag{5}$$

where σ_d^t is the uniaxial tensile stress at which damage commences and E_0 is the undamaged Young's modulus. The damage criterion is enforced by computing the elastic complementary energy function as damage progresses:

$$\beta(\boldsymbol{\sigma}^T \mathbf{D}_e \boldsymbol{\sigma})^{1/2} - (\mathbf{r})^t \leq 0. \tag{6}$$

The damage flow rule defines the damage softening and is given by

$$\dot{d} = \dot{\mu}^t \frac{\partial(G(\bar{\tau}^t, d)^t)}{\partial \tau} \tag{7}$$

where $\dot{\mu} \geq 0$ is the damage consistency parameter and defines damage loading/unloading conditions according to the Kuhn-Tucker relations

$$\dot{\mu} \geq 0, g(\bar{\tau}, r) \leq 0, \dot{\mu} g(\bar{\tau}, r) = 0. \tag{8}$$

In addition, to simplify the calculations in damage analysis, the damage multiplier $\dot{\mu}$ is defined so that

$$\dot{\mu} = \dot{r}. \tag{9}$$

From the consistency of the damage condition in Equation (2) it is given that

$$\dot{\bar{\tau}} = \dot{r} = \dot{\mu}. \tag{10}$$

According to Equation (10), the definition (3) we have

$$\dot{\mu} = \frac{\gamma^2}{\bar{\tau}} \boldsymbol{\sigma}^T \mathbf{D}_e^{-1} \dot{\boldsymbol{\sigma}}. \tag{11}$$

$(\partial G / \partial \bar{\tau})^t$ defines the damage rate with respect to the undamaged elastic complementary norm. If the damage potential function G is assumed to be independent of d , substitution of Equation (10) into Equation (7) will lead to:

$$d = G \tag{12}$$

with the undamaged condition being enforced so that

$$\left\{ G(\mathbf{r}^t) \right\}_{(\mathbf{r})^t = (\mathbf{r})^0} = 0. \tag{13}$$

Damage accumulation functions is given by:

$$\mathbf{G}((r)^t) = 1 - \frac{(r)^0(1-A)}{(r)^t} - A \exp[B((r)^0 - (r)^t)] \tag{14}$$

For no damage, $\mathbf{G}(r)^t = 0$. The characteristic material parameters, A and B, would generally be obtained from experimental data.

3. DAMAGE CRITERION

The damage criterion is defined as a function of the free energy Ψ_0 of the undamaged material, expressed in terms of undamaged principal stresses $\sigma_i^{p,0}$:

$$\mathbf{F} = K(\sigma^{p,0}) \sqrt{2\rho_0 \Psi_0} - 1 = \frac{K(\sigma^{p,0})}{\sqrt{E^0}} \sqrt{\sum_{i=1}^3 (\sigma_i^{p,0})^2} - 1 \leq 0 \tag{15}$$

where: ρ_0 is the density in the material configuration.

The terms of the above equation have the following meaning:

$$K(\sigma^{p,0}) = \frac{r}{\sqrt{2\rho_0 (\Psi_t^0)_L}} + \frac{1-r}{\sqrt{2\rho_0 (\Psi_c^0)_L}}, \tag{16}$$

$$r = \frac{\sum_{i=1}^3 \langle \sigma_i^{p,0} \rangle}{\sum_{i=1}^3 |\sigma_i^{p,0}|}, \tag{17}$$

$$2\rho_0 (\Psi_{t,c}^0)_L = \sum_{i=1}^3 \langle \pm \sigma_i^{p,0} \rangle \epsilon_i, \tag{18}$$

$$(\Psi_0)_L = (\Psi_t^0)_L + (\Psi_c^0)_L. \tag{19}$$

In these equations $(\Psi_{t,c}^0)_L$ represent the part of the free energy developed when the tension/compression limit is reached. Taking into account that the tension and compression strengths are $f_t = \sqrt{(2\rho_0 \Psi_t^0 E_0)_L}$ and $f_c = \sqrt{(2\rho_0 \Psi_c^0 E_0)_L}$ respectively, and substituting the last definition in the Equation (16), the damage function can be written as:

$$\mathbf{F} = \bar{\sigma} - f_c \leq 0 \tag{20}$$

where

$$\bar{\sigma} = [1 + r(n-1)] \sqrt{\sum_{i=1}^3 (\sigma_i^{p,0})^2} \quad (21)$$

with $n = \frac{f_c}{f_t}$. The advantage of the yield criterion written in Equation (21) is that any yield function \mathbf{F} can be used always as long as it is homogeneous and of first order in stresses (Mohr-Coulomb, Drucker-Prager).

4. GLOBAL DAMAGE IMPLEMENTATION

The idea for global damage indices definition stemmed from a macroscale analogy with the microscale local damage index definition. Thus, the starting point for deducing a global structural damage index is Equation (22), which defines local damage as a relation between the actual free energy Ψ of the damaged material and the elastic free energy Ψ_0 of a fictitious undamaged material.

$$\Psi(\boldsymbol{\varepsilon}, d) = (1-d)\Psi_0(\boldsymbol{\varepsilon}) = (1-d) \left(\frac{1}{2\rho_0} \boldsymbol{\varepsilon}^T \boldsymbol{\sigma}^0 \right). \quad (22)$$

It seemed natural to reach this objective by integrating the pointwise Equation (22) over a finite mass, as follows:

$$\Psi = (1-d)\Psi_0 \Rightarrow \mathbf{W}_p = \int_V \rho_0 \Psi dV = \int_V (1-d)\rho_0 \Psi_0 dV = (1-D)\mathbf{W}_p^0 \quad (23)$$

where D^* is the global damage indices of the considered structural mass, $\mathbf{W}_p^0 = \int_V \rho_0 \Psi_0 dV$ is its fictitious ever-elastic potential energy due to the actual strains and \mathbf{W}_p is the actual potential energy. Solving Equation (23) for D , yields the final expression:

$$D^* = 1 - \frac{\mathbf{W}_p}{\mathbf{W}_p^0} = \frac{\int_V \rho_0 \Psi_0 dV - \int_V (1-d)\rho_0 \Psi_0 dV}{\int_V \rho_0 \Psi_0 dV} = \frac{\int_V d\rho_0 \Psi_0 dV}{\int_V \rho_0 \Psi_0 dV}. \quad (24)$$

In a finite element context, expression (24) takes the following operational form:

$$D^* = 1 - \frac{\sum_e \mathbf{a}^T \int_{V^{(e)}} \mathbf{B}^T \boldsymbol{\sigma} dV}{\sum_e \mathbf{a}^T \int_{V^{(e)}} \mathbf{B}^T \boldsymbol{\sigma}^0 dV} \quad (25)$$

where \sum_e denotes the sum over a number of finite elements, \mathbf{a} is the mesh nodal displacement vector, \mathbf{B} is the strain displacement matrix, $V^{(e)}$ is the volume of each finite element (e), $\boldsymbol{\sigma}$ is the actual stress vector and $\boldsymbol{\sigma}_0$ is the stress vector should the material preserve its original characteristics and undergo the actual strains.

CONCLUSION

In this paper the author presented a damage model which can be applied successfully to assess the structural conditions and estimate the safety level and durability of historical masonry constructions under static and dynamic loading. The global damage indices provides accurate quantitative data on the state of any component subpart of a damaged structure and its importance to the overall structural behaviour, being of invaluable help to the task of assessing the reliability, safety and definition of adequate repair or retrofitting strategies.

References

1. Maier, G., Nappi, A. Papa, E. Damage models for masonry as a composite material: a numerical and experimental analysis. *Constitutive Laws for Engineering Materials*, ASME Press, New York, 1991.
2. Kachanov, L.M. Continuum model of medium with cracks. *ASCE J. Engng Mech.*, vol. 106: p. 1039-1051, 1980.
3. Park, Y.J., Ang, A.S. Mechanistic seismic damage model for reinforced concrete. *ASCE, J. Struct. Engng*, vol. 111: p. 722-739, 1985.
4. Pijaudier-Cabot, G., Bazant, Z.P. Non local damage theory. *ASCE J. Engng Mech.*, vol. 113: p. 1512-1533, 1987.
5. Gambarotta, L., Lagomarsino, S. Damage in brick masonry shear walls. *Fracture and Damage in Quasibrittle Structures: Experiments, Modelling and Computer Analysis*, p. 463-472, 1994.

A New Form of the Active Moments Method

Constantin Ionescu

Civil Engineering, University, Iassy, Zip code: 700482, Romania

Summary

The paper desires to pay a tribute to Professors A. Şesan and N. Orlovski, which professed last century at the Faculty of Civil Engineering and Installations from Iasi.

These professors imagined a calculation procedure for frames, named active moment method, as a response to the displacement (deformation) method.

The structure calculation by displacement methods is conducted on a base system, obtained by introducing fictive connections which deters the possible displacement of the nodes – revolutions and translations.

The elements in question in the displacement method are the nodes real displacements (written Z_i). Under the exterior forces action and displacements, on the elements in question direction, in the complementary connections appear reactions. Total reactions from complementary connections must be equal to zero. This way it can be obtained the condition equations.

Despite the active moments method, the basic system is similar to that in the displacements method, but the element in question are “active moments” of nodes M_i and displacement (kinematic chains), M_A .

The active moment is defined as the moment which by its action on the base system, on the node “ i ” or in the degree of freedom “ a ”, creates the real displacement of the node “ i ”, and the real displacement of the nodes which are part of the kinematic chain “ a ”.

The condition equations from the active moments method expresses the structure static equilibrium and has two types: nodes equilibrium equations and kinematic chains equilibrium equations. Must be mentioned the fact that none of the papers written by the authors didn’t demonstrated the way in which the equilibrium equations have been obtained.

In the present paper have been obtained the equilibrium equations by active moments method by using the girder, node and nodes and beams chain equilibrium conditions with the help of the methodology "Gh. Em. Filipescu". This way has been obtained calculation relations for the extremity moments more general than the ones used in the displacements method, relations (4.6.) and (4.19.).

Also, it has been distinguished an alternative of the active moments method, where the elements in question are node active moments and active displacement forces.

KEYWORDS: structure calculus, condition equations, active moments, active forces, displacements, rigidities.

1. INTRODUCTION

The engineering technique evolution, in different time periods, has been determined by the necessity of refuge and attendance of the human activities which imposed a diversified volume of constructions. Due to this fact, has increased the number of problems connected to the search of different constructive forms which could better undertake the actions with a minimal construction materials consume.

The resistance structures composition and calculation has been made, long ago, based on the experience and only slightly on the theoretical elements.

Latter, based on the phenomena observation have been established constructive rules and calculation models, repetitively verified on the constructions. Generalizing the experience and development of the experimental researches have been developed the theoretical calculation basis for the constructions.

The current stage of theory development and structure calculus is due to engineers and science people who have discovered the solutions for the problems of the resistance structures design and execution for different constructions by experimental methods but also by theoretical ways.

Considering the investigations, have resulted general calculation methods, main principles of construction organization and future horizons of the researches in the area of one of the most interesting branches of the Construction Mechanics and Construction Dynamics.

In the science people gallery, which have contributed to the development of Construction Mechanics can be mentioned J.C.Maxwell, O. Mohr, K. Culman, L. Cremona, pe S. Timošenko, I.P. Prokofiev and others.

In Romania, great engineers and professors as Gh. Em. Filipescu, A. Beleş, M. Hanganu, C. Avram, Alex. Gheorghiu, A. Şesan, M. Ifrim, N. Orlovski and others have obtained remarkable results in the area of Constructions Static and Dynamics.

2. STATEMENT OF EQUILIBRIUM CONDITION

In the paper “The frame calculation by circumvolution method” published by A. Şesan and N. Popescu, in 1954, in the Journal of University “Al. I. Cuza” and

Polytechnic Institute in Iasi, are presented several definitions regarding the static structures calculus undetermined by displacements method.

It is mentioned that in that moment were known two methods of expressing the equilibrium equations. The first one had been published in Wien, in 1943, by R. Guldán. The equilibrium condition was expressed by two types of equations:

- Equilibrium equations on node ($\Sigma M_i = 0$):

$$d_i \varphi_i + \sum_k K_{ik} \varphi_i + K_{is} \Delta_{is} + K_{ij} \Delta_{ij} + S_i = 0 \quad (2.1)$$

- Equilibrium equations of floor ($\Sigma T_k = 0$):

$$\sum_u \overline{K} \varphi_s + \sum_a \overline{K}_j \varphi_j + D_u + S_u = 0 \quad (2.2.)$$

In these equilibrium equations have been made the notations:

- $\varphi_i, \varphi_k, \varphi_s$ – nodes unknown angular displacements;
- Δ_k – unknown linear displacements of the nodes;
- K_{ik} – rigidity at circumvolution of a bar extremity;
- \overline{K}_s – rigiditatea la deplasare transversală a unei extremități de bară;
- S_i, D_u și S_u – terms resulted from the actions effect.

Starting from the same base system with stucked displacements, I.P.Procofiev has published, in 1948, another form of static equilibrium equations:

- Node equilibrium equations:

$$\sum_{j=1}^N r_{ij} Z_j + \sum_{s=a}^G r_{is} Z_s + R_{ip} = 0 \quad i = 1, 2, \dots, N \quad (2.3.)$$

- Kinematic chain equilibrium equations:

$$\sum_{i=1}^N r_{si} Z_i + \sum_{e=a}^G r_{se} Z_e + R_{sp} = 0; \quad s = a, b, \dots, G \quad (2.4.)$$

Where: Z_1, \dots, Z_j are nodes angular unknown displacements ,
 Z_k, \dots, Z_n – nodes linear displacements.

Analyzing the two forms of the equilibrium equations statement, it can be observed that the first way in which it is used the forces equilibrium ($T = 0$), expressed by forces projections on perpendicular directions on beams, diminishes the application area only to frames with floors parallel beams. The second way, presented by Prokofiev, is based on effects overlapping (of the diagrams) and it is more general

than the first one, because it increases the methods area of application also to the frames with inclined pillars.

It must be mentioned also the paper of P. Mazilu, in Bucharest, in 1946, entitled: “The Frames Calculation – Displacements and Virtual Mechanical Work in Cross Method”. The paper has been elaborated, as the author says, between 1942 –1943 and “introduces in Cross Method the principle of virtual displacements and virtual mechanical work”.

In the same direction is written also the paper “Another Form of the Condition Equations for the Deformation Method” with the authors: A. Şesan and N. Popescu. The authors demonstrate that “the use of mechanical work for the condition equations establishment – node and displacement – can be generalized for any frames type”.

The cited article and the paper named “Variants and Simplification of the Moments Distribution Method”, published by A. Sesan and N. Orlovski, puts the basis of active moments method by introducing the notions of node and chain active moment.

In this paper, it is mentioned the use of “revolutions and displacements” as unknown elements of the condition equations which is a “disadvantage”, because it operates with “insignificant” values, “modified” by multipliers and because of that the authors propose to express the equilibrium condition by elements in question - “active moments”.

3. ABOUT THE “ACTIVE MOMENTS” METHOD

The “active moments” method was created in 1954 by professor A. Şesan and his collaborators: N. Orlovski and N. Popescu. This is an alternative of displacements method which operates with unbalanced moments: “active moments“ of nodes, \mathbf{M}_i and displacement (kinematic chains), \mathbf{M}_a .

The active moment is defined as the moment which by activating, on the base system, on “i” node or in the liberty degree “a”, determines the node “i” real displacement, also the real displacement of the node which are part from the kinematic chain “a”.

The condition equations in the active moments method express the structure of static equilibrium and are of two types:

Nodes equilibrium equations:

$$\sum_i M = 0; \quad -M_i + \sum_{j=1}^N \mu_{ij} M_j + \sum_a^G \mu_{ia} M_a + \mathfrak{m} = 0; \quad (i = 1, 2, \dots, N); \quad (3.1.)$$

- Kinematic chains equilibrium equations:

$$\sum_a M = 0; \quad -M_a + \sum_{i=1}^N \mu_{ai} M_i + \sum_b^G \mu_{ab} M_b + m_a = 0; \quad (a = a,b,\dots,G); \quad (3.2.)$$

Where have been done the notations:

$$\mu_{ij} = -d_{ji} t_{ji}; \quad \mu_{ji} = -d_{ij} t_{ij}; \quad \mu_{ij} \neq \mu_{ji}; \quad (3.3.)$$

$$\mu_{ia} = \sum_i \pm v'_{ij,a}; \quad v'_{ij,a} = \frac{\overline{K}_{ij} \beta_{ij,a}}{\sum_A (\overline{K}_{ij} + \overline{K}_{ji}) \beta_{ij,a}}; \quad (3.4.)$$

$$\mu_{ai} = \frac{1}{\beta_a} \sum_a d_{ij} (1 + t_{ij}) \beta_{ij,a}; \quad \mu_{ia} \neq \mu_{ai}; \quad (3.5.)$$

$$\mu_{ab} = -\frac{1}{\beta_a} \sum_{a,b} (v'_{ij,a} + v'_{ji,b}) \beta_{ij,a}; \quad \mu_{ab} \neq \mu_{ba}; \quad (3.6.)$$

$$m_i = \sum_j m_j; \quad m_a = \frac{1}{\beta_a} (\sum_a (m_j + m_j) \beta_{i,a} + \sum_k P_k \delta_{k,a}); \quad (3.7.)$$

For these coefficients calculation are used the rigidities for the rotation of the bars extremities and for the transversal displacement of the bars extremities, \mathbf{K}_{ij} și \mathbf{K}_{ij}^ψ , the distribution and transmission: \mathbf{d}_{ij} , and \mathbf{t}_{ij} and two proportionality coefficients: β_{ij} și β_A .

The proportionality coefficient of the bar rotation \mathbf{ij} noted β_{ij} is calculated by considering a bar rotation which is equal to the unit, by which can be determined the other bars rotations.

If we consider that on a fictive bar acts an active moment, \mathbf{M}_A , than the proportionality coefficient of this bar is β_A . The calculus is done with the relation:

$$\beta_a = \frac{\sum_a (\overline{K}_{ij}^\psi + \overline{K}_{ji}^\psi) \beta_{ij,a}^2}{\sum_a (\overline{K}_{ij}^\psi + \overline{K}_{ji}^\psi) \beta_{ij,a}} \quad (3.8.)$$

4. DIRECT DEVICE FOR CONDITION EQUATION DEDUCTION IN THE METHOD OF “ACTIVE MOMENTS”

The deformed position of a certain frame can be defined by the mean of nodes displacements: rotations and translations.

The nodes angular displacements ($z_i, i = 1, 2, 3, \dots, N$) are independent variables, while the linear displacements ($z_s, s = a, b, c, \dots, G$) are interdependent by the mean of a number of parameters equal to the number of liberty degrees of the kinematic system, obtained by introducing articulations in nodes and in bearing constraint. The result is that the number of independent parameters, which geometrically define the deformed position of a structure, equals the nodes number to which is added the number of degrees of the frame elastic liberty. The nodes translations are part of a kinematic chain which relies on a single parameter, z_s .

For a bar **ij**, the rotation noted ψ_{ij} is expressed considering the parameter z_s with the relation:

$$\psi_{ij,s} = \beta_{ij,s} z_s \tag{4.1.}$$

Where $\beta_{ij,s}$ is the bar rotation **ij** when the parameter $z_s = 1$.

4.1. The girder equilibrium conditions

We extract a bar **ij** from a base system, of a certain structure, corresponding to the displacements method, activated by burdens and displacements (nodes rotation and bar rotation), fig.4.1. The general expressions of the end moments can be expressed as:

$$\begin{aligned} M_{ij} &= M_{ij}(z_i) + M_{ij}(z_j) + M_{ij}(\psi_{ij}) + M_{ij}(p) \\ M_{ji} &= M_{ji}(z_i) + M_{ji}(z_{jj}) + M_{ji}(\psi_{ij}) + M_{ji}(p) \end{aligned} \tag{4.2.}$$

Or as notations in fig.4.1:

$$\begin{aligned} M_{ij} &= K_{ij} z_i + t_{ji} K_{ji} z_j - \overline{K_{ij}^{\psi}} \psi_{ij} - m_{ij} \\ M_{ji} &= t_{ij} K_{ij} z_i + K_{ji} z_j - \overline{K_{ji}^{\psi}} \psi_{ij} + m_{ij} \end{aligned} \tag{4.3.}$$

In the case in which the bar **ij**, considered in the research, is component of different chains and nodes corresponding to the liberty degrees **a, b, c, ..., G**, than the expression of bar rotation can be written as a sum of rotations corresponding to each liberty degree:

$$\psi_{ij} = \psi_{ij,a} + \psi_{ij,b} + \psi_{ij,c} + \dots = \sum_{s=a}^G \psi_{ij,s} \tag{4.4.}$$

or taking into consideration the relation (4.1):

$$\psi_{ij} = \sum_{s=a}^G \beta_{ij,s} z_s \tag{4.5.}$$

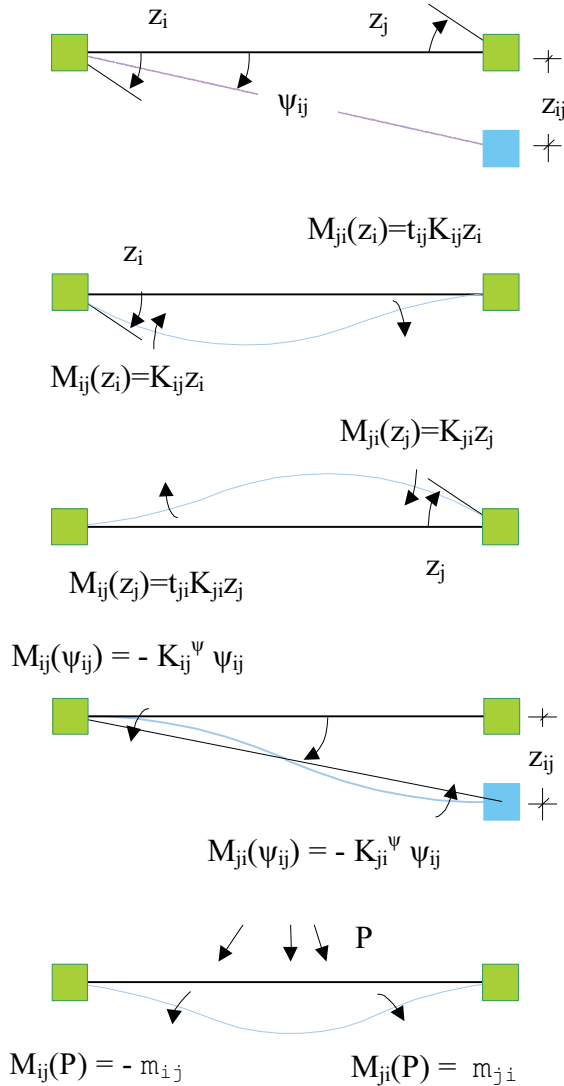


Fig. 4.1 Situations of girder and node loads considering the statement of equilibrium conditions – bar end moments ij for different load situations

The end moments, the relations (4.2.), as per relations (4.4.) and (4.5.) and notations from fig.4.1, become:

$$\begin{aligned}
 M_{ij} &= K_{ij}z_i + t_{ji}K_{ji}z_j - \sum_{s=a}^G \overline{K_{ij}^\psi} \beta_{ij,s} z_s - m_j \\
 M_{ji} &= t_{ij}K_{ij}z_i + K_{ji}z_j - \sum_{s=a}^G \overline{K_{ji}^\psi} \beta_{ji,s} z_s + m_j
 \end{aligned}
 \tag{4.6.}$$

4.2. Node equilibrium conditions

Considering a node *i* taken from a certain structure, fig. 4.2., in which compete several bars, activated by a couple M_i . The node will rotate. The node rotation measurement, z_i , will equal each bar extremity rotation measure which competes in the node. In each bar extremity the end moments, which appear are proportional to the rotation measurement z_i ($M_{ij} = K_{ij}z_i$).

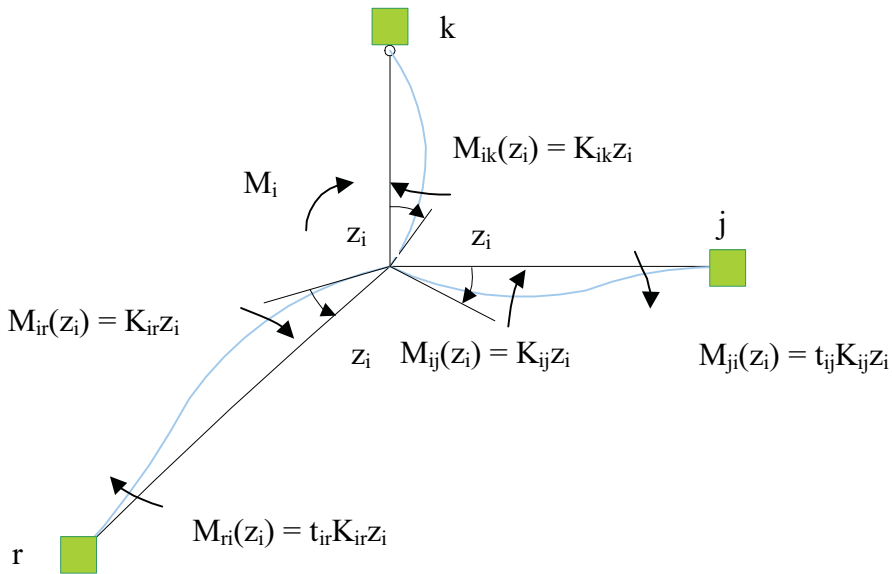


Fig. 4.2 The end moments of the bars which compete in node *i* when the node is loaded with a rotation of node, z_i , or with an active moment of node, M_i

Expressing the node *i* equilibrium, by a moment's equation:

$$\sum_i M_i = 0; \quad \Rightarrow M_i = \sum_{j=1}^{N_j} K_{ij} z_i
 \tag{4.7.}$$

Where:

$$z_i = \frac{1}{\sum_{j=1}^{N_i} K_{ij}} M_i \tag{4.8.}$$

Where - N_i represents the number of nodes connected by bars to node i .

4.3. Chain equilibrium condition

It is detached, from a certain frame, fig. 4.3.a., a chain of bars and nodes corresponding to a liberty degree, depending on the parameter z_s . We act on this chain with an active moment, M_s , which determines the real displacement, z_s , or, the rotations, $\psi_{ij,s}$, without the node to have the possibility to rotate.

We express the equilibrium of these bars and nodes chain by a moment's equation:

$$\sum_s M = 0 \quad \Rightarrow M_s = \sum_{ij=1}^{B_s} (\overline{K_{ij}^\psi} + \overline{K_{ji}^\psi}) \psi_{ij,s} \tag{4.9.}$$

And considering the relation (4.1.) it is obtained:

$$M_s = z_s \sum_{ij=1}^{B_s} (\overline{K_{ij}^\psi} + \overline{K_{ji}^\psi}) \beta_{ij,s} \tag{4.10.}$$

Where:

$$z_s = \frac{1}{\sum_{ij=1}^{B_s} (\overline{K_{ij}^\psi} + \overline{K_{ji}^\psi}) \beta_{ij,s}} M_s \tag{4.11.}$$

Where - B_s number of bars for the chain s .

In order to determine the reaction from the connection of liberty degree it turns to the faulty in fig. 4.3.c. and the displaced in fig.4.3.d. The articulated scheme of the nodes and bars chain loaded with the moments on the bars and the reaction R_s is in equilibrium. The equilibrium is expressed by an equation of virtual mechanical work by producing a kinematic displacement compatible with the connections. It results:

$$R_s \Delta^{ar} - \sum_{ij}^{B_s} (\overline{K_{ij}^\psi} + \overline{K_{ji}^\psi}) \psi_{ij,s} \psi_{ij,s}^{ar} = 0 \tag{4.12.}$$

Or

$$R_s \Delta^{ar} - \sum_{ij=1}^{B_s} (\overline{K_{ij}^\psi} + \overline{K_{ji}^\psi}) \beta_{ij,s} z_s \beta_{ij,s} \Delta^{ar} = 0 \tag{4.13.}$$

Where

$$R_s = \sum_{ij=1}^{B_s} (\overline{K_{ij}^\psi} + \overline{K_{ji}^\psi}) \beta_{ij,s}^2 z_s \tag{4.14.}$$

And

$$z_s = \frac{1}{\sum_{ij=1}^{B_s} (\overline{K_{ij}^\psi} + \overline{K_{ji}^\psi}) \beta_{ij,s}^2} R_s \tag{4.15.}$$

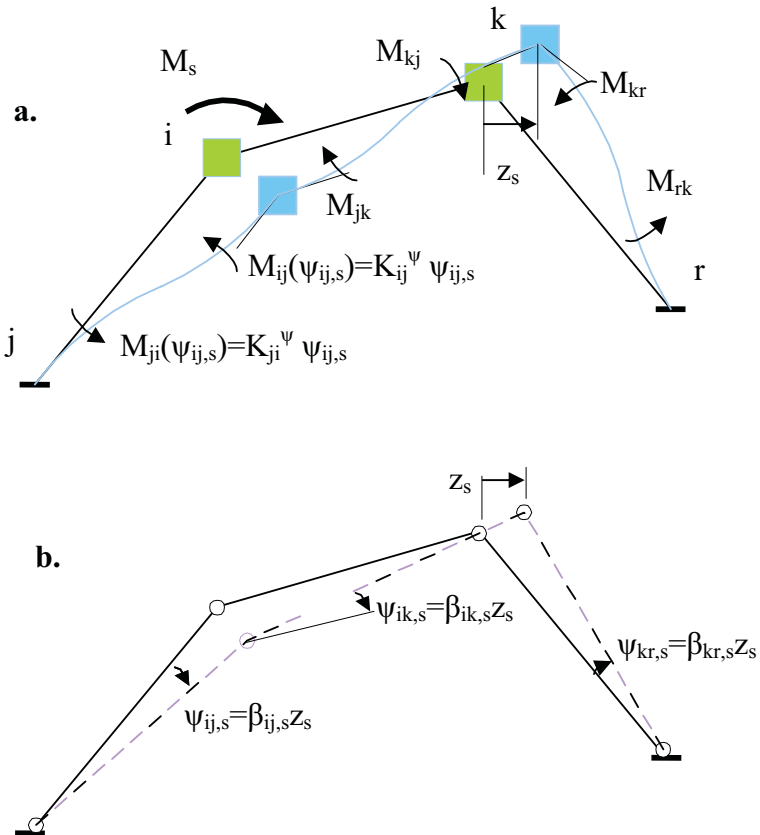


Fig.4.3. Loading situations for a nodes and bars chain in order to express the equilibrium condition: a. Bars and nodes chain loaded with the active moment of displacement, M_a ; b. the connection between the bar rotation, $\psi_{ij,s}$ and displacement z_s ;

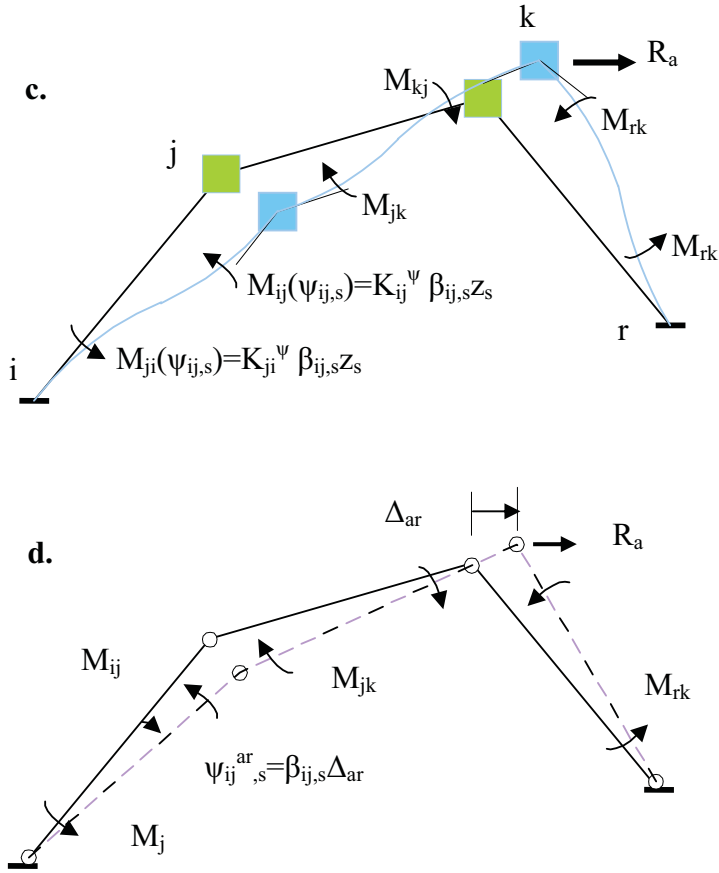


Fig .4.3 (continuance) Loading situations for a nodes and bars chain in order to express the equilibrium condition: d. The articulated scheme for a bars chain having in the bars extremities applied end moments, M_{ij} and the reaction from the liberty degree hardcore; c. Nodes and bars chain loaded with the real displacement z_s , on the liberty degree direction has been introduced the corresponding reaction R_a

Equalizing the relations (4.11.) and (4.15) it results:

$$\beta_s = \frac{R_s}{M_s} = \frac{\sum_{ij=1}^{B_s} (\overline{K_{ij}^{\psi}} + \overline{K_{ji}^{\psi}}) \beta_{ij,s}^2}{\sum_{ij=1}^{B_s} (\overline{K_{ij}^{\psi}} + \overline{K_{ji}^{\psi}}) \beta_{ij,s}} \quad (4.16.)$$

Or

$$R_s = \beta_s M_s = \frac{\sum_{ij=1}^{B_s} (\overline{K_{ij}^\psi} + \overline{K_{ji}^\psi}) \beta_{ij,s}^2}{\sum_{ij=1}^{B_s} (\overline{K_{ij}^\psi} + \overline{K_{ji}^\psi}) \beta_{ij,s}} M_s \quad (4.17.)$$

β_s is, from the active moments method point of view, the rotation of a fictive bar on which would act the active displacement moment.

Based on the relations, (4.8.), (4.11.) and (4.16.) can be written the general expressions of bar moments loaded with burdens, with node active moments, \mathbf{M}_i , and active displacement moments, \mathbf{M}_s , or with node active moments and active displacement force, \mathbf{R}_s :

$$M_{ij} = \frac{K_{ij}}{\sum_{j=1}^{N_i} K_{ij}} M_i + t_{ji} \frac{K_{ji}}{\sum_{i=1}^{N_j} K_{ji}} M_j - \sum_{s=a}^G \frac{\overline{K_{ij}^\psi} \beta_{ij,s}}{\sum_{ij=1}^{B_s} (\overline{K_{ij}^\psi} + \overline{K_{ji}^\psi}) \beta_{ij,s}} M_s - m_j \quad (4.18.)$$

$$M_{ji} = t_{ij} \frac{K_{ij}}{\sum_{j=1}^{N_i} K_{ij}} M_i + \frac{K_{ji}}{\sum_{i=1}^{N_j} K_{ji}} M_j - \sum_{s=a}^G \frac{\overline{K_{ji}^\psi} \beta_{ij,s}}{\sum_{ij=1}^{B_s} (\overline{K_{ij}^\psi} + \overline{K_{ji}^\psi}) \beta_{ij,s}} M_s - m_j \quad (4.19.)$$

Also,

$$M_{ij} = d_{ij} M_i + t_{ji} d_{ji} M_j - \sum_{s=a}^G v_{ij,s} M_s - m_j \quad (4.20.)$$

$$M_{ji} = t_{ij} d_{ij} M_i + d_{ji} M_j - \sum_{s=a}^G v_{ji,s} M_s + m_j$$

And

$$M_{ij} = d_{ij} M_i + t_{ji} d_{ji} M_j - \sum_{s=a}^G v'_{ij,s} R_s - m_j \quad (4.21.)$$

$$M_{ji} = t_{ij} d_{ij} M_i + d_{ji} M_j - \sum_{s=a}^G v'_{ji,s} R_s + m_j$$

Where:

$$d_{ij} = \frac{K_{ij}}{\sum_{j=1}^{N_i} K_{ij}}; \quad v_{ij,s} = \frac{\overline{K_{ij}^\psi} \beta_{ij,s}}{\sum_{ij=1}^{B_s} (\overline{K_{ij}^\psi} + \overline{K_{ji}^\psi}) \beta_{ij,s}}; \quad v'_{ij} = \frac{\overline{K_{ij}^\psi} \beta_{ij,s}}{\sum_{ij=1}^{B_s} (\overline{K_{ij}^\psi} + \overline{K_{ji}^\psi}) \beta_{ij,s}^2}; \quad (4.22.)$$

Observation: 1. the expressions 4.8 and 4.11 indicate the fact that the real displacements of the nodes can be determined based on the node and displacement active moments.

2. Analyzing the relations (4.3.), (4.6.) and (4.20.) we can say that the last two relations are more general, because the end moments are applicable to any straight bar from a static undetermined structure, with rigid nodes, loaded with burdens, node rotations and parameters of liberty degrees, node active moments and active displacement moments.

It is considered, a certain structure driven by a force system. The structure will deform and in the bars extremities appear bending moments, determined by the relations (4.5), (4.18) and (4.19). In order to determine the elements in question: nodes different displacements (\mathbf{z}_i și \mathbf{z}_s) or, node and displacement active moments (\mathbf{M}_i și \mathbf{M}_s) we will use the methodology of Gh. Em. Filipescu. In this method are being used the labile base systems activated by the given forces and the end moments (\mathbf{M}_{ij} , \mathbf{M}_{ji}). Are being used two types of equations:

- Continuity equations. In the case studied, here, in the paper, these equations reduced to the level of each bar, brought us to the relations (4.5), (4.18) and (4.19);
- Static equilibrium equations:

$$\sum_{j=1}^{N_i} M_{ij} = 0; \quad i = 1, 2, 3, \dots, N \tag{4.23.}$$

$$LMV_{(s)} = 0; \quad s = a, b, c, \dots, G \tag{4.24.}$$

Explaining the equations (4.23) and (4.24) by end moments, the relations (4.5), (4.19), and (4.21), can be obtained these equation systems:

$$\sum_{j=1}^{N_i} K_{ij} z_i + \sum_{j=1}^{N_i} t_{ij} K_{ij} z_j - \sum_{s=a}^G \overline{K_{ij}^v} \beta_{ij,s} z_s - \sum_{j=1}^{N_i} m_j = 0 \tag{4.25.}$$

$$\begin{aligned} & \sum_{ij=1}^{B_s} K_{ij} (1+t_{ij}) \beta_{ij,e} z_i + \sum_{ij=1}^{B_s} K_{ij} (1+t_{ij}) \beta_{ij,e} z_j - \sum_{s=a}^G \sum_{ij=1}^{B_s} (\overline{K_{ij}^v} + \overline{K_{ji}^v}) \beta_{ij,s} \beta_{ij,e} z_s + \\ & + \sum_{ij}^{B_s} (-m_j + m_i) \beta_{ij,e} + \sum_{k=1}^{N_p} P_k \delta_{k,e} = 0; \quad i = 1, 2, \dots, N: \quad i \neq j; \quad e = a, b, \dots, G; \end{aligned} \tag{4.26.}$$

Or

$$r_{ii}z_i + \sum_j r_{ij}z_{jj} + \sum_s r_{is}z_s + R_{ip} = 0; \quad i \neq j; \quad i = 1, 2, \dots, N; \quad (4.27.)$$

$$\sum_i r_{si}z_i + \sum_j r_{ij}z_j + \sum_s r_{se}z_s + R_{sp} = 0; \quad i \neq j; \quad e = 1, 2, \dots, G; \quad (4.28.)$$

And

$$\sum_{j=1}^{N_i} d_{ij}M_i + \sum_{j=1}^{N_i} t_{ji}d_{ji}M_j - \sum_{s=a}^G \sum_{j=1}^{N_i} v_{ij,s}M_s - \sum_{j=1}^{N_i} m_j = 0; \quad i \neq j; \quad i = 1, 2, \dots, N; \quad (4.29.)$$

$$\begin{aligned} & \sum_{ij=1}^{B_s} d_{ij} (1+t_{ij}) \beta_{ij,e} M_i + \sum_{ij=1}^{B_s} d_{ji} (1+t_{ij}) \beta_{ij,e} M_j - \sum_{s=a}^G \sum_{ij=1}^{B_s} (v_{ij,s} + v_{ji,s}) \beta_{ij,s} \beta_{ij,e} M_s + \\ & + \sum_{ij}^{B_s} (-m_j + m_j) \beta_{ij,e} + \sum_{k=1}^{N_p} P_k \delta_{k,e} = 0; \quad i = 1, 2, \dots, N; \quad i \neq j; \quad e = a, b, \dots, G; \end{aligned} \quad (4.30.)$$

Or

$$M_i + \sum_j \mu_{ij}z_j + \sum_s \mu_{is}M_s + m_p = 0; \quad (4.31.)$$

$$\sum_i \mu_{si}M_i + \sum_j \mu_{sj}M_j + \sum_e \mu_{es}M_e + m_{sp} = 0; \quad (4.32.)$$

Also

$$\sum_{j=1}^{N_i} d_{ij}M_i + \sum_{j=1}^{N_i} t_{ji}d_{ji}M_j - \sum_{s=a}^G \sum_{j=1}^{N_i} v'_{ij,s}R_s - \sum_{j=1}^{N_i} m_j = 0; \quad i \neq j; \quad i = 1, 2, \dots, N; \quad (4.33.)$$

$$\begin{aligned} & \sum_{ij=1}^{B_s} d_{ij} (1+t_{ij}) \beta_{ij,e} M_i + \sum_{ij=1}^{B_s} d_{ji} (1+t_{ij}) \beta_{ij,e} M_j - \sum_{s=a}^G \sum_{ij=1}^{B_s} (v'_{ij,s} + v'_{ji,s}) \beta_{ij,s} \beta_{ij,e} R_s + \\ & + \sum_{ij}^{B_s} (-m_j + m_j) \beta_{ij,e} + \sum_{k=1}^{N_p} P_k \delta_{k,e} = 0; \quad i = 1, 2, \dots, N; \quad i \neq j; \quad e = a, b, \dots, G; \end{aligned} \quad (4.34.)$$

Regarding the previous relations certain comments must be done, such as:

- The relations (4.27) and (4.28) represent the condition equations system for a structure static undetermined, in the displacement method. The elements in question are the displacements. The free terms are reactions, and the coefficients are unitary reactions and are determined with the above relations:

$$r_{ii} = \sum_{j=1}^{N_i} K_{ij}; \quad r_{ij} = t_{ij} K_{ij}; \quad (4.35.)$$

$$r_{is} = -\sum_{j=1}^{N_i} \overline{K_{ij}^{\psi}} \beta_{ij,s}; \quad r_{si} = \sum_{ij=1}^{B_s} K_{ij} (1 + t_{ji}) \beta_{ij,s}; \quad (4.36.)$$

$$r_{es} = \sum_{ij=1}^{B_s} (\overline{K_{ij}^{\psi}} + \overline{K_{ji}^{\psi}}) \beta_{ij,s} \beta_{ij,e}; \quad R_{ip} = -\sum_{k=1}^{N_i} m_j; \quad (4.37.)$$

$$R_{ep} = \sum_{ij=1}^{B_e} (-m_j + m_j) \beta_{ij,e} + \sum_{k=1}^{N_p} P_k \delta_{k,p}; \quad (4.38.)$$

- The relations (4.21) and (4.32) represent the condition equation system for a structure static undetermined, in the method of active moments. The elements in question are node and bars active moments. The free terms and coefficients are determined with the relations:

$$\mu_{ii} = \sum_{j=1}^{N_i} d_{ij}; \quad \mu_{ij} = t_{ji} d_{ji}; \quad i \neq j; \quad (4.39.)$$

$$\mu_{is} = -\sum_{j=1}^{N_i} v_{ij,s}; \quad \mu_{si} = \sum_{ij=1}^{B_s} d_{ij} (1 + t_{ij}) \beta_{ij,s}; \quad i \neq j \quad (4.40.)$$

$$\mu_{ej} = \sum_{ij=1}^{B_e} d_{ji} (1 + t_{ji}) \beta_{ij,e}; \quad \mu_{es} = -\sum_{ij=1}^{B_s} (v_{ij,s} + v_{ji,s}) \beta_{ij,e}; \quad (4.41.)$$

$$m_{ip} = -\sum_{j=1}^{N_i} m_j; \quad m_{ep} = \sum_{ij=1}^{B_e} (-m_j + m_j) \beta_{ij,e} + \sum_{k=1}^{N_p} P_k \delta_{k,e} \quad (4.42.)$$

- The relations (4.33) and (4.34) represent the condition equations system for a structure static undetermined, in an alternative of active moments method. The elements in question are node active moments and active displacement forces.

4.5. The indirect device for condition equation deduction from active moment methods starting from the equation system of the displacement method.

Corroborating the relations (4.8) with (4.35) and (4.11) with (4.16) and (4.37) for $e = s$, can be obtained the expressions:

$$z_i = \frac{1}{r_{ii}} M_i; \tag{4.43.}$$

$$z_s = \frac{\beta_s}{r_{ss}} M_s; \tag{4.44.}$$

Are introduced the relations (4.43) and (4.44) in the condition equation system of the displacement method (2.3) and (2.4), results:

$$\frac{r_{ii}}{r_{ii}} M_i + \sum_j \frac{r_{ij}}{r_{jj}} M_j + \sum_s \frac{r_{is}}{r_{ss}} M_s + R_{ip} = 0; \tag{4.45.}$$

$$\sum_i \frac{r_{si}}{r_{ii}} M_i + \sum_j \frac{r_{sj}}{r_{jj}} M_j + \sum_s \frac{r_{se}}{r_{ss}} \beta_s M_s + R_{sp} = 0; \tag{4.46.}$$

After dividing the equation (4.46.) by β_s it is obtained:

$$\sum_i \mu_{si} M_i + \sum_j \mu_{sj} M_j + \sum_e \mu_{es} M_e + m_{sp} = 0; \tag{4.47.}$$

$$M_i + \sum_j \mu_{ij} z_j + \sum_s \mu_{is} M_s + m_p = 0; \tag{4.48.}$$

The equation system (4.45) and (4.46) is identical with (4.31) and (4.32), and the system (4.47) and (4.48) is identical with the equation system formed from (2.3) and (2.4). Consequently, between the coefficients and free terms of displacement method and active moment method are the relations:

$$\mu_{ii} = \frac{r_{ii}}{r_{ii}} = 1; \quad \mu_{ij} = \frac{r_{ij}}{r_{jj}}; \quad \mu_{is} = \frac{r_{is}}{r_{ss}}; \tag{4.49.}$$

$$\mu_{si} = \frac{r_{si}}{r_{ii}} \frac{1}{\beta_s}; \quad \mu_{sj} = \frac{r_{sj}}{r_{jj}} \frac{1}{\beta_s}; \quad \mu_{se} = \frac{r_{se}}{r_{ss}}; \tag{4.50.}$$

$$m_p = R_{ip}; \quad m_{sp} = \frac{R_{sp}}{\beta_s}; \tag{4.51.}$$

3. CONCLUSION

Have been obtained the equilibrium equations from active moment method by using the equilibrium conditions for girder, node and nodes and bars chain by the mean of "Gh. Em. Filipescu" methodology. The equation system obtained in subchapter 4.2., and the relation (4.27.), has interchangeable lateral coefficients.

Has been identified a variant of active moments method, where the elements in question are node active moments and displacement active forces.

Have been obtained calculus relations for end moments more general than the ones used in displacement method, the relations (4.6) and (4.19).

References:

1. Orlovschi, N. I., Construction static, vol. II, Static undetermined structures, part 1,2,3, Rotaprint I.P. "Gh. Asachi" Iași, 1975 (in Romanian).
2. Șesan, A., Orlovschi, N. I., Variants and simplifications of moments distribution method, Construction theory and practice, Iași no. 1, 1954 (in Romanian).
3. Șesan, A., Orlovschi, N. I., A generalization of moments distribution methods. Studies and researches, Academia, R. P. Romania, filial Iași, nr. 3-4, 1955 (in Romanian).
4. Șesan, A., Popescu, N., Another form of the condition equations of deformation method, Construction Theory and Practice, Iași nr. 2, 1955 (in Romanian).
5. Amariei, C. I., Construction static – Static undetermined structures, vol. II, Rotaprint I.P. "Gh. Asachi" Iași, 1981 (in Romanian).

Laboratory analysis in B.L.W.T. – priorities in insuring a safety curtain walling design

Elena Carmen Teleman, Elena Axinte

Civil and Industrial Constructions Dept., Faculty of Civil Engrg., T.U. "Gh. Asachi" Iasi, Romania

Summary

In the last half of century, the mankind is confronted with a new, most serious problem, determined by the global warming phenomenon and in particular, in the last years, Romania has already been confronted with the severe consequences of these climatic changes. A dramatic increase of the number of strong winds with speeds over 100 km/h in temperate climatic zones had been the cause of disastrous effects in terms of human lives and enormous material.

The design of very high buildings is a current modern concept but a greater complexity is imposed even from the first stage because of the importance of a realistic evaluation of the costs of investment. The balance between the investment costs and the safety level imposed during the service life time or in fact the risk involved by its exploitation is the designers most capital decision.

The latest solutions of steel glass façades are in fact glass panes of grate dimensions sustained in various manners by steel lattice structures or steel rods. Their important sensibility to every movement of the main structure, the influence of temperature variations upon the fixing details and hence upon the glass itself are almost exceeded by the effects of wind dynamic action directly supported by this envelope.

The last decades brought many scientific studies on these intricate systems and almost all of them are directed towards a more realistic evaluation of all the effects of the wind pressure upon light curtain walling.

Along the conditions imposed in the design of these elements in order to cope with wind pressure, the paper presents some of the results of several studies on models in the wind boundary layer wind tunnel of the Laboratory of Aerodynamics from the Faculty of Civil Engineering in Iasi. These results are directed towards a thorough evaluation of extreme values of wind pressure coefficients and also focus on the vibrations induced to the elements of the envelope by the dynamic effects of wind action, a most important comfort and safety criteria.

KEYWORDS: steel-glass envelopes, maxima wind pressure coefficients, spectral power, frequency of vibration, wind boundary layer tunnel

1. INTRODUCTION

Neglecting due to lack of knowledge of the extension of wind effects upon the antropic area had in the recent past year most disastrous consequences [1]. The last decades of the XXth century are marked by the development of the science of building aerodynamics, a domain where the meteorology and the theory of probabilities meet and mix together with the structural engineering concepts. The design of a multi-storey structure is a process with a high degree of complexity and the important effort involved in the project justifies the equilibrium between an economic cost of execution and the risk assumed for the exploitation period of time. After a rich experience has been achieved, it seems that the design of the envelope of a multi-storey building affects in a highest degree the safety level for the exploitation period of time. The light materials used for these envelopes, like glass, thermo-insulating materials, steel or aluminium skeleton vary widely their mechanical characteristics: dilatation coefficient, elastic modulus, strength and strain but in the process of design of the perimetral cladding the common factor of all these materials is that together they have to stand up against the effects of wind dynamic action.

In these conditions the design of a multi storey structure to strong wind gusts and their effects upon the envelope becomes an important preliminary stage because by modelling the interaction between the wind and the future structure and anticipating the structural response, benefic modifications of its aerodynamic shape may improve the dynamic behaviour. Also, by studying the environmental conditions imposed to the building important decisions may be taken in order to avoid unpleasant effects of the urban implantations. Notorious laboratories for the Aerodynamics of Structures from all over the world play an important role in this preliminary process.

For at least 50 years the humanity is confronted with a new and most serious problem: the dramatic climatic changes due to global warming, whose multiple and severe consequences Romania has already experienced. A rather realistic prognoses of wind motion at global scale along with the estimation of the local effects inside the structure of the boundary layer in different environments became priorities in insuring the security in the exploitation of the buildings because their consequences at the economic scale are huge. The amplification of the number of strong winds with speeds of more than 100 km/h in temperate zones and of the number of hurricanes with wind speeds of more than 200 km/h in tropical and subtropical zones increased dramatically the costs of reconstructions and repair in the last decades and unfortunately they were the cause of important human casualties, and sometimes disasters at human scale. In the same time, the insurances costs increased in some countries, like Great Britain ten times in the last 50years [2].

Many of the environmental conditions imposed to a high rise building amplify the effects of wind dynamic actions: increased speeds in shore areas, turbulences due to perturbations of urban wind profile in the big cities area, vicinity with other buildings of similar size etc., the implication being the distribution of the wind pressure/suction on the surface of the building [3]. Due to an important scientific knowledge accumulated in this respect, the architects and engineers are able to master the shape and types of structures adopted for these high rise buildings. A good example is the Milo Turning Tower, project of the Spanish architect Santiago Calatrava and for the time being, the highest building in Europe (245 m), whose torsioned shape reduces the vortices and diminishes the local pressures on the surface of the envelope [4].

2. PARTICULARITIES IN THE DESIGN OF MODERN CURTAIN WALLING

2.1. *Types and design criteria*

The requirements for transparent envelopes of the buildings are, no matter to which codes for practice we are referring to, based on the following criteria [5], [6], [7]:

- dimensions and tolerances;
- strength and serviceability;
- fire protection;
- thermal and physical functions insured;
- other specific criteria imposed by serviceability functions.

As steel and glass are preponderant in the structure of transparent facades, a fundamental need is to predict the glass behaviour in facades, in order to achieve both performance and economy.

The conventional supporting structures of steel-glass facades are those in which the glass panes carry their dead load and the afferent wind load depending on their surface; the panes are supported by steel window frames which transfer the loads to the main structure of the building. Normally, the glass frame producer designs the panes including glass, sealing and fasteners and gives the necessary requirements for the designer of the load bearing structure.

In the last decades, a very wide number of studies were directed towards the behaviour of the glass panels under different exploitation conditions. Vertical movements of the main structure of the building may be important but usually are situated between +5.0 mm and -25 mm but the expansion/contraction of the glass itself in vertical panels determine movements of 17.5 mm to -12 mm, important tension stresses being accumulated at the corners of the panels or on the edges, depending on the supporting system.

As the movements of the supporting system of the glass panels must follow the movements of the main structure of the building, after a rich experience was gathered in research studies, limitation of the maximum deformations of the glass under wind action in the middle of the panels are imposed: δ_1 is 1:175 from the span; also, deformations of the supporting frame must be limited so δ_2 , δ_3 are no more than 1:175 of the span.

Also, preventing the lateral buckling phenomenon for the supporting elements under local pressure/suction impose limits for their slenderness; it was assumed of 1:100 from the span for steel beams and 1:360 from the span in the case of lattice girders [5].

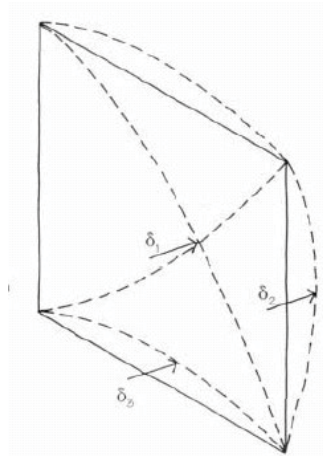


Fig. 1. Deflections of the steel-glass panels: δ_1 - deflection in the middle of the panel; δ_2 , δ_3 – deflections in the middle of the edges, on the supports [5]

The last decades imposed new solutions for transparent facades on the market, being the result of applicability of new technologies combined with the demand of higher performances. Hybrid –supported facades are greater surfaces of glazing whose supporting structure is characterized by the replacement of either a horizontal beam or a vertical column by a stainless steel cable or rod (fig.2.a., fig. 3) [6]. In the solution presented, the vertical cables take dead load of glass panes and the wind load also. If greater surfaces (higher glass facades) are considered, a horizontal truss (or more) is designed in order to take the wind action and to limit the deflections of the glass consequently. A particular type represents the suspended glass facades for which the cable supported mechanism prevents only wind loads, the glass panes supporting their own weight (fig. 2.b).

The hybrid-supported structure concept is based on the fact that the cables and rods remain in tension so one of the key structural design problems for these envelopes

is the thermal expansion, which might cause structural instability so normally, the cables are pre-stressed. If the height becomes too big, the pre-stressing force into the cables is not enough to overcome the effects of thermal expansion and for these situations, springs are used for each vertical truss to pre-stress the cables and rods. The design imposes for a non-linear analysis for obtaining the stresses, deformations and the natural frequency response. The literature specifies that a certain amount of trial and error is required to balance the rod and catenary system with the floor spring (fig. 4.).

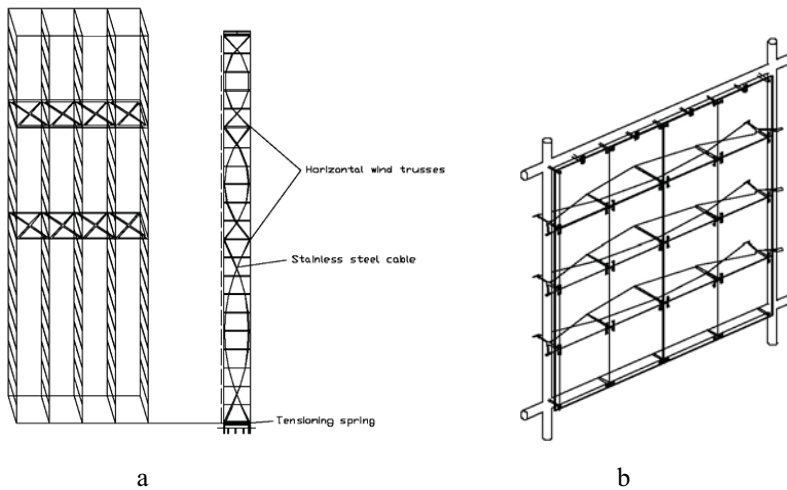


Fig. 2.a, b. Steel-glass façades: a)-hybrid-supported glass façade; b)-cable supported suspended glass façade [6]

For these types of envelopes, deformation becomes of capital importance and the permissible deformation is established for the most frequent wind loads compatible not only with the glass or cladding system involved but also with the joints and the fastening systems. As the deflections of the cable truss are concentrated around the holes drilled in the glass, uncontrolled values of efforts may increase the risk of producing the fatigue phenomenon in the glass [6], [7].

Requirements for the design of the glass panels in limit states design impose the validation of the relationships for maximum stresses and maximum deflection defined with the following relationships [6], [7]:

$$\sigma_{\max} = k \cdot \left(\frac{a}{t}\right)^2 \cdot q_d \quad (1)$$

$$\delta_{\max} = k' \cdot \frac{a^4}{t^3} \cdot \frac{q^k}{E} \quad (2)$$

where:

- a -length of shorter edge of the pane;
- t - thickness of the glass pane;
- q_d – uniform pressure load on the panel in the ultimate state for design;
- k, k' - coefficient that takes into account the aspect ratio of the panel and also the normalized value of the load necessary to reduce the calculations from non-linear to linear case.;
- E -elastic modulus of the glass pane;
- q_k - the value of wind load pressure in the limit state of serviceability.

2.2. Studies considering the security in exploitation of light envelopes design

2.2.1. Accuracy in the determination of realistic values of wind pressure action

The cladding is generally designed to sustain the efforts due to wind dynamic action. Several factors influence the design criteria in this respect [7]:

- wind attack angle;
- internal pressure inside the building;
- risks involved by the presence of accidental wide openings in the facade which would lead to the alteration of internal pressure;
- amplification of wind suctions in the corners of buildings;
- effects of the alteration of the environmental conditions during the life time upon the distribution of wind pressures on the surface of the building and also, the effects of vicinity.

Imposed by the necessity of national standard regulations of design, execution and exploitation of curtain walling systems in Romania and in order to insure the security level imposed by the Romanian legislation a code for practice was elaborated: NP 102-04, issue nr. 170/15.02.2005 [8], according to which, whichever is the curtain walling system proposed by the designer, it must be tested for the comfort criteria, particularly from the wind action point of view (chapter 5.2.5. *Efforts upon curtain walls due to wind dynamic action*). The tests will consider for each system separately: local reference wind pressure according to the height above the ground, gust factor considering the specific dynamic behaviour of the structural main system and the peak factors applied to local pressure coefficients, considering the dynamic characteristics of the facade panel.

Serious lack of data makes these requirements onerous. For example, if a safety level is imposed, a reference wind pressure value superior to that corresponding to a 10 years recurrence will be adopted. The recommendation is to extrapolate the

values of a Gumbel I or Frechet II distribution of extremes based on the observation data from of I.N.M.H. Bucuresti, Filaret station. But since, the distribution regards only one station it will not correspond with accuracy for all over the surface of the Romanian territory and since the recommendation specify that the designer should adopt any other type of data in order to insure the security level, in fact it is non-operational for other zones than the one mentioned.

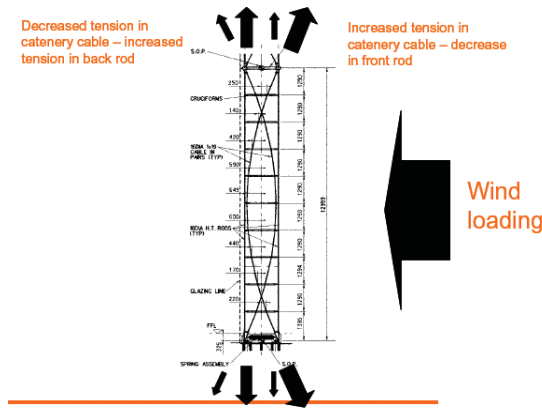


Fig. 3. Working system of a hybrid supported façade [5].

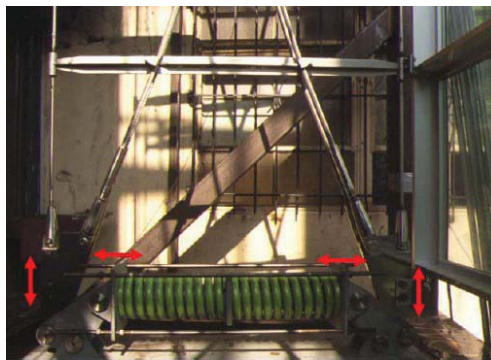


Fig. 4. Dissipative system for the wind: floor spring joint (Korean World Trade Center) [7].

Testing the curtain wall panels considering the cumulative effects of both dynamic behaviour of the main structural system and the dynamic behaviour of the steel-glass panel is difficult to achieve. The safety factor adopted in the limit state design theory is a function of two other random variables: safety index, β and the coefficient of variation of the wind action (speed/pressure), v . Considering a log-normal distribution, the safety factor is defined by [9]:

$$\phi = e^{0.75\beta v} \quad (3)$$

It is important to observe that, if a normal distribution is considered, then the safety index has usually values between 2.5 and 4.5; in this case the probability of failure during the service life is placed between 1/100 and 1/10⁶.

The usual formulation of the wind pressure in the codes for design against wind action all over the world is:

$$w = q_{ref} \cdot c_e \cdot c_g \cdot c_p \cdot A \quad (4)$$

where:

- q_{ref} - reference wind dynamic pressure;
- c_e - exposing factor;
- c_g - peak factor;
- c_p - pressure coefficient;
- A - surface of the area exposed to wind pressure.

Bearing in mind that all the measured values are random and analyzed through the statistics methods, a global coefficient of variation of wind action will be obtained from the formulae:

$$v = \sqrt{v_{q_{ref}}^2 + v_{c_e}^2 + v_{c_g}^2 + v_{c_p}^2} \quad (5)$$

In the process of design, the extreme values of wind pressure or suction themselves influence the security level imposed. Modern techniques of measuring in boundary layer wind tunnels have an increased degree of accuracy and the latest values of the variation coefficients reported are considerably lower than the ones stipulated by the various design codes, mostly due to the variation of the pressure coefficient c_p . As a general conclusion, the variation coefficient according to design code is 0.36 the partial safety factor being thus 2.25 in opposition with a variation factor of 0.18 obtained through wind tunnel measurements leading to a safety factor of 1.59 (β is 3.0 in both cases). An increased value of safety factor is based on local pressure coefficients obtained from general tests which are not giving a certainty of the pressure coefficients and offer only a rough and sometimes insecure evaluation of the wind action on the surface of the building [9], [10].

As the instantaneous pressure coefficient c_p is a process fully described through statistic methods, the maxima/minima values of pressure are defined by the algebraic sum between the mean pressure values and the product of the amplification of the variation factor which is named in all the codes for structural design to wind action as the peak factor, g or c_g with the value of the standard deviation (or the r.m.s.):

$$g_k(t) = \pm \frac{\hat{c}_{p,k}(t)(\tilde{c}_{p,k}(t)) - \bar{c}_{p,k}(t)}{\sigma_{p,k}(t)} \quad (6)$$

where:

- $g_k(t)$ - local peak factor in the point k on the surface of the building at the time t ;
- $\hat{c}_{p,k}(t)(\tilde{c}_{p,k}(t))$ - local extreme values of maxima/minima of instantaneous pressure in the point k on the surface of the building at the time t ;
- $\bar{c}_{p,k}(t)$ - local mean value of the instantaneous positive (or negative) pressure in the point k and at the time t ;
- $\sigma_{p,k}(t)$ - root mean square (or standard deviation).

Although the codes specify that a conservative value of the peak factor may be taken as 3.5 to predict the extreme values of wind pressure from the mean values obtained for a certain position on the surface of the building, numerous studies developed showed that since in certain situations this peak factor may have values three times bigger, it is not wise however, when it comes for the design of the wall cladding of a high rise building to limit the evaluations of extremes only to the value mentioned above.

2.2.2. Consideration of wind-induced vibrations in design of light envelopes

In the design of glass facades slenderness and long spans are often imposed for both glass panes and frame structures and this may lead to dynamical problems when a flexible structure with low natural frequency is exposed to gusty winds [11]. Wind induced vibrations may damage the sealants, loosen fasteners and cause inconvenience to occupants of the building. In ENV 1991-2-4, 1995 it is stated that the fundamental natural frequency f_0 should be always higher than 5 Hz, regardless to the wind speed in order to avoid vibrations induced by dynamic wind loads [7]. Under the mentioned value, the dynamic behaviour of the structure must be separately analyzed, though the methods are not specified. A F.E.M. modelling of the glass pane and its frame provide an accurate analysis [6], [7], but in this case a time-history description of the wind dynamic action is desired as an input.

2. STUDIES IN THE LABORATORY OF BUILDINGS

AERODYNAMICS CONCERNING CURTAIN WALLS DESIGN

During the last decade, the studies in the laboratory of Aerodynamics of the Civil Engineering Faculty were directed towards developing the local instantaneous pressure measurement techniques of sampling on rigid models of buildings placed

in urban environment and with different levels of height along with refining the acquisition methods and processing the data obtained [13], [14], [15].

In parallel, a calibration of the results was developed, showing where the accuracy of measuring must be increased. By elaborating a module of programs under MATLAB the statistic data were analyzed, mainly for the coefficients of wind pressure. Several programs were developed:

- TB1.M...TB3.M – program for the determination of the pressure/suction coefficients-mean, peak and standard deviations, tracing the isopleths with polynomial interpolation functions and graphics of variation of the aerodynamic coefficients on the surface of the models;
- GPD.M- program for the determination of the peak factor c_g of the local instantaneous pressure (mean, r.m.s. and maxima values, histograms and regression lines); also for the validation of the acquisition data (fig. 5.a, b);
- TREC.M – program of determination of the variation coefficient ν for different averaging periods;
- TST_PSD.M – program for the determination of the spectral power and spectral density in its normalized shape (fig. 6.a, b).

The last program enlighten the values of the frequencies that gather the majority of the spectral densities, the frequencies around 5 Hz being very important for the study as it was mentioned in the subchapter 2.2.1. This program was considered to be the best way to identify the critical values of frequencies that might superpose on the natural frequencies of the glass-steel panes.

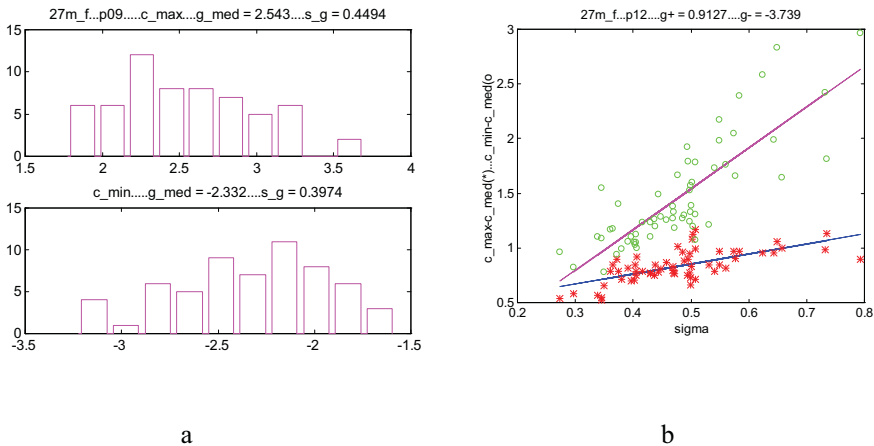


Fig. 5.a, b. Programs under MATLAB elaborated during the studies in the boundary layer wind tunnel in the Civil Engineering Faculty in Iasi: a)-Program GPD.M for the determination of peak factors; b)- Calibration of the peak factor values.

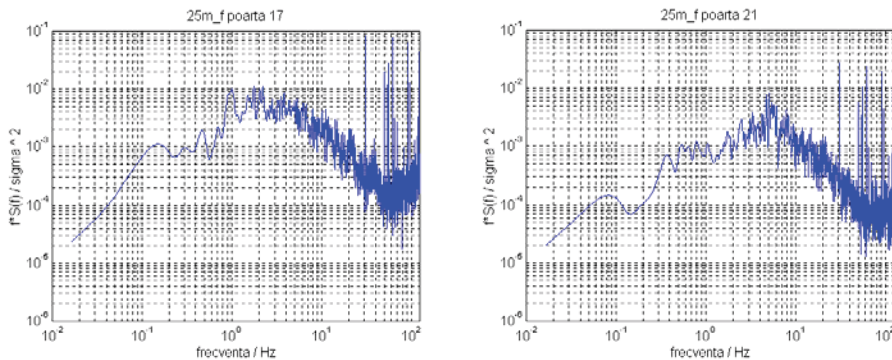


Fig. 6.a, b. Spectral densities normalized and traced in the program TST_PSD.M.: a) pressure signal processed; b)- suction signal processed.

3. CONCLUSIONS

Modeling the turbulences localized on the surface of the buildings and responsible of numerous accidents more or less severe was transferred into the numerical simulation sphere. The analysis of the fluctuating pressures was put into evidence by a spatial evaluation of the spectral density all over the surface of the structure, allowing the elaboration of an accurate method of design to wind dynamic action at least of the most common shapes of buildings [10] are presented in Eurocode 1 and also in the Romanian code NP 082-04. *Design Code. Basis of the structural design and evaluation of the actions on structures. Wind action* [16], [17].

Still, by refining the methods of evaluation of wind tunnel data of pressure on the surface of the buildings many precious data for specific situations imposed by the environmental conditions or architectural solutions are put into evidence.

The design of the transparent façades of glass and different solutions for the steel framing call for simulations by F.E.M. methods of the system dynamic behaviour using time history registrations of wind pressure. These simulations can be validated afterwards by tests on larger scales (or natural scales) of specimens of facade panels.

References

1. www.news.softpedia.com, Sci/Tech News Staff - *Uragane mai multe din cauza încălzirii globale* (in Romanian)
2. Brian Smith, Tom Wyatt, *Structures, Dynamics and Wind a 10-th review*, 8th Biennial Scruton Lecture, Wind Engineering Society, 2003

3. Soligo, Michael, Vicepresident of Rowan Williams Davies & Irwin Inc.(RWDI) , Ontario, Canada- *High Rise Buildings in Hurricane Areas*, Technotes, Issue No. 2b
4. <http://www.turningtorso.com>
5. Mike Otlet, Head of Structural Engineers ATKINS-*The role of a structural engineer in the design of a façade*, ATKINS, U.K. april 2006
6. Jusi Kallioniemi-*Joints and fastenings in steel glass facades*, Helsinki University of Technology, Depart. of Civil and Environmental Engineering, Laboratory of Steel Structures, Ph.D. Thesis, 1999, Helsinki, Finland
7. Aki Vuolio- *Structural Behaviour of Glass Structural in Facades*, Helsinki University of Technology, Laboratory for Steel Structures Publications, 2003, TKK TER 27, Helsinki, Finland
8. “*Normativ pentru proiectarea si montajul peretilor cortina pentru satisfacerea cerintelor de calitate prevazute de legea 10/1995*”, NP 102-04, aprobat ord. nr. 170/2005
9. Peter A. Irwin- *Developing Wind Engineering Techniques to Optimize Design and Reduce Risk*, Conference on Wind Engineering 2006 (WES 06), Glasgow, U.K., www.ukwes.bham.ac.uk
10. Scott Gamble P. Eng.- *Wind Tunnel Testing – A Breeze Through*, Structure Magazine, nov. 2003
11. Peter Irwin, president of Rowan Williams Davies & Irwin Inc.(RWDI) , Ontario, Canada- *Motion Criteria in High Rise Buildings*, Technotes issue no. 2c
12. Scott L. Gamble, Roger J. Mittenburg, Michael D. Cicci, Marco Accardo (RWDI, Guelph, Ontario, Canada)-*Prediction of Local Exterior Wind Pressures from Wind Tunnel Studies Using Time History Analysis Approach*, Americas Conference on Wind Engineering, 2001.
13. Teleman, C.-*Contributii privind alcatuirea si calculul cladirilor multietajate cu structura metalica*, Teza de doctorat, 2000, U.T. “Gh. Asachi” Iasi (in Romanian)
14. Teleman, E.-C., Axinte, E., Sillion, R.- *Trends of Actual Computer Assistance for Laboratory Studies in Boundary Layer Wind Tunnel*, “Computational Civil Engineering 2006”, International Conference, Iasi, Romania 26 may
15. Carmen Teleman, Elena Axinte- *Calibration Methods of Data Obtained in Boundary Layer Wind Tunnel*, Buletinul Institutului politehnic din Iasi, Tomul XLVIII (LII), fasc 1-2. Constructii. Arhitectura, pp. 95-101
16. *Cod de proiectare. Bazele proiectarii si actiuni asupra constructiilor. Actiunea vantului NP-082-04.* (in Romanian)
17. XP ENV 1991-2-4/2000- Eurocode 1: *Bazele calculului si actiuni pe structuri – Partea 2-4: Actiuni asupra structurilor- Actiunea vantului (P 06-102-4)* (in Romanian)

FEM 3D analysis of RC frame foundations of rotary cement kiln

Grzegorz Dmochowski, Przemysław Siwiec and Piotr Berkowski

Faculty of Civil Engineering, Wrocław University of Technology, Wrocław, PL50-370, Poland

Summary

Results of 3D finite element analysis of damaged foundations for cement tubular oven are presented in a paper. The foundation consists of four RC frames modeled for analysis using solid FE with 24 d.o.f. each. Serviceable and temperature loads, as well as loads from pre-stressing are taking into account. The frames, primary designed as 2D structures, are sensitive for out-of-plane and temperature loads. The additional effects of stresses from these loads should be taking into consideration during FEM analysis.

KEYWORDS: rotary cement kiln, RC foundation, spatial numerical model, FEM analysis

1. DESCRIPTION OF THE FOUNDATION

The support structure of rotary kiln under consideration was built in the early 1950s. It consists of four reinforced concrete solid frames spaced at equal intervals. The lowest frame is denoted by number 1 and the other by respectively 2, 3 and 4.

As part of rotary kiln retrofitting, frame 4 was to be torn down and an additional frame was to be placed next to frame 1 whereby the latter practically would not carry any loads. The other two frames: frame 2 and frame 3 were to continue to be in service and be subjected to additional loads. Because the two frames were considerably damaged it was necessary to determine their serviceability.

The foundation named frame 2 had been made as an RC frame embedded in the foundation plate. A static scheme with one column in the form of a rocker with both its ends articulated had been adopted. The other column had been rigidly fixed in the plate. The frame's spandrel beam had been thermally protected with an about 20 cm thick concrete overlay. In the course of its service considerable horizontal displacements of the kiln's foundation were observed. Therefore in the early 1980s the structure was strengthened by tensioning. The rigid-rigid column, the frame's spandrel beam and the joint connecting the members were subjected to tensioning.

The bowstrings were made from $\phi 5$ mm strings combined into L1+6+12+18 ropes, with two ropes running on each side of the foundation and concreted.

The technical condition of frame 2 varied. The foundation plate was found to be in good condition. The foundation had not undergone settlement and was undamaged. The columns were in satisfactory condition. The concrete reinforcement cover was found not to have loosened or cracked. The frame's spandrel beam was in bad condition. It was found to have sagged by 3-4 cm. The spandrel beam's undersurface was cracked and its reinforcement cover was loose over a considerable area. When the loosened cover was removed, reinforcement in the form of superficially corroded #35 square bars was revealed. Also the spandrel beam's entire top surface was found to be corroded.

The foundation named frame 3 had been built as a stiff frame, considerably long (8.6 m) along the kiln's axis, embedded in the RC plate. There were two platforms: one for a motor and one for the kiln's rotary bearing on the frame. The top surface of the frame was thermally protected with a 20 cm thick concrete overlay. The foundation plate was in good condition: no excessive settlements or damage were found. The columns were in satisfactory condition. They were uncracked and their reinforcement cover was found not to be loose. The frame's spandrel beam was in bad condition since it had been subjected not only to considerable service loads and temperature impacts but also to the destructive action of grease escaping from the motor driving the rotary kiln. Lubricant leaks were visible on the spandrel beam plate's undersurface.

2. FOUNDATION MATERIALS' STRENGTH PROPERTIES AND EXPLOITATION CONDITIONS

2.1. Concrete

On the basis of the fragmentary documentation which survived in the cement plant's archive it was found that the design strength of the foundation concrete had been assumed to be $R_w = 160 \text{ kG/cm}^2$ which corresponds to current concrete grade B12.5-B15. According to non-destructive test results, the concrete in the frames could be classified as class B10 at the most. Therefore concrete parameters: $R_{bb} = 4.8 \text{ MPa}$ and $R_b = 5.8 \text{ MPa}$ were assumed for further calculations.

2.2. Reinforcing steel

In the surviving fragment of the design, smooth reinforcing steel $\phi 20$, $\phi 30$ and $\phi 35$ with allowable stress $\sigma_d = 1200 \text{ kG/cm}^2$, corresponding to a design strength R_a of

about 106 MPa, was specified. The lower steel strength had probably been adopted in view of the considerable diameters of the structural reinforcement.

2.3. Foundation tensioning

The spandrel beam, the column and the joint of frame 2 had been tensioned using double steel ropes, made from $\phi 5$ mm strings forming a steel rope of type L1+6+12+18, running on both sides of the foundations. The nominal rope breaking force of 1130 kN had been assumed. The ropes were tensioned with a force amounting to 60% of the nominal force. Thus the tensioning force had been $S = 2700$ kN. From the way in which the ropes were secured it one could be concluded that the spandrel beam had been tensioned above the neutral axis, as shown in Figures 1 & 2.

2.4. Exploitation temperature

Considering that the concrete overlay protecting the foundation against temperature effects was 20 cm thick the foundation had been assumed to be subjected at its surface to a temperature field of $+40^{\circ}\text{C}$, decreasing at every $10^{\circ}\text{C}/\text{m}$ towards the column’s base.

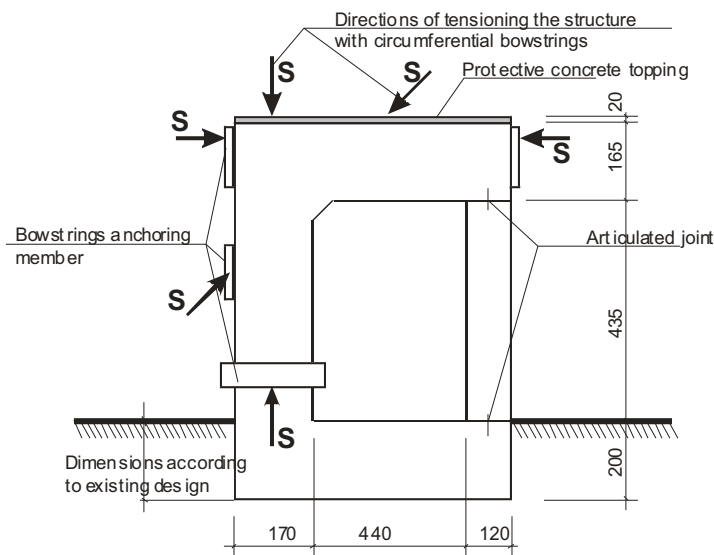


Figure 1. Frame 2. Structural and tensioning scheme

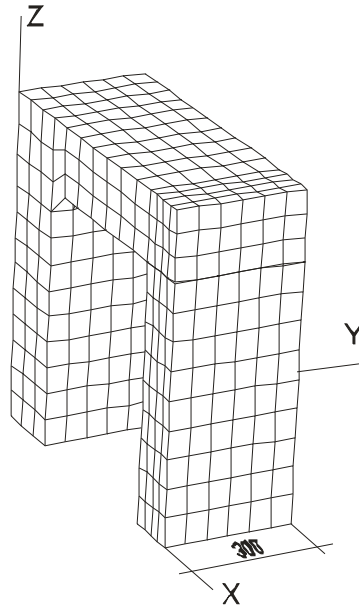


Figure 2. Frame 2. Division into finite elements

3. ANALYTICAL MODELS OF FOUNDATIONS

Program MES DIANA was used for the numerical analysis [4]. Linear physical and geometric relations were assumed for the material and the structure. Isoparametric 3-D finite elements HX24L, described by eight nodes, were used to build the models (Figure 3). In order to obtain more precise results a $3 \times 3 \times 3$ Gaussian points integration scheme (triangles in Figure 3) was adopted.

In such finite elements stresses σ_{yy} and strains σ_{zz} are constant in direction x and they can linearly change in directions y and z . Stresses σ_{yy} and σ_{zz} and strains σ_{yy} and σ_{zz} respectively in directions x , y and z behave similarly. A uniformly distributed load or a load linearly variable along each edge can be applied to each wall of the finite element. The latter can also be loaded with temperature which may be different in each of its nodes. The displacements and deformations of the frames are given for the nodes while the stresses are given for the finite element's centre of gravity.

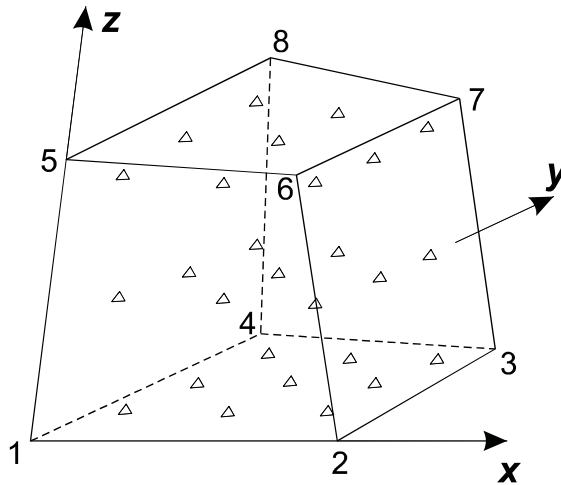


Figure 3. FEM element HX24L

The division of frame 2 model into finite elements is shown in Figure 2. 1022 nodes and 640 brick elements were used to create the model. The articulated joint between the spandrel beam and the rocker column was modelled using short articulated-articulated bars.

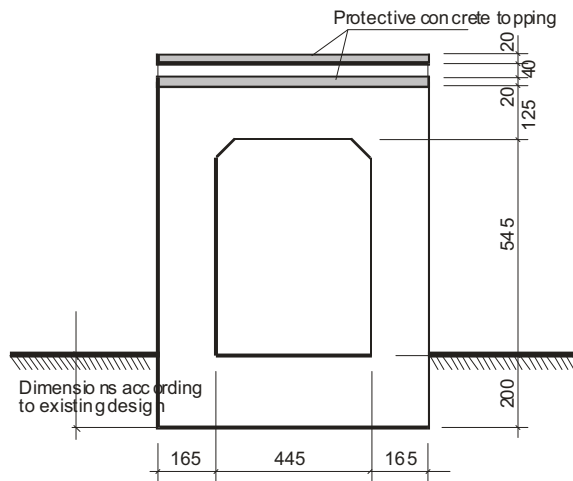


Figure 4. Frame 3. Structural scheme

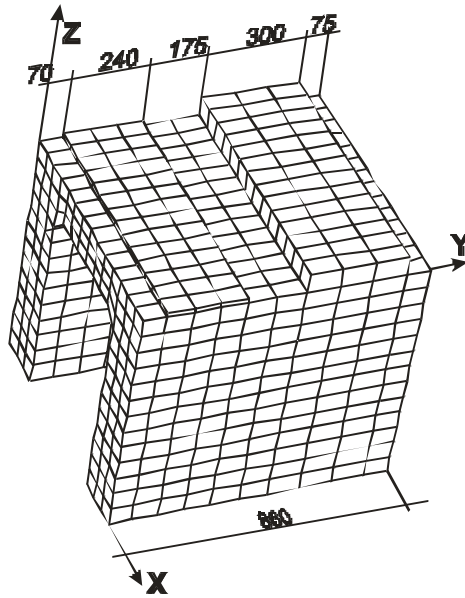


Figure 5. Frame 3. Division into finite elements

The model of frame 3 was created using 1660 nodes and 1104 brick finite elements.

The following load schemes were adopted for frame 2:

- the foundation dead load,
- the characteristic rotary kiln load,
- the design rotary kiln load,
- the frame tensioned with bowstrings,
- loading with a temperature field.

The following load schemes were adopted for frame 3:

- the foundation dead load,
- the characteristic rotary kiln load,
- the design rotary kiln load,
- loading with a temperature field.

The numerical 3-D model calculations were verified for a static flat bar scheme.

4. ANALYSIS OF RESULTS

The check of the deformations of frame 2 confirmed the latter's susceptibility to horizontal loads. The total horizontal displacements of the spandrel beam,

calculated in the elastic phase, exceeded 5 mm. Taking into account material plasticization, deformations about 2.5 cm were yield, i.e. above the permissible values.

The results of the numerical analysis, in the form of σ_{xx} and σ_{yy} graphs for frame 2 are shown in Figure 6 and for frame 3 in Figure 7. In both structures the stresses in the elements lying on the spandrel beam’s edge and in its middle (along axis Y) were analyzed. In addition, stresses in the region of the elevated spandrel beam under the motor driving the kiln were taken into account in frame 3. The results are presented for the design service loads, the tension of frame 2 and the temperature increase load.

The total force tensioning the undersurface of the spandrel beam in frame 2 was 3326.4 kN. The load-bearing capacity of the reinforcement with a surface area as in the design was to 2259 kN, which means that it was insufficient to carry the loads. Similarly in frame 3, the total force tensioning the spandrel beam’s undersurface was 3345 kN, which means that for the same assumed reinforcement it exceeded the spandrel beam’s load-bearing capacity.

An analysis of stresses σ_{xx} in the spandrel beam of frame 2 shows only a slight influence of the temperature load on the degree of strain of the structure. The stresses due to an increase in temperature amount to merely 10% of the service loads, which confirms that lowly over-rigid structures are resistant to this kind of load.

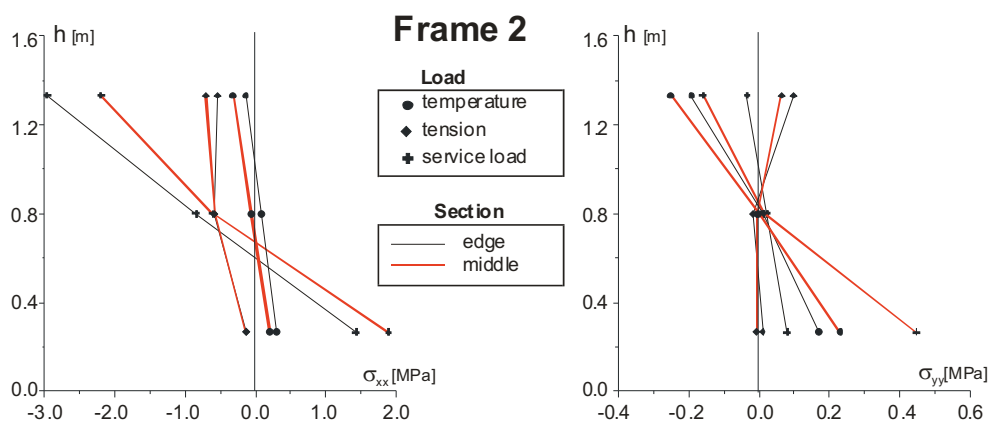


Figure 6. Frame 2. Stresses σ_{xx} and σ_{yy}

The effect of the stresses produced by tensioning was somewhat stronger. But due to the point of application of the steel ropes in the spandrel beam the expected reduction in tensile stress in the spandrel beam’s bottom zone was slight (below 10%) while the deflection of the spandrel beam increased. The increase in tensile stress σ_{yy} in the middle of the spandrel beam thickness was significant: considering

that the design tensile strength is 580 kPa it may explain the appearance of cracks propagating perpendicularly to the kiln's axis. This means that the spatial aspect of the behaviour of the spandrel beam should have been taken into account in the design.

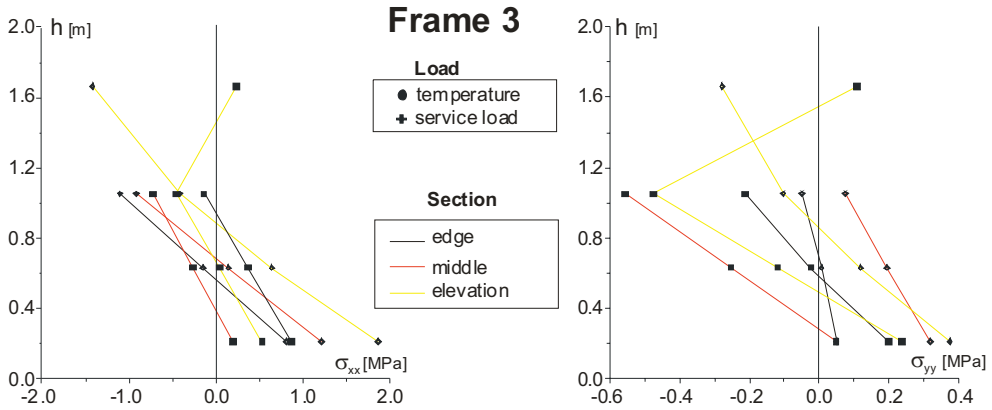


Figure 7. Frame 3. Stresses σ_{xx} and σ_{yy}

In frame 3 the temperature load impact was much greater. Stresses σ_{xx} produced by temperature were nearly as high as the ones due to the design service load whereas stresses σ_{yy} exceeded them significantly. Interesting was the appearance of tensile stresses in the spandrel beam's top zone thickened in order to mount the motor. The stresses did not exceed the concrete's tensile strength but as a result of the long-lasting action of temperature they might cause cracking in and damage to the spandrel beam's top surface.

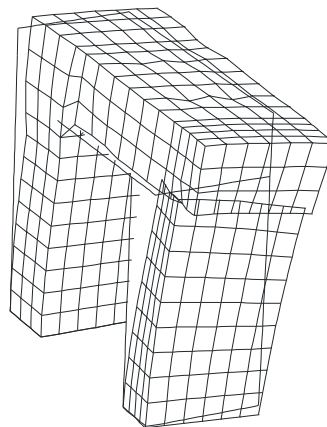


Figure 8. Deformation of frame 2

Similarly as in frame 2, the share of tensile stresses σ_{yy} (acting along the kiln's axis) produced by the service loads was found to be considerable. The stresses were responsible for the appearance of cracks perpendicular to the rotary kiln's axis.

Figure 8 shows the deformations of frame 2 under the service load, the tension and the temperature field. The deformations of frame 3 under the service load and the temperature field are shown in Figure 9.

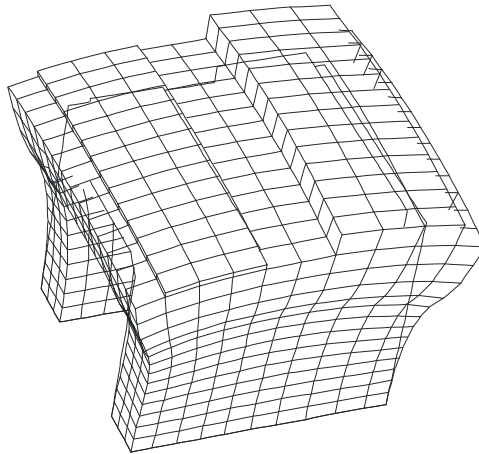


Figure 9. Deformation of frame 3

5. CONCLUSIONS

From the numerical analyses the following conclusions were drawn:

The load-bearing capacity of the spandrel beams in the investigated rotary kiln support frames was insufficient to carry the design loads.

The originally adopted static scheme in the form of a frame with one rocker column was susceptible to horizontal displacements which might increase if disturbances in the operation of the kiln occur or if the kiln components would be nonaxially assembled.

The cracks in the spandrel beam of frame 3, running perpendicularly to the kiln's axis, were the result of the spandrel beam's spatial work neglected in the original design.

When designing rotary kiln support frames it should be taken into account the increase in stress, due the thermal field, particularly when the static scheme should be changed for one with two rigid columns.

The 3-D frame model calculations have confirmed the fact that tensile stresses in the column and in the spandrel beam were concentrated closer to their axes and not at their outer surfaces. Therefore additional reinforcement should be provided to carry these stresses.

References

1. Lipiński, J., *Foundations for machines*, Arkady, Warsaw, 1985, (in Polish).
2. Polish Standard PN-84/B-03264 – Concrete, reinforced-concrete and prestressed structures. Structural analysis and design, (in Polish).
3. Kobiak, J., Stachurski, W., *RC structures*, Vol. 1, Arkady, Warsaw, 1984, (in Polish).
4. DIANA, Finite element analysis, Element library, User's manual – release 6.1, TNO Building and Construction Research.
5. Comparison of design loads, POLTEGOR-Projekt Ltd., (in Polish).
6. Design of rotary kiln foundations (in Polish), B.B.P. No. 4 in Gliwice, the Opole Branch, 1950, Extracts, (in Polish).
7. Dmochowski, G., Siwiec, P., Spatial analysis RC frame foundations of rotary cement plant kiln, *Current scientific and research problems in building*, Ed. Warmińsko-Mazurski University, 2000, (in Polish).

Flood routing using ‘Femme’

L. De Doncker¹, P. Troch¹, R. Verhoeven¹,
K. Buis², P. Meire²

¹*Hydraulics Laboratory, Ghent University, Ghent, 9000, Belgium*

²*Ecosystem Management Research Group, University of Antwerp, Wilrijk, 2610, Belgium*

Summary

The environment ‘Femme’ (‘a flexible environment for mathematically modelling the environment’) is used to model ecological processes as the transport of nutrients and pollutants. The program is user-friendly and based on a Fortran modular open source code and uses a lot of integrated integration tools. For the study of the interaction of ecological processes and flow in the river, a realistic modelling of the surface water flow is necessary. Here, the implementation of a one dimensional hydrodynamic model for surface water flow in ‘Femme’ is reported.

Because of the lack of hydrodynamic information in the ecological model, the kinematic and parabolic equations are implemented first. They describe accurate the time shift of the wave. The simplification to the parabolic and the kinematic equations allow a faster and easier solution. The parabolic model is known as the convection-diffusion equation and describes the translation and attenuation of the wave in open channels and is valid for short stretches with mild slopes. The kinematic model doesn’t take into account the flattening of the wave and corresponds less with the realistic deformation of waves.

First, the context of the research is presented in the introduction. Further, the importance of hydraulic modelling is illustrated. The study area and the modeling environment are further developed. As a conclusion, some calculation results are enclosed.

KEYWORDS: ecosystem modelling, environmental engineering, flood routing, vegetated rivers.

1. INTRODUCTION

This paper is part of the multidisciplinary research project ‘A fundamental study on exchange processes in river ecosystems’ (University of Antwerp, Vrije Universiteit Brussel, Ghent University, 2004 - 2007). The overall research aim is to study the diverse physical and biological processes in margins and inundation areas of water courses and how their interactions determine the exchange of water, dissolved

compounds and particulate matter. This paper will give an introduction on hydraulic modelling. The first action is exploring the possibilities of surface water modelling, to add in a later phase the vegetational processes. Simplified modelling equations are used.

2. FLOOD ROUTING

2.1 Importance of Hydraulic Modelling

River hydraulics is characterised by changing discharges and water levels due to rain fall. Studies about this topic have although to take into account this non-permanent character of the flow. Time shift and flattening of the peak of the wave can be remarked by studying waves at two different places in rivers as can be seen on Figure 1. The hydrograph of the wave is shown in section I as well as in the more downstream section II.

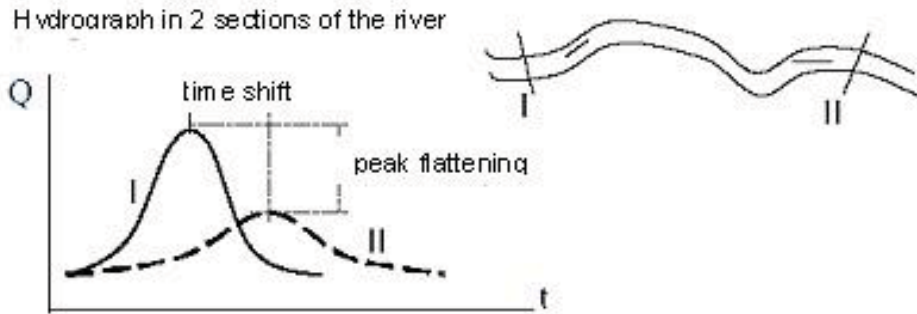


Figure 1: Hydrograph in 2 sections of the river

Description of this phenomenon, i.e. non-permanent flow of surface water is done by the Saint-Venant equations which include the continuity equation (1) and the momentum equation (2):

$$\frac{\partial Q}{\partial x} + B \frac{\partial h}{\partial t} = 0 \quad (1)$$

$$\frac{\partial Q}{\partial t} + \frac{\partial}{\partial x} \left(\frac{Q^2}{A} \right) = gA \left(S_0 - S_f - \frac{\partial h}{\partial x} \right) \quad (2)$$

with Q = discharge [m^3/s], B = section width at water surface [m], h = water depth [m], g = gravity [m/s^2], A = wetted cross section area [m^2], $S_0 = \tan \alpha$ = bottom slope [m/m], S_f = energy gradient needed to overcome frictional resistance of channel bed and banks in steady flow = friction slope [m/m].

2.2 Study Area: the river Aa

Focus of the study is the downstream part of the river Aa (Fig. 2), this is the stretch between weir 3 and weir 4, a distance of 1.4 km, near the village of Poederlee. In this area the interaction between groundwater, surface water and vegetation will be studied. Regular measurements of discharge and water level allow to gather data to calibrate the model.

The catchment basin of the river Aa is situated in the region of Antwerp and is hydrographical part of the Nete basin. More than 40 % of the water in the Nete basin is going to the river Aa, which is although an important river. The river Aa flows into in the Kleine Nete near the city of Grobbendonk. The origin of the river Aa is found near the communities of Merksplas and Turnhout and is streaming through Turnhout, Gierle, Gielen, Poederlee and Vorselaar. The river Aa has a total length of 36.8 km and the drainage area is about 23,700 ha.

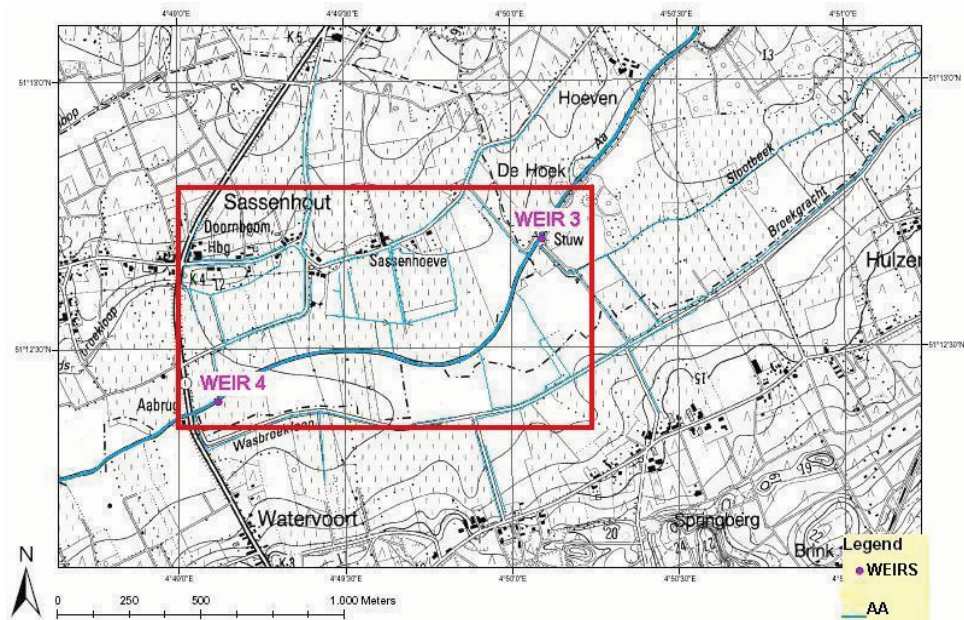


Figure 2: The river Aa

2.3 Simplified Saint-Venant Equations

The Saint-Venant equations can be simplified in some typical cases which can be easily solved. For rivers with a small slope, the acceleration terms are negligible and the equation is known as a parabolic model, which is the convection-diffusion equation. The model describes the attenuation of the wave due to storage and friction.

The maximum discharge will decrease and the minimum discharge will increase in the downstream direction, due to the influence of the diffusion parameter D . So, the wave will become flatter and wider, because the total amount of water has to be the same.

When also the distance between two sections is short, the peak flattening is negligible and the most simplified model is the kinematic model which includes only the friction and the translation of the wave. Peak flattening is not incorporated.

Equations (3) and (4) present respectively the parabolic and kinematic wave model, with D = diffusion parameter, responsible for peak flattening and C = convection parameter, responsible for the translation of the wave. D and C are variables and depend of the values of the discharge and the water level. Therefore, the solution can only be obtained by numerical models.

$$D \frac{\partial^2 Q}{\partial x^2} = C \frac{\partial Q}{\partial x} + \frac{\partial Q}{\partial t} \quad (3)$$

$$C \frac{\partial Q}{\partial x} + \frac{\partial Q}{\partial t} = 0 \quad (4)$$

$$C = -\frac{1}{B} \left(\frac{\frac{\partial S_f}{\partial h}}{\frac{\partial S_f}{\partial Q}} \right) = -\frac{1}{B} \left(\frac{\partial Q}{\partial h} \right) \quad (5)$$

$$D = \frac{1}{B} \left(\frac{1}{\frac{\partial S_f}{\partial Q}} \right) \quad (6)$$

The values of D and C depend of the discharge and the water height and can be found in a numerical way. Values mentioned in (Verhoeven, 2006) are 10^4 to 10^6 m/s for D and $C = 1.5$ to $1.8V$ (with V the average velocity). Calculations in this

study resulted in other values as $D = 250$ m/s and $C = 0.29$ m/s, which is the translation velocity of the wave and can also be seen on Figure 3. Best values are obtained by fitting the calculation result on measured values or on more detailed simulation results as obtained with the Saint-Venant equations.

In a first phase, the cross sections are simplified to rectangular or trapezoidal sections. Comparison with the effective geometry of the river Aa has shown that the differences are only small (De Doncker et al., 2005).

2.4 The Hydraulic Model ‘Femme’

‘Femme’ or ‘a flexible environment for mathematically modelling the environment’ is developed by NIOO (Netherlands Institute of Ecology) (Soetaert et al. (2004)). ‘Femme’ is a modelling environment for the development and application of ecological time dependent processes by use of numerical integration in the time of differential equations. The program is written in Fortran.

‘Femme’ consists of a wide range of numerical calculations and model manipulations (as integration functions, forcing functions, linking to observed data, calibration possibilities, etc.). These technical possibilities allow the user to focus on the scientific part of the model and detailed research of the model without the confrontation with real program linked problems.

‘Femme’ is focused on ecosystem modelling, is open source (no black box) and exists of a modular hierarchical structure (implementation of different models next to each other). What was missing up till now was the implementation of a hydrodynamic surface water model to couple ecology and surface water in each timestep.

For the study of the interaction of ecological processes and flow in the river, a realistic modelling of the surface water flow is necessary. Here, the implementation of a one dimensional hydrodynamic model for surface water flow in ‘Femme’ is reported.

2.5 Implementation of the Flow Equations in ‘Femme’

The hydrodynamic model for the transmission of the wave in the river has to be implemented in ‘Femme’. Differential equations were converted into algebraic equations using the finite difference scheme. Forward discretisation of the equations in time and central discretisation in space is carried out.

Implementation of the hydrodynamic model in ‘Femme’ can be done by using the characteristics of this environment. Discretisation in space has to be implemented in the code, the integration routine for timestepping is incorporated in the code.

Further, ‘Femme’ will be used for the integrated hydrodynamic – ecological modeling. Therefore, it is not advisable to model complex ecological processes with simplified conceptual hydrodynamic models. In this multidisciplinary approach, different research areas have to be integrated to study properly the interaction between surface water and vegetation.

2.6 Calculation Results

2.6.1 Kinematic versus parabolic wave model

The kinematic and the parabolic model are built into the ‘Femme’ environment. As a first verification of the model, a stretch of a river is modelled. The wave, measured upstream, has a triangular hydrograph $Q(t)$ as indicated in gray dashed line at Figure 3 and Figure 4.

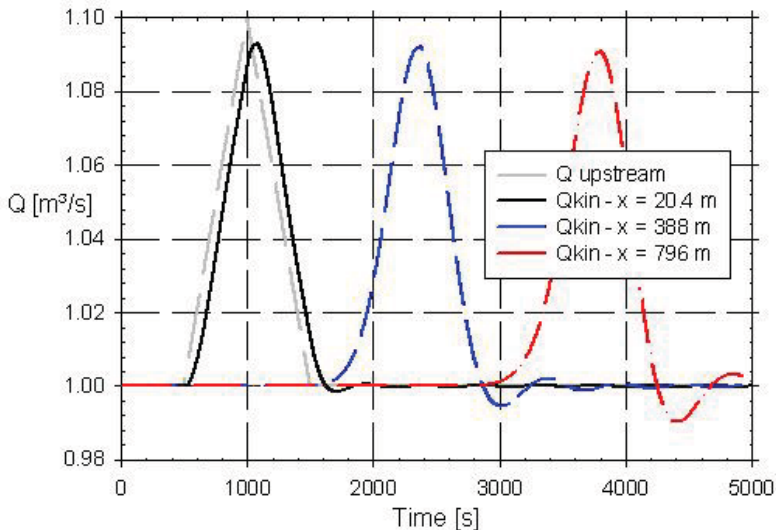


Figure 3: Use of the kinematic wave model: results at different distances

The kinematic as well as the parabolic model calculates the transmission of the wave. The resulting hydrograph at 20.4 m, 388 m and 796 m from the upstream boundary is indicated at Figure 3 and Figure 4. The total length of the channel is 1000 m. The channel is rectangular, has a bottom width of 10 m and a water height of 1 m. The Manning coefficient is $0.05 \text{ m}^{-1/3} \text{ s}$.

In Figure 3, the use of a kinematic model is illustrated. The time shift indicates that the wave moves from upstream to downstream with a constant celerity, without peak flattening. The small decrease of the peak discharge is due to the numerical (non-physical) dispersion as a consequence of the discretisation. Small wiggles at

the base flow are due to the triangular hydrograph, which is not natural and contains discontinuities.

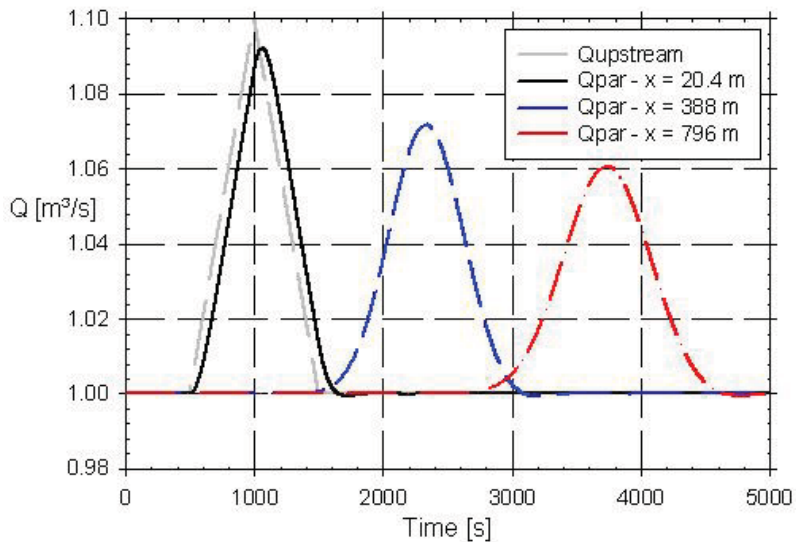


Figure 4: Use of the parabolic wave model: results at different distances

In numerical modeling, a good choice of timestep Δt and cell width Δx is necessary. These values have to be sufficient small to not to miss any effects (e.g. peak discharges) and to be sufficient large to minimize the calculation time. The Courant-Friedrichs-Lewy condition (CFL, Cunge et al.) determines a relation between the time step and the grid size separation to solve the partial differential equations in a convergent way.

For an explicit scheme, it means that the solution will be numerical stable. So, for using the explicit solution scheme of the kinematic and parabolic model, attention have to be paid at this criteria.

This condition can be avoid by using an implicit scheme for solving the Saint-Venant equations (as the Preissmann scheme). Time steps can be taken larger, which is useful for long simulation periods, and the solution will be stable.

The parabolic model, used for the results of Figure 4 contains an extra diffusion term. Next to the time shift, also the peak flattening in the downstream direction can be seen.

2.6.2. Variation of the Manning coefficient

Further, some calculations about the influence of the roughness coefficient n are carried out. Three different values of this friction factor are used: $n = 0.05 \text{ m}^{-1/3}\text{s}$, $n = 0.2 \text{ m}^{-1/3}\text{s}$ and $n = 0.5 \text{ m}^{-1/3}\text{s}$. These are values derived from the research carried out in the river Aa. Winter values were low, due to the low amount of vegetation in the river. In spring and summer, biomass starts to increase and results into higher Manning coefficients.

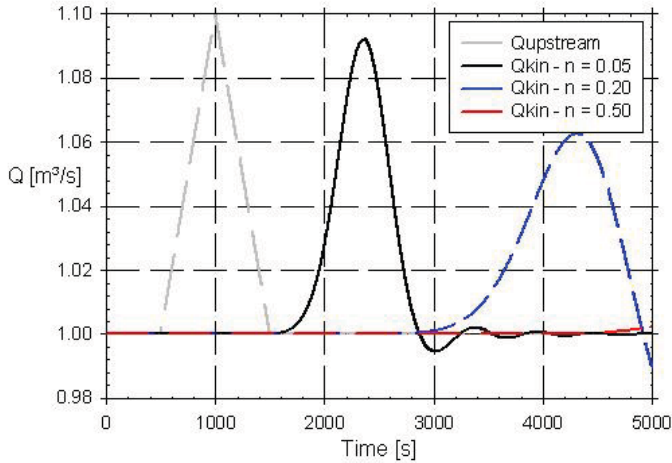


Figure 5: Use of the kinematic wave model: result at the same distance ($x = 388 \text{ m}$) for different values of the Manning coefficient n

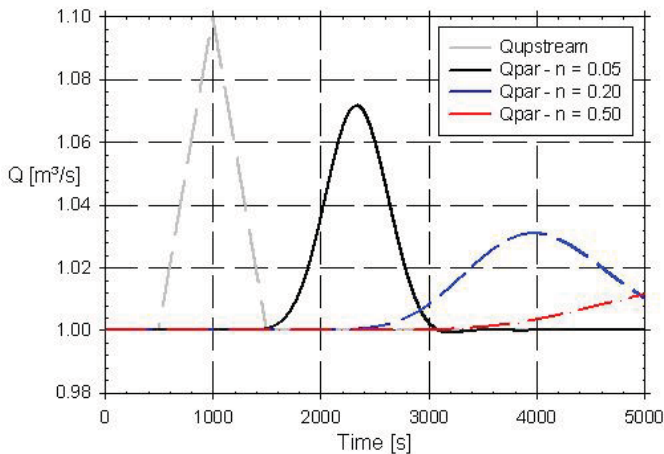


Figure 6: Use of the parabolic wave model: result at the same distance ($x = 388 \text{ m}$) for different values of the Manning coefficient n

Differences between winter and summer up to a factor 10 are not rare. As can be seen, the presence of more macrophytes cause obstruction in the channel. For a certain amount of water, it is more difficult for the water to pass and so the discharge will be lower, just as the peak value of the discharge. More vegetation in the river results in a higher friction coefficient of Manning.

2.6.3 Use of the Saint-Venant equations

After having modeled the simplified kinematic and parabolic equations, the proliferation of the triangular hydrograph is also modeled using the Saint-Venant equations. These results can be seen on Figure 7 and Figure 8. Figure 7 shows the results at different sections when the Manning coefficient is set constant ($n = 0.05 \text{ m}^{-1/3} \text{ s}$).

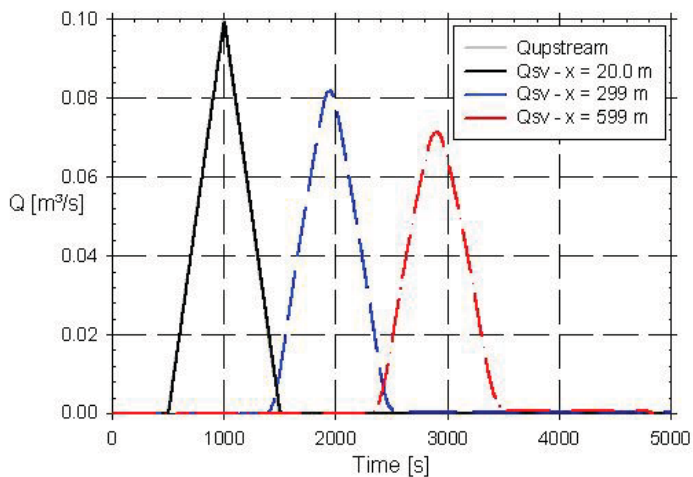


Figure 7: Use of the Saint-Venant equations: result at different distances

At Figure 8, the influence of this friction coefficient in a certain section ($x = 299 \text{ m}$) can be seen. The total stretch is 10,000 m and upstream and downstream boundary conditions have to be added, which is different compared to the simplified equations.

The parabolic and kinematic model use the upstream boundary condition and start to calculate one cell after the other. In contrary, the Saint-Venant equations use both boundaries and need well balanced initial conditions. Calculation of the surface water level for permanent steady state flow over the total length of the channel can be a good start and can serve initial conditions. Further more, boundary conditions are important because both of them have influences in the different cells.

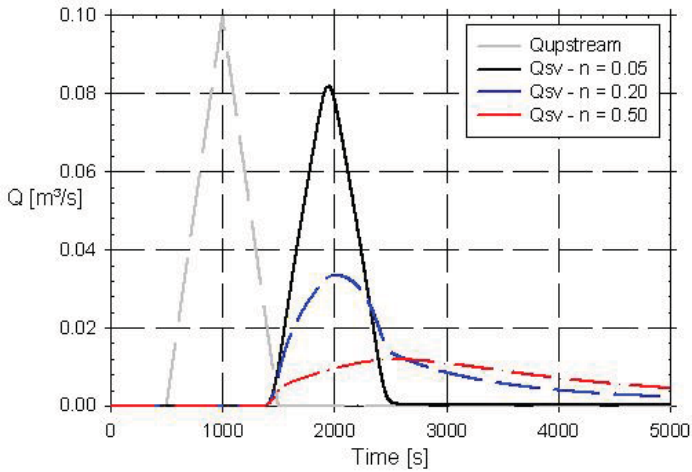


Figure 8: Use of the Saint-Venant equations: result at the same distance ($x = 299$ m) for different values of the Manning coefficient n

Concerning the morphology of the channel, the slope is important for the water levels in the channel. This bottom slope has an influence on the friction slope S_f (water surface slope). A constant slope of 0 can eliminate that influence.

3. CONCLUSIONS

'Femme' has been used as environment for the description and propagation of waves in rivers. As a study area, the river Aa was selected and its characteristics were implemented in 'Femme'.

By this, three kind of models to simulate the propagation of waves in channels are considered. As can be seen, the one model is more accurate as the other, but accurateness includes also a higher degree of complexity. So depending of the situation and the kind of results that have to be obtained, one model can be chosen.

While studying a variety of ecosystem cases, different wave models (based on the kinematic, parabolic and Saint-venant equations) or even a constant discharge can be used in the hydraulic calculation.

Acknowledgements

This research is funded by the FWO (Fund for Scientific Research) - Flanders (G.0306.04). It is part of the multidisciplinary research project 'A fundamental study on exchange processes in river ecosystems' (University of Antwerp, Vrije

Universiteit Brussel, Ghent University, 2004 - 2007). The overall objective is to study the physical and biological exchange processes in margins and inundation areas of water courses and how their interactions determine the exchange of water, dissolved compounds and particulate matter.

Thanks to Mr. Martin Van Daele and Mr. Stefaan Bliki for their assistance with the discharge measurements.

This research is funded by the FWO (Fund for Scientific Research) - Flanders (G.0306.04).

References

1. Abbott, M. B. et al., *Unsteady Flow in Open Channels*, Vol. 1, Ed. by Mahmood, K. and Yevjevich, V., 1975.
2. Buis, K., Anibas, C., Banasiak, R., De Doncker, L., Desmet, N., Gerard, M., Van Belleghem, S., Batelaan, O., Troch, P., Verhoeven, R. and Meire, P., *A multidisciplinary study on exchange processes in river ecosystems*, W3M, Wetlands: Monitoring, Modelling, Management, 22 – 25 September, Wierzba, Poland, 2005.
3. Cunge, J., Holly, F. and Verwey, A., *Practical aspects of computational river hydraulics*, Pitman Advanced Publishing Program, London, 1980.
4. Chow, V.T., *Open Channel Hydraulics*, McGraw-Hill, New York 1959.
5. Chow, V.T., Maidment, D. R., Mays, L.W., *Applied Hydrology*, McGraw-Hill, New York 1988.
6. De Doncker, L., Troch, P., Verhoeven, R., *Influence of aquatic weed growth on the flow resistance of the river Aa*, 6th FirW PhD Symposium, 30th November 2005, Ghent University, Belgium.
7. Soetaert, K., de Clippele, V., Herman, P., ‘Femme’, a flexible environment for numerically modeling the environment, Manual, NIOO-CEME, Yerseke, The Netherlands.
8. Verhoeven, R., Water beheer en waterbeheersing, course for civil engineers, part C: ‘*Afvoer en berging van water*’.

Simulation of cooling tower collapse on the basis of non-linear concrete model and FEM analysis

Przemysław Siwiec, Sebastian Toś

Department of Civil Engineering, Wrocław University of Technology, Wrocław, Poland

Summary

In this paper authors attempt to take advantage of a non-linear model of material to create a mathematical model of the cooling tower, and further, taking advantage of the non-linear FEM analysis, they try to recover numerically the course of the collapse. Both for concrete, as well as for steel, an elasto-plastic model of material characterized by specific plasticity criteria has been assumed.

KEYWORDS: cooling tower, non-linear analysis, elasto-plastic material model, FEM analysis

1. INTRODUCTION

The main purpose of design process is to bestow an object a form, shape and guarantee proper technical parameters in order to fulfill its functions and safety of service. As soon as the erecting process begins the object is under influence of destructive factors and interactions tending to ruin it. The purpose of the structure designer is to predict these factors and to counteract properly. Nevertheless crashes do occur. Therefore the new assignment appears: to determine causes and failure sequences. Being in the know with the failure course we are able to determine the safety conditions of a similar already existing structure and to undertake proper improving actions.

In this paper the authors have tried to create a proper numerical model of the reinforced concrete (RC) cooling tower and to investigate the failure course of RC cooling tower in 1987.

2. THE FAILURE SEQUENCE

The failure of over 100 m high RC cooling tower was one of the most spectacular crashes in Poland. On 7th February 1987 at 7 p.m. the RC cooling tower suddenly collapsed. At the level of 38th concreting cycle almost the whole perimeter of its

shell was cut. Only from the north-east side a deep interstice appeared (Fig. 1). At the moment of the failure the RC cooling tower was under regular service. Till that day the object had been exploited uninterruptedly for 23 years and it was considered to be in the best technical state of all six identical RC cooling towers in the battery.

The most characteristic in this failure was the lack of clear cause. On that day it was light windy: 3–5 m/s, so the wind factor could not be the main reason. The unusual influences such as sound waves caused by supersonic airplanes or underground earthquakes were excluded, too. The RC cooling tower collapsed as if under its own weight.

According to the initial investigations [8] — carried out from February to April 1987 — it has been established that at the most of the fracture the concrete was crumbled, cracked and not condensed. At the whole of the fracture perimeter reinforcement bars without any traces of rupture were found. Some of them were strongly crumpled, some cambered downwards only. A few of them were cambered upwards, too.



Fig. 1 RC Cooling tower after the collapse

The examination of the concrete and reinforcement strength of the RC cooling tower confirmed their satisfactory quality. The strength of most of concrete samples reached over 20 MPa.

The initial estimation of collapse causes has revealed concrete corrosion of the operating contact zone leading to loss of the shell stability [8]. However this phenomenon seemed to be too simple and incomplete especially in consideration of the fact of strong winds occurring only a few days before the failure.

A following hypothesis has been proposed: the proximate cause of failure was the improperly performed operating contact zone which in result of variable winds and

corrosion factors led to loss of the whole shell stability. In order to prove this hypothesis the nonlinear FEM analysis on the numerical model of RC cooling tower has been performed, with use of the DIANA system.

3. DESCRIPTION OF THE NUMERICAL MODEL

3.1 Geometry

In order to properly analyze the proposed thesis the numerical model of 100 m high RC cooling tower has been created.

Eight-node shell elements of CQ40 [13] type have been used for creating the numerical model of the bicurvature shell structure. These elements allow to introduce the variable shell thickness in every node so the numerical model has no rapid stiffness changes.

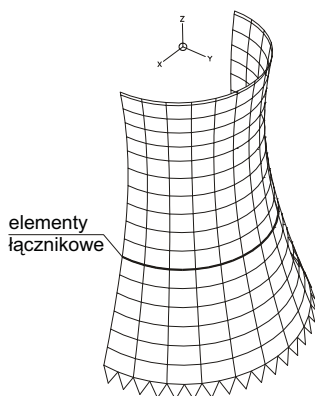


Fig. 2 Numerical model

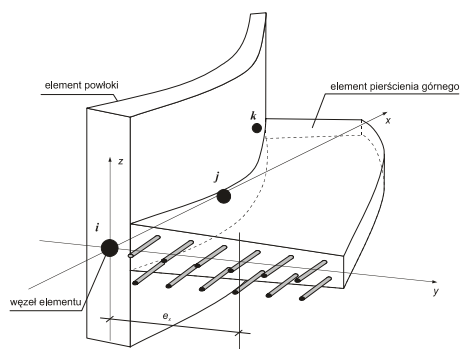


Fig. 3 Elements of upper shelf

The structure has been divided into 17 rings with 12 final elements in every ring (for the half of the structure) — see Fig. 2 [3].

The stiffening ring has been created with the three-node rod elements of CL18B type (Beurnoulli) with 6 degrees of freedom in every node. Their cross-section has been eccentricity founded (shifted in relation to) on the net of nodes in order to model the stiffening shelf properly. Due to possibility of unrestricted cross-section shape modeling, the actual trapezoid-shaped shelf has been created — see Fig. 3.

The load carrying poles have been modeled with the rectilinear elements of L13BE type (circle-shaped in cross-section) and they have been connected in a rigid way with the shell elements and with the fundamentals.

The DIANA system allows to model the reinforcement as the settled inserts, bound with the mother element and make its stiffness increase. The reinforcement elements have no degrees of freedom of their own so their deformation is determined by the deformation of the mother element. It means that there is no slip phenomenon between the concrete and the reinforcement. Generally it is possible to insert the reinforcement in the mother final element in unrestricted way — regardless of its geometry.

Two kinds of the reinforcement have been used in the numerical model of the RC cooling tower: the linear inserts (rods) settled in rod elements, and the net inserts settled in shell elements. Tab. 1 shows the area of used inserts [8].

All final elements used in the numerical model have been numerical integrable and for each of the groups the modified integral-points-set has been used:

- Poles elements had eight Gauss’s integral points at their cross-section surface, evenly distant from the rod center. Three integral zones with 8 points in each one at the rod length have been used (according to the Gauss’s rule).
- Upper shelf elements had nine Gauss’s integral points at their cross-section surface (3×3) and three integral points groups distributed at the rod length (according to the Gauss’s rule).

Tab. 1. The reinforcement area

Element	Area
Load carrying poles	0.34%
Upper shelf	0.28%
Outer horizontal reinforcement	0.25%
Inner horizontal reinforcement	0.25%
Outer vertical reinforcement	0.20%
Inner vertical reinforcement	0.20%

- The reinforcement settled in elements had the integral schemes analogical with their mother elements: three Gauss’s points at the length for rods and 3×3 Gauss’s integral points for reinforcement nets of shell elements.

In order to investigate the simulation of the failure course, the FEM numerical model has been created in which the connecting elements have been used in order to model the linear damage zone properly [13].

The characteristic feature of these elements is the possibility of physical disconnection into two parts after exceeding the tensile strength. The connecting elements of the N6IF type have defined stiffness against compression/tension and shearing.

Tab. 2. The material parameters

Parameter	
Young's modulus	26·106 kPa
Poisson ratio	0.1667
Density	23 kN/m ³
Compression strength	11 500 kPa
$\sin \phi$	0.5
$\sin \psi$	0.5
Tensile strength	900 kPa
Damage energy G_f	500 kNm/m ²
Weakenig model	Hordijk
Tangential stress ratio β	0.01

In order to create the numerical model properly in accordance with the actual structure, the connecting elements in damage zone (3 to 5 elements long) had the stiffness of the weakened concrete (Hordijk's model - see Tab. 2) and their shearing stiffness has been equal with the reinforcement bar shearing stiffness. The stiffness of the rest of the connecting elements has been defined as equal with the stiffness of the shell elements.

3.2. The material

All final elements had nonlinear characteristics [2] and their parameters have been based partly on published investigations results of the analyzed object and partly on the design project documentation and expert opinions on the cooling tower [7, 8]. There has been taken into consideration the material ductility described by the Drucker-Prager's constitutive model in the compressed zone for the concrete elements.

For the tensile zone the smeared cracks model has been used [14, 15]. The winding effect of the load carrying RC poles has been modeled by increasing the strength parameters of concrete. On the basis of the in situ investigations the concrete strength of $f_c=20$ MPa has been assumed whereas for the RC poles it has been increased to $f_c=25$ MPa [8]. The Tab. 2 shows the nonlinear concrete parameters.

Tab. 3 Values of the α parameter

d_{\max} [mm]	α
8	4
16	6
32	10

The most important parameter describing the material in the cracked zone is the damage energy G_f . Its value has been based on the recommendations of the CEB-FIB Model Code (1990), which allowed to estimate the damage energy on the basis of the strength investigations according to the relationship:

$$G_f = \alpha f_{ck}^{0,7} \tag{1}$$

where f_{ck} is the compression strength, depends on the maximum aggregate size (Tab. 3).

Fig. 4 shows the concrete performance for the biaxial state of stress. Fig. 5 shows the H-M-H criterion for steel.

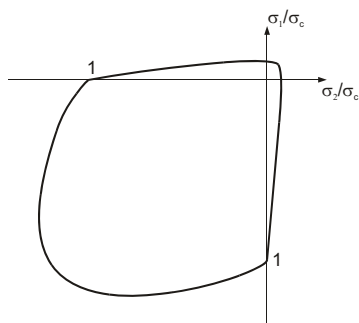


Fig. 4 Biaxial state of stress for concrete

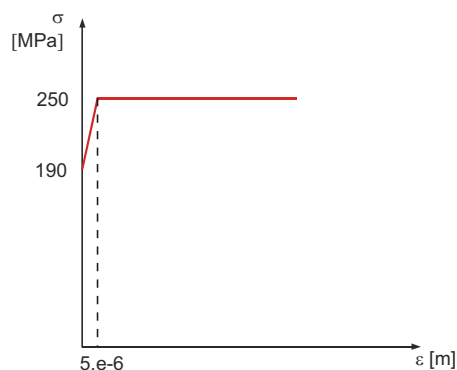


Fig. 5 The steel stiffening model

4. THE LOADS

In the calculation carried out only the deadweight and the wind have been considered [1]. They were the most important factors and most significant for the structure effort. Other loads such as: temperature, hydraulic pressure, unequal insolation effects, unequal foundations subsiding and other exceptional loads have been neglected. As far as the general question is considered taking into account all of these loads will allow to determine the global state of the structure effort.

During the numerical analysis process the structure has been loaded in a few phases:

- First the deadweight was loaded (incrementally) till the nonlinear load coefficient L_f reached the value equal to 1.0.

- Then the wind load was added (incrementally) till the nonlinear load coefficient L_f reached its maximum value.

5. THE TECHNIQUE OF THE NONLINEAR PROBLEM TRACING

In order to solve the nonlinear problem the standard Newton-Raphson's algorithm and the energetic norm of the results convergence control have been used. In nonlinear process the *arc-length* technique based on tracing the selected node displacement has been used in order to control the load growth. At each stage of the load increment the node displacement (degree of freedom) towards the selected direction has been analyzed. Every time the most deformed node - in the previous stage of the analysis - has been taken into account. Calculations have been stopped as soon as the lack of convergence has occurred.

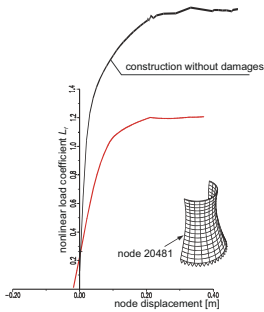


Fig. 6 The structure answer curves

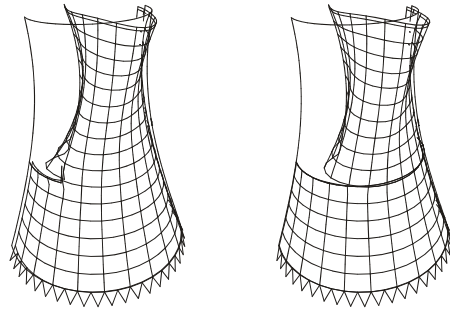


Fig. 7 The deformation development in RC cooling tower under the wind load

The structure performance under the increasing load has been investigated with use of the structure response curve, which described the chosen node displacement as a function of the load increase (defined as the nonlinear load coefficient L_f).

6. THE NUMERICAL SIMULATION OF THE COLLAPSE SEQUENCE

According to the proposed hypothesis it has been assumed that the primary damage area of the operating contact zone reached up to 21 m (three elements of the half-ring). In order to fulfill the symmetry conditions the interstice has been located at the windward side. This is a particular case yet it is sufficient for the essence of the

analyzed matter. The numerical analysis indicates the possibility of the primary shell damage development caused by the wind loads without collapse of the whole structure.

Assuming the variable wind directions, it is probable that the progressive interstice growth up to the whole perimeter would occur. At the next calculation stage the interstice has been assumed as long enough and the cooling tower has been deadweight loaded only. At further stages the size of the totally damaged material in the interstice has been varied. The run of the structure response curve is shown in the Fig. 8 and the deformation development - in the Fig. 9.

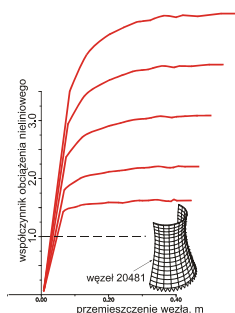


Fig. 8. The structure response curves due to development of initial crack.

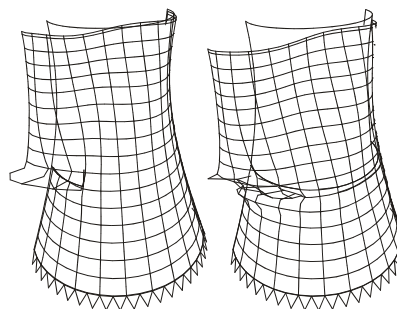


Fig. 9. The deformation development in RC cooling tower under the deadweight

The deformation character confirms the conclusion of locally violent variable displacement character. Displacement occurs within the area of one ring above and one ring below the interstice. What is worth noticing is the deformation form of the upper part of the shell.

At the area close above the interstice the shell goes outwards from its perimeter while the rest of the shell goes towards the inside. According to the above scheme only a small part of the shell should collapse outside the cooling tower and the whole rest of it should collapse towards the inside.

7. THE FAILURE SEQUENCE DETAILS

Phase 1 — improper composition of the concrete mixture, its impurities or not sufficiently careful assembly phase caused the material imperfection which increased during the service of the cooling tower [5, 6]. The negative coincidence was localization of this imperfection in the zone of the highest structure effort — i.e. at of the tower height [3]. At this moment it is impossible to exclude the geometrical imperfection in the analyzed zone, too.

Phase 2 —increasing material degradation process caused by accelerated corrosion of the cracked concrete brings about the interstice or the weakened material zone. Then the variable winds and frost penetration cause enlarging of this zone. It is possible that the weakened zone still holds its geometrical shape in spite of total loss of its strength parameters due to internal cracking. This would explain the fact that the Electric Power Station employers had not noticed the shell defect. Undoubtedly the interstice initiation took place at the operating contact zone.

Phase 3 — when the strong winds cause the increasing of the interstice up to its critical length, further interstice length growth begins which results from the deadweight of the cooling tower only. At first this process was not violent as it was restrained by the reinforcement and could last even for a few days until the moment of a violent collapse. If only the stronger puff of wind occurred during this time, the collapse would undoubtedly have taken place sooner.

The confirmation of the presented above hypothesis of the failure sequence is the occurrence of the most of the concrete debris at the eastern side of the cooling tower. According to the presented model the failure process started exactly above the area where the concrete debris was found outside the cooling tower.

8. CONCLUSION

In this paper the numerical model of the RC cooling tower has been created with consideration of material and geometrical nonlinearity. This model has been investigated on the basis of 100 m high RC cooling towers commonly built in Poland. The presented numerical model enables simulation of the process occurring during regular RC cooling tower exploitation. The numerical model analysis allows the precise determination of the causes and the failure course. Due to possibility of failure results verification — especially the concrete debris localization — the presented numerical model has been proved reliable.

References

1. Siwiec P., Szechinski M.: *Zelbetowa chłodnia kominowa obciążona wiatrem* — Inżynieria i Budownictwo, nr 3, 1997.
2. Siwiec P., Strouven P., Moczko A.: *Study of steel bar corrosion by experimental and analytical simulation* — DIANA Computational Mechanics '94, ed. Kusters M. A., Hendriks A. N., Kluwer Academic Publishers, Dordrecht — 1994.
3. Siwiec P.: *Nieliniowa analiza statyczno-wytrzymałościowa uszkodzonej, żelbetowej chłodni kominowej* — doctor's thesis, The Institute of the Building Engineering, Wrocław 2001.
4. Zabiello Z., Hawre L.: *Problemy oceny stanu technicznego chłodni kominowych w kontekście awarii chłodni nr 6* — The Science-technical Conference: The durability of the RC cooling towers, Czocha — 1989.
5. Persona M.: *Z badań doświadczalnych chłodni kominowych Elektrowni Turow* — The Science-technical Conference: The durability of the RC cooling towers, Czocha — 1989.

6. 6. Persona M., *Wybrane zagadnienia z badan zelbetowych chlodni kominowych* — Chłodnie Kominowe. Efektywne systemy ochrony i napraw, Sympozjum, Jelenia Góra 1991.
7. 7. Persona M., Szechinski M.: *Remark on failure of a reinforced concrete cooling tower* — IABSE Colloquium, Stuttgart 1991.
8. 8. Persona M., Stus R., Szechinski M.: *Okreslenie przyczyn katastrofy budowlanej chlodni kominowej nr 6 oraz ustalenie stanu technicznego czesci niezawalonej pod katem mozliwosci wykorzystania dla ukkladu chlodzacego Elektrowni Turow* — Reports of the Institute of the Building Engineering, Wrocław University of Technology, SPR no. /87.
9. 9. Persona M. i zespól: *Wyniki badan i ocena stanu technicznego konstrukcji plaszczu chlodni kominowej nr 6 w elektrowni Turow* — Reports of the Institute of the Building Engineering Wrocław University of Technology, SPR nr 43/89.
10. 10. Owczarzy J.: *Katastrofy zelbetowych chlodni kominowych* — The Science-technical Conference: The durability of the RC cooling towers, Czocha — 1989.
11. 11. Niku S. M.: *Finite Element Analysis of Hyperbolic Cooling Towers* — Lecture Notes in Engineering, ed. Brebbia C. A., Orszag S. A., Springer-Verlag 1986.
12. 12. Golczyk M.: *Analiza techniczna przyczyn i skutkow uszkodzen i zniszczen hiperboloidalnych powlok chlodni kominowych* — The Science-technical Conference: The durability of the RC cooling towers, Czocha — 1989.
13. 13. DIANA Finite Element Analysis, *User's Manual*, Release 6.2 — TNO Building and Construction Researche, Delft 1996.
14. 14. Blaauwendraad J.: *Numerical Methods in Structural Mechanics* — Delft University of Technology — 1993.
15. 15. De Borst R.: *Computational Methods in Non-linear Solid Mechanics* — Delft University of Technology, series B20, Delft 1993.

Unsteady axial Poiseuille flow of a Bingham fluid in an annulus

Irene Daprà, Giambattista Scarpi
DISTART, University of Bologna, 40136, Italy

Summary

Several fluids which are of interest in civil engineering, as bentonite, montmorillonite, slurries, behave as Bingham fluids, i.e. fluids which present a yield stress. This paper investigates numerically the start-up, the cessation and some pulsating flows of a Bingham plastic between two coaxial cylinders. The constitutive law presents a discontinuity for zero shear rate which introduces severe difficulties in solving any problem of unsteady motion, both analytically and numerically. A suitable way to avoid the obstacle is to regularize the constitutive equation using a smooth function to approximate the Bingham law. The adopted function depends usually on a parameter: as it tends to infinity the model tends (in distribution theory sense) to the true Bingham law. Several models have been used in literature to regularize the rheological behaviour of a viscoplastic fluid: in this paper a new constitutive equation is proposed, based on the error function (erf). The velocity fields have been calculated using an implicit finite difference method. The numerical results confirm that the time required to reach the final steady state is infinite for start-up, whereas it is finite for stopping. In the pulsating flow the mean velocity of the plug in a period and the mean rate of flow increase owing to the non linearity of the material.

KEYWORDS: Bingham fluid, unsteady flow, Poiseuille flow, flow in annulus.

1. INTRODUCTION

Bingham fluids such as bentonite and montmorillonite are used to solve many engineering problems for example in drilling, in pile works and in rock consolidation. Bentonite is the base material in drilling: it cools the drill and reduces wear, consolidates the excavation, goes back up in the annulus between wall and stick bringing to the surface the debris.

Bingham fluids require the application of a greater shear stress than a critical value, the yield stress, to begin to move. After yielding, the rheological behaviour is that of a Newtonian fluid, while in the core region the material moves as a solid body. Many unsteady flows of Newtonian fluids admit analytical solution in closed form:

the same problems for a Bingham fluid are obviously more difficult to solve because of the non linearity of the constitutive law.

The discontinuity in the constitutive equation at zero shear rate introduces severe difficulties for analytical and even for numerical solutions. To overcome that, Glowinski [1] suggested regularising the constitutive law, substituting the discontinuous function with a continuous one, which, when a given parameter tends to an assigned limit, usually zero or infinity, tends (at least in the sense of distributions theory) to the true Bingham law. Several proposals for regularisation have been made in literature; the most used is that proposed by Papanastasiou [2]. An interesting analysis of advantages and disadvantages of continuous models with exhaustive literature is given by Frigaard and Nouar [3].

Characteristic of a Bingham fluid is the fact that its stopping time is finite, whereas Newtonian fluids and generally any fluid without yield stress need an infinite time to stop. Glowinski [4] and Huilgol et al. [5] give a theoretical upper bound for the stopping time for pipe and plane flow. Chatzimina et al. [6] study numerically the cessation of the Couette and Poiseuille flow of a Bingham fluid using the Papanastasiou model comparing the numerical results with the theoretical predictions. Many authors have written in the past about unsteady flow of Bingham fluids; among these we recall for example Duggin [7] which gives a numerical solution for the start-up flow in a circular pipe; Papanastasiou and Boudouvis [8] solve numerically flow problems in generalised conduits. Hammad [9] studies the pulsatile flow for different waveforms of the pressure gradient. Daprà and Scarpi give an analytical solution to the start-up problem in a circular pipe.

This paper investigates numerically the start-up, the cessation and some pulsating flows of a Bingham plastic between two coaxial cylinders. A new model based on the error function is proposed to regularize the constitutive equation.

2. CONSTITUTIVE EQUATIONS

Being \mathbf{v} , \mathbf{T} and $\dot{\boldsymbol{\gamma}}$ the velocity vector, the stress tensor and the rate of strain tensor, the constitutive equation of a Bingham fluid is

$$\left\{ \begin{array}{ll} \dot{\boldsymbol{\gamma}} = 0 & \tau \leq \tau_0 \\ \mathbf{T} = \left(\frac{\tau_0}{\dot{\boldsymbol{\gamma}}} + \mu \right) \dot{\boldsymbol{\gamma}} & \tau \geq \tau_0 \end{array} \right. \quad (1)$$

where τ_0 is the yield stress and μ is the viscosity of the fluid. To avoid the singularity in the constitutive equation, it is possible to substitute the rheological law (1) with a continuous function. In 1987 Papanastasiou suggested the equation

$$\mathbf{T} = \left[\frac{\tau_0 \left[1 - \exp(-m\dot{\gamma}) \right]}{\dot{\gamma}} + \mu \right] \dot{\gamma} \quad (2)$$

The authors propose the following relation which is continuous and infinitely derivable everywhere

$$\mathbf{T} = \left[\frac{\tau_0}{\dot{\gamma}} \operatorname{erf}(k\dot{\gamma}) + \mu \right] \dot{\gamma} \quad (3)$$

where, as usual,

$$\operatorname{erf}(x) = \frac{2}{\sqrt{\pi}} \int_0^x e^{-t^2} dt \quad (4)$$

is the error function.

3. AXIAL FLOW IN A CONCENTRIC ANNULUS

3.1. Steady flow

The geometry is shown in Fig. 1. The flow is one-dimensional and the momentum equation is:

$$-\frac{\partial p}{\partial x} + \frac{1}{r} \frac{\partial(r\tau)}{\partial r} = \rho \frac{\partial u}{\partial t} \quad (5)$$

where x is the direction of the motion, r the radial coordinate, p the pressure, τ the shear stress, u the velocity, ρ the fluid density and t the time. Eq. (1) becomes

$$\left\{ \begin{array}{ll} \frac{\partial u}{\partial r} = 0 & \tau \leq \tau_0 \\ \tau = \tau_0 \operatorname{sgn}\left(\frac{\partial u}{\partial r}\right) + \mu \frac{\partial u}{\partial r} & \tau \geq \tau_0 \end{array} \right. \quad (6)$$

where

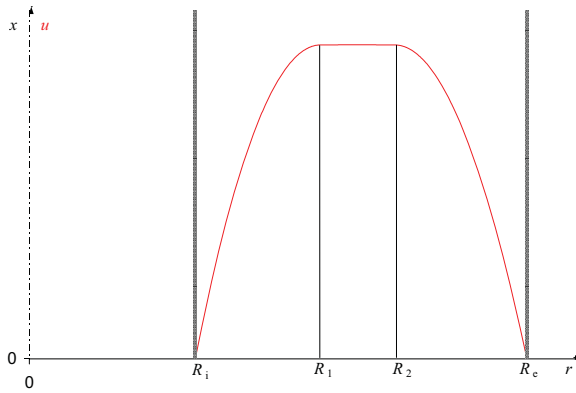


Fig. 1. Flow geometry

$$\operatorname{sgn}\left(\frac{\partial u}{\partial r}\right) = \begin{cases} -1 & \frac{\partial u}{\partial r} < 0 \\ 1 & \frac{\partial u}{\partial r} \geq 0 \end{cases} \quad (7)$$

Putting $-\frac{\partial p}{\partial x} = \bar{P}$, the steady solution for a Bingham fluid is then

$$\begin{cases} u = u_1 = \frac{1}{\mu} \left(-\frac{\bar{P}r^2}{4} + a \ln r - \tau_0 r + b_1 \right) & R_i \leq r \leq R_1 \\ u = u_2 = \frac{1}{\mu} \left(-\frac{\bar{P}r^2}{4} + a \ln r + \tau_0 r + b_2 \right) & R_2 \leq r \leq R_e \\ u = u_1(R_1) = u_2(R_2) & R_1 \leq r \leq R_2 \end{cases} \quad (8)$$

$R_1 \leq r \leq R_2$ being the unyielded region, where the material behaves as a solid. The equation

$$a \ln \frac{R_e \left(-\tau_0 + \sqrt{\tau_0^2 + 2a\bar{P}} \right)}{R_i \left(\tau_0 + \sqrt{\tau_0^2 + 2a\bar{P}} \right)} + \tau_0 \left(R_e + R_i - \frac{\sqrt{\tau_0^2 + 2a\bar{P}}}{\bar{P}} \right) - \frac{\bar{P}}{4} (R_e^2 - R_i^2) = 0 \quad (9)$$

allows to evaluate a and

$$b_1 = \frac{\bar{P}R_i^2}{4} - a \ln R_i + \tau_0 R_i \quad (10)$$

$$b_2 = \frac{\bar{P}R_i^2}{4} - a \ln R_i - \tau_0 R_i \quad (11)$$

$$R_1 = \frac{-\tau_0 + \sqrt{\tau_0^2 + 2a\bar{P}}}{\bar{P}} \quad (12)$$

$$R_2 = \frac{\tau_0 + \sqrt{\tau_0^2 + 2a\bar{P}}}{\bar{P}} \quad (13)$$

the amplitude of the plug is then

$$R_2 - R_1 = \frac{2\tau_0}{\bar{P}} \quad (14)$$

The rate of flow Q , which allows to calculate the mean velocity V , is

$$Q = \int_{R_i}^{R_1} 2\pi r u_1 dr + \pi (R_2^2 - R_1^2) u_1 + \int_{R_2}^{R_e} 2\pi r u_2 dr \quad (15)$$

Using the hydraulic radius $R = \frac{\pi (R_2^2 - R_1^2)}{2\pi (R_1 + R_2)} = \frac{R_2 - R_1}{2}$ as reference length, eq. (8)

and (15) give

$$\begin{aligned} V = \frac{R^2 \bar{P}}{\mu (\eta_e^2 - \eta_i^2)} & \left\{ c \left(\eta_2^2 \eta_e^2 \ln \frac{\eta_1 \eta_e}{\eta_2 \eta_i} - \frac{\eta_e^4}{2} + \frac{\eta_2^2 \eta_e^2}{2} + \eta_i^2 \eta_e^2 - \frac{\eta_1^2 \eta_e^2}{2} \right) + \right. \\ & + \frac{\eta_e^4}{8} - \frac{\eta_i^4}{8} + \frac{1}{8} (\eta_2^2 - \eta_1^2)^2 - \frac{1}{4} \eta_2^2 (\eta_e^2 - \eta_i^2) + \frac{1}{2} (\eta_2 - \eta_1) \cdot \\ & \left. \cdot \left(\frac{\eta_1^3}{3} - \frac{\eta_e^3}{3} - \frac{\eta_i^3}{3} - \eta_1 \eta_2^2 - \frac{2}{3} \eta_2^3 + \eta_2 \eta_i \eta_e + \eta_2^2 \eta_e \right) \right\} \quad (16) \end{aligned}$$

where $\eta_e = R_e / R$, $\eta_i = R_i / R$, $\eta_1 = R_1 / R$, $\eta_2 = R_2 / R$ and $c = \frac{a}{R_e^2 \bar{P}}$

3.2. Unsteady flow

Introducing the following dimensionless quantities: $\xi = x / R$, $\eta = r / R$, $v = u / V$, $\theta = \tau R / \mu V$, $\theta_0 = \tau_0 R / \mu V = Bn$, $P = \bar{P} R^2 / \mu V$, $K = kV / R$, $T = t\mu / \rho R^2$, eq. (5) becomes:

$$P + \frac{1}{\eta} \frac{\partial(\eta\theta)}{\partial\eta} = \frac{\partial v}{\partial T} \tag{17}$$

The constitutive equation

$$\theta = B \operatorname{erf} \left(K \frac{\partial v}{\partial \eta} \right) + \frac{\partial v}{\partial \eta} \tag{18}$$

is plotted in Fig. 2.

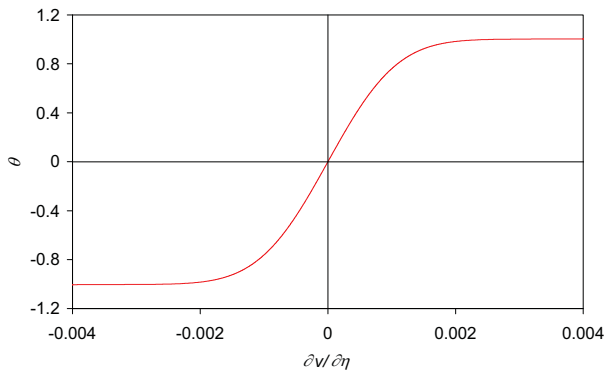


Fig. 2. Regularized constitutive equation

Substituting (1) in (17)

$$P + \left[\frac{2KBn}{\sqrt{\pi}} \exp \left(- \left(K \frac{\partial v}{\partial \eta} \right)^2 \right) + 1 \right] \frac{\partial^2 v}{\partial \eta^2} + \frac{1}{\eta} \left[\frac{\partial v}{\partial \eta} + B \operatorname{erf} \left(K \frac{\partial v}{\partial \eta} \right) \right] = \frac{\partial v}{\partial T} \tag{19}$$

For a coaxial pipe of dimensionless internal radius η_i and external radius η_e , the boundary conditions are:

$$v(\eta_i, T) = v(\eta_e, T) = 0 \quad \forall T \tag{20}$$

Moreover

$$\left. \frac{\partial v}{\partial \eta} \right|_{\eta_1} = \left. \frac{\partial v}{\partial \eta} \right|_{\eta_2} = 0 \quad v(\eta_1) = v(\eta_2) \tag{21}$$

3.2.1. Start-up flow

A suddenly positive pressure gradient $P = P_0$ is applied to the fluid at rest. P_0 gives rise to a unit non-dimensional mean velocity in steady state and must be greater than $2Bn$ in order for the fluid to move. The initial condition for eq. (19) is

$$v(\eta, T) = 0 \quad \eta_i \leq \eta \leq \eta_e \quad T < 0 \quad (22)$$

3.2.2 Cessation of flow

The constant pressure gradient P_0 applied to the fluid in steady flow is suddenly cancelled.

Conditions at $T = 0$ are

$$\begin{cases} v = v_1 = -\frac{P_0 \eta^2}{4} + A \ln \eta R - \eta Bn + B_1 & \eta_i \leq \eta \leq \eta_1 \\ v = v_2 = -\frac{P_0 \eta^2}{4} + A \ln \eta R + \eta Bn + B_2 & \eta_2 \leq \eta \leq \eta_e \\ v = v_1(\eta_1) = v_2(\eta_2) & \eta_1 \leq \eta \leq \eta_2 \end{cases} \quad (23)$$

where, referring to eqs. (9)-(11), $A = \frac{a}{\mu V}$, $B_1 = \frac{b_1}{\mu V}$ and $B_2 = \frac{b_2}{\mu V}$

3.2.3 Pulsatile flows

Two different pressure wave are imposed to a fluid at rest

a) rectangular wave

$$P = P_0 \sum_{n=0}^{\infty} \left[H(T - n(T_1 + T_2)) - H(T - n(T_1 + T_2) - T_1) \right] \quad (24)$$

where $H(T)$ is the unit step function; in a period $T_0 = T_1 + T_2$ the pressure gradient P is equal to P_0 for the first time interval T_1 and $P = 0$ for the second one T_2 .

b) sinusoidal wave superimposed to a constant pressure gradient P_0 :

$$P = P_0 (1 + \varepsilon \sin 2\pi f T) \quad (25)$$

where f is the frequency.

4. NUMERICAL RESULTS

The numerical calculations have been carried out for coaxial pipes with $\eta_i = 8$ and $\eta_e = 10$: the annulus width is thus 20% of the radius of the external pipe; the dependence of the unyielded core extension $\eta_2 - \eta_1$ on the Bingham number in steady state is plotted in Fig. 3.

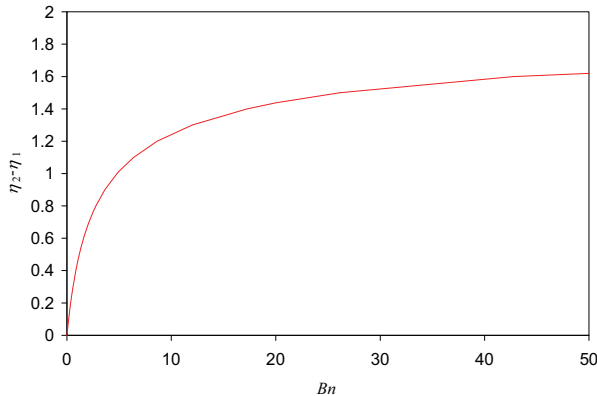


Fig. 3. Solid plug amplitude versus Bingham number

Eq. (19) with boundary conditions (20), (21) and the appropriate initial conditions is solved using an implicit finite difference method. The numerical procedure has been first validated for a Newtonian fluid, for which the analytical results are well known.

Numerical experiments indicated that the maximum value for parameter K in order to obtain valid results can be estimated as $K = 5000 \frac{\eta_2 - \eta_1}{Bn}$. If K exceeds this value, the numerical procedure can exhibit instabilities. A uniform spatial grid of 1000 points has been adopted, using a time step equal to $4 \cdot 10^{-6}$. Smaller time steps give the same results, whereas greater ones can generate instabilities. The difference between the steady-state velocity profile obtained with the numerical solution and the theoretical one for a true Bingham fluid is less than 1%.

a) Start-up

Fig. 4 illustrates the numerical steady velocity profile for Bingham fluids, with $Bn = 1, 2, 3, 10$ and for a Newtonian one, which can be considered as a Bingham fluid with $Bn = 0$. Fig. 5 shows the development of the plug velocity versus time for the same values of Bn .

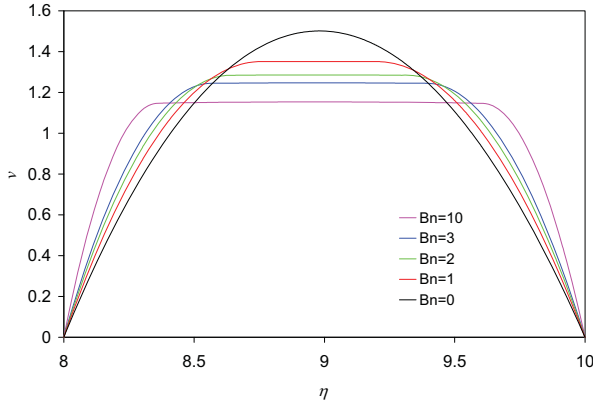


Fig. 4. Steady velocity profiles

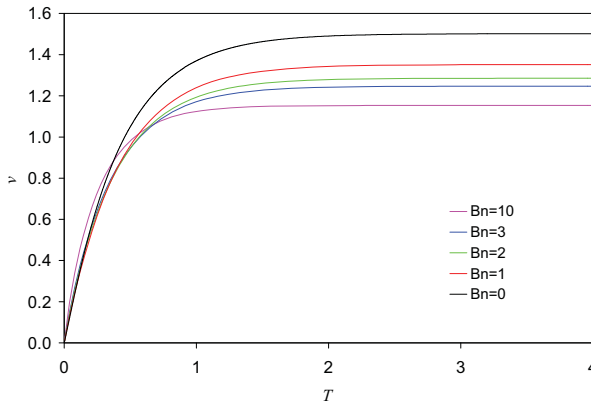


Fig. 5. Start-up: solid plug velocity versus time

b) Cessation of flow

Unlike Newtonian fluids and generally any fluid without yield stress which need an infinite stopping time, Bingham fluids require a finite time T_s to reduce to zero the velocity. Glowinski [5] [6] and Huilgol et al. [7] gave a theoretical upper bound for the stopping time for Poiseuille and plane flow. Fig 6 shows the rate of flow as function of time at different Bingham numbers. As expected, the rate of flow decreases the more rapidly the greater Bn is. Fig 7 shows the time needed to reduce the rate of flow to 10^{-3} and 10^{-5} respectively, as function of Bn : the difference between the two obtained values of time becomes appreciable only if $Bn > 10$. The time required to reduce the rate of flow to 10^{-5} can be considered as the stopping time.

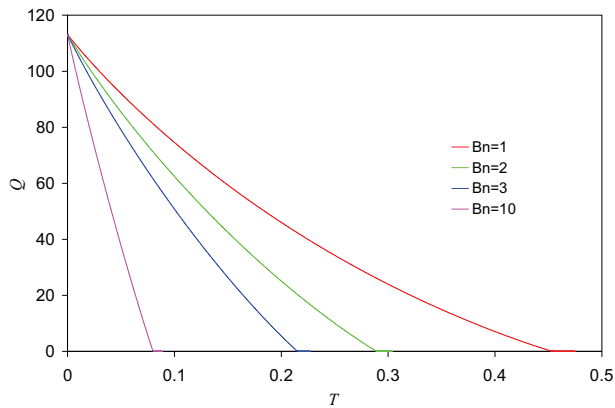


Fig. 6. Cessation of flow: discharge as a function of time

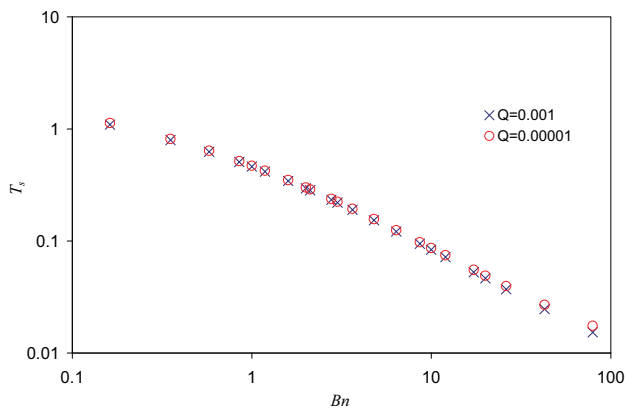


Fig. 7. Cessation of flow: stopping time T_s versus Bingham number

c) Pulsatile flows

For a rectangular wave, Fig 8 illustrates the core velocity versus time for some values of Bn ; referring to eq. (24) $T_1 = 2$ and $T_2 = T_1/10$. For $Bn = 10$ the fluid completely stops for a time length about equal to $T_2/2$.

For a sinusoidal wave like eq. (25), putting $Bn = 5$, Figs 9-10 show the time development of plug velocity for some values of ε and frequency $f = 0.05$ and $f = 0.5$ respectively. For $f = 0.05$ and $\varepsilon = 0.5$ the movement stops for a time length of about 15% of the period. Calling v_s, v_{max}, v_{min} the steady, the maximum and the minimum plug velocity respectively, $v_{max} - v_s$ is always greater than

$v_s - v_{\min}$, for all values of ε . The quantity $\delta = [(v_{\max} - v_s) - (v_s - v_{\min})] / v_s$ can be considered as an index of the asymmetry of the velocity with respect to the steady value. Fig. 11 shows δ versus frequency at different ε . Being always $\delta > 0$ it is easy to deduce that the mean rate of flow in a period increases owing to the non linearity of the constitutive equation.

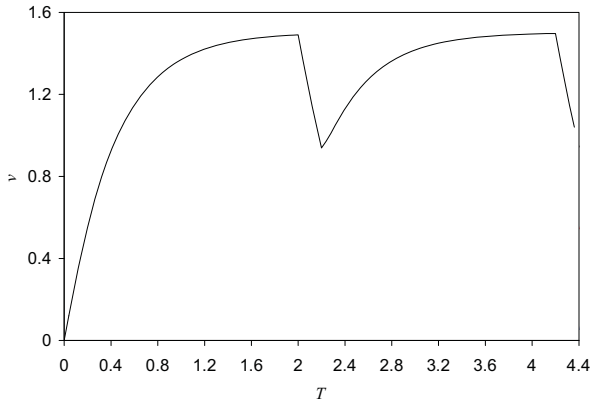


Fig. 8. Rectangular wave: plug velocity versus time

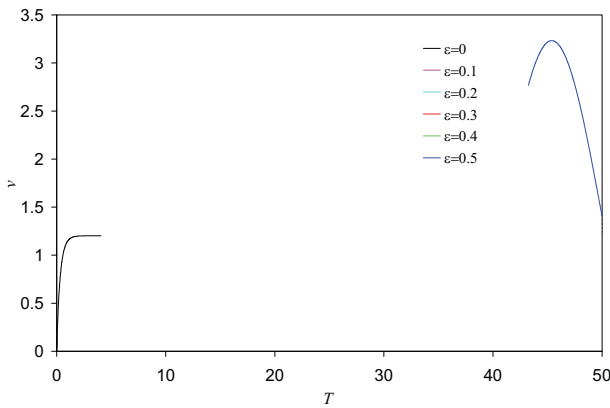


Fig. 9. Sinusoidal wave: plug velocity versus time; $Bn = 5, f = 0.05$

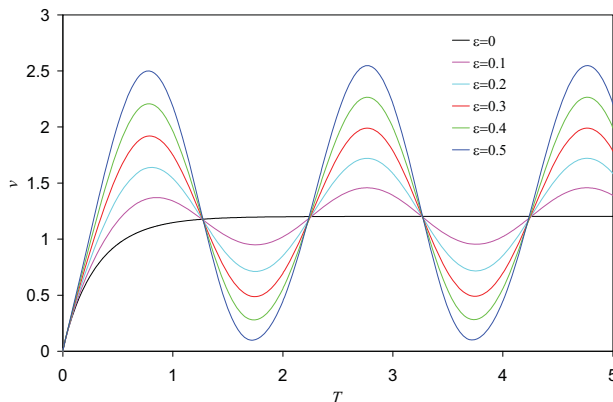


Fig. 10. Sinusoidal wave: plug velocity versus time; $Bn = 5, f = 0.5$

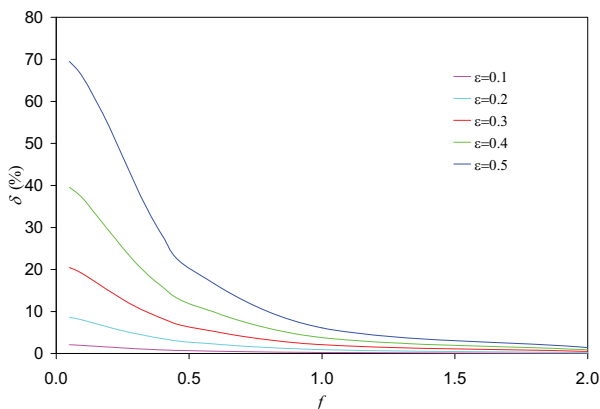


Fig. 11. Sinusoidal wave: δ versus frequency

5. CONCLUSIONS

Unsteady motion of a Bingham fluid in coaxial pipes has been examined numerically. The momentum equation has been written using a regularized constitutive equation proposed by the authors, based on the error function. The solution has been carried out via an implicit finite difference method; numerical experiments indicated that the maximum value for the parameter of the rheological model in order to obtain valid results is $K = 5000 \frac{\eta_2 - \eta_1}{Bn}$. If K exceeds this value,

the numerical procedure can exhibit instabilities. An uniform spatial grid of 1000 points has been adopted, using a time step equal to $4 \cdot 10^{-6}$. Four different motions have been considered: start-up, cessation and two pulsatile flows. The analysis of start-up flow has been useful to validate the numerical procedure comparing the obtained asymptotic solution to the well known analytical one. In the cessation the rate of flow decreases the more rapidly the greater Bn is: the stopping time which is infinite for Newtonian fluids becomes finite for Bingham fluids and decreases for increasing Bn . In pulsatile flow, applying a rectangular pressure gradient the flow can completely stop for some time if the Bingham number is sufficiently great. The superposition of a sinusoidal wave to the steady pressure gradient gives rise to an increment of the mean discharge in a period, owing to the non linearity of the constitutive equation.

References

1. Glowinski, R., *Numerical methods for nonlinear variational problems*, Springer-Verlag, New York, 1984.
2. Papanastasiou, T.C., Flows of materials with yield, *J. Rheol.* 31 (5), 385-404, 1987.
3. Frigaard, I.A., Nouar, C., On the usage of viscosity regularisation methods for visco-plastic fluid flow computation, *J. Non-Newtonian Fluid Mech.* 127, 1-26, 2005.
4. Glowinski, R., Sur l'écoulement d'un fluide de Bingham dans une conduite cylindrique, *J. de Méc.* 13, 601-621, 1974.
5. Huilgol, R.R., Mena, B., Piau, J.M., Finite stopping time problems and rheometry of Bingham fluids, *J. Non-Newtonian Fluid Mech.* 102, 97-107, 2002.
6. Chatzimina, M., Georgiou, G.C., Argyropaidas, I., Mitsoulis, E., Huilgol, R.R., Cessation of Couette and Poiseuille flows of a Bingham plastic and finite stopping times, *J. Non-Newtonian Fluid Mech.* 129, 117-127, 2005.
7. Duggins, R. K., The commencement of flow of a Bingham plastic fluid, *Chem. Eng. Sci.*, 27, 1991-1996, 1972.
8. Papanastasiou, T.C., Boudouvis A. G., Flows of viscoplastic materials: models and computation, *Comp. and Struct.*, 64, (1-4), 677-694, 1977.
9. Hammad, K. J., Unsteady pipe flows of a viscoplastic non-Newtonian fluid: effects of pressure gradient waveform, *Proc. ASME FED*, 247, 197-204, 1998.
10. Daprà, I., Scarpi, G, Start-up flow of a Bingham fluid in a pipe, *Meccanica*, 40, 49-63, 2005.

Formation of lime efflorescence on concrete and concrete products

Tomáš Fojtík¹, Jiří Brožovský²

^{1,2} Faculty of Civil Engineering, Brno University of Technology, Brno, 602 00, Czech Republic

Summary

Many specialists from all over the world occupied themselves with the problem of efflorescence formation on concrete and on concrete products. This problem is nearly as old as the concrete itself. The fact that to this very day, the problems of efflorescence formation course and of formed efflorescence elimination is not yet clearly defined up to now, shows how extensive and difficult is this task. This paper concerns the problems of efflorescence formation on concrete and concrete products depending on some conditions to which the concrete is exposed.

KEY WORDS: concrete, concrete product, lime efflorescence, primary, secondary

1. INTRODUCTION

Is the efflorescence on the surface of concrete the demonstration of its degradation? This form of degradation is in contrast with the sulphate corrosion or with other forms of corrosion not dangerous in light of structural properties and the efflorescence has not major effect on the durability of concrete structures. Nevertheless the efflorescence which occurs on the surface of concrete products mostly in the form of white "spots" or layers is an esthetic defect which can significantly influence the quality of concrete soffit products.

The efflorescence consists from inorganic salts or hydroxides which are leached out from concrete (from the cement stone or from the aggregate). The hydrous solution of these salts is transported by the system of capillary tubes in concrete. It evaporates on the surface of the concrete and reacts with atmospheric CO₂ or SO₂ (produced in a high degree by the industrial production). The efflorescence is formed largely in the form of salts (chiefly as sodium, potassium and mainly as calcium sulphates or carbonates). The main component is as a rule CaCO₃.

The occurrence of efflorescence is typical on the surface of concrete alternately soaked and dried or exposed to the action of pressure water. Less frequent factors of efflorescence formation on concrete surface are:

- The proportion of individual concrete components and their total concentration in the bearing hydrous solution,

- The relative air humidity in the surrounding atmosphere (ϕ [%]). It depends on the solubility degree of individual components and on RH whether the given salts crystallize in the pores or on the surface of the material. The crystallization in pores is one of the building materials significant destruction factors [1, 2, 3].

2. LIME EFFLORESCENCE

It is formed by calcium carbonate (CaCO_3) which is formed by the action of atmospheric carbon dioxide (CO_2) in humid medium on calcium hydroxide ($\text{Ca}[\text{OH}]_2$) liberated during maturing (hydration) of concrete [3].

2.1. Primary lime efflorescence

The primary lime efflorescence is formed only for a limited period from the concrete or concrete products production by the reaction of calcium hydroxide (this is the component of both, the hardened concrete and the hardened lime mortar) with the atmospheric CO_2 under moisture, in the surface layers of concrete products.

2.2. Secondary lime efflorescence

The secondary lime efflorescence is formed during the whole service life of concrete by reaction of the calcium hydroxide leached out on the surface of products with the atmospheric carbon dioxide under presence of moisture.

By the effect of atmospheric CO_2 the in water insoluble calcium carbonate is transformed after a longer period in the in water soluble calcium hydrogen carbonate $\text{Ca}[\text{HCO}_3]_2$.

The secondary efflorescence does not in contrast to the primary efflorescence form only lighter spots on the surface of concrete but it constitutes on the surface crystalline substance, which dusts off as removable dust.

Consequently, after this transformation of the calcium carbonate the lime efflorescence disappears. The time of calcium carbonate conversion into calcium hydrogen carbonate is approximately 1,5 till 3 years (in dependence on internal and outer conditions, first of all on climatic effects) [2, 3].

3. MECHANISMS INFLUENCING FORMATION OF LIME EFFLORESCENCE

The frequency of lime efflorescence formation on concrete depends on many variables. These are first of all the water content (w and ϕ) and the content of the atmospheric CO_2 [3].

It is necessary to mention that no less than from 75 % the formation of all efflorescence on concrete is caused by the “lack of technological discipline” in the production and the remaining 25 % is the result of the concrete components chemism.

3.1. The main conditions supporting the formation of lime efflorescence on concrete:

- The high w/c ratio,
- Temperature,
- Porosity,
- Improper admixtures,
- Mixing and compacting conditions,
- Additives,
- Water tightness,
- Treatment conditions,
- Capillarity,
- Content of free lime,
- Proportion of cement and aggregate in concrete,
- CO_2 content in the atmosphere,
- Time of products storing,
- Type of construction,
- The storing of products [1,2,3].

4. MEASURES ELIMINATING THE FORMATION OF LIME EFFLORESCENCE IN THE PRODUCTION

4.1. Measures and methods limiting the efflorescence formation used in production

- Elimination or limiting of causes mentioned in chapter 3.1,
- Utilization of additives which contribute to following possible effects:
 - Interruption of capillary tubes and on this way the undesirable mass transfer,

- Increase of water tightness, waterproofing of capillary pores,
- Chemical fixing of lime to insoluble product [3].

4.2. Means and methods removing the already formed efflorescence

As a rule the lime efflorescence can be removed sufficiently mechanically, for instance by sweeping it up. Also special means can be used. The concentrated preparation is diluted with water and after the concrete surface was saturated with water and the superfluous water was removed, the diluted preparation is applied on the surface of the product by means of a brush or sponge. After the efflorescence is dissolved the surface is washed down with water.

If it is not possible to remove the lime efflorescence by one of readily available products, it is possible to apply a special procedure. We can use for instance the 3% solution of hydrochloric acid, phosphoric acid or the solution of some organic acid (for instance acetic acid or oxalic acid etc.) It is necessary to take into account that in the case of lime efflorescence dissolution with acids the shade of concrete products colour and the structure of the surface can change, because the acids attack and disintegrate together with the efflorescence also the cement stone [1, 3].

5. EXPERIMENTAL MEASUREMENTS

5.1. Division of experimental works

Considering the fact, that the formation of efflorescence is influenced by quite a number of factors, the most important effects were selected for testing, namely the general effect of the surroundings and of the concrete composition.

5.1.1. Determination of efflorescence formation conditions

The aim was the laboratory testing of concrete samples of concrete with exactly defined variant composition, exposed to different types of surroundings.

5.1.2. Determination of concrete composition on the formation of the efflorescence

Test pieces with exactly defined proportion of concrete components were prepared in this phase. The test pieces were tested consequently for the dependence of lime efflorescence formation on the type of used concrete, on the method of concrete compacting during the production of these test pieces, on the proportion of cement and aggregate and on the value of w/c ratio.

5.1.3. Determination of efflorescence formation conditions in dependence on the composition of concrete

The aim was to make test pieces with the constant w/c ratio and with variable proportion between cement and aggregate and to expose it to different types of surroundings.

5.2. Methods of testing

5.2.1. Determination of conditions for efflorescence formation

The made concrete prisms were stored in following surroundings:

- Water bath ($t = 20 \pm 2^\circ\text{C}$),
- Laboratory surroundings ($t = 20 \pm 2^\circ\text{C}$, RH = 40 – 60 %),
- Air tight chamber with 98 % of CO₂ concentration,
- Hot air drier ($t = 50^\circ\text{C}$),

The influence of these surroundings was monitored on the formation of efflorescence. The extent of concrete surface coverage with efflorescence was determined and evaluated by optical microscopy and its mineralogical composition was detected by means of X-ray diffraction analysis.

5.2.2. Determination of the concrete composition influence on the formation of efflorescence

The made test pieces were exposed to surroundings in which the most efflorescence was formed during the preceding phase and the effect of the concrete composition was described on the efflorescence formation at varying:

- Kind of cement (locality),
- Way of concrete compacting,
- Proportion of cement and aggregate,
- Water-cement ratio.

5.2.3. Determination of efflorescence formation conditions in dependence on the concrete composition

The prepared concrete prisms with the cement and aggregate proportion 1:5 or 1:6 were placed into following surroundings:

- Climatic chamber – for the period of 24 hours, temperature 28°C and RH 95 %,
- Normal atmospheric surroundings (outdoor) – for the period of 24 hours,
- Drier – for the period of 6 hours, temperature 60°C.

The effect of climatic conditions on the formation of efflorescence was subsequently monitored on these test pieces and the results were compared with results obtained in the phase I (article 5.2.1.)

5.3. Results of individual phases of work

5.3.1. Determination of efflorescence formation conditions

All efflorescence which arises on the test pieces during this work is so-called primary efflorescence. This is formed only during the limited period from the concrete or concrete products production by the reaction of calcium hydroxide with atmospheric CO_2 in humidity on surface layers of concrete products.

The secondary efflorescence is formed by the effect of atmospheric CO_2 and it is transferred after longer period from the in water insoluble CaCO_3 into in water soluble calcium hydrogen carbonate $\text{Ca}[\text{HCO}_3]_2$. This process lasts longer time.

The test pieces made from the cement CEM I 42,5 R from the cement plant Mokrá, and from the aggregate Bratčice with constant proportion of cement and aggregate 1:3 and with the water-cement ratio $w = 0.5$ with vibration and by manual stamping. The test pieces were exposed for 28 days to individual surroundings and we can state that:

- The formation of efflorescence does not take place in surroundings with fluctuating pressure and relative air humidity with the temperature 50°C and higher,
- In laboratory surroundings at $t = 20 \pm 2^\circ\text{C}$, constant atmospheric pressure and in relative air humidity varying from 40 to 60% the efflorescence is admittedly formed but not so quickly as in the water medium with the temperature $t = 20 \pm 2^\circ\text{C}$. On the other hand the efflorescence which was already on the surface of the test pieces before they were placed into this surroundings increased moderately their volume,
- In the chamber with constant atmospheric pressure and the temperature $t=20\pm 2^\circ\text{C}$ with the content of 98% of CO_2 is the efflorescence formed only in small quantity, but when we have put into the chamber a sample which already contained on the surface efflorescence the efflorescence quantity increased (volumetrically, no the surface area),
- Unambiguously the most favorable conditions for the formation of efflorescence is the aqueous medium with the temperature of $t = 20 \pm 2^\circ\text{C}$. In this medium even after 14 days of storing always new efflorescence was formed while in other media the growth of it was stagnating,
- The most important factor influencing the formation of efflorescence is besides the temperature of surroundings the value of the relative humidity (RH) and the rate of air circulation,
- Quick overlapping of the surface with efflorescence takes place after placing the prisms in the chamber with elevated concentration of CO_2 but in a definite moment the formation of new efflorescence stops. The elevated CO_2 concentration in the atmosphere results in the closing of pores on the surface by the formed efflorescence and in the stagnation of its further formation,

- We observed the rapid increase of efflorescence after placing the concrete into water bath at the temperature $t = 20 \pm 2^\circ\text{C}$ for the period of at least 28 days,
- When we have taken out the samples from the water storing after 28 days, have removed the efflorescence and placed the samples once more into this surroundings, the growth of efflorescence did not start again.

5.3.2. Determination of the concrete composition influence on the formation of efflorescence

- We can state that the intensity of efflorescence formation is not direct proportional to the increasing value of water ratio, i.e. the value of water ratio doesn't affect the size of efflorescence formation,
- We can further state that with the increasing proportion of cement and aggregate the intensity of efflorescence growth increases,
- The type of cement has an effect on the formation of efflorescence. The intensity of concrete surface coating with efflorescence was in our case with both types of cements nearly identical but in some cases we observed still a higher intensity of efflorescence formation in the case of concrete made from cement CEM I 42.5 R from the cement plant Mokra. The contributing case can be the higher content of CaO in the cement CEM I 42.5 R Mokra in comparison with the cement CEM I 42.5 R from the cement plant Hranice,
- The way of compacting in the concrete manufacture can have a significant influence on the formation of efflorescence. The efflorescence during water storage was formed practically on all samples, naturally the concrete compacted by vibro-pressing was much more resistant against the formation of efflorescence in comparison with concrete made only by ramming.

5.3.3. Determination of efflorescence formation conditions in dependence on the concrete composition

The test was carried out in laboratory conditions to precise the hypothesis concerning the efflorescence formation in hot air driers which is connected with the velocity of surface desiccation and with the water vapour diffusion. Two sets of prisms with different ratio of cement and aggregate were placed into the hot air drier, in the damping box and in the laboratory surroundings.

- In the phase I more efflorescence was formed on the concrete surface in the case of the cement : aggregate proportion 1,5 contrary to the proportion 1:6,
- The main effort was of course to describe the processes in the hot air drier during the period of 24 hours since the placing of samples. The rapid desiccation of concrete during the first 8 hours caused intensive formation of efflorescence. Of course the surface of concrete is after 24 hours practically without efflorescence,
- The obtained efflorescence was submitted to X-ray diffraction analysis, which confirmed the similarity of efflorescence concerning the mineralogical

composition. In cements of CEM I 42.5 R type from both the cement plant Mokrá and the cement plant Hranice the prevailing mineral component in efflorescence is calcite.

6. CONCLUSION

We can state following the theoretical analyses and practical realized tests that the less favourable atmospheric conditions under which the formation of efflorescence takes place in a high degree are the temperatures 0 – 5°C in the morning hours of autumn months. The period of fresh concrete products storing has no effect on the quantity of efflorescence, it is rather the measure against their formation which can be easily realized in every manufacturing plant or during the production.

The first condition for the minimization of the lime efflorescence formation is the dosing of optimal batch water quantity for perfect hydration and for achieving of concrete high compactness with small rate of absorption. This can be achieved by the addition of adequate additives and admixtures.

It is further necessary to prevent during the hardening of concrete both its desiccation and the water condensation on its surface owing to the cold surrounding atmosphere. This can be achieved by the use of so-called maturing chambers during the hardening of concrete products.

The type of the used cement with different chemical and mineralogical compositions can affect the formation of possible lime efflorescence.

The tests which we have performed verified the influence of some variables on the possibility of lime efflorescence formation on concrete. It is necessary to remember that the efflorescence formation is influenced by a number of further factors which could not be included into this work.

The further development in this area should be directed towards the deeper understanding of the efflorescence formation reasons under the effect of further outer factors. This research should help to prevent or at least to minimize the formation of efflorescence on concrete and in this way to increase the esthetic value of concrete.

Acknowledgements

The work was supported by the MSM 0021630511 plan: Progressive Building Materials with Utilization of Secondary Raw Materials and their Impact on Structures Durability.

References

1. Matoušek, M., Drochytka, R.: *Atmospheric Corrosion of Concretes*, IKAS Praha, 1998, ISBN 80-902558-0-9.(in Czech)
2. Pytlík, P., *Concrete Technology*, Brno: Naše vojsko, 1994. ISBN 80-206-0434-0. (in Czech)
3. Kresse, P., Efflorescence-Mechanism of occurrence and possibilities of prevention, Research Centre of the company BAYER AG Krefeld-Uerdingen, published in the Journal: *Betonwerk-Fertigteile-Technik (BFT)*.

The use of computer means in representation of the ruled surfaces

Monica Gheorghiu and Mirela Chelcea

*Descriptive Geometry, Engineering Graphics and Graphics Computer Programs Department,
Technical University of Civil Engineering, Bucharest, Romania*

Summary

Teaching the Descriptive Geometry by the means of the computer is a recent attempt to make the subjects more understandable and to facilitate the approach of the students to some difficult subjects. This work makes a connection between a 3D representation of some examples of this chapter and their orthogonal projections, the final target of the Descriptive Geometry using the possibility of animation provided by an adequate "software", for example the program "AutoCAD 3D".

KEYWORDS: ruled surfaces, Descriptive Geometry, orthogonal projections, paraboloid, cylindroid, helicoid, hyperboloid.

1. INTRODUCTION

Teaching Descriptive Geometry is, without any doubt, unless a first for the system of university Rumanian education, but a recent attempt to align itself with the last tendencies of education. A particular effort of those who teach is presumed in order to provide such a course of Descriptive Geometry, regarding the adaptation of the means of presenting the matters using an adequate "software", for example the program "AutoCAD 3D". This is why this work is a first step in attempting to build a system of teaching and of evaluation based on the computer.

The subject of this work belongs to the applicable part of this matter and, although it attracts the interest of the student, it is considered as having a high level of difficulty. The presentation in 3D of the ruled surfaces, axonometric, apply the intuition of onlooker and this is why provides a complete sight of the subject however complicate would be.

The successive transformation of that, in images 2D, meaning in orthogonal projections, can easily be done by using the Autocad 3D or other programs which makes possible to use animation 3D. This manner of presenting simultaneously the two methods to visualize can provide a certain easiness to discern the main orthogonal projections in a unit space and can lead to obtain the capacity to

represent in orthogonal projection on any plane of the objects however complicated they are.

The authors also consider that the 3D representation based on the computer of the various types of ruled surfaces, as well as the connection between these views of the examples suggested to be solved and their orthogonal projections could make this subject not only understandable but also more attractive. The elements, which compose certain surfaces, are proposed to be identified in the assembly and to be represented in the usual system of projections.

The following stages were established in the presentation of the subject, in order to fulfil the requests of the problem: the view of the final representation of the defined surface, the 3D representation of it, the turn around of the 3D view, the orthogonal projections due to this proceeding, the 3D and 2D view of the constituent elements and finally, the way to form the surface.

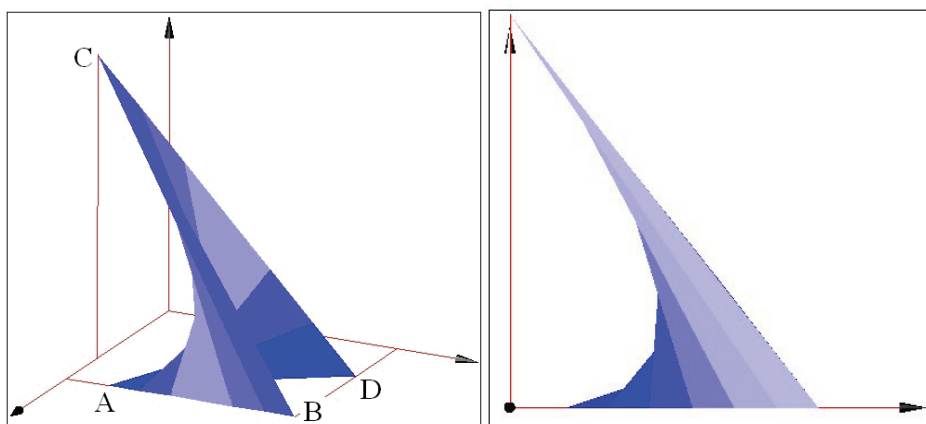


Figure 1. Paraboloid – axonometric representation and projection on the plane [W]

2. EXAMPLES

2.1. Paraboloid

2.1.1. Paraboloid. First example

The figured paraboloid could have the following parameters: first directrix – line AB, second directrix – line CD, with A, B and D in [H] and C in [V]. AB is parallel to Oy, BD parallel to Ox (see Figure 1).

2.1.2. Paraboloid. Second example

The application could also require the representation of the symmetrical surface in relation with base plane (see Figure 2).

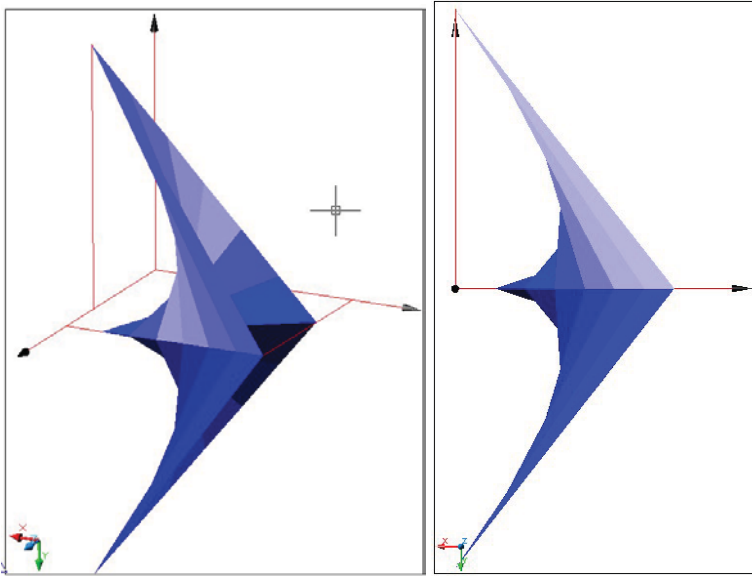


Figure 2. Paraboloid – axonometric representation and projection on the plane [W]

2.2. Conoid

2.2.1. Conoid. First example

This complex problem demands to draw the ruled surface with directrix I a semicircle with the centre the point M and radius 30mm, which belongs to the plane that makes a 60° angle to plane [H], and directrix II the segment ST, 20 mm long, on a line perpendicular to [W].

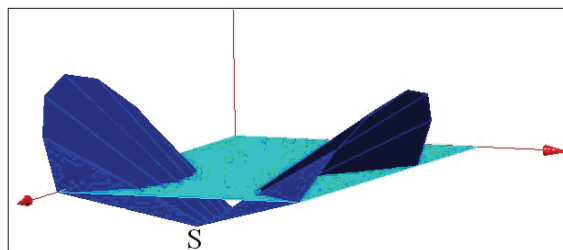


Figure 3. Conoid – axonometric representation

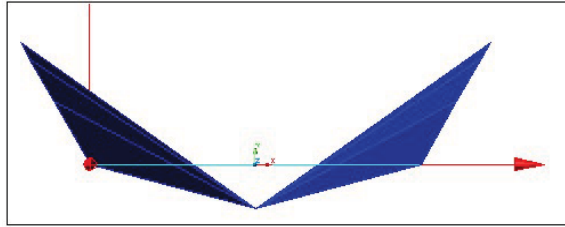


Figure 4. Conoid – projection on the plane [W]

The other request is to represent also the symmetrical surface to the plane that includes points s and T and is parallel to plane [V] and finally to solve the problem of intersection between the rolled surface and plane [H], the requirement could modify as follows: (see Figures 3 and 4).

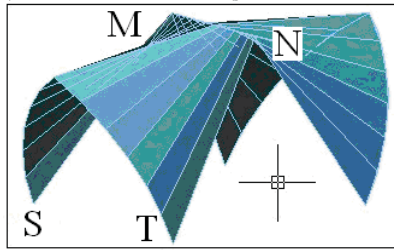


Figure 5. Cylinderoid – axonometric representation

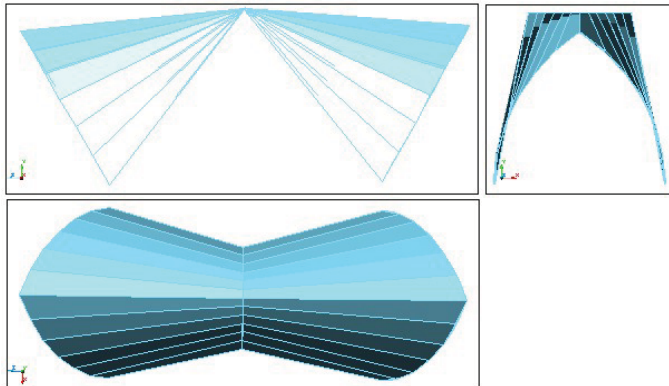


Figure 6. Cylinderoid –projection on the plane [V], [W] and [H]

2.2.2. Conoid. Second example

The surface which is suggested to represent is formed by two symmetrical conoids. The first one has the first directrix in a plane inclined at an angle of 60° to the horizontal, composed of 2 circle arcs with a 65 mm radius, passing through points

S and T in [H], positioned between [H] and their point of intersection, above [H] with S and T while directrix II segment MN, which belongs to a line which is perpendicular to [V].

The second conoid is the symmetrical of the first relative to [W] passing through M and N (see Figures 5 and 6).

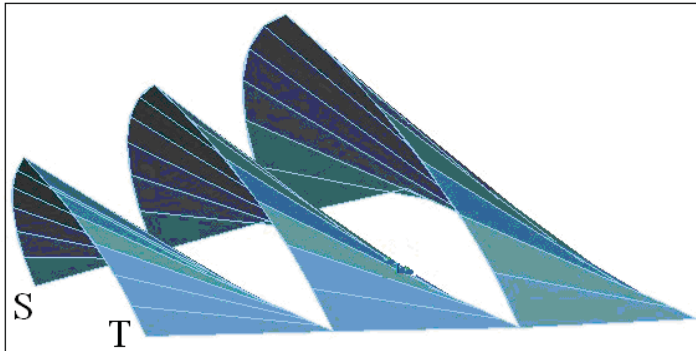


Figure 7. Cylinderoid – axonometric representation

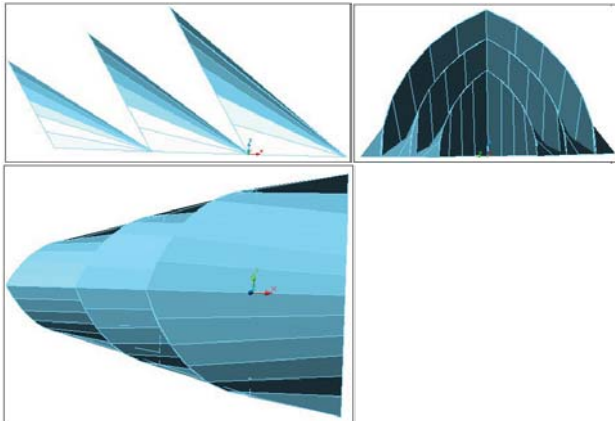


Figure 8. Cylinderoid – projection on the plane [V], [W] and [H]

2.2.3. Conoid. Third example

The surface of this example is made by three units, from among the first conoid has the first directrix in a plane oriented at an angle of 60° to the horizontal, composed of 2 circle arcs with a 65 mm radius, passing through points S and T in [H], while directrix II segment S1T1 from [H], (see Figure 7).

The second conoid has directrix I in a plane oriented at an angle of 60° to the horizontal, composed of 2 circle arcs with a 80 mm radius, passing through points S1 and T1, positioned between [H] and their point of intersection, above [H] while directrix II segment S2T2 in [H].

The third conoid has directrix I in a plane oriented at an angle of 60° to the horizontal, composed of 2 circle arcs with a 95 mm radius, passing through points S2 and T2, positioned between [H] and their point of intersection, above [H] while directrix II segment S3T3 in [H] (see Figure 8).

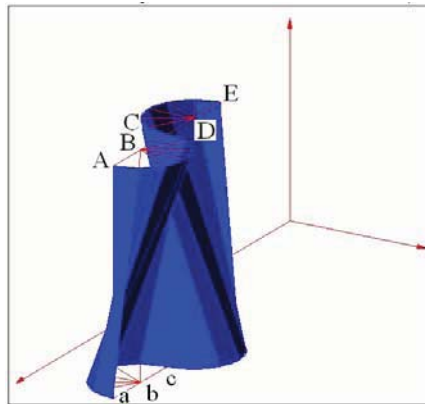


Figure 9. Proposed application. Cylindroid – axonometric representation

2.3 Cylindroid

2.3.1. Cylindroid. First example

The request of this problem is to make an axonometric representation of the cylindroid with directrix I – two semicircles with centers B and D respectively, in a plane parallel to [H], directrix II – two semicircles with centers b and d respectively, in plane [H].

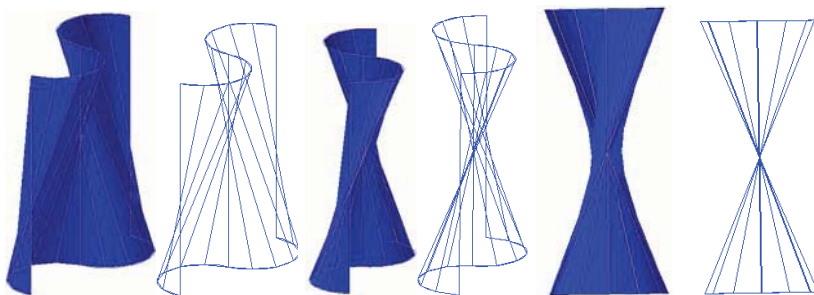


Figure 10. Cylindroid – the rotation of the surface until we see the projection to plane [W]

The semicircles with centers b and D are between plane [V] and a plane parallel to [V] determined by points A, E and a. The semicircles with centers B and d are on the other side of the plane determined by A, E and a, mentioned above (see Figures 9, 10, 11 and 12).

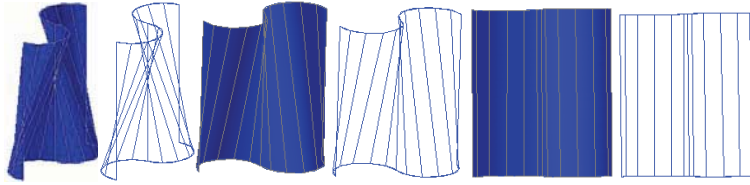


Figure 11. Cylindroid – the rotation of the surface until we see the projection to plane [V]

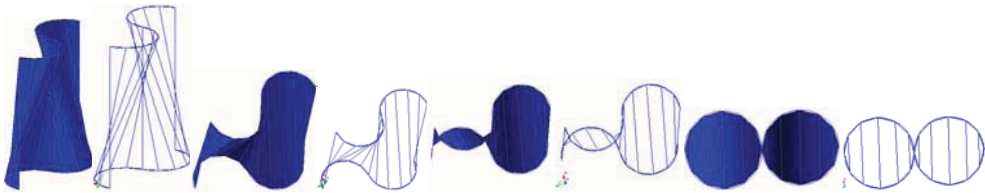


Figure 12. Cylindroid – the rotation of the surface until we see the projection to plane [H]

The problem may be extended by adding the request to repeat the obtained cylindroid surface several times, or by rotating the surface and so changing the data (see Figures 13 and 14).

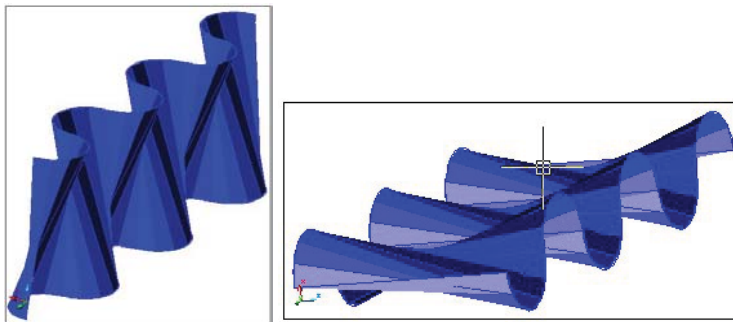


Figure 13. Cylindroid – axonometric representation

2.3.2. *Cylindroid. Third example*

It is required to draw the ruled surface that has both curves circle arcs with a radius of 30 and 50mm respectively, in a plane that makes a 60^0 angle to plane [H]. Point M is the middle of the segment representing the cord sub-stretched by both

directrices. It is also required to represent the symmetrical surface to this one relative to the plane that includes point N and is parallel to plane [V] (see Figure 15).

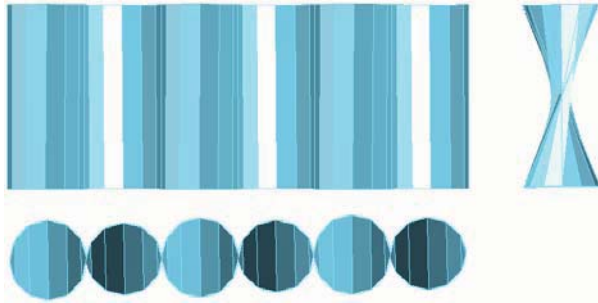


Figure 14. Cylindroid – projection on the plane [V], [W] and [H]

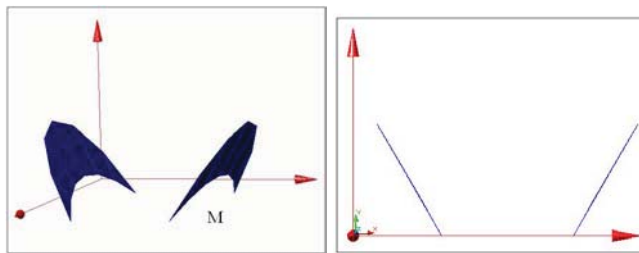


Figure 15. Cylindroid – axonometric representation and projection on the plane [W]

2.3.3. *Cylindroid. Fourth example*

The problem requires the representation of a ruled surface that has the following parameters: first directrix the segment ST, second directrix a circle arc with a radius of 225mm and the corresponding cord SR. It is also required to represent the surface that is symmetrical to it relative to the parallel plane [V] that includes points S and T (see Figure 16).

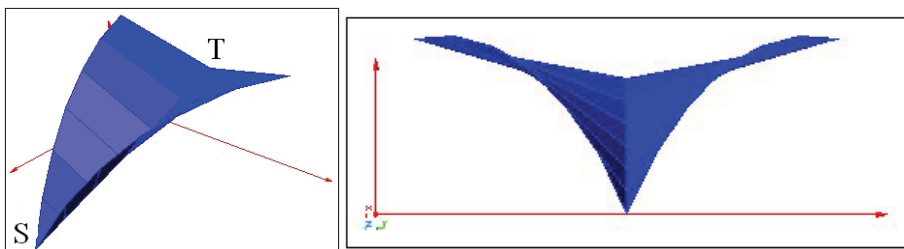


Figure 16. Cylindroid – axonometric representation and projection on the plane [W]

2.3.4. *Cylindroid. Fifth example*

The surface to be represent is a cylindroid that has directrix I is a circle arc on the semicircle with the radius 45 and the center S, in a plane parallel to [V], above [H], inscribed between its point of intersection with [H] and point R on the semicircle, directrix II is also a circle arc, in a plane perpendicular to [H], that makes with the plane of directrix I an angle of 150, derived from a semicircle with a radius of 70, above [H], that intersects directrix I in point R. Also draw this cylindroid's symmetrical relative to the plane of the first directrix (see Figures 17, 18, 19 and 20).

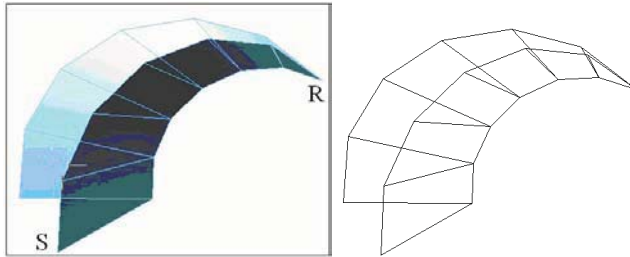


Figure 17. Cylindroid – axonometric representation

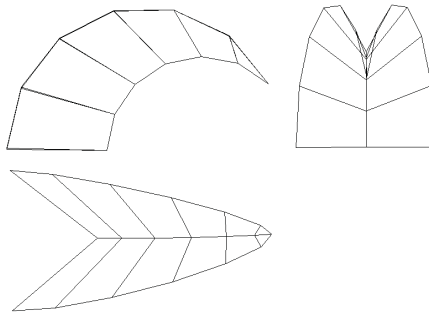


Figure 18. Cylindroid – projection on the plane [V], [W] and [H]

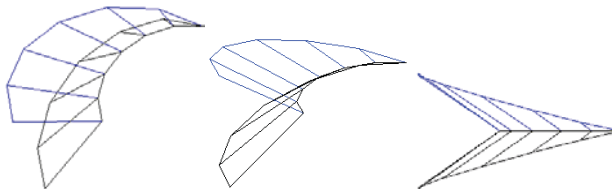


Figure 19. Cylindroid – the rotation of the surface until we see the projection to plane [H]

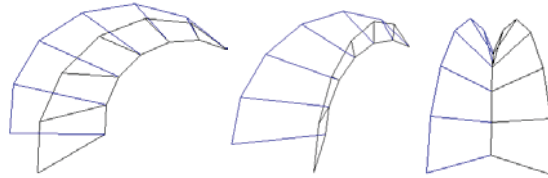


Figure 20. Cylindroid – the rotation of the surface until we see the projection to plane [W]

2.3.5. *Cylindroid. Sixth example*

The problem demands to represent a ruled surface with directrix I in a plane parallel to [W] determined by points S and T, made up of circle arc derived from a semicircle with a 20mm radius, centre S, with all points more distanced from [H] than from S and the tangents to this circle, symmetrical to the sS segment, starting from point T and T1 respectively, T’s symmetrical relative to s. Directrix II has the same shape as directrix I, is parallel to it at a distance of 20 mm, in a plane parallel to [W], at a distance of 90 mm from it. Figure also the ruled surface symmetrical to this one relative to the plane of the second directrix. Figure also the ruled surface which is symmetrical to the one obtained up to now, relative to the plane of the last figured directrix (see Figure 21 and 22).

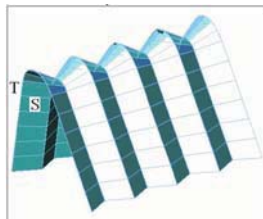


Figure 21. Cylindroid – axonometric representation

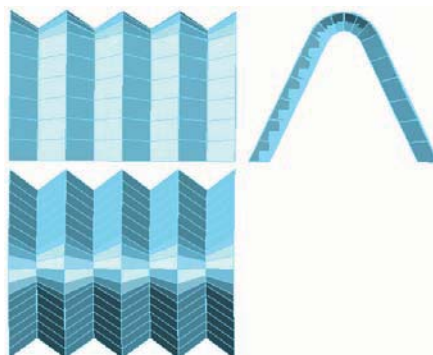


Figure 22. Cylindroid – projection on the plane [V], [W] and [H]

2.4 Helicoidal Surfaces

2.4.1. Helicoidal Surfaces. First example

The problem target is the axonometric representation of the group formed by 4 identical adjoining helicoidal surfaces (see Figures 23 and 24), with directrices belonging to a cylindrical surface generated thus:

- surface I, directrix I starting from point A and directrix II from B,
- surface II, directrix I starting from point B and directrix II from C,
- surface III, directrix I starting from point C and directrix II from D,
- surface IV, directrix I starting from point D and directrix II from A.

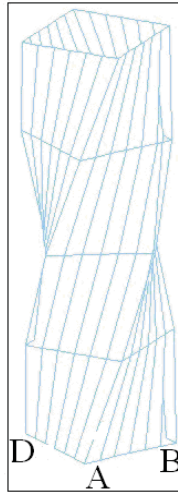


Figure 23. Helicoidal surfaces – axonometric representation and projection on plane [W]

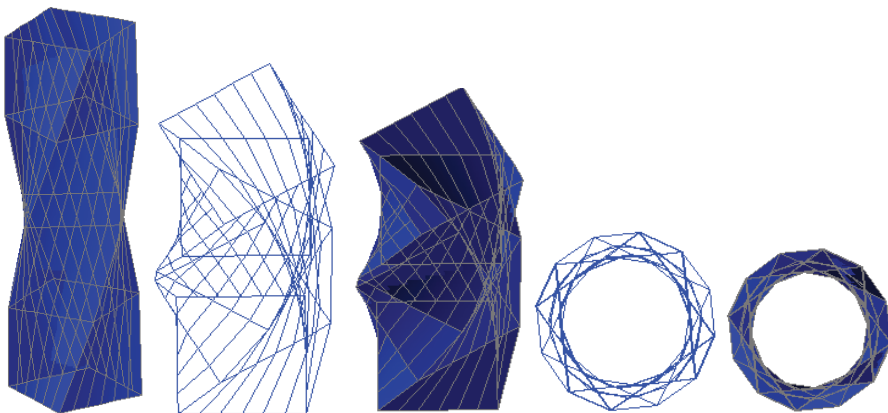


Figure 24. Helicoidal surfaces – axonometric representation and projection on plane [H]

The first rulings of each surface belong to plane [H] and make up a square ABCD with a side of 30 mm. The plane containing the second rulings for each surface is at a distance of 30 mm from [H], while these rulings together make up a square, rotated to the previous one in [H] by 30° . Each of the next ruling planes is at a distance of 30 mm from the previous one and the square made up by these rulings is rotated by 30° to the previous plane.

The last directrices are in a plane situated at a distance of 120 mm from [H].

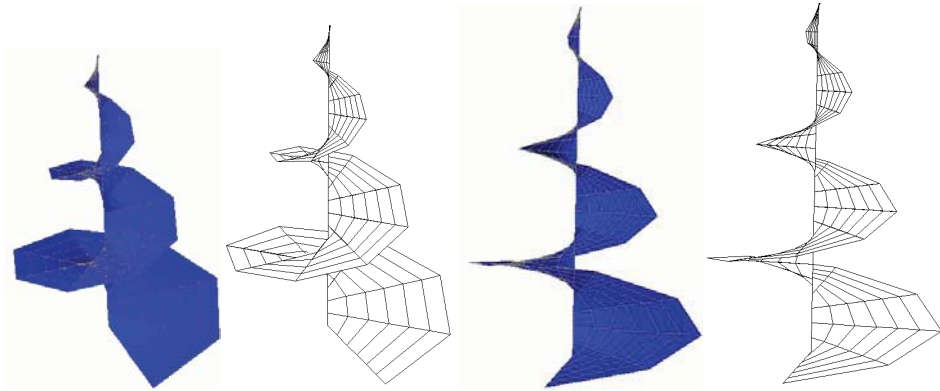


Figure 25. Helicoidal surfaces – axonometric representation and projection on plane [W]

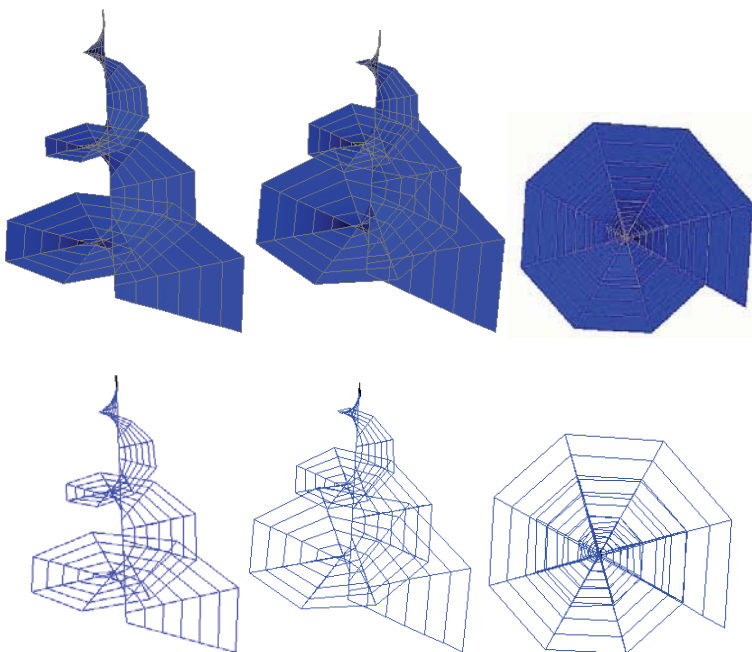


Fig. 26. Helicoidal Surface – rotation of the surface until the projection to plane [H] is seen

2.4.2. Helicoidal Surfaces. Second example

It is demanded to represent the helicoidal surface with a directrix plane in plane [H], which has directrix I a line perpendicular to [H] through the point H(60,60,0) and directrix II a curve belonging to a conoidal surface, with the basis a circle with center H and radius 48 mm. Each ruling is to be in a plane situated at a distance of 5 mm to the previous ruling's plane, rotated by 45°, and with a length 2mm less than it (see Figures 25 and 26).

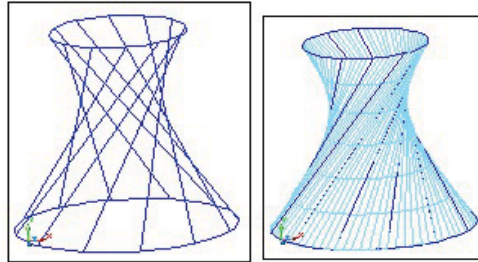


Figure 27. Hyperboloid – axonometric representation

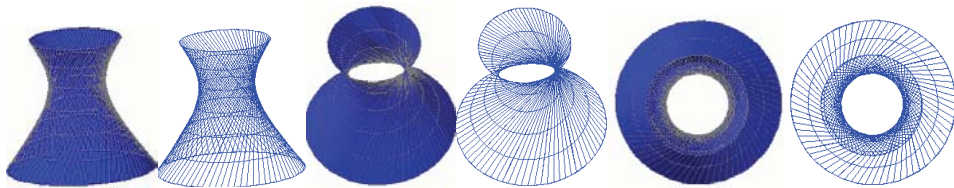


Figure 28. Helicoidal Surface – the rotation of the surface until we see the projection to plane [H]

2.5. Hyperboloid

2.5.1. Hyperboloid. First example

It is required to trace the ruled surface with both basic curves circles, directrix I is the circle with centre S and radius 50 mm in [H], directrix II a circle with radius 30 and centre T in a plane parallel to [H] at a distance of 90 mm from it. The divergence between the horizontal projections of the ends of the segment representing a directrix, is 120° for each directrix (see Figure 27 and 28).

2.5.2. Hyperboloid

If the ruled surface described by the above data, but with a divergence of 150° is represent (see Figure 29 and 30) some differences will be noticed, the main one would be that the interior diameter is smaller in the second case than in the first.

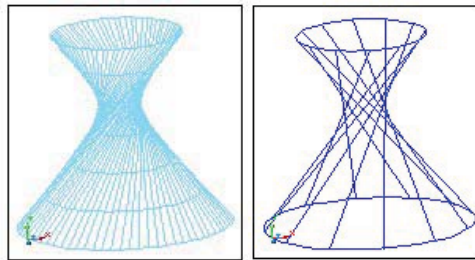


Figure 29. Cylindroid – axonometric representation

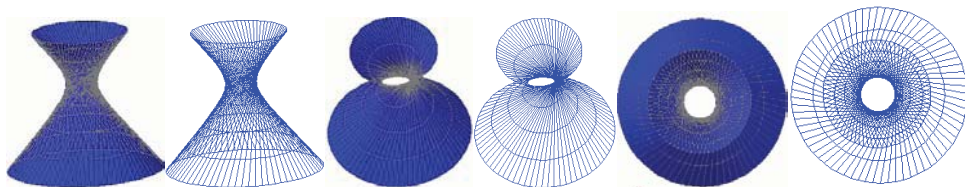


Figure 30. Helicoidal Surface – the rotation of the surface until we see the projection to plane [H].

3. CONCLUSIONS

The new manner of teaching provides not only a maximum efficiency of the study, but, essential more, it radically changes the approach of the students to the geometrical representation. It also makes them involved and responsible in the relationship with their own training to fulfil the university conditions and stimulates simultaneously their creativity.

References

1. Gheorghiu, M., Chelcea, M., *Descriptive Geometry, Problems*, MATRIX ROM Publisher, ISBN 973-755-015-3, Bucharest, 2006. (in Romanian).
2. Gheorghiu, M., Chelcea, M., *Famous buildings as models for ruled surfaces*, The 2nd International Conference on engineering graphics and design – ICEGD - Galați, Romania – 2007.

Numerical studies on the seismic performance of three structural systems

Horațiu Mociră, Eugen Panțel

Faculty of Civ. Eng., Technical University, Cluj-Napoca, 400027, Romania

Summary

For many years, the basic intent of the building code seismic provisions has been to provide buildings with an ability to withstand intense ground shaking without collapse, but potentially with some significant structural damage.

The damage to buildings, transportation structures and lifelines wrought by the 1989 Loma Prieta earthquake, the 1994 Northridge earthquake, and the 1999 Hanshin earthquake near Kobe, has forced structural engineers, disaster response agencies and building officials to carefully consider seismic response of the building environment in terms of performance rather than life-safety.

Civil engineering structures normally rely on their ability to dissipate energy to resist dynamic forces such as strong earthquakes. In recent years, to keep the vibration of these structures within the functional and serviceability limits and to reduce structural and architectural damage caused by extreme loads, different passive protective systems have been proposed. Addition of energy dissipation devices (EDDs) is considered one of the viable strategies for enhancing the seismic performance of building structures. For many building structures, EDDs may provide considerable performance improvement or cost saving.

This paper provides a comparison of the performance indices of a three story building with three different structural systems – moment frame, viscously damped frame and a base isolated frame. Fluid viscous damping and base isolation have the same objective of significantly decreasing the response of a structure to earthquake excitation. With both fluid viscous damping and base isolation it is possible to have a structure remain within the elastic region, so there is no permanent deformation from a seismic event. Each of the models were analyzed as linear structures and subjected to time histories for 3 different earthquakes of Vrancea type. The non-dimensional performance indices considered for the models are: Peak Drift ratio, Peak Base Shear and Peak Level Acceleration.

In summary, the viscously damped frame has the best overall relative performance of the three framing schemes. The base isolated frame is better than moment frame.

KEYWORDS: steel frames, passive control, base isolation, viscous damper, time history analysis.

1. INTRODUCTION

Earthquakes represent one of the most damaging disasters. Repairing an area that has experienced an earthquake is an expensive and difficult process. Engineers have introduced different techniques to prevent a large amount of the damage typically caused by earthquakes. The use of passive energy dissipation devices represents a feasible alternative to improve seismic behavior of structures by reducing the structural damage resulting from environmental disturbances [1].

Damping is one of many different methods that have been proposed for allowing a structure to achieve optimal performance when is subjected to an earthquake. The level of damping in a conventional elastic structure is very low, and hence the amount of energy dissipated during transient disturbances is also very low. During strong motions, conventional structures usually deform beyond their elastic limits, and eventually fail or collapse.

The concept of supplemental dampers added to a structure assumes that much of the energy input to the structure will be absorbed by supplemental devices [2]. An ideal damper will be able to reduce both stress and deflection in the structure. Fluid viscous dampers operate on the principle of fluid flow through orifices. A stainless steel piston travels through chambers that are filled with silicone oil. The pressure difference between the two chambers cause silicon oil to flow through an orifice in the piston head and seismic energy is transformed into heat.

Seismic isolation is another alternative for protecting structures from earthquakes. The philosophy behind this method is based on minimizing the earthquake induced forces transferred to the superstructure. During the past 20 years, seismic isolation has emerged as one of the most promising retrofitting strategies for improving the seismic performance of existing buildings. It is also an attractive approach for new construction when conventional design is not suitable or economical [3], [4].

Japan, New Zealand, and a number of European countries pioneered the use of seismic isolation in civil engineering structures. More recently, the United States has begun to implement isolation technology in bridges. In the seismic isolation approach, the superstructure mass is uncoupled from seismic ground motions. This is also referred to as "superstructure" isolation. It uses special types of bearings called "seismic isolation bearings," which are placed below the superstructure and on top of the substructure (foundation). In the event of a strong earthquake, they add flexibility to the structure, by elongating its period and dissipating energy. It could also give rise to large relative displacements across the isolator interface; this can be controlled by incorporating damping elements in the bearing or by adding supplemental dampers.

2. THE STRUCTURE, DAMPERS, BASE ISOLATORS, LOADS

2.1. The structure

Because the majority of buildings in Romania are less than three stories in height, a three story steel frame was selected as a reference frame. The structure was designed as a conventional SMRF (Figure 1) to provide a benchmark for seismic performance comparison with passive control systems. The following design parameters according to P100-1/2006 were used to design SMRF [5]:

- importance class II $\gamma=1,2$
- design ground acceleration $a_g=0,24\text{cm/sec}^2$
- $T_c=1,6$ sec
- behavior factor $q=6$

All connections between beams and columns are assumed rigid connections.

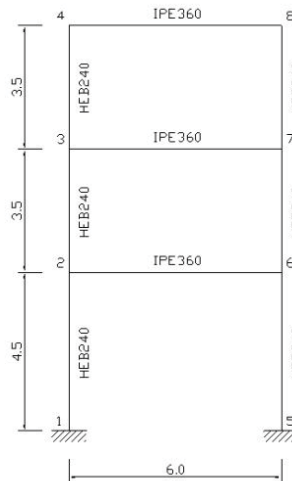


Figure 1. 3 Storey Moment Frame

The structure was then modified by the addition of fluid viscous dampers (Figure 2) or base isolators (Figure 3) to improve the seismic performance, with no attempt made to redesign the main frame elements.

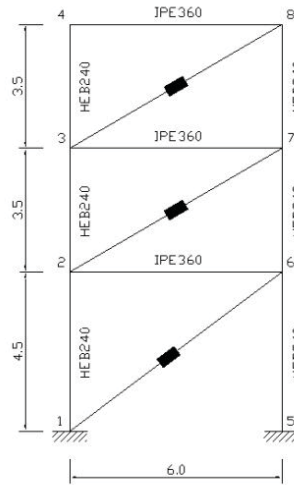


Figure 2. 3 Storey Frame with Linear Viscous Dampers

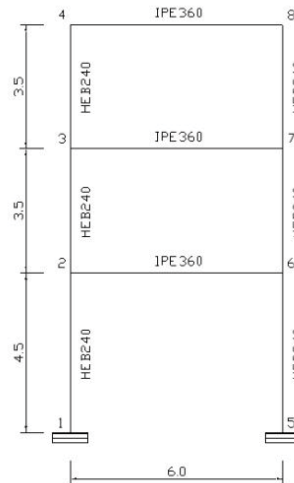


Figure 3. 3 Storey Frame with Base Isolators

2.2. The dampers

The linear viscous dampers (Figure 4) will be installed with a diagonal brace configuration. The inherent damping ratio of the structure is assumed to be 5%, and

the total effective damping ratio of the whole system is designated at 20% of critical.

The damping coefficient used for all dampers is $c=245\text{kN}\cdot\text{sec}/\text{m}$. In this example, the linear effective stiffness is set to zero so that pure damping behavior is achieved.

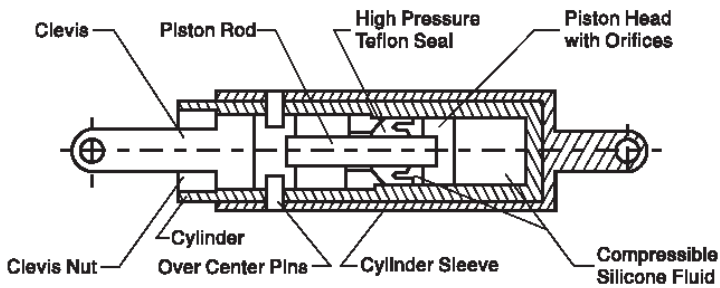


Figure 4. TAYLOR DEVICES Viscous Damper

2.3. The base isolators

The isolators are of elastomeric type (Figure 5) and have been chosen from FIP INDUSTRIALE catalog, according to the vertical reactions requirements [6].

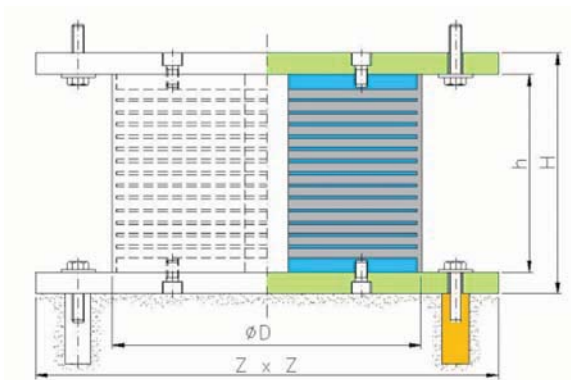


Figure 5. FIP INDUSTRIALE Base Isolator

The selected isolators SI-S 400/78, have the following specifications:

Mechanical properties: Vertical load $V=570\text{kN}$; Horizontal stiffness $=0.64\text{kN}/\text{mm}$.

Geometrical characteristics: Diameter $D=400\text{mm}$; Total height $Z=450\text{mm}$.

2.4. The loads

The seismic performance of these structural systems was studied using linear response-history analysis. Three scaled artificial earthquakes of Vrancea type, that matched on average a P100-1/2006 Provisions response spectrum were used for analysis.

3. NUMERICAL RESULTS

The results of the time history analyses are presented and discussed. Comparisons are made of estimated base shear, interstory drift and floor acceleration.

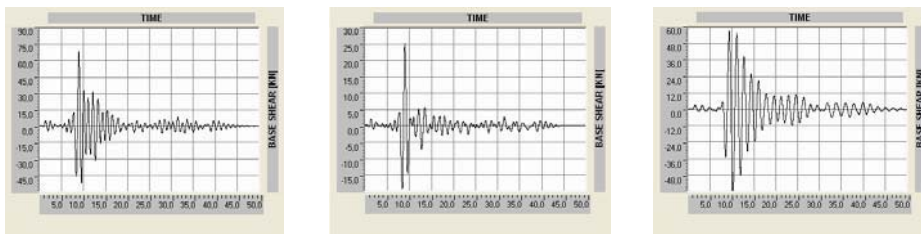


Figure 6. Base Shear for Vrancea type earthquake

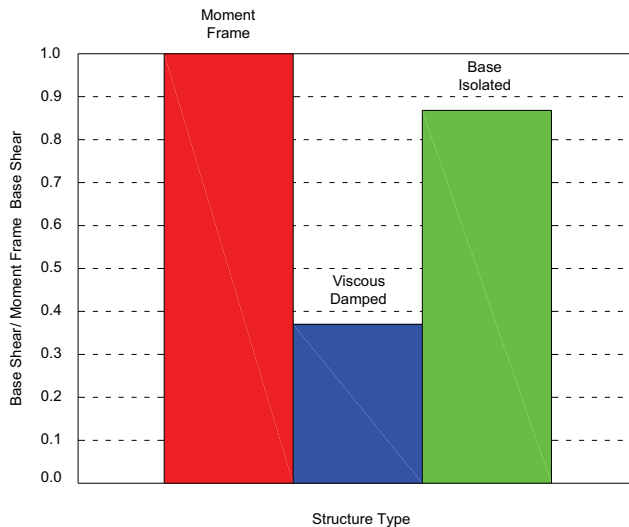


Figure 7. Normalized Maximum Value of Base Shear

3.1. Base shear

Figures 6 and 7 show a comparisons of base shears for the three structural schemes that were studied. Viscous dampers are extremely effective in reducing the base shear of the frame, whereas the addition of base isolators results in a modest reduction in base shear.

3.2. Interstory drift

This is a code design parameter and is something most engineers focus upon during the design process. From a damageability perspective, it is a measure that impacts damage to the framing system, building façade and windows, piping, ductwork and partitions.

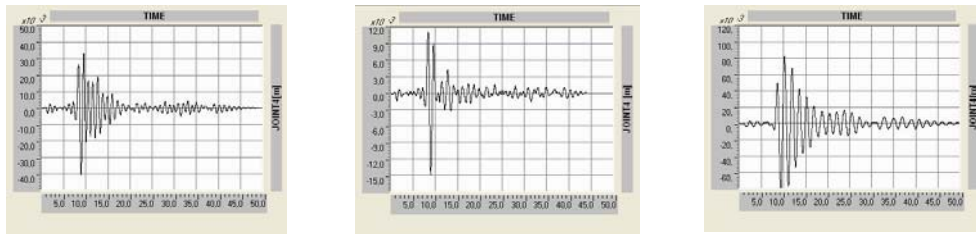


Figure 8 Top floor displacements

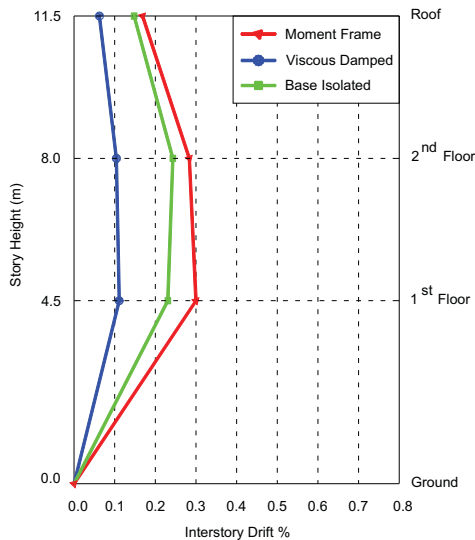


Figure 9 Interstory Drift

Results proved that control methods were successful in reducing the floor displacements of the structure (Figure 8). The viscously damped frame reduced the maximum drift by 63.30%, whereas the base isolated frame reduced the maximum drift by 23.90%. Figure 10 shows a comparison of maximum values of interstory drift for all framing schemes, normalized to the moment frame.

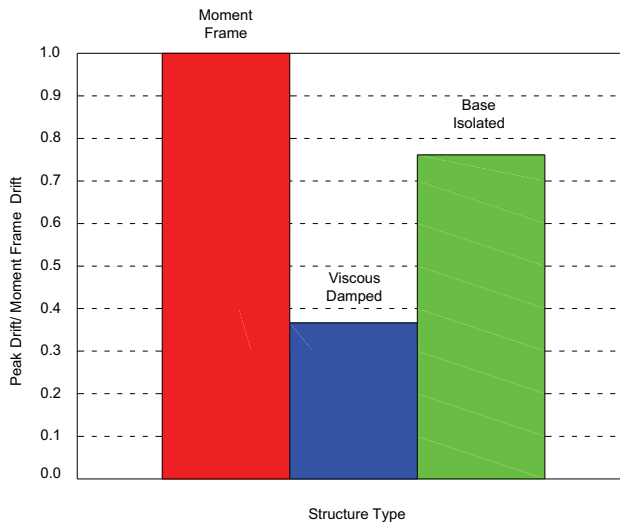


Figure 10 Normalized Maximum Value of Interstory Drifts

3.3. Floor accelerations

This parameter is almost never taking into account in the design process, because it requires a time history analyses to obtain it. From the damageability perspective it is the measure that impacts damage to the ceiling and lights, electrical and mechanical equipment, elevators and the building contents.

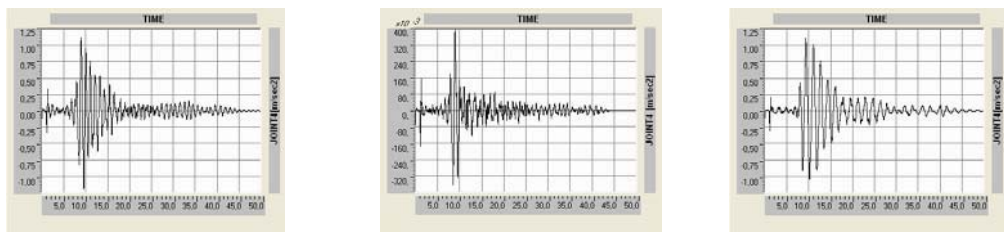


Figure 11 Top floor accelerations

In assessing the acceleration performance, the viscously damped frame has the best performance (Figure 11). The viscously damped frame reduced the maximum floor acceleration by 66.90%, whereas the base isolated frame reduced the maximum floor acceleration by 9.20% (Figure 12).

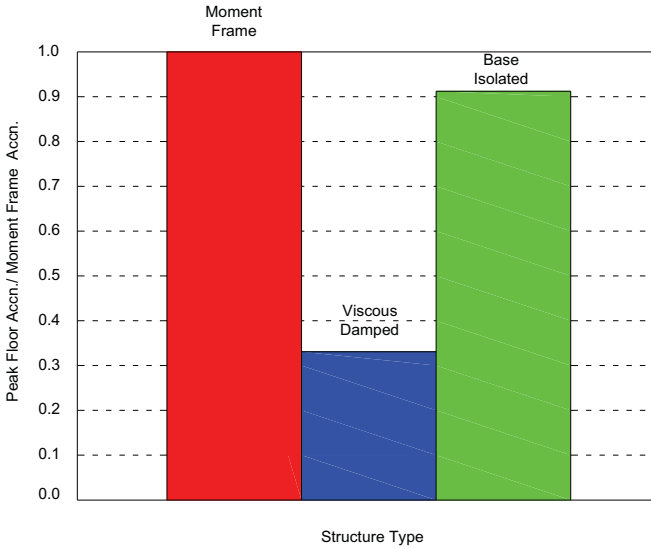


Figure 11 Normalized Peak Floor Accelerations

3.4. Performance indexes

For each control approach considered (i.e. viscous damper and base isolation), the uncontrolled response of the structure was compared with the controlled response [7].

The non-dimensional performance indexes considered in this study are Peak Base Shear (PI_1), Peak Drift ratio (PI_2), Peak Level Acceleration (PI_3).

They are defined as follows: $PI_1 = \frac{F_{b,c}^{max}}{F_{b,u}^{max}}$; $PI_2 = \frac{\delta_c^{max}}{\delta_u^{max}}$; $PI_3 = \frac{\ddot{x}_c^{max}}{\ddot{x}_u^{max}}$; where:

$F_{b,u}^{max}$; $F_{b,c}^{max}$ - the maximum base shear of the uncontrolled/controlled frame;

δ_u^{max} ; δ_c^{max} - the maximum inter storey drift ratio of the uncontrolled/controlled frame;

\ddot{x}_u^{max} ; \ddot{x}_c^{max} - the maximum absolute floor acceleration of the uncontrolled/controlled frame.

The results presented in Table 1 show that the viscously damped frame was the most effective in reducing the building’s response.

Table 1. Performance index for peak base shear, peak drift and peak acceleration

Cases	Performance Index			% Reduction		
	PI ₁	PI ₂	PI ₃	Base Shear	Story Drift	Acc
Viscous Damped	0.367	0.367	0.331	63.30	63.30	66.90
Base Isolated	0.869	0.761	0.908	13.10	23.90	9.20

4. CONCLUDING REMARKS

The objective of the paper is to evaluate the efficiency of two passive control systems. This paper has presented a comparative study of seismic performance (base shear, interstory drift and floor acceleration) of a three story steel building. The three story moment resisting frame was designed according to P100-1/2006 Provisions and then retrofitted with viscous dampers and base isolators. The structure was subjected to linear time history analyses for different earthquakes of Vrancea type.

The above numerical results presented for the three story one bay frame can not be generalized. The analyses show that the seismic performance of the viscously damped frame significantly exceeds that of the other framing schemes. The three story base isolated frame had better performance than the three moment frame.

These parameters indicate that structural and non-structural damages are significantly reduced in the case of viscously damped frame.

The results emphasize that seismic performances of the building depend upon the structural framing scheme chosen for that building.

References

1. Miyamoto, H.K., Singh, J.P., Performance of Structures with Passive Energy Dissipators, *Earthquake Spectra*, 2002.
2. Haskell, G., Lee, D., Fluid Viscous Damping as an Alternative to Base Isolation, *Technical papers from Taylor Devices*, 2004.
3. Alhan, C., Gavin, H., *Parametric Analysis of Passive Damping in Base Isolation*, 16th ASCE Engineering Mechanics Conference, Seattle, 2003.
4. Alexa, P., Mociran, H., Mathe, A., *Passive control of semirigid steel structures*, Computational Civil Engineering, Iasi, 2005.
5. P100-1/2006, Code for seismic design of residential buildings, agrozootehnical and industrial structures. (in Romanian).
6. www.fip-group.it
7. Rama Raju, K., et al., Optimum Distribution of Viscous Fluid Dampers in Multi-Storied Buildings, *International Conference on Structural Stability and Dynamics*, Florida, 2005.

Identification Methods of the Nonlinear Systems Subjected to Seismic Actions

Doina Stefan, Violeta-Elena Chitan

¹Structural Mechanics, Technical University "Gh. Asachi" Iasi, 700050, România

Summary

The need to identify the nonlinear systems subjected to stochastic actions led to the development of the classical and/or deterministic methods toward some methods capable to take into account the improved models for structure and excitation.

The identification of the nonlinear systems can be carried out using specific approaches that are based on the reparability hypotheses or on the change of the nonlinear system with an equivalent linear system that has the features closely related to the initial one.

Current nonlinearities that occur in the structural response during a strong earthquake are geometrical and/or physical (nonlinearity of the stiffness and the damping). In order to underline the nonlinearity of the stiffness, in this paper we take advantage of the modeling method for the structural response using a non-stationary linear model and the parameter identification of the equivalent stationary linear model, both for the SDOF and the NDOF systems.

Explaining the nonlinearity of the stiffness can be done in two specific ways: the structure response modeling through the nonstationary linear model and the parameter identification of the equivalent stationary linear model; the real stiffness valuation of the structure during each vibration cycle using the internal force calculus of the structure.

KEYWORDS: nonlinear system, stationary linear model, nonlinearity of the stiffness, structural response.

1. INTRODUCTION

In the context of continuous efforts to improve the knowledge in the field of dynamic-seismic behavior of a building, the direction is toward the study of structural behavior starting from the tests in situ.

This kind of approach gives the means for: structural quality and security level checking in the conditions of real exploitation; validation of the existent analytical

models of behavior, also for the a-priori hypotheses of the structural response prediction; knowledge accumulation, necessary to improve the dimensioning methods and the well argued working out of the new behavior models.

Knowing precisely or often good enough the features of a system implies the discerning use of various theoretical and experimental approaches. The system identification doesn't mean anything else but the convenient processing of some information achieved from the tests, in order to obtain a physical or mathematical model, as simple and easy-to-use as possible.

An identification process consists of: the choice of the model structure; the choice of the criterion to compare the model with the real structure; estimation of the model parameters.

The need to identify the nonlinear systems subjected to stochastic actions led to the development of the classical and/or deterministic methods toward some methods capable to take into account the improved models for structure and excitation. For this reason, the non-linear system identification can be carried out using specific approaches that are based on the reparability hypotheses or on the change of the nonlinear system with an equivalent linear system that has the features closely related to the initial one.

Current nonlinearities that occur in the structural response during a strong earthquake are physical and/or geometrical. In the case of physical non-linearity the equations of motion settled in the hypothesis of visco-elastic linear behavior do not remain valid already, and generally, the forces that occur are expressed using non-linear functions, with respect to displacement and velocity, this leading to the non-linear stiffness and non-linear damping.

To underline the non-linear stiffness, two methods are usually carried out: the structural response modeling using a non-stationary linear model and the parameter identification of the equivalent stationary linear model; the estimation of the effective structural stiffness during each cycle of vibration using the computation of internal structural forces.

2. THE EQUIVALENT LINEARIZATION METHOD

Using the fact that linear systems are solved easily, the study of the nonlinear systems can be performed with sufficient accuracy by changing the nonlinear system with an equivalent linear system having the features closely related to the initial one. This technique of linearization for the systems subjected to stochastic actions was proposed for the first time by Booton in 1953.

2.1. SDOF Systems

The simplest mechanical system is the SDOF oscillator, which has the equation of motion as follows:

$$m\ddot{y}(t) + h(y, \dot{y}) = f(t) \tag{1}$$

where:

- y , \dot{y} , \ddot{y} are denoting the displacement, velocity and acceleration;
- h (y , \dot{y}) denotes a function that describes the nonlinearity of the oscillator;
- f(t) denotes the stochastic action.

The linearization method consists of the change of nonlinear oscillator with an equivalent linear one. Equation (6.6) becomes:

$$m\ddot{\tilde{y}}(t) + c_{eq}\dot{\tilde{y}}(t) + k_{eq}\tilde{y}(t) = f(t) \tag{2}$$

where:

- y , \dot{y} , \ddot{y} are denoting the displacement, velocity and acceleration of the equivalent linear system;
- c_{eq} denotes the viscous damping of the equivalent system;
- k_{eq} denotes the stiffness of the equivalent linear system;
- (c_{eq} and k_{eq} must be found out).

It is normaly to say that the nonlinear system and the equivalent linear system do not have identically motions, so the solutions y , \dot{y} , \ddot{y} do not verify exactly the equation (2), this becoming:

$$m\ddot{\tilde{y}}(t) + h(\tilde{y}, \dot{\tilde{y}}) = f(t) + \varepsilon(t) \tag{3}$$

where: $\varepsilon(t)$ is the error that allows the measurement of the difference between the equations (1) and (2).

$$\varepsilon(t) = h(\tilde{y}, \dot{\tilde{y}}) - c_{eq}\dot{\tilde{y}}(t) - k_{eq}\tilde{y}(t) \tag{4}$$

In order to find out c_{eq} and k_{eq} , the error $\varepsilon(t)$ must have the minimum value. This method suggests a minimization process for $\varepsilon(t)$, starting from the identity:

$$\frac{\partial E[\varepsilon(t)^2]}{\partial C_{eq}} = \frac{\partial E[\varepsilon(t)^2]}{\partial K_{eq}} = 0 \quad (E[\varepsilon(t)^2] - \text{math operator}) \tag{5}$$

Developing the equation (5) we obtain the system:

$$\begin{aligned} K_{eq} &= \frac{E[h \cdot \tilde{y}]E[\dot{\tilde{y}}^2] - E[h \cdot \dot{\tilde{y}}][\tilde{y} \cdot \dot{\tilde{y}}]}{E[\tilde{y}^2]E[\dot{\tilde{y}}^2] - E[\tilde{y} \cdot \dot{\tilde{y}}]^2} \\ C_{eq} &= \frac{E[h \cdot \dot{\tilde{y}}]E[\tilde{y}^2] - E[h \cdot \tilde{y}][\tilde{y} \cdot \dot{\tilde{y}}]}{E[\tilde{y}^2]E[\dot{\tilde{y}}^2] - E[\tilde{y} \cdot \dot{\tilde{y}}]^2} \end{aligned} \tag{6}$$

where:

h is as a matter of fact $h(y, \dot{y})$;

$E[\tilde{y}, h(\tilde{y}, \dot{\tilde{y}})]$ and $E[\dot{\tilde{y}}, h(\tilde{y}, \dot{\tilde{y}})]$ can be expressed as functions of y and

\dot{y} and c_{eq} and k_{eq} are functions depending on the terms of the covariance matrix, denoted $cov[Y]$ and having the following format:

$$cov[Y] = \begin{bmatrix} E[\tilde{y}, \dot{\tilde{y}}] & E[\tilde{y}, \tilde{y}] \\ E[\dot{\tilde{y}}, \tilde{y}] & E[\dot{\tilde{y}}, \dot{\tilde{y}}] \end{bmatrix} \quad (7)$$

2.2. NDOF Systems

The nonlinear NDOF system has the following equation of motion:

$$M\ddot{y}(t) + h(y, \dot{y}) = f(t) \quad (8)$$

where:

$f(t)$ is a representative gaussian process of the excitation;

$W(t)$ is a stationary gaussian process;

$g(t)$ is a vector with terms as functions that are measurable in time;

y is the displacement vector.

$$f(t) = W(t) \cdot g(t) \quad (9)$$

The equivalent linear system has the form:

$$M\ddot{\tilde{y}} + C_{eq}\dot{\tilde{y}} + K_{eq}\tilde{y} = f(t) \quad (10)$$

where:

C_{eq} is the equivalent damping matrix that depends on the time (because $g(t)$ is not constant);

K_{eq} is the equivalent stiffness matrix.

The vector of errors is defined by the relation:

$$\varepsilon(t) = h(\tilde{y}, \dot{\tilde{y}}) - C_{eq}(t)\dot{\tilde{y}} - K_{eq}(t)\tilde{y} \quad (11)$$

This vector is computed as a function of variables of the linear system and it is minimized using the least square criterion. The $C_{ij}(t)$ and $K_{ij}(t)$ coefficients from the $C_{eq}(t)$ and $K_{eq}(t)$ matrices are computed from:

$$\begin{aligned} \frac{\partial E[\varepsilon^T(t)\varepsilon(t)]}{\partial C_{ij}(t)} &= 0 \quad i = 1, N \quad ; \quad j \leq i \\ \frac{\partial E[\varepsilon^T(t)\varepsilon(t)]}{\partial K_{ij}(t)} &= 0 \end{aligned} \quad (12)$$

Using equation (11) we can write:

$$\begin{aligned}
 E[h(\tilde{y}, \dot{\tilde{y}})\tilde{y}^T] - C_{eq}(t)E[\dot{\tilde{y}}, \dot{\tilde{y}}^T] - K_{eq}(t)E[\tilde{y}, \tilde{y}^T] &= 0 \\
 E[h(\tilde{y}, \dot{\tilde{y}})\dot{\tilde{y}}^T] - C_{eq}(t)E[\tilde{y}, \tilde{y}^T] - K_{eq}(t)E[\dot{\tilde{y}}, \dot{\tilde{y}}^T] &= 0
 \end{aligned}
 \tag{13}$$

From above, the $C_{ij}(t)$ and $K_{ij}(t)$ terms can be obtained.

The excitation is a gaussian one, this leading to a gaussian response and allowing to write the $E[h(\tilde{y}, \dot{\tilde{y}}), \tilde{y}^T]$ and $E[h(\tilde{y}, \dot{\tilde{y}}), \dot{\tilde{y}}^T]$ terms as functions of the $Y(2n \times 2n)$ covariance matrix terms. The computation of the $E[h(\tilde{y}, \dot{\tilde{y}}), \tilde{y}^T]$ and $E[h(\tilde{y}, \dot{\tilde{y}}), \dot{\tilde{y}}^T]$ terms is easily carried out if we assume the fact that the displacements and velocities are two by two independent.

$$C_{ij}(t) = E\left[\frac{\partial h_i(\tilde{y}, \dot{\tilde{y}})}{\partial \tilde{y}}\right] \quad K_{ij}(t) = E\left[\frac{\partial h_i(\tilde{y}, \dot{\tilde{y}})}{\partial \dot{\tilde{y}}}\right]
 \tag{14}$$

$$Y = \begin{bmatrix} E[\tilde{y}\tilde{y}^T] & E[\tilde{y}\dot{\tilde{y}}^T] \\ E[\dot{\tilde{y}}\tilde{y}^T] & E[\dot{\tilde{y}}\dot{\tilde{y}}^T] \end{bmatrix}
 \tag{15}$$

The linear system has $n(n+1)/2$ unknowns, which are the $C_{ij}(t)$ and $K_{ij}(t)$ $i=1,n$ terms and they are computed with respect to the terms of the $Y(t)$ matrix.

3. NONLINEAR SYSTEM IDENTIFICATION. THE MODEL OF THE NONLINEAR OSCILLATOR

It is considered the fact that the measured response at the roof level can be modeled using the nonlinear oscillator, which has the equation of equilibrium as follows:

$$\ddot{y} + f(y, \dot{y}) = -p\ddot{y}_{ter}
 \tag{16}$$

Assuming for the mass and the damping to remain constant, and for the stiffness to be variable, the force f has the expression:

$$f = c_0\dot{y} + k_0(t)y
 \tag{17}$$

where:

- c_0 is the damping constant over the unit of mass;
- $k_0(t)$ is the structural stiffness over the unit of mass.

The equation (16) can also be written:

$$\ddot{y} + c_0\dot{y} + k_0(t)y = -p\ddot{y}_{ter}
 \tag{18}$$

In order to compute the response of the assumed model, the non-linear differential equation (17) must be solved for each iteration step of the numerical algorithm for minimization.

The equation of equilibrium in incremental variables is:

$$\Delta\ddot{y} + c_0\Delta\dot{y} + k_0(t)\Delta y = -p\Delta\ddot{y}_{ter} \tag{19}$$

where:

$$\begin{aligned} \Delta\ddot{y} &= \ddot{y}(t + \Delta t) - \ddot{y}(t) \\ \Delta\dot{y} &= \dot{y}(t + \Delta t) - \dot{y}(t) \\ \Delta y &= y(t + \Delta t) - y(t) \\ \Delta\ddot{y}_{ter} &= \ddot{y}_{ter}(t + \Delta t) - \ddot{y}_{ter}(t) \end{aligned} \tag{20}$$

There are many ways to solve the equation (19). The best one is the step-by-step approach. The dynamic equilibrium is stable at the beginning and at the end of each time step Δt , inside in which it is assumed a linear variation of acceleration and the structural features remaining constant during all the range (fig.1).

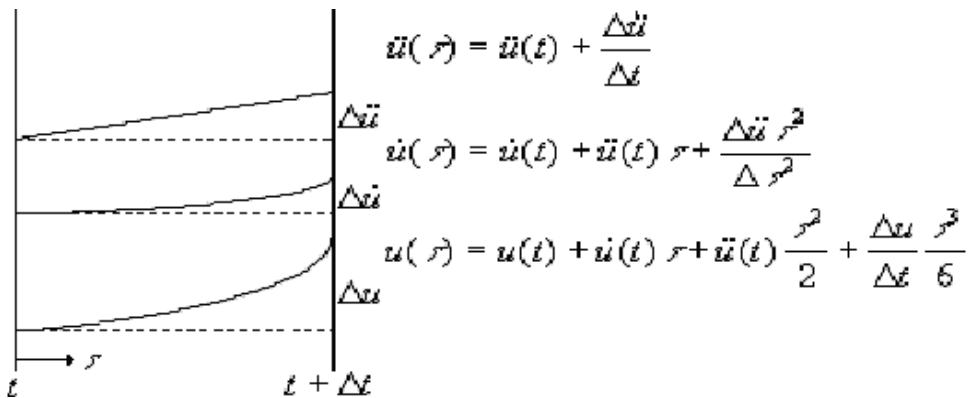


Figure 1. The dynamic equilibrium

The incremental values for velocity and displacement are:

$$\Delta\dot{y}(t) = \dot{y}(t)\Delta t + \Delta\ddot{y}(t) \frac{\Delta t}{2} \tag{21}$$

$$\Delta y(t) = \dot{y}(t)\Delta t + \ddot{y}(t) \frac{\Delta t^2}{2} + \Delta\ddot{y}(t) \frac{\Delta t}{2} \tag{22}$$

Using the incremental displacement as a basic variable, one can obtain the incremental acceleration from equation (22), which is after substituted in equation (21), this leading to:

$$\Delta\ddot{y}(t) = \frac{6}{\Delta t^2} \Delta y(t) - \frac{6}{\Delta t^2} \Delta \dot{y}(t) - 3\ddot{y}(t) \quad (23)$$

$$\Delta\dot{y}(t) = \frac{3}{\Delta t^2} \Delta y(t) - 3\dot{y}(t) - \frac{\Delta t}{2} \ddot{y}(t) \quad (24)$$

Substituting equations (23) and (24) in equation (19) we obtain:

$$\left[\frac{6}{\Delta t^2} \Delta y(t) - \frac{6}{\Delta t^2} \Delta \dot{y}(t) - 3\ddot{y}(t) \right] + K_0 \left[\frac{3}{\Delta t} \Delta y(t) - 3\dot{y}(t) - \frac{\Delta t}{2} \ddot{y}(t) \right] + K_0(t) \cdot \Delta y(t) = -p\ddot{y}_{ter} \quad (25)$$

or:

$$\tilde{K}(t) \cdot \Delta y(t) = \Delta \tilde{y}_{ter} \quad (26)$$

where:

$$\tilde{K}(t) = \frac{6}{\Delta t^2} + \frac{3}{\Delta t} C_0 + K_0 \quad (27)$$

$$\Delta \tilde{y}_{ter} = -p\Delta \ddot{y}_{ter} + \frac{6}{\Delta t} \dot{y}(t) + 3\ddot{y}(t) + C_0 \left[3\dot{y}(t) + \frac{\Delta t}{2} \ddot{y}(t) \right] \quad (28)$$

Therefore, the incremental displacement is computed starting from equation (26) and dividing the effective incremental load by the effective stiffness.

4. CONCLUSIONS

A nonlinear system can be defined as a system that doesn't obey to the superposition principles. This "non-property" occurs to the extremely various systems for which it doesn't exist general solving methods, but only special methods, adapted to each class of problems.

The identification of the nonlinear systems can be carried out using specific approaches that are based on the reparability hypotheses or on the change of the nonlinear system with an equivalent linear system that has the features closely related to the initial one.

Current nonlinearities that occur in the structural response during a strong earthquake are geometrical and/or physical (non-linearity of the stiffness and damping). In this paper we take advantage of the modeling method for the structural response using a non-stationary linear model and the parameter identification of the equivalent stationary linear model, in order to underline the nonlinearity of the stiffness.

References

1. Afra H., P.Argoul, *Identification du comportement sismique des batiments et comparaison avec les donnees reglementaires*, 1990, Annales des Ponts et Chausees, pag.50-65. (in French)
2. Eykhoff P., *Identificarea sistemelor*, 1977, Ed. Tehnica, Bucuresti. (in Romanian, translation from English)
3. Guihot Pascal, *Analyse de la reponse de structures non lineaires sollicitees par des sources d'excitation aleatoire*. These de doctorat de l'Universite de Paris VI, 1999. (in French)
4. Stefan Doina, *Identificarea sistemelor mecanice cu aplicatii la calificarea seismia a unor cladiri si echipamente din componenta Centralelor Nuclearo-Electrice*, Teza de doctorat, Univ. Tehnica “Gh. Asachi”, ian., 1996, Iasi. (in Romanian)

ISBN 978-973-8955-14-1



MANIFESTARI STIINTIFICE